VISCOUS FLUID FLOW OVER AN EXPONENTIALLY STRETCHING PERMEABLE SHEET WITH HALL EFFECT AND CONVECTIVE THERMAL CONDITION

A THESIS SUBMITTED TO
NATIONAL INSTITUTE OF TECHNOLOGY WARANGAL, (T.S.)
FOR THE AWARD OF THE DEGREE OF
DOCTOR OF PHILOSOPHY
in
MATHEMATICS

by

JAGADEESHWAR PASHIKANTI
(Roll No. 714048)

UNDER THE SUPERVISION OF
Dr. D. SRINIVASACHARYA

DEPARTMENT OF MATHEMATICS
NATIONAL INSTITUTE OF TECHNOLOGY
WARANGAL
TELANGANA STATE, INDIA

MAY 2018

C E R T I F I C A T E

This is to certify that the thesis entitled " **Viscous Fluid Flow over an Exponentially Stretching Permeable Sheet with Hall Effect and Convective Thermal Condition** " submitted to National Institute of Technology Warangal, for the award of the degree of ***Doctor of Philosophy***, is the bonafide research work done by **Mr. JAGADEESHWAR PASHIKANTI** under my supervision. The contents of this thesis have not been submitted elsewhere for the award of any degree.

Dr. D. Srinivasacharya
Professor
Department of Mathematics
National Institute of Technology,
Warangal, T.S., INDIA

.

DECLARATION

This is to certify that the work presented in the thesis entitled **"Viscous Fluid Flow over an Exponentially Stretching Permeable Sheet with Hall Effect and Convective Thermal Condition"**, is a bonafide work done by me under the supervision of **Dr. D. SRINIVASACHARYA** and has not been submitted elsewhere for the award of any degree.

I declare that this written submission represents my ideas in my own words and where others' ideas or words have been included, I have adequately cited and referenced the original sources. I also declare that I have adhered to all principles of academic honesty and integrity and have not misrepresented or fabricated or falsified any idea / data / fact /source in my submission. I understand that any violation of the above will be a cause for disciplinary action by the Institute and can also evoke penal action from the sources which have thus not been properly cited or from whom proper permission has not been taken when needed.

Jagadeeshwar Pashikanti

Roll No. 714048

Date:_____

Dedicated to

My Family, My Teachers

&

Sri Sai Baba

ACKNOWLEDGEMENTS

It is a rare privilege and boon that I could associate myself for pursuing my research work with Dr. D. Srinivasacharya, Professor of Mathematics, National Institute of Technology Warangal, India. I sincerely record my gratitude for his invaluable guidance and constant encouragement throughout the preparation of this thesis and his involvement and meticulous supervision while my work was in progress. With his inimitable qualities as a good teacher, he chiseled my path towards perfection. Ever since I met him, he has been a perpetual source of inspiration, divine guidance, encouragement and enlightenment. He is responsible for making the period of my research work as an educative and enjoyable learning experience. He has been a great source of motivation and inspiration. The thesis would not have seen the light of the day without his unrelenting support and cooperation. I deem it a privilege to have worked under his amiable guidance. My vocabulary is inadequate to express my gratitude. I also thank to madam Smt. D. Jayasrinivasacharya for her hospitality and her patience during our elongated discussions.

I am grateful to Prof. D. Srinivasacharya, Head, and former Heads, Prof. Debashis Dutta and Prof. J. V. Ramana Murthy, Department of Mathematics for providing necessary help and support throughout my research period.

I take this opportunity to thank the retired Prof. G. Radhakrishnamacharya and Prof. Y. N. Reddy, Department of Mathematics for his valuable suggestions, moral support and encouragement during my stay.

I thank the members of the Doctoral Scrutiny Committee, Prof. K. N. S. Kasi Viswanadham, Prof. J. V. Ramana Murthy, Department of Mathematics and Prof. P. Nageswar Rao, Department of Chemistry for their valuable suggestions, moral support and encouragement while my work was in progress.

I place on record my gratitude to all the faculty members of the Department of Math-

ematics, for their constant encouragement. Also, I am grateful to Prof. D. S. Kesava Rao, former Head, Department of Humanities and Social Sciences for his kind support.

I express my sincere thanks to the Director, National Institute of Technology, Warangal for awarding me Institute Fellowship (MHRD, GoI) to carry out my research work. I thank him for his kind support and encouragement at every stage of this endeavor.

I owe my special thanks to Dr. J. Pranitha, Dr. Ch. Ramreddy, Dr. K. Kaladhar, Dr. M. Krishna Prasad for their support. I thank G. Madhava Rao, Md. Shafeeurrahaman, Mrs. K. Hima Bindu, Mrs. T. Pradeepa, G. Venkata Suman, Ch. Venkata Rao, P. Naveen, all other research colleagues in the Department of mathematics and my friends, who helped me during my Ph.D for being cooperative and also for making my stay in the NITW campus fruitful and enjoyable every moment.

My deepest gratitude to my Mother, P. Veeralaxmi and in-laws, R. Sammireddy and R. Vijaya for their continuous support and constant encouragement over the years. My thanks, choked with emotion, to my innocent daughters P. Akshitha and P. Nikshitha for their understanding and adjustment while I missed them, when I was engrossed in my research. All of their love and affection have been motivating force behind what I am today.

Finally, and most importantly, I would like to thank my better half, R. Swapna for her support, prayers, patience and understanding that were vital to complete this dissertation. Without her help and encouragement, I would not have been finished this thesis.

. Jagadeeshwar Pashikanti

A B S T R A C T

The thesis consists of NINE chapters. In each chapter, we consider two different physical conditions on the sheet i.e. when the sheet is (i) subjected to thermal convective boundary condition and (ii) maintained at uniform wall temperature with Hall effect. Chapter 1 provides an introduction to the concepts in Newtonian fluid, heat and mass transfer and a review of the pertinent literature. Chapter 2 presents the effect of thermal radiation and chemical reaction in a viscous fluid flow over an exponentially stretching sheet. Chapter 3 investigates the effect of Joule heating on the viscous flow over an exponentially stretching sheet. Chapter 4 deals the numerical solution of influence of cross-diffusion effects on the flow of viscous incompressible fluid due to the exponentially stretching sheet. Chapter 5 studies the effect of variable fluid properties and heat source/sink on the laminar viscous flow on an exponentially stretching sheet. Chapter 6 presents the influence of thermophoresis and viscous dissipation effects of incompressible viscous fluid flow due to a sheet stretching exponentially. Chapter 7 studies the double dispersion effects in a laminar slip flow of electrically conducting viscous fluid over an exponentially stretching permeable sheet. Chapter 8 explores the influence of homogeneous-heterogeneous reactions in presence of thermal radiation on the laminar slip flow of viscous incompressible fluid on an exponentially stretching sheet.

Except for case (a) of chapters 3 and 6 and both cases of chapters 7 and 8, in all the chapters, the governing non-linear ordinary differential equations and their associated boundary conditions are linearized by using successive linearization method and then solved numerically by using Chebyshev spectral collocation method. For the case of non-similar equations, in the above-mentioned chapters, a local similarity and non-similarity method is used to transform the governing partial differential equations into ordinary differential equations and then solved by using Successive linearization method together with Chebyshev spectral collocation method. The effects of convective heat transfer coefficient(Biot number), Hall parameter, magnetic parameter, thermal radiation, chemical reaction, Joule heating, cross-diffusion effects, variable viscosity, variable thermal conductivity, heat source or sink, thermophoresis, viscous dissipation, double dispersion effects, homogeneous and heterogeneous reactions are considered on the flow characteristics such as the velocity, temperature and concentration distributions along with the local heat and mass transfer coefficients and are presented through graphs. The last chapter (Chapter 9) gives key findings of the thesis and scope of the work for further study.

NOMENCLATURE

$\tilde{a}, \tilde{b}$	Concentrations of the chemical species $\tilde{A}$ and $\tilde{B}$	V_*	Variable wall mass transfer velocity
$\tilde{a}_0$	Positive constant	N_*	Slip velocity
$\tilde{A}, \tilde{B}$	Chemical species	N_0, V_0	Constants
Bi	Biot number	g	Gravitational acceleration
$\mathbb{B}$	Buoyancy ratio	Gr	Grashof number
$\tilde{C}$	Concentration	h_f	Convective heat transfer coefficient
C_w	Wall concentration		
C_∞	Ambient concentration	k_c, k_s	Rate constants
c_p	Specific heat capacity	K	Measures the strength of the homogeneous reaction
c_s	Concentration susceptibility	K_s	Measures the strength of the heterogeneous (surface) reaction
K_T	Thermal diffusion ratio		
T_m	Mean fluid temperature	k^*	Mean absorption coefficient
T_w	Wall temperature	L	Characteristic length
D	Molecular diffusivity	$Nu_{\tilde{x}}$	Local Nusselt number
$\tilde{D}_e$	Effective molecular diffusivity	Pr	Prandtl number
D_A, D_B	Diffusion coefficients	R	Radiation parameter
q_w	Heat flux	$Re_{\tilde{x}}$	Local Reynolds number
q_m	Mass flux	Re	Reynolds number
S	Suction/Injection parameter	Sc	Schmidt number
U_*	Stretching velocity	J	Joule heating parameter
U_0	Reference velocity	Q	Heat source

Q_0	Constant
k_1	Rate constant
k_0	Constant
k_p	Permeability of porous medium
K_p	Porosity parameter
H_a	Magnetic parameter
q_1	Heat source parameter
x	Streamwise coordinate
Ec	Eckert number
S_r	Soret number
D_f	Dufour number
$Sh_{\tilde{x}}$	Local Sherwood number
$\tilde{T}$	Temperature
T_f	Convective wall temperature
T_∞	Ambient temperature
T	Dimensionless temperature
C	Dimensionless concentration
κ	Thermal conductivity
D_γ	Thermal dispersion parameter
D_χ	Solutal dispersion parameter
ϵ	Thermal conductivity parameter
τ	Thermophoresis parameter
θ_r	Viscosity parameter
η	Similarity variable
τ_e	Electron collison time
ω_e	Cyclotran frequency of electrons
λ	Velocity slip parameter
μ	Dynamic viscosity
ν	Kinematic viscosity
ρ	Density of the fluid
σ^*	Stefan-Boltzmann constant
σ	Electrial conductivity
τ_w	Wall shear stress
ψ	Stream function

Greek Symbols

α	Thermal diffusivity
$\tilde{\alpha_e}$	Effective thermal diffusivity
β_T	Coefficients of thermal expansion
β_C	Coefficients of solutal expansion
γ	Chemical reaction parameter
β_h	Hall parameter

Subscripts

w	Wall condition.
∞	Ambient condition.

Superscript

$\prime$	Differentiation with respect to η.

Contents

[1]Case(a):Accepted for publication in "**Lecture Notes in Mechanical Engineering**",
Case(b):Published in "**Frontiers in Heat and Mass Transfer**" (2018) 9(37) (2017) 1–10

[2]Case(a):Communicated to "**Mathematical Sciences**",
Case(b):Published in "**Nonlinear Engineering - Modeling and Application**" 6(2) (2017) 101–114

[3] Case(a):Published in "**International Journal of Engineering, TRANSACTIONS A**" 31(1) (2018) 120–127,
Case(b):Communicated to "**Propulsion and Power Research**"

[4] Case(a):Accepted for publication in "**Modelling, Measurement and Control B**" 87(1) (2018) 7–14,
Case(b):Published in "**International Journal of Energy for a Clean Environment** " 19(1-2) (2018) 67–83

[5] Case(a): Communicated to "**International Journal of Applied Mechanics and Engineering**", Case(b) Communicated to "**Journal of the Association of Arab Universities for Basic and Applied Sciences**"

[6] Case(a): Communicated to "**International Journal of Engineering Science**", Case(b) Communicated to "**Journal of Molecular Liquids**"

[7] Case(a): Communicated to "**Nonlinear Engineering - Modeling and Application**", Case(b) Communicated to "**International Journal of Chemical Reactor Engineering**"

Chapter 1

Preliminaries and Review

1.1 Introduction

Fluid mechanics deals with the behavior of liquids and gases at rest or in motion. It stands central to much of science and engineering and impacts defense, transportation, manufacturing, environment, medicine, energy, etc. It encompasses a vast variety of practical problems ranging from the flow of blood in capillaries to flow of oil in huge pipelines and from the flight of birds to supersonic flights of airplanes. This subject is proven to be a highly exciting and challenging subject of modern sciences in view of its applications in every aspect our daily life. The quest for deeper understanding of the subject has not just enlivened the development of the subject itself but has additionally proposed the progress in the supporting areas, such as applied mathematics, numerical computing, and experimental techniques.

The fluid dynamics due to a stretching surface has ever increasing applications in industry as well as in certain technological processes. When sheets are being manufactured, molten material is pulled from the slit and stretched to obtain required thickness [5]. The eminence of such products is determined by both the kinematics of stretching and the simultaneous

heating or cooling during the process. This situation is similar to continuous pulling of plastic sheets in the manufacturing of plastic bags and rubber sheets. It is important to study the velocity of the stretching surface relative to the point of extrusion [115]. In all these processes, the quality of the final product, as well as the cost of production, is affected by the rate of heat transfer and mass transfer on the stretching surface, and knowledge of cooling fluid and its flow properties. The rate at which the sheet is drawn from the extrusion slit is described in a number of different ways namely; linear, continuous, unsteady and nonlinear such as exponential. In most studies it is assumed that the velocity of the stretching sheet is need not be linearly proportional to the distance from the extrusion slit [50].

Many chemical engineering processes like those in metallurgy and polymer extrusion Fig. (2.2.4)) (image is taken from Abel *et al.* [2]) involve the cooling of a molten liquid (polymer solution, molten metal, etc.) by drawing it into a cooling liquid, sometimes referred as the ambient liquid. While drawing the molten liquid into the cooling system it is sometimes stretched (as in the case of polymersheet extrusion). The stretching imparts a unidirectional orientation to the extrudate, thereby improving its fluid mechanical properties (see [29]). The problem of stretching sheet is thus a fundamental one and arises in many practical situations that are similar to the polymer extrusion and metallurgical processes. Some of these are listed below:

- Continuous stretching, rolling, manufacturing of polymer sheets.
- Drawing, annealing, tinning of copper wires.
- Cooling of an infinite metallic plate in a cooling path.
- Boundary Layer along a liquid film in condensation processes.
- Manufacture of materials by extrusion process and heat-treated materials traveling between a feed and wind-up rolls or conveyer belts.
- Glass blowing, paper production, crystal growing, etc.

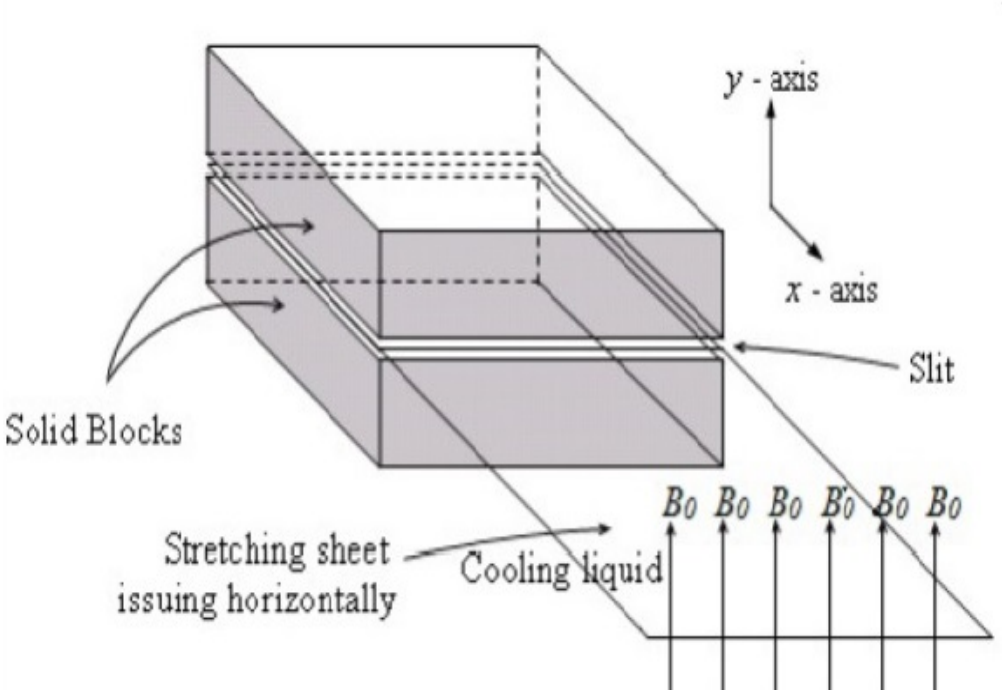

Figure 1.1: Schematic diagram of a polymer extrusion process

In a polymer extrusion process, the fluid mechanical properties desired for the ultimate outcome (sheet being stretched) depend mainly on the rate of cooling. The liquid which is basically meant to cool the stretching sheet plays an important role in determining the property sought for the final product. It is imperative therefore to consider two important aspects in this physically interesting problem:

- Proper choice of cooling liquid.
- Regulation of the flow of the cooling liquid.

An appropriate and advantageous choice of cooling liquid in all these processes is Newtonian fluid. Hence, the laminar flow, heat and mass transfer over a stretching sheet in a Newtonian fluid has received considerable interest by several researchers.

1.2 Newtonian fluids

The great majority of most common fluids (liquids and gases) such as water, gasoline, honey, organic solvents, oils, air, steam, nitrogen or rare gases are characterized as Newtonian fluids. These fluids resist movement or the movement of an object through the fluid. The magnitude of the resistance to this deformation is represented by the viscosity of the fluid. The study of a Newtonian fluid flow gained much attention in last few decades because of their industrial and engineering applications.

A Newtonian fluid is a fluid that exhibits a viscosity that remains constant regardless of any external stress that is placed upon it, such as mixing or a sudden application of force. Another way to describe these fluids is that they obey Newtons law of viscosity or a linear relationship between viscosity and shear stress i.e. the shear stress induced by flow is proportional to the rate of the strain and the constant of proportionality is the fluid's viscosity.

The equations governing the flow of incompressible Newtonian fluids are

$$\frac{\partial \rho}{\partial t} + \rho(\nabla \cdot \vec{q}) = 0 \tag{1.1}$$

$$\rho\left(\frac{\partial \vec{q}}{\partial t} + (\vec{q}\cdot\nabla)\vec{q}\right) = \rho\vec{f} - \nabla p + \mu\nabla^2\vec{q} \tag{1.2}$$

where $\vec{q}$ is the velocity vector and p is the fluid pressure, ρ is the density of the fluid and $\vec{f}$ is the body force per unit mass.

1.3 Basic Terminology

Heat Transfer

Heat transfer means the exchange of internal energy between individual elements or regions of the medium considered. It always occurs from higher temperature region to lower temper-

ature region. There are three modes by which the heat transfer occurs. They are conduction, convection and radiation. The molecular transport of heat in bodies or between bodies in the thermo dynamical system is referred to as conduction. Convection is concerned with the fluid medium and/or the fluid in the medium. The heat transfer due to the movement of fluid from one region to the other region in the medium is called convection. Radiation heat transfer is a mechanism in which the internal energy of a substance is converted into radiant energy. The transport of heat by convection together with conduction is known as convective heat transfer. Further, forced, free and mixed convection are three classification of convection. To compute the heat transfer rate in the medium, the temperature distribution or temperature field is to be determined from the heat or energy (conservation of energy) equation.

$$\rho\, c_p \left(\frac{\partial \tilde{T}}{\partial t} + \vec{q} \cdot \nabla \tilde{T} \right) = \nabla.(\alpha \nabla \tilde{T}) \tag{1.3}$$

where $\tilde{T}$, c_p and α are the local equilibrium temperature, the specific heat capacity at constant pressure and the thermal diffusivity of the medium, repsectively.

Radiation

Heat transfer due to the emission of electromagnetic waves is known as thermal radiation. The importance of radiation becomes intensified at high absolute temperature levels. It is well known that the thermal radiation heat transfer does not require any intermediate medium by electromagnetic waves, or photons, which may travel a long distance without interacting with the medium. Thus thermal radiation is of great importance in vacuum and space applications. The transfer of energy by radiation depends on differences of the individual absolute temperature of the bodies. In the presence of thermal radiation, the energy equation (1.3) reduce to

$$\rho\, c_p \left(\frac{\partial \tilde{T}}{\partial t} + \vec{q} \cdot \nabla \tilde{T} \right) = \nabla.(\alpha \nabla \tilde{T}) + \nabla q_r \tag{1.4}$$

The radiation heat flux is q_r, under the Rosseland approximation [102] can be written as

$$q_r = -\frac{4\sigma^*}{3k^*}\frac{\partial \tilde{T}^4}{\partial \tilde{y}} \tag{1.5}$$

where σ^* is Stefan-Boltzman constant and k^* is coefficient of mean absorption. We assume the variation in the fluid phase temperature inside the flow to be appropriately minimum such that $\tilde{T}^4$ may be shown as a linearly continuous function of the temperatures and enlarged in a Taylor Series around T_m and removing highest order terms, we get $\tilde{T}^4 = 4T_m^3\,\tilde{T} - 3T_m^4$.

Viscous Dissipation

Viscous dissipation or dissipation is referred as transforming the energy taken from the motion of the fluid by the viscosity into internal energy. This process is partially irreversible. The energy conservation equation by including viscous dissipation is given by

$$\rho\, c_p \left(\frac{\partial \tilde{T}}{\partial t} + \vec{q}\cdot\nabla\tilde{T}\right) = \nabla.(\alpha\nabla\tilde{T}) + \Phi \tag{1.6}$$

where Φ is the dissipation function representing the work done against viscous forces, which is irreversibly converted into internal energy. It is defined as $\rho\Phi = \lambda_d\,(\nabla\cdot\vec{q})^2 + 2\mu\,(D:D)$

Mass Transfer

The tendency of a component in a mixture to travel from a region of high concentration to one of low concentration is called mass transfer. Mass transfer occurs by two mechanisms Diffusion mass transfer and Convective mass transfer. Diffusion mass transfer may occur either due to concentration gradient or temperature gradient or pressure gradient. Convective mass transfer is a mechanism in which mass is transferred between the fluid and the solid surface as a result of movement of matter from the fluid to the solid surface or fluid. The species mass flux can be determined from the statement of conservation of mass species,

which is given by

$$\frac{\partial \tilde{C}}{\partial t} + \vec{q} \cdot \nabla \tilde{C} = \nabla.(D \nabla \tilde{C}) \tag{1.7}$$

where $\tilde{C}$ is the concentration and D is the solutal diffusivity.

Chemical Reaction

Chemical reaction is the reaction in which the rate of reaction is directly proportional to the species concentration. Depending on the occurrence at an interface or as a single-phase volume reaction, the chemical reaction can be termed as either heterogeneous or homogeneous or both homogeneous and heterogeneous. With first order chemical reaction, the equation (1.7) can be written as

$$\frac{\partial \tilde{C}}{\partial t} + \vec{q} \cdot \nabla \tilde{C} = \nabla.(D \nabla \tilde{C}) - k_1(\tilde{C} - C_0) \tag{1.8}$$

where k_1 is the rate of chemical reaction.

Chemical reaction effect on the fluid flow is of considerable significance in chemical technology, materials processing systems and hydrometallurgical industries. The research on fluid flow with chemical reaction effects can help to design the chemical processing equipment, chemical diffusion in disk electrode modeling, carbon monoxide reactions in metallurgical mass transfer and kinetics, optical materials processing, and formation and dispersion of fog, etc. Several investigators have analyzed the impact of chemical reaction on the flow, heat and mass transfer through channels, pipes and annular region.

Cross-diffusion effects

When heat and mass transfer arise at the same time in a moving liquid, the relations between the fluxes and the driving abilities are of complex nature. It has been observed that an energy flux can be generated not only by temperature gradients but also by concentration gradients. “The mass flux can be generated by temperature gradients and this embodies the

Thermal diffusion, also called thermo-diffusion or Soret effect [89]. The heat flux induced by a concentration gradient is called Dufour or diffusion-thermo effect".

The modified energy and concentration equations, in steady state, with the Soret and Dufour effects, are given by

$$\vec{q} \cdot \nabla \tilde{T} = \nabla \cdot (\alpha \nabla \tilde{T} + D_{TC} \nabla \tilde{C}) \tag{1.9}$$

$$\vec{q} \cdot \nabla \tilde{C} = \nabla \cdot (D \nabla \tilde{C} + D_{CT} \nabla \tilde{T}) \tag{1.10}$$

where D_{CT}/D is the Soret number and D_{TC}/α and is Dufour number.

Magnetohydrodynamics

Magnetohydrodynamics (MHD) is the branch of continuum mechanics which deals with the mutual interaction between the magnetic field and electrically conducting fluid. If the magnetic field is present in an incompressible, electrically conducting fluid, then it interacts with the fluid by means of body force and body couple per unit mass. In the absence of gravitational effects, the regular magneto-fluid dynamics assumption is $\rho\vec{f} = \rho_e\vec{E} + \vec{J} \times \vec{B}$, where ρ_e is the free charge density, $\vec{E}$ is the electric field, $\vec{B}$ is the total magnetic field, and $\vec{J}$ is the current density and given by the Ohm's law $\vec{J} = \sigma\left[\vec{E} + \vec{q} \times \vec{B}\right]$. Since $\vec{J} \times \vec{B} \gg \rho_e E$, the later can be neglected. Hence, by adding the electromagnetic force term to the momentum equation of the fluid, the fluid dynamical aspects of MHD can be studied. The equation of motion of MHD Newtonian fluid will have the form

$$\rho\left(\frac{\partial \vec{q}}{\partial t} + (\vec{q} \cdot \nabla)\vec{q}\right) = \rho\vec{f} - \nabla p + \mu\nabla^2\vec{q} + \vec{J} \times \vec{B} \tag{1.11}$$

The total magnetic field in the medium is the sum of the applied magnetic field and induced magnetic field due to the motion of a conducting liquid in an applied magnetic field. The motion of a conducting fluid through a magnetic field induces electric currents and the fluid experiences a force. This force is called Lorenz force ($\vec{J} \times \vec{B}$) and it alters the motion of the fluid.

Hall Effect

"The presence of a magnetic field, in the flow of electric current through a conductor, applies a transverse force on the moving charge carriers that tend to push them to one side of the conductor. All accumulation of charge along the edges of conductors will adjust this magnetic effect, producing a quantifiable voltage between two sides of the conductor. The existence of quantifiable transverse voltage is known as Hall effect" named after E. H. Hall who discovered it in 1879.

The study of fluid flow with Hall current effects has important engineering applications in problems of magnetohydrodynamics generators and Hall accelerators as well as in flight magnetohydrodynamics. If the electron-atom collision frequency is assumed to be relatively high, the Hall effect cannot be neglected in which a current is induced in the direction normal to both the electric and magnetic fields. In this case, the generalized ohms law (current density) [110] is given by

$$\vec{J} = \sigma\Big[\vec{E} + \vec{q} \times \vec{B} - \eta(\vec{B} \times \vec{J})\Big] \tag{1.12}$$

where η is the Hall factor.

Joule Heating

James Prescott Joule(1841) was the first to studey the Joule heating effect. It is also known as ohmic heating or resistive heating. When an electric current pass through an electrolyte, it causes Joule heating. It is produced by intercommunication among the atomic ions that compose the body of the conductor and moving charged particles that form the current. In this process, some of the kinetic energy is converted into the heat and as a result temperature of the body increases. The rise in the temperature of the fluid translates to nonuniform properties of the fluid, such as a change in density and conductivity of the fluid. Changes in the applied electric potential field and the flow field are among some of the factors that alter the properties of the fluid.

Thermophoresis

The thermophoresis is a mechanism in which small particles migrate in the direction of decreasing thermal gradient. It is quite significant in radioactive particle deposition in nuclear reactor safety simulations, aerosol particle sampling, deposition of silicon thin films etc.

Variable fluid properties

In most of the engineering applications, the thermophysical properties of the fluid, especially viscosity and thermal conductivity may vary with temperature. Therefore, to predict the heat transfer rate accurately, it is necessary to take into account this variation of viscosity and thermal conductivity. Different researchers have taken the variations of the viscosity and thermal conductivity as different functions of temperature, time etc.. Lai and Kulacki [51] assumed that the fluid viscosity μ varies as an inverse linear function of the temperature $\tilde{T}$ i.e.,

$$\frac{1}{\mu} = \frac{1}{\mu_\infty}\left(1 + \delta(\tilde{T} - T_\infty)\right) \tag{1.13}$$

where δ is a thermal property of the fluid and μ_∞ is the constant value of coefficient of viscosity at far away from the surface.

Similarly, Slattery [100] and Chaim [13] assumed that the fluid thermal conductivity α varies as a linear function of temperature i.e.,

$$\alpha = \alpha_o(1 + \epsilon T) \tag{1.14}$$

where $\epsilon = E(T_w - T_\infty)$ is the thermal conductivity parameter, E is a constant depending on the nature of the fluid and T_w is the surface temperature. The variation of ϵ can be taken in the range as $-0.1 \leq \epsilon \leq 0$ for lubrication oils, $0 \leq \epsilon \leq 0.12$ for water and $0 \leq \epsilon \leq 6$ for air.

Boundary Layer Approximation

The boundary layer theory was presented by Ludwig Prandtl in 1904. The main idea was to divide the flow into two parts. The smaller part is a thin layer in the vicinity of solid surface in which the effects of viscosity are felt. This thin layer near the solid surface is called boundary layer. Although the boundary layer is thin, it plays an essential role in fluid dynamics. The thickness of the boundary layer is a function of the ratio between inertial forces and viscous forces, that is, the Reynolds number. The concept of boundary layer can be used to simplify the Navier-Stokes equations to such an extent that it becomes possible to tackle a large number of practical problems of great importance.

Boussinesq Approximation

For sufficiently small isobaric changes in temperature and concentration, the fluid density depends linearly on temperature and concentration differences, which is called as a linear Boussinesq approximation (discussed in detail by Tritton [113]) and is given by

$$\rho = \rho_\infty[1 - \beta_T(\tilde{T} - T_\infty) - \beta_C(\tilde{C} - C_\infty)] \tag{1.15}$$

where ρ_∞ is the fluid density, T_∞ is the ambient temperature,C_∞ is the ambient concentration at some reference point in the medium, β_T is the coefficient of thermal expansion and β_C is the coefficient of solutal expansion, which are given by

$$\beta_T = -\frac{1}{\rho}\left(\frac{\partial\rho}{\partial\tilde{T}}\right)_{p,C} \tag{1.16a}$$

$$\beta_C = -\frac{1}{\rho}\left(\frac{\partial\rho}{\partial\tilde{C}}\right)_{p,T} \tag{1.16b}$$

Equation (1.16) is a good approximation for the variation of density. This states that

i. all variations in fluid properties can be completely ignored except for density in momentum equation.

ii. the density is considered to vary with temperature and concentrations only, and its variations can be ignored everywhere except where they give rise to buoyancy force.

1.4 Boundary Conditions

The governing equations for the velocity and temperature fields are partial differential equations. Which are applicable at every point in a fluid that is being modeled as a continuum. When they are integrated into any given situation, it can be expected to see arbitrary functions or constants appear in the solution. To evaluate these, an additional statement of velocity, temperature fields and their gradients at the natural boundaries of the flow domain are needed. Such statements are known as boundary conditions.

The question of the conditions to be satisfied by a moving fluid in contact with a solid body was one of considerable difficulty for a long time, A short historical note on the conditions at the surface of the contact of a fluid with sold of the body is presented in Goldstein [32]. During the nineteenth century three different hypotheses were put forward by various authors at various times. According to the first, the velocity is the same at a solid wall as that of the solid itself, and changes continuously in the fluid, which has everywhere the same properties. The second was put forward by Girard in the discussion of his experiments on the flow of liquids through tubes. He supposed that a very thin layer of fluid remains completely attached to the walls. Further, Girard assumed that the rest of the fluid slips over it. He also supposed that if the walls are of the same material everywhere, the layer has a constant thickness, so that its surface presents to the current the same irregularities as those of the wall itself. Also, he assumed that the thickness of the layer depends on the curvature of the wall and on the temperature. He took it to be different for different liquids or different materials of the walland to become zero for liquids which do not wet the wall. In such cases he supposed that the liquid slips over the surface, Thirdlyfrom the same molecular hypotheses which led him to the equations of motion of a viscous fluid, Navier deduced that there is slipping at a solid boundary, and this slipping is resisted by a force proportional to the relative velocity. Since the tangential stress on the solid wall at any point is the same

as the stress at a neighbouring internal point of the fluid, this is equivalent to the boundary condition $\beta u = \mu \frac{\partial u}{\partial n}$ for flow in the one direction along a plane wall, where u is the velocity, the differentiation is along the normal away from the wall, and β is a constant, such that $\frac{\mu}{\beta}$ is a length. This length is zero if there is no slip. A brief historical, theoretical and experimental summary by several researchers along with the validations on the three conditions is given by Goldstien (pp 667-680). As it was generally accepted and adopted in the book by Goldstien that the slip, if it takes place, is thin or a quasi solid layer of the fluid, the slip boundary condition at the boundary of the surface is considered in the present thesis.

The different boundary conditions for the velocity (no-slip condition and slip condition), and temperature (uniform temperature, heat flux, and convective conditions) are given below.

No-slip Condition

In no-slip boundary condition, the fluid is in contact with a wall will have the same velocity as the velocity of the wall. Often, the walls are not moving, so as the fluid velocity is zero. In drag flows, the velocity of the wall is finite and the fluid velocity is equal to the wall velocity.

$$\vec{q}_{(\text{at the boundary})} = \vec{q}_{\text{wall}}$$

Slip Condition

Generally accepted boundary condition on the solid surface is no-slip condition. Navier [75] suggested that fluid slips at the solid boundary and slip velocity depends linearly on the shear stress.

$$\overline{q}_{\text{wall}} = \zeta \, \overline{\tau}_{\text{wall}}$$

where ζ is the slip length or slip coefficient. The measure of the slip is called slip length. Factors that affect the slip length include weak wall fluid attraction, surface roughness, and high shear stress. If $\zeta = 0$, then the general assumed no-slip boundary condition is obtained.

Isothemral/Flux conditions

In most usual situations, heat transfer takes place in a fluid moving near a wall heated or cooled at a temperature different from that of the fluid. In this case, the boundary conditions are expressed at the fluid/solid interface. The most usual conditions consist of one of the following simplified assumptions:

1. The fluid/solid interface is at a uniform temperature : $T_{\text{fluid}} = T_{\text{solid}} = \text{constant}$
2. The heat flux is uniform on the interface : $q_w = -K_f\,(n.\nabla T)$.

Convective Boundary Conditions

Recently, a novel mechanism for the heating process has drawn the involvement of many researchers, namely, convective boundary condition (CBC), where the heat is supplied to the convecting fluid through a bounding surface with a finite heat capacity. Further, this results in the heat transfer rate through the surface being proportional to the local difference in temperature with the ambient conditions [65].

$$-K_f\,(n.\nabla T) = h(T_{\text{surface}} - T_\infty)$$

where h is the heat transfer coefficient, T_∞ is the ambient temperature.

1.5 Successive Linearization Method

The Successive Linearisation Method (SLM) is proposed and developed by Makukula *et al.* [59] and Motsa and Sibanda [69]. This method linearizes the governing nonlinear equations. To solve the nonlinear boundary value problem in an unknown function $z(x)$ using SLM, we assume that $z(x)$ is approximated by

$$z(x) = z_r(x) + \sum_{m=0}^{r-1} z_m(x) \tag{1.17}$$

where $z_r(x)$ is an unknown function and $z_0(x)$, $z_1(x) \cdots z_{r-1}(x)$ are known approximate solutions. The unknown function $z_r(x)$ can be determined by solving the linearized differential equation in $z_r(x)$ obtained by substituting (1.17) in the given nonlinear differential equation and linearizing the resulting differential equation using Taylor's series expansion. Hence, the subsequent solutions $z_r(x), r \geq 1$, are obtained by successively solving the linear equations for $z_r(x), r \geq 1$ given that the previous guess $z_{r-1}(x)$ is known. The initial guess $z_0(x)$ is chosen such that it satisfy the given boundary conditions.

Any numerical scheme can used to solve the above iterative sequence of linearized differential equations. The SLM method has been successfully applied to a wide variety of scientific models over finite and semi-infinite intervals. The SLM approximation was applied to boundary value problems which possess smooth solutions.

1.6 Chebyshev Spectral Collocation Method

The Chebyshev spectral collocation method ([12, 21, 112]) is based on the Chebyshev polynomials defined on the interval $[-1, 1]$. To solve a differential equation, in an unknown function $z(x)$, on $[-1, 1]$, first descritize the interval $[-1, 1]$ using the following $N + 1$ Gauss-Lobatto collocation points

$$\xi_j = \cos \frac{\pi j}{N}, \quad j = 0, 1, 2, ..., N \tag{1.18}$$

Next, the unknown function $z(x)$ and its derivatives are approximated at the collocation points as follows

$$z(\xi) = \sum_{k=0}^{N} z(\xi_k) T_k(\xi_j) \quad \frac{d^{\boldsymbol{r}} z}{dx^{\boldsymbol{r}}} = \sum_{k=0}^{N} \left[\frac{2}{(b-a)} \mathbf{D}_{kj} \right]^{\boldsymbol{r}} z(\xi_k), \tag{1.19}$$

where T_k is the k^{th} Chebyshev polynomial defined by $T_k(\xi) = \cos(k \cos^{-1} \xi)$, and $\mathbf{D}$ being

the Chebyshev spectral differentiation matrix whose entries are defined as ([12, 21, 112])

$$\left.\begin{aligned}
&\mathbf{D}_{00} = \tfrac{2N^2+1}{6} \\
&\mathbf{D}_{jk} = \tfrac{c_j}{c_k}\tfrac{(-1)^{j+k}}{\xi_j-\xi_k}, \;\; j \neq k; \;\; j,k = 0,1,2\cdots,N, \\
&\mathbf{D}_{kk} = -\tfrac{\xi_k}{2(1-\xi_k{}^2)}, \;\; k = 1,2\cdots,N-1, \\
&\mathbf{D}_{NN} = -\tfrac{2N^2+1}{6}
\end{aligned}\right\} \tag{1.20}$$

Substituting equations (1.18)-(1.19) into the given differential equation, we get the following system of the algebraic equation

$$\mathbf{A}_{r-1}\mathbf{X}_r = \mathbf{R}_{r-1}, \tag{1.21}$$

in which A_{r-1} is a square matrix of order $(N+1)\times(N+1)$ while X_r and R_{r-1} are $(N+1)^{th}$ order coloumn vectors. Writing the boundary conditions in terms of Chebyshev polynomials, incorporating them in the above system of equations and solving the reduced system of algebraic equations, we obtain the solution of the given differential equation. If the domain is $[a,b]$, then it will be transformed to the domain $[-1,1]$ by using the using suitable transformation.

1.7 Literature Review

The heat and mass transfer in the boundary layer flow on a continuously stretching surface is of considerable importance both from theoretical and practical points of view because of their wider applications to polymer technology and metallurgy. Sakiadis [91] was the first to study the boundary layer behavior on continuously moving solid surface, which is the Blasius type of flow. Griffith [33] studied the boundary layer behavior on moving continuous cylindrical surfaces. In this study, velocity distribution was experimentally measured and the temperature and concentration profiles were theoretically calculated. Erickson [28] investigated the boundary layer behaviour on a moving continuous flat plate with suction by considering the transverse velocity component as nonzero at the surface of the plate. An

extension to this, Crane [18] studied this flow problem, where stretching sheet whose velocity is proportional to the distance from the slit. The flow in this case has certain similarities with tile Hiemenz boundary layer flow near a stagnation point in which the main velocity in the outer flow is proportional to the distance from the stagnation point. Gupta and Gupta [37] considered the flow, heat and mass transfer on a permeable stretching sheet with suction. Vleggaar [116] investigated heat and momentum transfer to continuously accelerating surface and concluded that the cooling of a monofilament proves to be independent of the drawing speed, which compares well with the results obtained in practice. Grubka and Bobba [34] analyzed the effect of power-law surface temperature variation on the heat transfer characteristics of a continuous, linearly stretching surface. Magyari and Keller [56] studied heat and mass transfer analysis of boundary layer flow on exponentially stretching continuous surface. Elbashbeshy [25] extended this work to porous media. Partha *et al.* [78] investigated the mixed convection flow and heat transfer from an exponentially stretching vertical surface in a quiescent fluid. From this study, it is noticed that the velocity boundary layer thickness is increased with the increase of both mixed convection and viscous dissipation parameters. Bidin and Nazar [11] analyzed numerical he effect of thermal radiation on the boundary layer flow over an exponentially stretching sheet. Mukhopadhyay *et al.* [70] investigated the mass transfer over an exponentially stretching sheet embedded in a stratified medium. Heat transfer analysis of water-based nanofluid over an exponentially stretching sheet was studied by Nadeem *et al.* [72]. Lare [52] discussed the Casson fluid flow of variable viscosity and thermal conductivity along exponentially stretching sheet embedded in a thermally stratified medium with exponentially heat generation. Zaib *et al.* [120] reported the micropolar fluid flow over an exponentially stretching sheet. Rehman *et al.* [87] investigated the heat transfer analysis for three-dimensional stagnation-point flow over an exponentially stretching surface.

The study of MHD flow of an electrically conducting fluid over an stretching sheet is of great importance in engineering applications, metallurgical and metal processing. Gupta [35] analyzed the effect of magnetic field on the heat transfer of a viscous electrically conducting fluid from a hot vertical plate. It is witnessed that the effect of the magnetic field is to

decrease the rate of heat transfer from the wall. Sato [93] considered viscous incompressible flow between two parallel plates under the transient electric and magnetic fields. Sparrow and Cess [101] investigated the free convection heat transfer due to the simultaneous action of buoyancy and induced magnetic forces. Singh and Cowling [98] presented the boundary layer flow up a hot vertical plate, in the presence of a uniform horizontal magnetic field normal to the plate. Kameswaran *et al.* [45] investigated the radiation effect on MHD Newtonian fluid over an exponentially stretching sheet. Seini and Makinde [94] investigated the MHD boundary layer flow due to the exponential stretching sheet with thermal radiation and observed that increasing the radiation parameter and the Eckert number increases the thermal boundary layer thickness whilst the reverse is observed for increasing values of the Prandtl number.

In most of the MHD flows reported in the literature, the Hall current term in the Ohm's law was ignored as it has no significant influence for smaller values of the applied magnetic field. However, when the strong magnetic field is utilized the effect of Hall current is very predominant. The study of effects of Hall current on MHD flows has been given much importance due to its widely spread applications in power generators and pumps, Hall accelerators, electric transformers, refrigeration coils, flight MHD, solar physics involved in the sunspot development, the solar cycle, the structure of magnetic stars, cool combustors, electronic system cooling, thermal energy storage, fiber and granular insulation, oil extraction and flow through filtering devices and porous material regenerative heat exchangers. Several investigators have analyzed the Hall currents on the fluid flow problems for different geometries. Katagiri [47] described the numerical investigation of the effects of Hall currents on the steady boundary layer flow of viscous incompressible and electrically fluid past a semi-infinite vertical plate. Pop and Soundalgekar [80] investigated the effect of the uniform transverse magnetic field and the Hall currents on the flow of an incompressible viscous, electrically conducting fluid past an infinite, porous plate. Gupta [36] studied the effects of Hall currents on the flow of an electrically conducting liquid past an infinite porous plate in the presence of a uniform transverse magnetic field with suction. Debnath *et al.* [20] studied the effects of Hall current on the unsteady hydromagnetic rotating fluid flow induced in a

viscous conducting liquid bounded by a porous flat plate with uniform suction or blowing. Pop and Watanabe [81] presented flow problem of free convection along a semi-infinite vertical flat plate taking the account of Hall effect. Eldahad and El-Aziz [26] investigated the effects of Hall and ion-slip currents with internal heat generation past a semi-infinite vertical plate. Megahed *et al.* [62] studied the heat and mass transfer along a semi-infinite vertical flat plate by taking the combined buoyancy force effects and Hall currents into account and observed that the transverse velocity being equal to zero when Hall parameter becomes very large. Abo *et al.* [27] investigated the influence of Hall current on the MHD mixed convective flow and heat transfer along an inclined continuously stretching surface with power-law variation in the surface temperature. Aziz [8] reported the effect of Hall current on the flow and of heat transfer over an unsteady stretching surface. Motsa and Shateyi [95] considered the significance of Hall currents and strong magnetic field on the unsteady flow and heat transfer of an electrically conducting fluid over an stretching surface. Pal [77] investigated the Hall currents effect with radiation over an unsteady stretching surface. Aurang and Sharidan [119] studied the effect of Hall currents with Soret and Dufour effects over an unsteady stretching surface. Zaman *et al.* [121] investigated the effects of Hall current on the flow of unsteady MHD axisymmetric second-grade fluid with suction over an exponentially stretching sheet. Nagalakshmi *et al.* [73] studied the unsteady flow of viscous incompressible fluid past an exponentially stretching sheet with thermal radiation, chemical reaction, and Hall current effects.

The heat transfer problems related to the convective boundary condition is more extensive and it occurs in realistic situations, where heat transfer occurs at the boundary surface to or from a fluid flowing on the surface at a known temperature and a known heat transfer coefficient, e.g. in heat exchangers, condensers, and re-boilers. Merkin [65] considered the natural convection boundary-layer flow on a vertical surface generated by Newtonian heating. Lin *et al.* [53] investigated the influence of viscous dissipation on the thermal entrance region laminar pipe flow heat transfer with convective boundary condition. Hamad *et al.* [38] studied the significance of hydrodynamic slip and thermal convective boundary conditions on the heat and mass transfer over a moving porous plate. Yacob and Ishak [117] discussed

the micropolar fluid flow past stretching or shrinking sheet using convective boundary condition. Rout *et al.* [90] analyzed the magneto-hydrodynamic flow including heat source and chemical reaction over a moving vertical plate under prescribed convective boundary condition. Mustafa *et al.* [71] investigated the flow and heat transfer characteristics over an exponentially stretching sheet in a nanofluid with convective boundary conditions. Rahman *et al.* [83] numerically solved the problem of steady boundary layer flow of a nanofluid past a permeable exponentially shrinking surface with the convective surface condition, using the Buongiornos mathematical nanofluid model. Khan *et al.* [48] studied the boundary layer flow of nanofluid past a bi-directional exponentially stretching sheet with the convective thermal condition. Ahmad and Mustafa [4] investigated the rotating flow of nanofluids induced by an exponentially stretching sheet with convective boundary conditions. Nayak *et al.* [76] reported the numerical simulation for three-dimensional steady flow of nanofluids passing through an exponentially stretching sheet in presence of magnetic field and convective boundary conditions. Reddy *et al.* [86] analyzed theoretically steady two-dimensional MHD flow of a Maxwell fluid over an exponentially stretching surface in the presence of velocity slip and convective boundary condition.

The thermal radiative heat transfer is very important in various propulsion devices for space vehicles, missiles, and aircrafts, manufacturing industries for the design of reliable equipment, nuclear plants and gas turbines. Thermal radiation effects become more important when the difference between the surface and the ambient temperature is large. Thus thermal radiation is one of the vital factors controlling the heat and mass transfer. Hussain *et al.* [43] explained the radiative hydromagnetic flow of Jeffrey nanofluid by an exponentially stretching sheet. Thermal radiation Effects on MHD boundary layer flow over an exponentially stretching surface were analyzed by Chaudhary *et al.* [17]. Further, It is observed that thickness of the velocity boundary layer, the local skin-friction coefficient and the local Nusselt number decreases with increasing value of the magnetic parameter. Remus and Marinca [88] studied the MHD viscous fluid flow over an exponentially porous stretching sheet accompanied by thermal radiation. Loganthan and Vimala [54] investigated the combined effects of MHD, suction, and radiation of a nanofluid over an exponentially stretching sheet

embedded in a thermally stratified medium. Hayat *et al.* [40] reported the unsteady flow caused by an inclined stretching sheet in a viscous nanofluid including stratification process due to both temperature and concentration in presence of thermal radiation.

In recent years, the engineers and researchers are intrigued to build the effectiveness of different mechanical frameworks and industrial machineries. Such sorts of challenges can be taken care of to diminish the temperature created because of Ohmic dissipation. Several researchers explored the impact of Joule heating on fluid flow and heat transfer at different conditions and found that it plays a prominent impact on MHD flows. Yadav and Sharma [118] investigated the effect of Joule heating on the MHD flow over an exponentially moving stretching sheet placed in a porous medium in presence of thermal radiation. Sreenivasulu *et al.* [105] analyzed the Joule heating, viscous dissipation, thermal radiation and magnetic field effects the flow past a permeable exponential stretching surface. Hari and Satya [9] explored the Joule heating effects on MHD mixed convection of a Jeffrey fluid over a stretching sheet with power-law heat flux. Hsiao [42] explored the micropolar nanofluid flow with MHD and viscous dissipation effects towards a stretching sheet with a multimedia feature in presence of Joule heating effects.

The process of transforming the energy taken from the motion of the fluid by the viscosity into internal energy, which is partially irreversible, is referred to as viscous dissipation. It may arise in free convection in several devices which are treated with large deceleration or operate at high rotative speed [30]. El-Aziz [24] discussed the laminar mixed convection flow of micropolar fluid over an exponentially stretching sheet with viscous dissipation effect. Raju *et al.* [85] investigated the influence of thermal radiation and magnetic field effects on the heat and mass transfer behavior of Casson fluid past an exponentially permeable stretching surface in presence of viscous dissipation. Adeniyan and Adigun [3] studied the natural convective MHD flow and heat transfer over an exponentially stretching sheet in an incompressible, electrically conducting fluid in the presence of viscous dissipation with Joule heating. The thermophoresis is a mechanism in which small particles migrate in the direction of decreasing thermal gradient. It is quite significant in radioactive particle deposition in nuclear reactor safety simulations, aerosol particle sampling, deposition of silicon thin films

etc. Goldsmith and May [31] were the first to estimate the thermophoretic velocity in the one-dimensional flow.

The Soret effect (thermal diffusion), the existence of a diffusion flux inview of a temperature gradient, become very noteworthy when the thermal gradient is very large. Whereas the energy flux caused by a concentration gradient is termed as the Dufour effect (diffusion-thermo). Generally, these effects are considered as second-order phenomenon and may become significant in areas such as petrology, hydrology, geosciences, etc. Eckert and Drake [22] recognized many instances when the importance of these effects cannot be neglected. Srinivasacharya and Ramreddy [108] investigated the Soret and Dufour effects on mixed convection flow, heat and mass transfers from an exponentially stretching surface. Sulochana *et al.* [109] investigated the cross-diffusion, viscous dissipation, heat source and chemical reaction effects on the flow of a nanofluid past an exponentially stretching sheet in a porous medium. Sravanthi [104] reported the MHD viscous fluid flow towards an exponentially stretching inclined porous sheet in the presence of Soret and Dufour effects with suction/blowing. are fewer investigators who addressed the importance of these effects on flow, heat, and mass transfer process over an exponentially stretching surface.

In most of the studies reported in the literature, the thermophysical properties of fluid were assumed to be constant. However, it is known that, fluid viscosity and fluid thermal conductivity may change with temperature. Applications include drawing of plastic films, wire drawing, paper production, glass fiber production, the study of spilling pollutant crude oil over the surface of the seawater, cooling of nuclear reactors, food processing, petroleum reservoir operations, casting and welding in manufacturing processes, and gluing of labels on hot bodies etc. In spite of its importance in many applications, this effect has received rather little attention. In recent years, fewer researchers have considered the effect of variable properties on the convective flows over stretching surfaces. Rahman [82] investigated the unsteady flow of incompressible laminar, electrically conducting and non-Newtonian fluid over a non-isothermal stretching sheet with variable viscosity and thermal conductivity in a porous medium. Siddheshwar *et al.* [97] studied the boundary layer flow behavior and heat transfer of a Newtonian fluid past an exponentially stretching sheet in presence of variable

viscosity. Megahed [64] described the flow and heat transfer of Powell-Eyring fluid over an exponentially stretching continuous permeable surface in the presence of heat flux and variable thermal conductivity.

The dispersion is the auxiliary effect of a porous medium on the fluid flow that happens because of mixing and recirculation of local liquid particles through convoluted ways framed by the permeable medium solid particles. There has been restored enthusiasm for concentrate double diffusive convection because of the impact of thermal and solutal dispersion. The thermal and solutal dispersion have applications in geothermal building applications, ceramic processing, sensible heat storage beds and petroleum recovery etc.,

The study of heat and mass transfer with chemical reaction has received considerable attention because of its importance in chemical and hydro-metallurgical industries such as the design of chemical processing equipment, polymer production, the manufacturing of ceramics or glassware etc. There are several chemically reacting systems which involve both homogeneous and heterogeneous reactions. Applications of this process occur in catalysis, biochemical systems, drying processes, combustion processes, metallurgical flows, cooling towers, etc. Generally, the interaction between the homogeneous reaction in the bulk of the fluid and heterogeneous reactions occurring on some catalytic surfaces is very complex and is involved in the production and consumption of reactant species at different rates both within the fluid and on the catalytic surfaces. Chaudhary and Merkin [14, 15] presented a model for homogeneous-heterogeneous reaction on uniform stream flow over a surface in which the heterogeneous reaction takes place by the first-order process and the homogeneous reaction by cubic autocatalysis method for equal and unequal diffusivities, respectively. Bachok *et al.* [10] investigated the effects of homogeneous and heterogeneous reactions on the steady boundary layer flow near the stagnation point on a stretching surface. Kameswaran *et al.* [46] analyzed the effects of homogeneous-heterogeneous reactions in nanofluid flow over a stretching or shrinking sheet placed in a porous medium saturated with a nanofluid. Abbas *et al.* [1] presented the effect of homogeneous and heterogeneous reactions on an electrically conducting viscous fluid near the stagnation-point past a permeable stretching or shrinking sheet. Masur *et al.* [61] reported the MHD homogeneous-heterogeneous reaction in a

nanofluid flow due to a permeable shrinking surface.

Suction or injection (blowing) of a fluid through the bounding surface can significantly change the flow field. Injection or withdrawal of fluid through a porous bounding wall is of general interest in practical problems such as film cooling, polymer fiber coating, coating of wires, etc. The process of suction and blowing has also its importance in many engineering activities such as in the design of thrust bearing and radial diffusers and thermal oil recovery. Suction is applied to chemical processes to remove reactants. Blowing is used to add reactants, cool the surface, prevent corrosion or scaling and reduce the drag.

1.8 Aim and Scope

The aim of the present thesis is to study the flow, heat and mass transfer due to steady, laminar incompressible viscous fluid over an exponentially stretching permeable sheet. The influence of suction/injection, velocity slip, Hall parameter, magnetic parameter, Richardson number (mixed convection parameter), Biot number, thermal radiation parameter, chemical reaction parameter, Joule heating parameter, Soret number, Dufour number, temperature dependent viscosity and thermal conductivity parameters, heat source/sink, viscous dissipation, thermophoresis, thermal and solutal dispersion parameters, porosity parameter, the strengths homogeneous and heterogeneous reaction rates on the flow characteristics such as the velocity, temperature, concentration, heat transfer rate and mass transfer rate are analyzed numerically. The problems considered deal with semi-infinite exponentially stretching sheet geometry for the two cases: when the sheet is (i) subjected to thermal convective boundary condition and (ii) maintained at uniform wall temperature with Hall effect.

1.9 Overview of the Thesis

This thesis is arranged into 9 chapters.

Chapter - 1 provides an introduction to the theory of viscous fluids, definitions of various

terms along with the equations of motion and magnetohydrodynamic (MHD) flows. A survey of related literature has been presented. Finally, brief introductions about the problems that we consider in the subsequent chapters are presented.

Chapter-2 analyzes the flow, heat and mass transports due to viscous fluid flow through a porous exponentially stretching sheet in the presence of thermal radiation and chemical reaction effects. The effects of magnetic, Hall parameter, chemical reaction, thermal radiation parameter, suction/injection parameter, Richardson number (mixed convection parameter) and Biot number on the non-dimensional velocities, temperature, concentration, heat, and mass transfer rates are discussed through graphs. The local skin-friction in $\tilde{x}$ and $\tilde{z}$-directions are presented in a tabular form for different values of velocity slip, magnetic, Hall parameter, Richardson number, chemical reaction and thermal radiation parameters.

In chapter-3, the heat and mass transfer for steady incompressible viscous fluid flow over a permeable exponentially stretching sheet is investigated in presence of Joule heating effect. The effects of magnetic, Hall parameter, suction/injection parameter, Richardson number (mixed convection parameter) and Biot number on the non-dimensional velocities, temperature, concentration are presented through graphs. The variation of heat and mass transfer rates in presence of Joule heating parameter, magnetic, Hall parameter, slip parameter, suction/injection parameter, Richardson number (mixed convection parameter) and Biot number are presented through graphs. Local skin-friction in $\tilde{x}$ and $\tilde{z}$-directions are presented in tabular form for diverse values of suction/injection, velocity slip, magnetic, Hall parameter, Joule heating parameter and mixed convection parameter.

Chapter-4 deals with the influence of Soret and Dufour effects due to steady, laminar slip flow of viscous incompressible fluid over an exponentially stretching sheet. The variation of non-dimensional velocities, temperature, concentration, heat, and mass transfer rates are presented through graphs for the physical parameters Tabular values for the skin-friction for various values of velocity slip, magnetic, Hall, mixed convection parameters, Soret and Dufour number, is displayed. It is seen that minor changes in Dufour and Soret numbers caused the major variations in the profiles.

Chapter-5 describes the impact of variable fluid properties on a steady, laminar incompressible and electrically conducting boundary layer flow of viscous fluid past an exponentially stretching sheet. The influence of variable viscosity parameter and thermal conductivity parameters, magnetic, Hall parameter, Biot number and heat source parameter on non-dimensional velocities, temperature, and concentration, local skin-friction, heat and mass rates are calculated and discussed quantitatively.

Chapter-6 presents the viscous fluid flow past a sheet, stretching exponentially, under the influence of thermophoresis and viscous dissipation effects. The non-dimensional velocities, temperature, and concentration profiles are obtained for various values of thermophoresis, magnetic, Hall parameter, slip parameter, suction/injection parameter, Richardson number, Eckert number and Biot number. The rate of local heat and mass transfers are presented graphically and discussed quantitatively for various values of the fixed parameters. The influence of thermophoresis parameter, Eckert number, velocity slip, magnetic, Hall parameter and Richardson number on local skin-friction in both directions is presented in a tabular form. The numerical results are compared and are found to be in good agreement with previously published results as special cases of the present investigation.

The objective of Chapter-7 is to describe the double dispersion on the laminar flow over an exponentially stretching porous surface in an incompressible electrically conducting viscous fluid with velocity at the boundary of the stretching surface. The influence of thermal and solutal dispersion parameters, velocity slip, thermal radiation parameter, magnetic and Hall parameters on non-dimensional velocities, temperature, concentration, the rate of heat and mass transfers is shown through graphs. Tabular values for the skin-friction for the various values of velocity slip, Hall parameter, thermal radiation, mixed convection, thermal and solutal dispersion parameters are displayed. The obtained results are compared with the previously published results for special cases.

The objective of Chapter-8 is to analyze the influence of homogeneous-heterogeneous reactions on the laminar slip flow of electrically conducting viscous fluid over an exponentially stretching porous surface. The variation of non-dimensional velocities, temperature and the rate of heat transfer for various values of magnetic, Hall parameter, thermal radia-

tion, mixed convection and suction/injection parameters is analyzed. Influence of strength of homogeneous-heterogeneous reactions together with all parameter, thermal radiation, mixed convection and suction/injection parameters on the variation of non-dimensional concentration and the rate of mass transfer of the fluid is analyzed and presented through graphs. The obtained results are compared with the previously published results for special cases. Tabular values for the skin-friction for the different values of velocity slip, Hall parameter, thermal radiation parameter, Richardson number, the strength of homogeneous-heterogeneous reaction is displayed. It is observed that both the skin-friction are not affected by the strength of heterogeneous-homogeneous reactions.

The main observation of the earlier chapters are summarized and the scope for further investigations are recorded in the final chapter (Chapter 9).

Considerable part of the work in the thesis is published/accepted for publication in journals. The remaining part is communicated for publications. The details are presented below.

List of papers published

1. "Slip viscous flow over an exponentially stretching porous sheet with thermal convective boundary conditions", *International Journal of Applied and Computational Mathematics*, Vol. 3(4) (2017), pp.3525–3537.

2. "Cross-diffusion effects on an exponentially stretching sheet in a doubly stratified viscous fluid", *Engineering Science and Technology, an International Journal*, Vol. 20 (2017), pp.1571–1578.

3. "MHD flow with Hall current and Joule heating effects over an exponentially stretching sheet", *Nonlinear Engineering - Modeling and Application*, Vol. 6(2) (2017), pp.101–114.

4. "Flow over an exponentially stretching sheet with Hall, thermal radiation, and chemical reaction effects", *Frontiers in Heat and Mass Transfer*, Vol. 9(37) (2017), pp.1–10.

5. "Flow over an exponentially stretching porous sheet with cross-diffusion effects and convective thermal conditions", *International Journal of Engineering (IJE), IJE TRANSACTIONS A*, Vol. 31(1) (2018), pp.120–127.

6. "Effect of variable viscosity, thermal conductivity and Hall currents on the flow over an exponentially stretching sheet with heat generation/absorption", *International Journal of Energy for a Clean Environment*, Vol. 19(1-2) (2018), pp.67–83.

7. "Effect of double stratification, cross-diffusion and Hall currents on the flow over an exponentially stretching sheet", *Journal of Nanofluids*, Vol. 7(5) (2018), pp. 961–973.

8. "Effect of variable properties on the flow over an exponentially stretching sheet with convective thermal conditions", *Modelling, Measurement and Control B*, Vol. 87(1) (2018), pp. 7–14.

List of papers accepted

9. "Effect of chemical reaction and thermal radiation on the flow over an exponentially stretching sheet with convective thermal conditions", *Lecture Notes in Mechanical Engineering*, (2018).

List of papers communicated

10. "Flow over an exponentially stretching sheet with Hall and cross-diffusion effects", Communicated to *Propulsion and Power Research*.

11. "Viscous flow over an exponentially stretching sheet with Hall, thermophoresis and viscous dissipation effects", Communicated to *Journal of the Association of Arab Universities for Basic and Applied Sciences*.

12. "Effect of Joule heating on the flow over an exponentially stretching sheet with convective thermal conditions", Communicated to *Mathematical Sciences*.

13. "Effect of viscous dissipation and thermophoresis on the flow over an exponentially stretching sheet", Communicated to *International Journal of Applied Mechanics and Engineering*.

14. "Effect of double dispersion and Hall currents on the flow over an exponentially stretching sheet", Communicated to *Journal of Molecular Liquids*.

15. "Flow over an exponentially stretching sheet with double dispersion and convective thermal conditions", Communicated to *International Journal of Engineering Science*.

16. "Homogeneous-heterogeneous reactions on the flow over an exponentially stretching sheet with Hall current", Communicated to *International Journal of Chemical Reactor Engineering*.

17. "Homogeneous-heterogeneous reactions on the viscous Flow on an exponentially stretching sheet with the convective thermal condition", Communicated to *Nonlinear Engineering - Modeling and Application*.

Chapter 2

Flow over an exponentially stretching sheet with thermal radiation and chemical reaction [1]

2.1 Introduction

The effect of thermal radiation on convective flows have applications in physics and engineering such as space technology, solar power technology, propulsion devices for aircraft and other industrial areas [115, 5, 25, 70, 88]. Animasaun *et al.* [6] investigated the motion of temperature dependent viscosity and thermal conductivity of steady incompressible laminar free convective MHD Casson fluid flow over an exponentially stretching surface with thermal radiation and exponentially decaying internal heat generation. Mabood *et al.* [55] investigated the MHD boundary layer flow of a viscous incompressible fluid over an exponentially stretching sheet including the effect of thermal radiation in the energy equation. On the other hand, the study of heat and mass transfer with chemical reaction has received considerable attention because of its importance in chemical and hydro-metallurgical industries

[1] Case(a):Accepted for publication in "**Lecture Notes in Mechanical Engineering**", Case(b):Published in "**Frontiers in Heat and Mass Transfer**" (2018) 9(37) (2017) 1–10

such as design of chemical processing equipment, polymer production, the manufacturing of ceramics or glassware etc. Eid [23] investigated the heat generation/absorption effects on the mixed convective flow of a nanofluid through a porous medium due to an exponentially stretching sheet in the presence of chemical reaction and magnetic field.

In this chapter, we investigate the influence of thermal radiation and chemical reaction on the viscous fluid flow over an exponentially stretching sheet. We consider two different physical conditions on the sheet i.e. when the sheet is (i) subjected to thermal convective boundary condition and (ii) maintained at uniform wall temperature with Hall effect. The influence of important parameters, namely, velocity slip, suction/injection, Hall parameter, and convective heat transfer parameter(Biot number) on the physical quantities of the flow, heat, and mass transfer rates are analyzed.

2.2 Formulation of the Problem

Consider a steady, two-dimensional, laminar slip flow of electrically conducting viscous incompressible fluid towards an exponentially stretching sheet. The ambient temperature and concentration of the fluid are T_∞ and C_∞, respectively. The Cartesian coordinate framework is considered by taking the positive $\tilde{x}-$axis along the sheet and $\tilde{y}-$axis orthogonal to the sheet so that the fluid occupies the space $\tilde{y} > 0$ (as shown in the Fig. (2.1)). The stretching velocity of the sheet is assumed as $U_*(\tilde{x}) = U_0\ e^{\frac{\tilde{x}}{L}}$ where $\tilde{x}$ is the distance from the slit and L is the reference length or scaling parameter. The suction/injection velocity of the fluid through the sheet is $V_*(\tilde{x}) = V_0\ e^{\frac{\tilde{x}}{2L}}$, where V_0 is the strength of suction/injection. Further, the slip velocity of the fluid is assumed as $N_*(\tilde{x}) = N_0\ e^{\frac{-\tilde{x}}{2L}}$, where N_0 is the velocity slip factor. The fluid is considered as non-scattering medium, to be gray and absorbing/emitting radiation. The radiative heat flux in the energy equation is described by the Rosseland approximation [102]. Also, it is assumed that there exists a homogenous chemical reaction of the first order with rate constant $k_1 = k_0 e^{\frac{\tilde{x}}{L}}$, where k_0 is constant, between the diffusing species and the fluid. With these assumptions, the equations governing the flow are given by

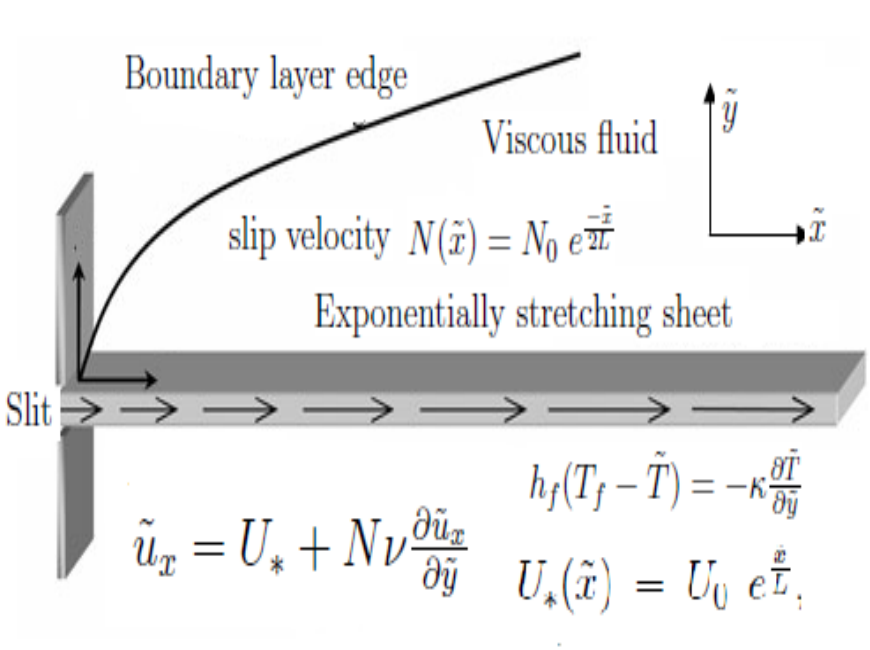

Figure 2.1: Schematic diagram with coordinate system

$$\frac{\partial \tilde{u}_x}{\partial \tilde{x}} + \frac{\partial \tilde{u}_y}{\partial \tilde{y}} = 0 \tag{2.1}$$

$$\tilde{u}_x \frac{\partial \tilde{u}_x}{\partial \tilde{x}} + \tilde{u}_y \frac{\partial \tilde{u}_x}{\partial \tilde{y}} = \nu \frac{\partial^2 \tilde{u}_x}{\partial \tilde{y}^2} \tag{2.2}$$

$$\tilde{u}_x \frac{\partial \tilde{T}}{\partial \tilde{x}} + \tilde{u}_y \frac{\partial \tilde{T}}{\partial \tilde{y}} = \alpha \frac{\partial^2 \tilde{T}}{\partial \tilde{y}^2} + \frac{16 T_\infty^3 \sigma^*}{3k^* \rho c_p} \frac{\partial^2 \tilde{T}}{\partial \tilde{y}^2} \tag{2.3}$$

$$\tilde{u}_x \frac{\partial \tilde{C}}{\partial \tilde{x}} + \tilde{u}_y \frac{\partial \tilde{C}}{\partial \tilde{y}} = D \frac{\partial^2 \tilde{C}}{\partial \tilde{y}^2} - k_1(\tilde{C} - C_\infty) \tag{2.4}$$

where $(\tilde{u}_x, \tilde{u}_y)$ is the velocity vector, $\tilde{C}$ is the concentration, $\tilde{T}$ is the temperature. D is the mass diffusivity, α is the thermal diffusivity, ρ is density, ν is the kinematic viscosity of the fluid, σ^* is the Stefan-Boltzmann constant, k^* is the mean absorption coefficient and c_p is specific heat capacity at the constant pressure.

In this chapter, two types (cases) of problems are considered. In first problem i.e. case (a), the sheet is subjected to convective thermal condition. In the second problem i.e. case (b), the sheet maintained at uniform wall temperature with Hall effect.

2.2.1 Case(a): Convective Thermal Condition

Assume that the sheet is either cooled or heated convectively through a fluid with temperature T_f and which induces a heat transfer coefficient h_f, where $h_f = h\sqrt{\frac{U_0}{2L}}e^{\frac{\tilde{x}}{2L}}$.

Hence, the conditions on the surface of the sheet are

$$\left.\begin{array}{l} \tilde{u}_x = U_* + N_*\nu\frac{\partial\tilde{u}_x}{\partial\tilde{y}},\ \tilde{u}_y = -V_*(\tilde{x}),\ h_f(T_f - \tilde{T}) = -\kappa\frac{\partial\tilde{T}}{\partial\tilde{y}},\ \tilde{C} = C_w \quad \text{at} \quad \tilde{y} = 0 \\ \tilde{u}_x \to 0,\ \tilde{T} \to T_\infty,\ \tilde{C} \to C_\infty \ \text{ as } \quad \tilde{y} \to \infty \end{array}\right\} \tag{2.5}$$

Introducing the stream functions through $\tilde{u}_x = -\frac{\partial\psi}{\partial\tilde{y}}$ and $\tilde{u}_y = \frac{\partial\psi}{\partial\tilde{x}}$ and then the following dimensionless variables

$$\left.\begin{array}{l} y = \tilde{y}\sqrt{\frac{U_0}{2\nu L}}e^{\frac{\tilde{x}}{2L}}, \quad \psi = \sqrt{2\nu L U_0}e^{\frac{\tilde{x}}{2L}}F(x,y), \\ \tilde{T} = T_\infty + (T_f - T_\infty)T(x,y), \quad \tilde{C} = C_\infty + (C_w - C_\infty)C(x,y) \end{array}\right\} \tag{2.6}$$

into Eqs. (2.1) - (2.4), we obtain

$$F''' + FF'' - 2F'^2 = 0 \tag{2.7}$$

$$\frac{1}{Pr}\left(1 + \frac{4R}{3}\right)T'' + FT' = 0 \tag{2.8}$$

$$\frac{1}{Sc}C'' + FC' - \gamma\, C = 0 \tag{2.9}$$

The conditions at the boundary reduces to

$$\left.\begin{array}{l} F(0) = S, \quad F'(0) = 1 + \lambda F''(0), \quad T'(0) = -Bi(1 - T(0)), \quad C(0) = 1 \ \text{ at } \quad y = 0 \\ F'(\infty) \to 0, \quad T(\infty) \to 0, \quad C(\infty) \to 0 \ \text{ as } \quad y \to \infty \end{array}\right\} \tag{2.10}$$

where $Bi = \frac{h}{\kappa}\sqrt{\nu}$ is the Biot number, $\gamma = \frac{2Lk_0}{U_0}$ is the chemical reaction parameter, $S = V_0\sqrt{\frac{2L}{\nu U_0}}$ is the suction($S > 0$) or injection($S < 0$) parameter, $Sc = \frac{\nu}{D}$ is the Schmidt number, $R = \frac{4\ \sigma^*\ T_\infty^3}{\kappa\ \kappa^*}$ is the radiation parameter, $\lambda = N_0\sqrt{\nu U_0/2L}$ is the velocity slip parameter, $Pr = \frac{\nu}{\alpha}$ is the Prandtl number and the prime denotes derivative with respect to y.

2.2.2 Skin Friction, Heat and Mass Transfer Coefficients

The wall shear stress is

$$\tau_\omega = \mu \left[\frac{\partial \tilde{u}_x}{\partial \tilde{y}}\right]_{\tilde{y}=0} \tag{2.11}$$

and the heat and mass transfers from the sheet respectively are given by

$$q_w = -\kappa \left[\frac{\partial \tilde{T}}{\partial \tilde{y}}\right]_{\tilde{y}=0} - \frac{4\sigma^*}{3k^*}\left[\frac{\partial \tilde{T}^4}{\partial \tilde{y}}\right]_{y=0} \quad \text{and} \quad q_m = -D\left[\frac{\partial \tilde{C}}{\partial \tilde{y}}\right]_{\tilde{y}=0} \tag{2.12a}$$

The non-dimensional skin friction $C_f = \dfrac{2\tau_\omega}{\rho U_*^2}$, the local Nusselt number $Nu_{\tilde{x}} = \dfrac{\tilde{x}q_w}{\kappa(T_f - T_\infty)}$ and the local Sherwood number $Sh_{\tilde{x}} = \dfrac{\tilde{x}q_m}{\kappa(C_w - C_\infty)}$, are given by

$$\left.\begin{aligned} \frac{\sqrt{Re_{\tilde{x}}}\ C_f}{\sqrt{2\tilde{x}/L}} = F''(0),\ \frac{Nu_{\tilde{x}}}{\sqrt{\tilde{x}/2L}\sqrt{Re_{\tilde{x}}}} = -\left(1+\frac{4R}{3}\right)T'(0),\ \text{and}\ \frac{Sh_{\tilde{x}}}{\sqrt{\tilde{x}/2L}\sqrt{Re_{\tilde{x}}}} = -C'(0) \end{aligned}\right\} \tag{2.13}$$

where $Re_{\tilde{x}} = \dfrac{\tilde{x}U_*(\tilde{x})}{\nu}$ is the local Reynold's number.

2.2.3 Solution of the Problem

The system of Eqs. (2.7) - (2.9) along with the boundary conditions (2.10) is solved numerically using the successive linearisation method (SLM) ([68], [60]). Using this method the non-linear governing equations reduce to a system of linear differential equations.

In this method, we assume that the independent vector $\mathbf{\Omega}(y) = [F(y), T(y), C(y)]$ can be expressed as

$$\mathbf{\Omega}(y) = \mathbf{\Omega}_r(y) + \sum_{n=0}^{r-1} \mathbf{\Omega}_n(y) \tag{2.14}$$

where $\mathbf{\Omega}_r(y)$, $(r = 1, 2, 3, ...)$ are unknown functions and $\mathbf{\Omega}_n(y)$ are the approximations which are obtained by recursively solving the linear part of the system of equations that

results from substituting (2.14) in (2.7) - (2.9).

The initial approximation $\mathbf{\Omega}_0(y)$ is chosen such that they satisfy the boundary conditions (2.10). Therefore $\mathbf{\Omega}_0(y) = \left(S + \frac{1}{1+\lambda} - \frac{1}{1+\lambda}e^{-y}, \quad \frac{Bi}{1+Bi}e^{-y}, \quad e^{-y}\right)$. The subsequent solutions F_r, T_r, C_r, $r \geq 1$ are obtained by successively solving the following linearized form of the equations which are obtained by substituting Eq. (2.14) in the governing equations (2.7) - (2.9).

$$F_r''' + \chi_{11,r-1}F_r'' + \chi_{12,r-1}F_r' + \chi_{13,r-1}F_r = \zeta_{1,r-1} \tag{2.15}$$

$$\chi_{21,r-1}F_r + \frac{1}{Pr}\left(1 + \frac{4R}{3}\right)T_r'' + \chi_{22,r-1}T_r' = \zeta_{2,r-1} \tag{2.16}$$

$$\chi_{31,r-1}F_r + \frac{1}{Sc}C_r'' + \chi_{32,r-1}C_r' - \gamma C_r = \zeta_{3,r-1} \tag{2.17}$$

where

$$\chi_{11,r-1} = \sum_{n=0}^{r-1} F_n, \;\; \chi_{12,r-1} = -4\sum_{n=0}^{r-1} F_n', \;\; \chi_{13,r-1} = \sum_{n=0}^{r-1} F_n'',$$
$$\chi_{21,r-1} = \sum_{n=0}^{r-1} T_n', \;\; \chi_{22,r-1} = \sum_{n=0}^{r-1} F_n, \;\; \chi_{31,r-1} = \sum_{n=0}^{r-1} C_n', \;\; \chi_{32,r-1} = \sum_{n=0}^{r-1} F_n,$$
$$\zeta_{1,r-1} = -\sum_{n=0}^{r-1} F_n''' - \sum_{n=0}^{r-1} F_n \sum_{n=0}^{r-1} F_n'' + 2\left(\sum_{n=0}^{r-1} F_n'\right)^2,$$
$$\zeta_{2,r-1} = -\frac{1}{Pr}\left(1 + \frac{4R}{3}\right)\sum_{n=0}^{r-1} T_n'' - \sum_{n=0}^{r-1} F_n \sum_{n=0}^{r-1} T_n',$$
$$\zeta_{3,r-1} = -\frac{1}{Sc}\sum_{n=0}^{r-1} C_n'' - \sum_{n=0}^{r-1} F_n \sum_{n=0}^{r-1} C_n' + \gamma \sum_{n=0}^{r-1} C_n$$

The boundary conditions reduce to

$$F_r(0) = \lambda F_r''(0) - F_r'(0) = F_r'(\infty) = T_r'(0) - BiT_r(0) = T_r(\infty) = C_r(0) = C_r(\infty) = 0 \tag{2.18}$$

The approximate solution for $\mathbf{\Omega}(y)$ is then obtained as

$$\mathbf{\Omega}(y) \approx \sum_{m=0}^{M} \mathbf{\Omega}_m(y) \tag{2.19}$$

where M is the order of SLM approximation.

Eqs. (2.15) - (2.17) are solved using the Chebyshev spectral collocation method [12]. To solve the problem by this method, first, the interval $[0, \infty)$ is replaced by the interval $[0, L]$, where L is a scaling parameter used to invoke the boundary condition at infinity. Again, the interval $[0, L]$ is transformed into the region [-1, 1] by

$$\frac{y}{L} = \frac{\xi + 1}{2}, \quad -1 \leq \xi \leq 1 \tag{2.20}$$

The unknown functions are approximated by the Chebyshev interpolating polynomials in such a way that they are collocated at the Gauss-Lobatto points defined as in Eq. (1.18). The function $\mathbf{\Omega}(y)$ is approximated at the Gauss-Lobatto points defined as in Eq. (1.18) i.e.,

$$\mathbf{\Omega}_r(\xi) = \sum_{k=0}^{N} \mathbf{\Omega}_r(\xi_k) T_k(\xi_j), \quad j = 0, 1, 2, ..., N \tag{2.21}$$

where T_k is the k^{th} Chebyshev polynomial.

The $\boldsymbol{r}^{th}$ order derivative in terms of Chebyshev spectral differentiation matrix $\mathscr{D}$ (defined in Eq. (1.19)) is given by

$$\frac{d^{\boldsymbol{r}}}{dy^{\boldsymbol{r}}} \mathbf{\Omega}_r(\xi) = \left(\frac{2}{L}\right)^{\boldsymbol{r}} \sum_{k=0}^{N} \mathscr{D}_{kj}^{\boldsymbol{r}} \mathbf{\Omega}_r(\xi_k), \quad j = 0, 1, 2, ..., N. \tag{2.22}$$

Substituting Eqs. (2.20) - (2.22) into Eqs. (2.15) - (2.17) leads to the following matrix equation

$$\mathbf{A}_{r-1} \mathbf{X}_r = \mathbf{R}_{r-1}, \tag{2.23}$$

subject to the boundary conditions

$$F_r(\xi_N) = \sum_{k=0}^{N} \mathbf{D}_{0k} F_r(\xi_k) = \sum_{k=0}^{N} (\lambda \mathbf{D}2_{Nk} - \mathbf{D}_{Nk}) F_r(\xi_k) = 0 \tag{2.24a}$$

$$\sum_{k=0}^{N} \mathbf{D}_{Nk} T_r(\xi_k) - Bi\ T_r(\xi_N) = T_r(\xi_0) = C_r(\xi_N) = C_r(\xi_0) = 0 \tag{2.24b}$$

In Eq.(2.23), $\mathbf{A}_{r-1}$ is a (3N + 3)×(3N + 3) square matrix and $\mathbf{X}_r$ and $\mathbf{R}_{r-1}$ are (3N + 3)×1

column vectors defined by

$$\mathbf{A}_{r-1} = \begin{bmatrix} A_{11} & A_{12} & A_{13} \\ A_{21} & A_{22} & A_{23} \\ A_{31} & A_{32} & A_{33} \end{bmatrix}, \quad \mathbf{X}_r = \begin{bmatrix} \mathbf{F}_r \\ \mathbf{\Theta}_r \\ \mathbf{\Phi}_r \end{bmatrix}, \quad \mathbf{R}_{r-1} = \begin{bmatrix} \mathbf{E}_{1,r-1} \\ \mathbf{E}_{2,r-1} \\ \mathbf{E}_{3,r-1} \end{bmatrix} \tag{2.25}$$

where

$$\begin{aligned}
&\mathbf{F}_r = [F_i(\xi_0), F_r(\xi_1), F_r(\xi_2), ..., F_r(\xi_{N-1}), F_r(\xi_N)]^T, \\
&\mathbf{\Theta}_r = [T_r(\xi_0), T_r(\xi_1), T_r(\xi_2), ..., T_r(\xi_{N-1}), T_r(\xi_N)]^T, \\
&\mathbf{\Phi}_r = [C_r(\xi_0), C_r(\xi_1), C_r(\xi_2), ..., C_r(\xi_{N-1}), C_r(\xi_N)]^T, \\
&\mathbf{E}_{1,r-1} = [\zeta_{1,r-1}(\xi_0), \zeta_{1,r-1}(\xi_1), \zeta_{1,r-1}(\xi_2), ..., \zeta_{1,r-1}(\xi_{N-1}), \zeta_{1,r-1}(\xi_N)]^T \\
&\mathbf{E}_{2,r-1} = [\zeta_{2,r-1}(\xi_0), \zeta_{2,r-1}(\xi_1), \zeta_{2,r-1}(\xi_2), ..., \zeta_{2,r-1}(\xi_{N-1}), \zeta_{2,r-1}(\xi_N)]^T \\
&\mathbf{E}_{3,r-1} = [\zeta_{3,r-1}(\xi_0), \zeta_{3,r-1}(\xi_1), \zeta_{3,r-1}(\xi_2), ..., \zeta_{3,r-1}(\xi_{N-1}), \zeta_{3,r-1}(\xi_N)]^T \\
&A_{11} = \mathbf{D}^3 + \chi_{11,r-1}\mathbf{D}^2 + \chi_{12,r-1}\mathbf{D} + \chi_{13,r-1}, \quad A_{12} = \mathbf{0}, \quad A_{13} = \mathbf{0}, \\
&A_{21} = \chi_{21,r-1}, \quad A_{22} = \tfrac{1}{Pr}\left(1 + \tfrac{4R}{3}\right)\mathbf{D}^2 + \chi_{22,r-1}\mathbf{D}, \quad A_{23} = \mathbf{0}, \\
&A_{31} = \chi_{31,r-1}, \quad A_{32} = \mathbf{0}, \quad A_{33} = \tfrac{1}{Sc}\mathbf{D}^2 + \chi_{32,r-1}\mathbf{D} - \gamma\mathbf{I}
\end{aligned}$$

Here $\mathbf{I}$ is an identity matrix of size (N +1)×(N +1). After modifying the matrix system (2.23) to incorporate boundary conditions (2.24), the solution is obtained as

$$\mathbf{X}_r = \mathbf{A}_{r-1}^{-1}\mathbf{R}_{r-1} \tag{2.26}$$

2.2.4 Result and Discussion

In order to validate the code generated, the results of the present problem have been compared with works of Magyari and Keller [56] as a special case by taking $S = 0$, $R = 0$, $\gamma = 0$, $\lambda = 0$, and $Bi \to \infty$ and found that they are in good agreement, as shown in Table. (2.1). The range of the parameters were chosen arbitrarily in order to study the impact of them on the physical quantities as $S = 0.5$, $\gamma = 0.5$, $\lambda = 1.0$, $R = 0.5$, and $Bi = 1.0$ unless otherwise mentioned.

Convergence of the method to the numerical results is achieved at the 20^{th} order of SLM

Table 2.1: *Comparative analysis for* $\frac{Nu_{\tilde{x}}}{\sqrt{\tilde{x}/2L}\sqrt{Re_{\tilde{x}}}}$ *by the current method for* $\lambda = 0$, $R = 0$, $\gamma = 0$, $S = 0$ *and* $Bi \to \infty$.

Nusselt number $\frac{Nu_{\tilde{x}}}{\sqrt{\tilde{x}/2L}\sqrt{Re_{\tilde{x}}}}$		
Pr	Magyari and Keller [56]	Present
0.5	0.330493	0.33053741
1	0.549643	0.54964317
3	1.122188	1.12208592
5	1.521243	1.52123757
8	1.991847	1.99183597
10	2.257429	2.25742182

approximation.

The influence of slip and suction/injection parameters on the fluid velocity is portrayed in the Figs. (2.2(a)) - (2.2(b)). It is evident from the Figs. 2.2(a) and (2.2(b)) that the rise in the slipperiness and the fluid suction diminish the velocity while the injection enhances the velocity. On the other hand, the skin-friction is enhancing with the slipperiness and reducing with the suction of the fluid as depicted in the Fig. (2.3).

The variation of the temperature distribution with λ, S, R and Bi is plotted through the Figs. (2.4(a)) - (2.4(d)). It is evident from the Fig. (2.4(a)) that the temperature is enhancing with the rise in the slipperiness. It is well known that wall suction reduces the thickness of thermal boundary layer and hence, reduction in temperature. This phenomenon is graphically presented in the Fig. (2.4(b)). However, the wall injection produces an exactly opposite nature. Figure (2.4(c)) illustrates that the temperature is enhancing with the rise in the value of thermal radiation and hence gain in thickness of thermal boundary. The variation of the temperature with Bi is presented in the Fig. (2.4(d)). A rise in the Biot number enhances the temperature. Further, for large large value of Biot number, the convective thermal condition from (2.10) transforms to $T(0) \to 1$, which signifies the constant wall condition. i.e., stronger convection leads to the higher surface temperatures which appreciably increases the temperature.

The influence of λ, S and γ on the concentration is shown graphically in Figs. (2.5(a))

- (2.5(c)). It is clear from the Fig. (2.5(a)) that an increase in the slipperiness rises the concentration. While, the wall injection is enhancing the fluid concentration as shown in the Fig. (2.5(b)). It is noticed from the fig. (2.5(c)) that the concentration of the fluid is increasing for the constructive reaction ($\gamma < 0$) and reducing for the destructive reaction ($\gamma > 0$).

The variations of the rate of heat transfer with S for diverse values of R, Bi and λ is portrayed through the Figs. (2.6(a)) - (2.6(c)). The rate of heat transfer is enhancing with the rise in the radiation parameter as shown in the Fig. (2.6(a)). Figure (2.6(b)) demonstrates that the rate of heat transfer is enhancing with the increase in the value of Bi. Figure (2.6(c)) shows that an increase in λ diminishes the rate of heat transfer. Further, it is noticed from these figures that the fluid suction enhances the rate of heat transfer.

The variation of the rate of mass transfer with S for different values of λ and γ is shown in the Figs. (2.7(a)) and (2.7(b)). It is observed from the Fig. (2.7(a)) that an increase in the slipperiness reduces the rate of mass transfer. On the other hand, an increase in the magnitude of chemical reaction parameter (positive values of γ) enhances the rate of mass transfer as shown in the Fig. (2.7(b)). Further, the rate of mass transfer is increasing with the fluid suction.

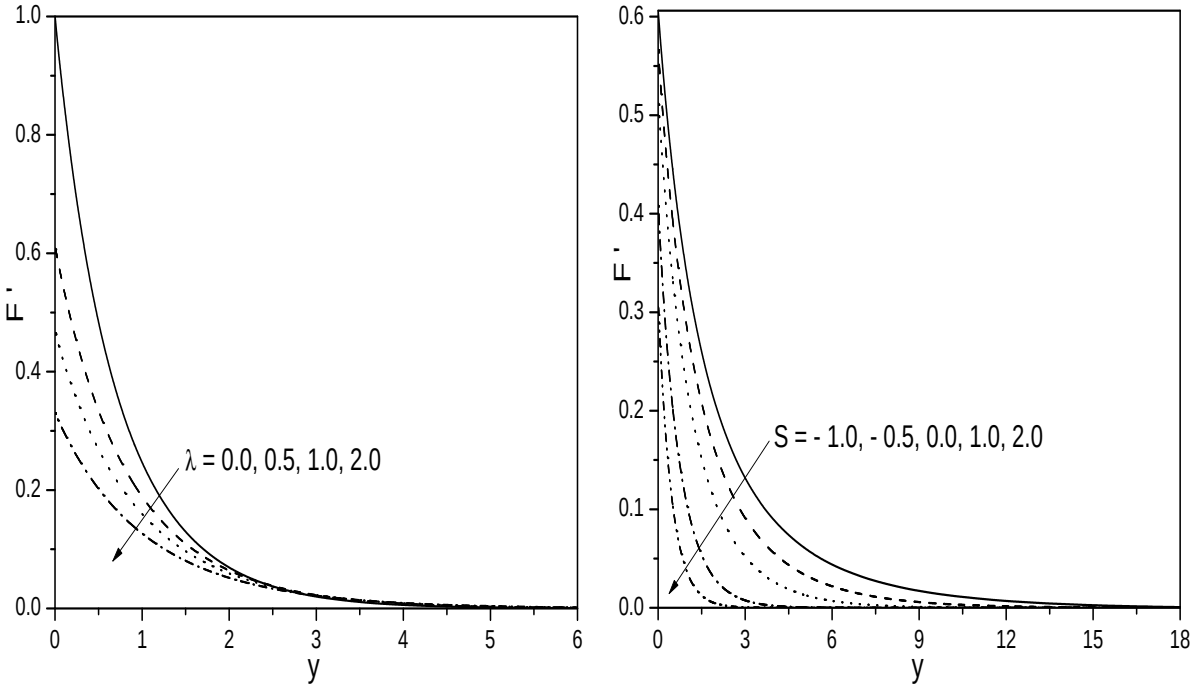

(a) (b)

Figure 2.2: *Effect of (a)λ, and (b)S on Velocity*

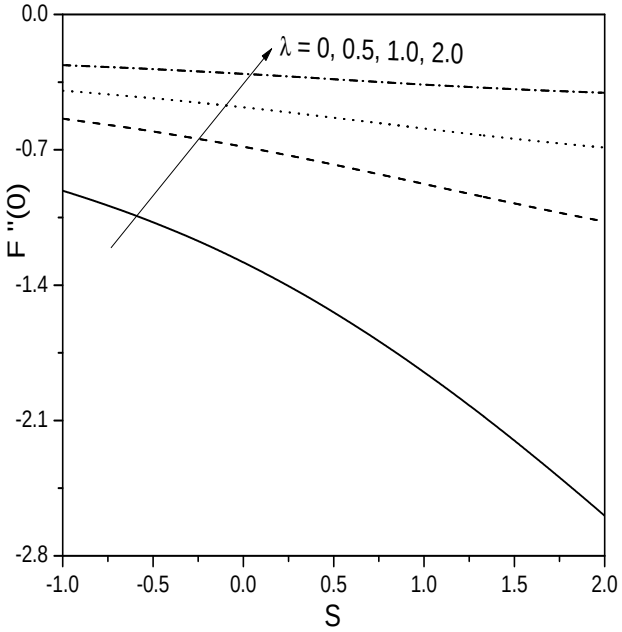

Figure 2.3: *Effect of* λ *on* $F''(0)$ *against* S

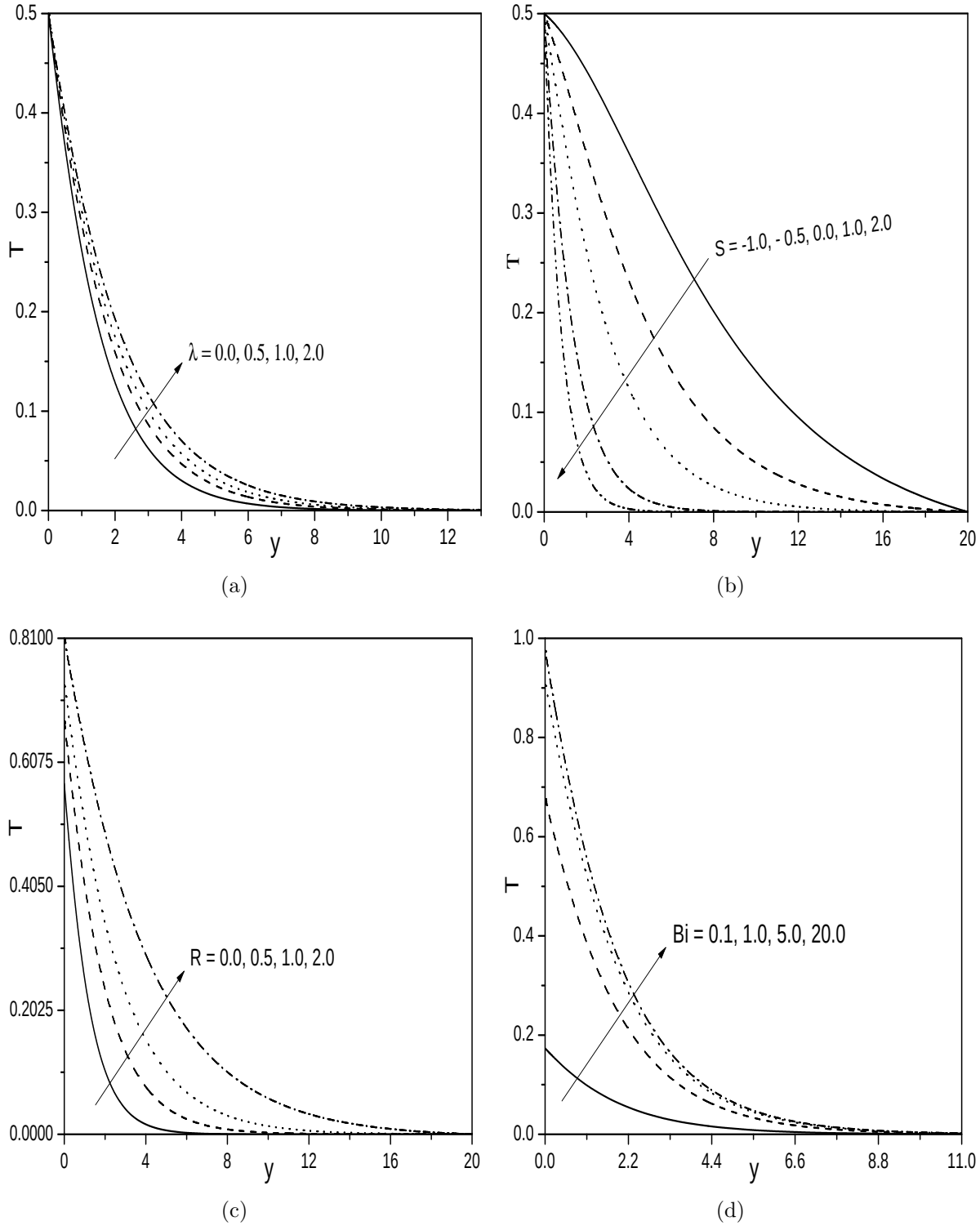

Figure 2.4: *Effect of (a)λ, (b)S, (c)R, and (d)Bi on T*

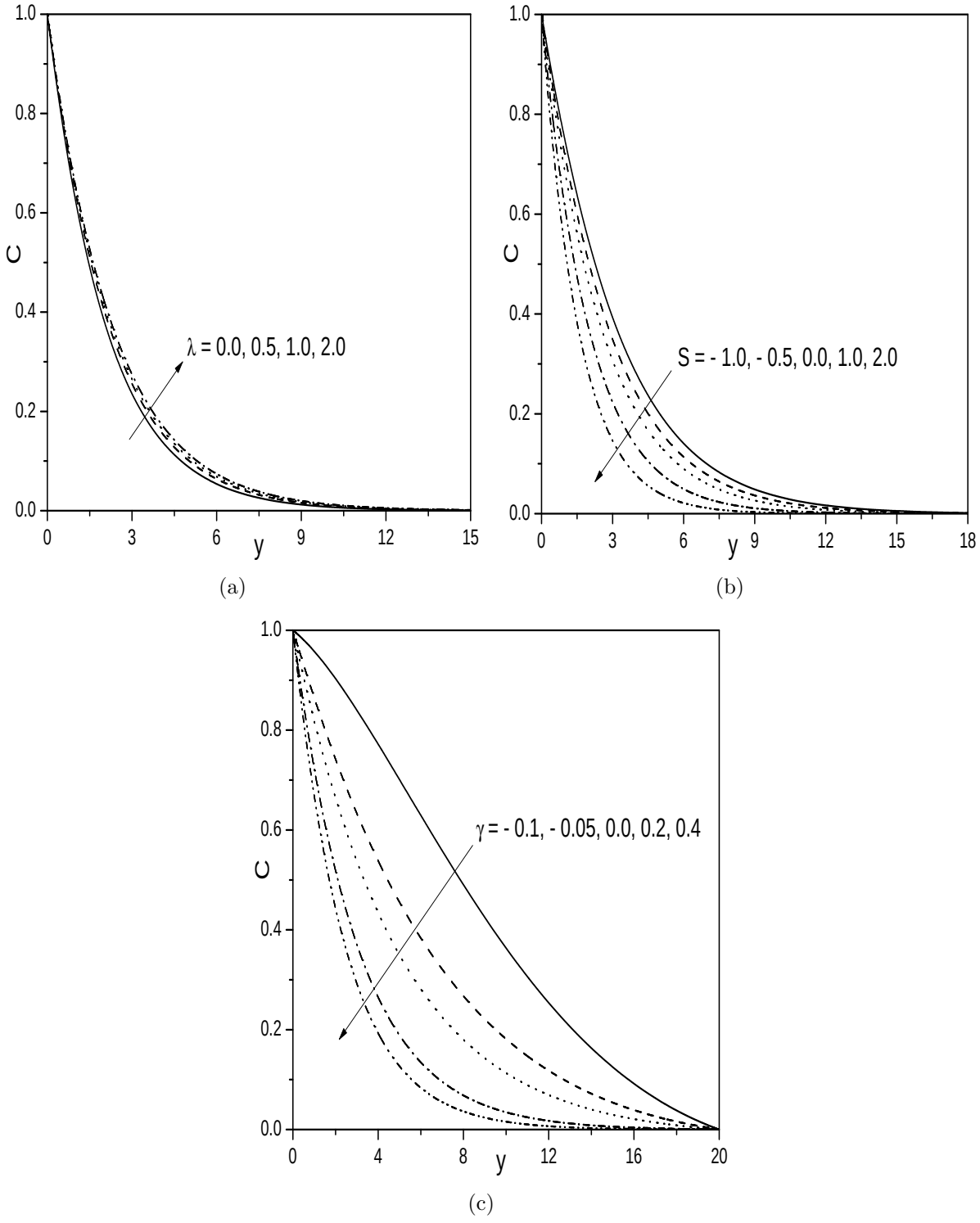

Figure 2.5: *Effect of (a)λ, (b)S, and (c)γ on C*

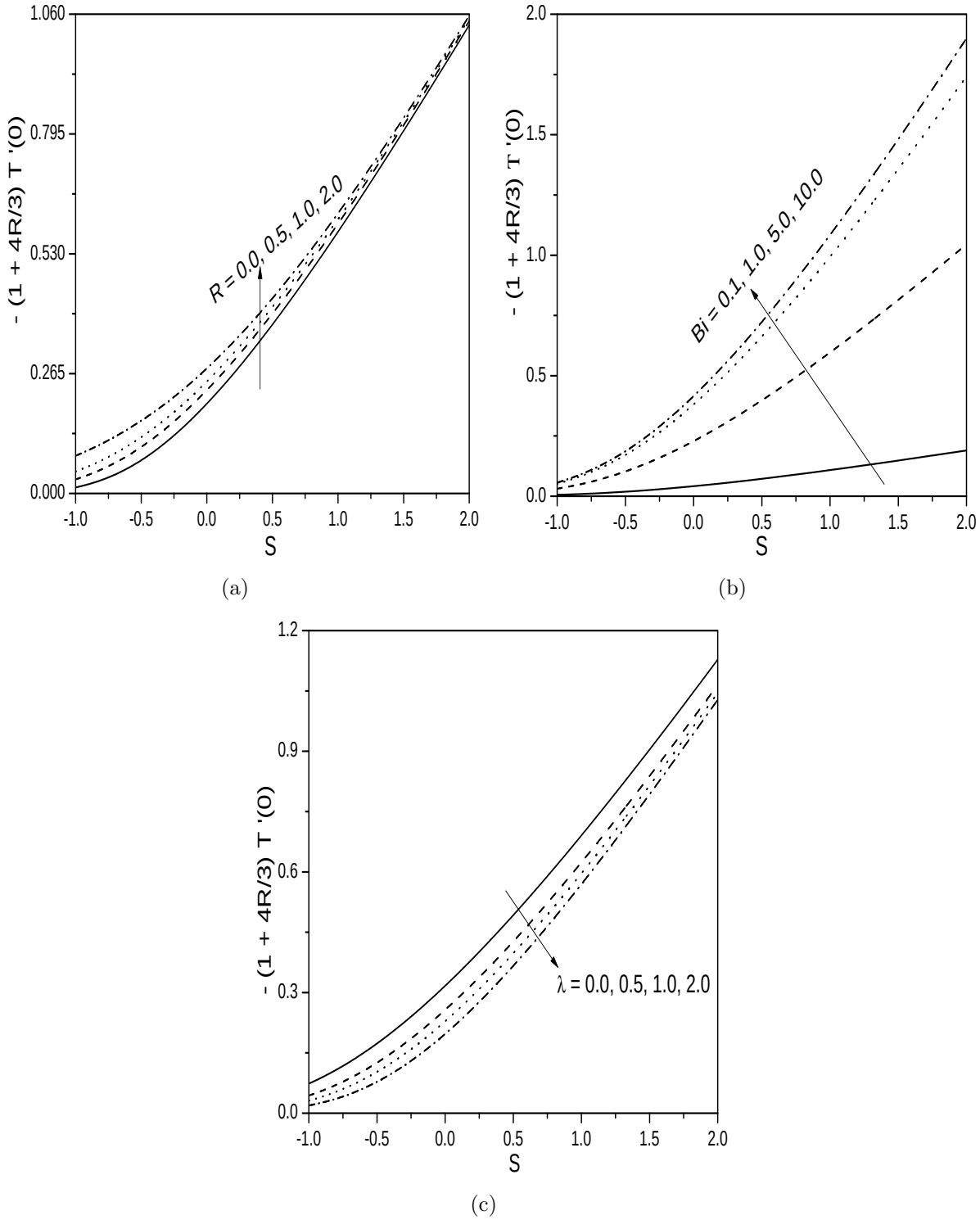

Figure 2.6: *Effect of (a)R, (b)Bi, and (c)*λ *on* $-(1+\frac{4R}{3})T'(0)$

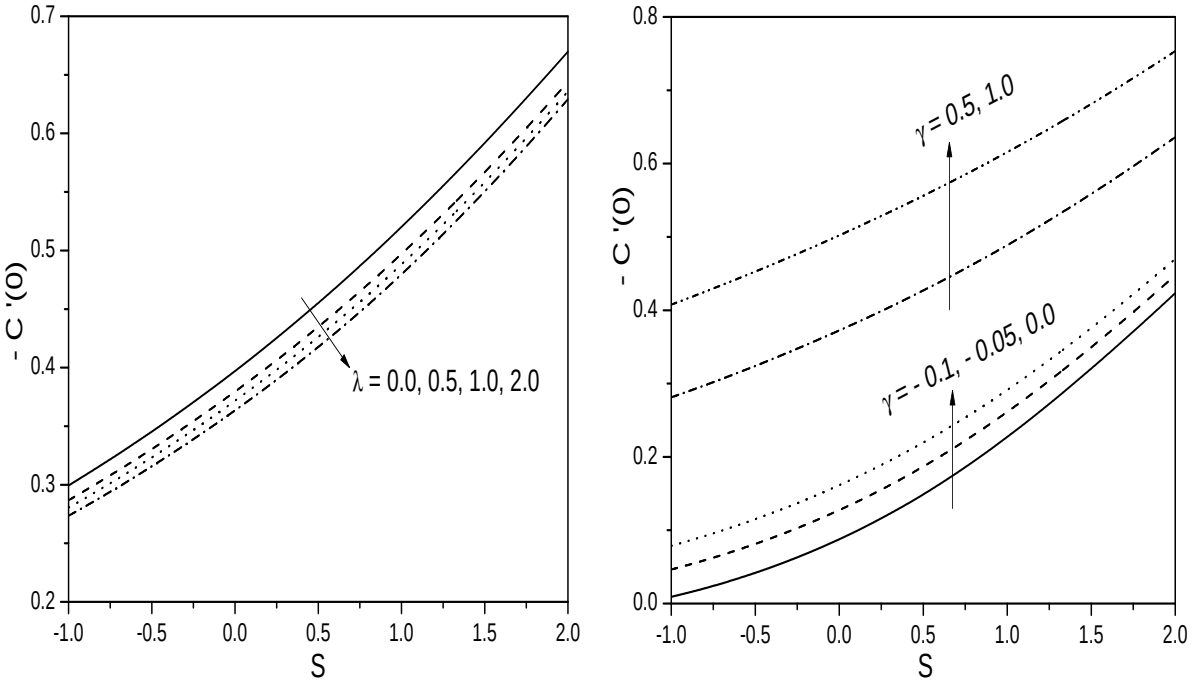

(a) (b)

Figure 2.7: *Effect of (a)*λ*, and (b)*γ *on* $-C'(0)$

2.2.5 Case(b): Uniform wall temperature with Hall effect

A magnetic field of strength $B(\tilde{x}) = B_0 e^{\frac{\tilde{x}}{2L}}$, where B_0 is the constant magnetic field, is applied orthogonal to the sheet as shown in the Fig. (2.8). The assumption of small magnetic Reynolds number allows to neglect the induced magnetic field in contrast to applied magnetic field. The Hall current is considered in view of relatively high electron-atom collision frequency. This assumption causes a cross flow in the $\tilde{z}$-direction, therefore the flow becomes three dimensional. Further, it is assumed that the sheet is maintained at uniform wall temperature and concentration $T_w(\tilde{x})$ and $C_w(\tilde{x})$, respectively. These values are assumed to be greater than the ambient temperature and concentration at any arbitrary reference point in the medium (inside the boundary layer). Under the Boussinesq approximation, the flow is governed by the equations (2.1), (2.3), (2.4) along with the following momentum equations

$$\tilde{u}_x \frac{\partial \tilde{u}_x}{\partial \tilde{x}} + \tilde{u}_y \frac{\partial \tilde{u}_x}{\partial \tilde{y}} = \nu \frac{\partial^2 \tilde{u}_x}{\partial \tilde{y}^2} + g\ \beta_T(\tilde{T} - T_\infty) + g\ \beta_C(\tilde{C} - C_\infty) - \frac{\sigma B^2}{\rho(1+\beta_h^2)}(\tilde{u}_x + \beta_h \tilde{u}_z) \quad (2.27)$$

$$\tilde{u}_x \frac{\partial \tilde{u}_z}{\partial \tilde{x}} + \tilde{u}_y \frac{\partial \tilde{u}_z}{\partial \tilde{y}} = \nu \frac{\partial^2 \tilde{u}_z}{\partial \tilde{y}^2} + \frac{\sigma B^2}{\rho(1+\beta_h^2)}(\beta_h \tilde{u}_x - \tilde{u}_z) \quad (2.28)$$

where $\tilde{u}_z$ is the velocity in $\tilde{z}$-direction.

The associated boundary conditions are

$$\left.\begin{aligned} &\tilde{u}_x = U_* + N_* \nu \tfrac{\partial \tilde{u}_x}{\partial \tilde{y}},\ \tilde{u}_y = -V_*(\tilde{x}),\ \tilde{u}_z = 0, \\ &T_w = T_\infty + T_0 e^{\frac{2\tilde{x}}{L}},\ C_w = C_\infty + C_0 e^{\frac{2\tilde{x}}{L}} \quad \text{at} \quad \tilde{y} = 0 \\ &\tilde{u}_x \to 0,\ \tilde{u}_z \to 0,\ \tilde{T} \to T_\infty,\ \tilde{C} \to C_\infty \ \text{ as } \ \tilde{y} \to \infty \end{aligned}\right\} \quad (2.29)$$

Substituting the following similarity transformations

$$\left.\begin{aligned} &\tilde{y} = y\sqrt{\tfrac{2\nu L}{U_0}} e^{\frac{-\tilde{x}}{2L}},\ \psi = \sqrt{2\nu L U_0} e^{\frac{\tilde{x}}{2L}} F, \\ &\tilde{u}_x = U_0 e^{\frac{\tilde{x}}{L}} F', \quad \tilde{u}_y = -\sqrt{\tfrac{\nu U_0}{2L}}\ e^{\frac{\tilde{x}}{2L}}(F + yF'), \quad \tilde{u}_z = U_0 e^{\frac{\tilde{x}}{L}} W \\ &\tilde{T} = T_\infty + T_0\ e^{\frac{2\tilde{x}}{L}} T,\ \tilde{C} = C_\infty + C_0\ e^{\frac{2\tilde{x}}{L}} C \end{aligned}\right\} \quad (2.30)$$

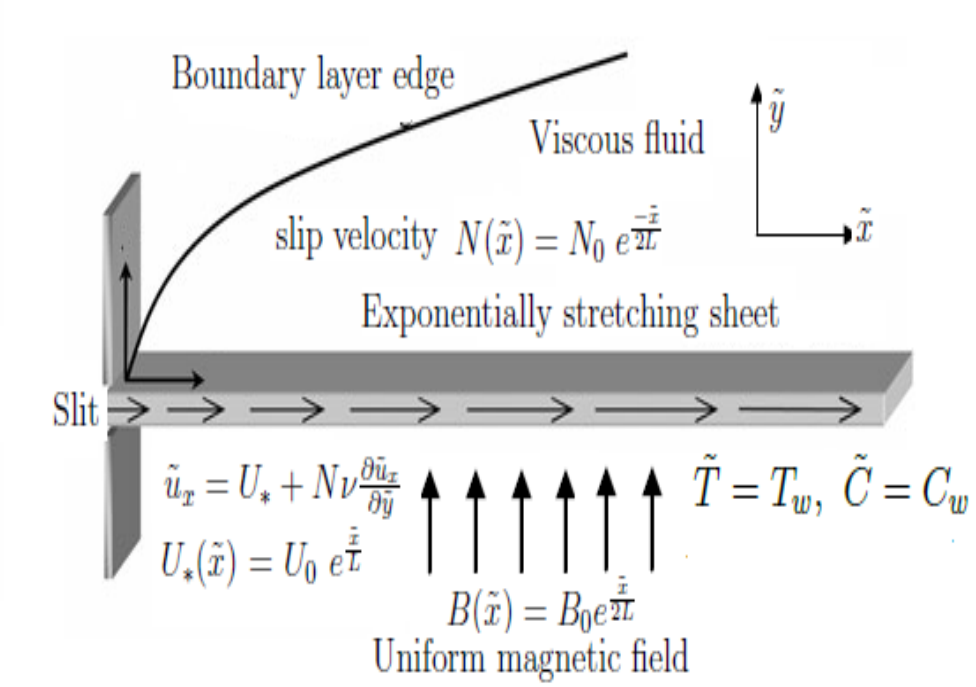

Figure 2.8: Schematic diagram with coordinate system

into the Eqs. (2.1), (2.27), (2.28), (2.3), and (2.4)

$$F''' + FF'' - 2F'^2 + 2Ri(T + \mathbb{B}C) - \frac{H_a}{1+\beta_h^2}(F' + \beta_h W) = 0 \tag{2.31}$$

$$W'' - 2F'W + FW' + \frac{H_a}{1+\beta_h^2}(\beta_h F' - W) = 0 \tag{2.32}$$

$$\frac{1}{Pr}\left(1 + \frac{4R}{3}\right)T'' + FT' - 4F'T = 0 \tag{2.33}$$

$$\frac{1}{Sc}C'' + FC' - 4F'C - \gamma C = 0 \tag{2.34}$$

The conditions (2.29) reduce to

$$\left.\begin{aligned} &F(y) = S,\ F'(y) = 1 + \lambda F''(y),\ W(y) = 0,\ T(y) = 1,\ C(y) = 1 \quad \text{at} \quad y = 0 \\ &F'(y) \to 0,\ W(y) \to 0,\ T(y) \to 0,\ C(y) \to 0 \quad \text{as} \quad y \to \infty \end{aligned}\right\} \tag{2.35}$$

where $Gr = \frac{g\beta_T T_0 L^3}{\nu^2}$ is the Grashof number, $Ri = \frac{Gr}{Re^2}$ is the mixed convection parameter, $H_a = \frac{2L\sigma B_0^2}{\rho U_0}$ is the magnetic parameter, $Re = \frac{U_0 L}{\nu}$ is the Reynold's number, $\beta_h = (\omega_e \tau_e)$ is

Hall parameter, τ_e is the electron collison time, ω_e is the cyclotran frequency of electrons and $\mathbb{B} = \frac{\beta_C\ C_0}{\beta_T\ T_0}$ is the buoyancy ratio. The other parameters are defined in case(a).

2.2.6 Skin Friction in $\tilde{x}$ and $\tilde{z}$-directions, Heat and Mass Transfer Coefficients

The wall shear stress in $\tilde{x}$- and $\tilde{z}$-directions are

$$\tau_{\omega\tilde{x}} = \mu \left[\frac{\partial \tilde{u}_x}{\partial \tilde{y}}\right]_{\tilde{y}=0}, \qquad \tau_{\omega\tilde{z}} = \mu \left[\frac{\partial \tilde{u}_z}{\partial \tilde{y}}\right]_{\tilde{y}=0} \tag{2.36a}$$

and the heat and mass transfers from the sheet respectively are given by

$$q_w = -\kappa \left[\frac{\partial \tilde{T}}{\partial \tilde{y}}\right]_{\tilde{y}=0} - \frac{4\sigma^*}{3k^*}\left[\frac{\partial \tilde{T}^4}{\partial \tilde{y}}\right]_{y=0} \quad \text{and} \quad q_m = -D\left[\frac{\partial \tilde{C}}{\partial \tilde{y}}\right]_{\tilde{y}=0} \tag{2.37a}$$

The non-dimensional skin friction in $\tilde{x}-$direction $C_{F\tilde{x}} = \frac{2\tau_{\omega\tilde{x}}}{\rho U_*^2}$, local skin-friction in $\tilde{z}-$direction $C_{F\tilde{z}} = \frac{2\tau_{\omega\tilde{z}}}{\rho U_*^2}$, the local Nusselt number $Nu_{\tilde{x}} = \frac{\tilde{x}q_w}{\kappa(T_w - T_\infty)}$ and local Sherwood number $Sh_{\tilde{x}} = \frac{\tilde{x}q_m}{\kappa(C_w - C_\infty)}$, are given by

$$\left.\begin{aligned} &\frac{\sqrt{Re_x}}{\sqrt{2\tilde{x}/L}} C_{F\tilde{x}} = F''(0), \quad \frac{\sqrt{Re_x}}{\sqrt{2\tilde{x}/L}} C_{F\tilde{z}} = W'(0), \\ &\frac{Nu_{\tilde{x}}}{\sqrt{\tilde{x}/2L}\sqrt{Re_{\tilde{x}}}} = -\left(1 + \frac{4R}{3}\right) T'(0), \quad \text{and} \quad \frac{Sh_{\tilde{x}}}{\sqrt{\tilde{x}/2L}\sqrt{Re_{\tilde{x}}}} = -C'(0). \end{aligned}\right\} \tag{2.38}$$

where $Re_{\tilde{x}} = \dfrac{\tilde{x}U_*(\tilde{x})}{\nu}$ is the local Reynold's number.

2.2.7 Solution of the problem

The system of Eqs. (2.31) - (2.34) along with the boundary conditions (2.35), is solved numerically, using the successive linearisation method.

Proceeding as in case (a), we obtain the following matrix equation

$$\mathbf{A}_{i-1}\mathbf{X}_i = \mathbf{R}_{i-1}, \tag{2.39}$$

subject to the boundary conditions

$$F_i(\xi_N) = \sum_{k=0}^{N} \mathbf{D}_{0k} F_i(\xi_k) = \sum_{k=0}^{N} (\lambda \mathbf{D}2_{Nk} - \mathbf{D}_{Nk}) F_i(\xi_k) = 0 \tag{2.40a}$$

$$W_i(\xi_N) = W_i(\xi_0) = T_i(\xi_N) = T_i(\xi_0) = C_i(\xi_N) = C_i(\xi_0) = 0 \tag{2.40b}$$

In Eq.(2.39), $\mathbf{A}_{i-1}$ is a (4N + 4)×(4N + 4) square matrix and $\mathbf{X}_i$ and $\mathbf{R}_{i-1}$ are (4N + 4)×1 column vectors defined by

$$\mathbf{A}_{i-1} = \begin{bmatrix} A_{11} & A_{12} & A_{13} & A_{14} \\ A_{21} & A_{22} & A_{23} & A_{24} \\ A_{31} & A_{32} & A_{33} & A_{34} \\ A_{41} & A_{42} & A_{43} & A_{44} \end{bmatrix}, \quad \mathbf{X}_i = \begin{bmatrix} \mathbf{F}_i \\ \mathbf{W}_i \\ \mathbf{\Theta}_i \\ \mathbf{\Phi}_i \end{bmatrix}, \quad \mathbf{R}_{i-1} = \begin{bmatrix} \mathbf{E}_{1,i-1} \\ \mathbf{E}_{2,i-1} \\ \mathbf{E}_{3,i-1} \\ \mathbf{E}_{4,i-1} \end{bmatrix} \tag{2.41}$$

where

$\mathbf{F}_i = [F_i(\xi_0), F_i(\xi_1), F_i(\xi_2), ..., F_i(\xi_{N-1}), F_i(\xi_N)]^T,$

$\mathbf{W}_i = [W_i(\xi_0), W_i(\xi_1), W_i(\xi_2), ..., W_i(\xi_{N-1}), W_i(\xi_N)]^T,$

$\mathbf{\Theta}_i = [T_i(\xi_0), T_i(\xi_1), T_i(\xi_2), ..., T_i(\xi_{N-1}), T_i(\xi_N)]^T,$

$\mathbf{\Phi}_i = [C_i(\xi_0), C_i(\xi_1), C_i(\xi_2), ..., C_i(\xi_{N-1}), C_i(\xi_N)]^T,$

$\mathbf{E}_{1,i-1} = [\zeta_{1,i-1}(\xi_0), \zeta_{1,i-1}(\xi_1), \zeta_{1,i-1}(\xi_2), ..., \zeta_{1,i-1}(\xi_{N-1}), \zeta_{1,i-1}(\xi_N)]^T$

$\mathbf{E}_{2,i-1} = [\zeta_{2,i-1}(\xi_0), \zeta_{2,i-1}(\xi_1), \zeta_{2,i-1}(\xi_2), ..., \zeta_{2,i-1}(\xi_{N-1}), \zeta_{2,i-1}(\xi_N)]^T$

$\mathbf{E}_{3,i-1} = [\zeta_{3,i-1}(\xi_0), \zeta_{3,i-1}(\xi_1), \zeta_{3,i-1}(\xi_2), ..., \zeta_{3,i-1}(\xi_{N-1}), \zeta_{3,i-1}(\xi_N)]^T$

$\mathbf{E}_{4,i-1} = [\zeta_{4,i-1}(\xi_0), \zeta_{4,i-1}(\xi_1), \zeta_{4,i-1}(\xi_2), ..., \zeta_{4,i-1}(\xi_{N-1}), \zeta_{4,i-1}(\xi_N)]^T$

$A_{11} = \mathbf{D}^3 + \chi_{11,i-1}\mathbf{D}^2 + \chi_{12,i-1}\mathbf{D} + \chi_{13,i-1}, \quad A_{12} = -\frac{H_a \beta_h}{1+\beta_h^2}\mathbf{I}, \quad A_{13} = 2Ri\mathbf{I}, \quad A_{14} = 2\mathbb{B}Ri\mathbf{I}$

$A_{21} = \chi_{21,i-1}\mathbf{D} + \chi_{22,i-1}, \quad A_{22} = \mathbf{D}^2 + \chi_{23,i-1}\mathbf{D} + \chi_{24,i-1}, \quad A_{23} = \mathbf{0}, \quad A_{24} = \mathbf{0}$

$A_{31} = \chi_{31,i-1}\mathbf{D} + \chi_{32,i-1}, \quad A_{32} = \mathbf{0}, \quad A_{33} = \frac{1}{Pr}\left(1 + \frac{4R}{3}\right)\mathbf{D}^2 + \chi_{33,i-1}\mathbf{D} + \chi_{34,i-1}, \quad A_{34} = \mathbf{0}$

$A_{41} = \chi_{41,i-1}\mathbf{D} + \chi_{42,i-1}, \quad A_{42} = \mathbf{0}, \quad A_{43} = \mathbf{0}, \quad A_{44} = \frac{1}{Sc}\mathbf{D}^2 + \chi_{43,i-1}\mathbf{D} + \chi_{44,i-1}$

Table 2.2: *Comparison of* $-F''(0)$ *and* $F(\infty)$ *calculated by the present method for* $S = 0$, $\lambda = 0$, $H_a = 0$, *and* $Ri = 0$.

	Magyari and Keller [56]	Present
$-F''(0)$	1.281808	1.28180856
$F(\infty)$	0.905639	0.90564370

Here **I** is an identity matrix of size (N +1)×(N +1). After modifying the matrix system (2.39) to incorporate boundary conditions (2.40), the solution is obtained as

$$\mathbf{X}_i = \mathbf{A}_{i-1}^{-1}\mathbf{R}_{i-1} \tag{2.42}$$

2.2.8 Results and Discussion

In order to validate the code generated, the results of the present problem have been compared with that of the results obtained by Magyari and Keller [56] as a special case by taking $Ri = 0$, $H_a = 0$, $S = 0$, $\lambda = 0$, $R = 0$, and $\gamma = 0$ and found that they are in good agreement, as presented in Table. (2.2). To study the effects of Hall parameter β_h, suction/injection parameter S, radiation parameter R and chemical reaction parameter γ, computations have been carried out in the cases of $Ri = 1.0$, $\mathbb{B} = 0.5$, $S = 0.5$, $\lambda = 1.0$, $\beta_h = 1.0$, $H_a = 2.0$, $R = 0.5$, and $\gamma = 0.5$.

Figures (2.9(a)) - (2.9(d)) interpret the variation of the velocities, temperature and concentration with S. It is seen from these figures that the velocities, temperature, and concentration are increasing with the increase in the injection parameter ($S < 0$). It is also perceived that the suction ($S > 0$) reduces both the momentum, thermal and concentration boundary layer thickness which, in turn, reduce the velocity, temperature, and concentration.

Figures (2.10(a)) - (2.10(d)) represent the behavior of the velocities, temperature and concentration with Hall parameter β_h. From figure (2.10(a)), it is observed that the tangential velocity increases with the increase in β_h. Figure (2.10(b)) shows that the cross flow velocity increases with an increase in the value of β_h. It is increasing near the plate and

then gradually decreasing. Figures (2.10(c)) and (2.10(d)) depict that the temperature and concentration are diminishing with an increase in the value of β_h.

The influence of γ on the velocities, temperature and concentration is presented in the figures (2.11(a)) - (2.11(d)). Figure (2.11(a)) depicts that the temperature is decreasing with an increase in the values γ. The same effect is observed on the secondary velocity as presented in the figure (2.11(b)). Further, from figure (2.11(c)), it is seen that the temperature is rising with an increase in the values of γ. The concentration reduces with the increasing values of γ as depicted in the figure (2.11(d)). This is due to the fact that the reaction-rate parameter is a decelerating agent, the conversion of the species takes place as a result of the chemical reaction and thereby reduces the concentration in the boundary layer.

The behaviour of both the velocities, temperature and concentration profiles with the radiation parameter R is exhibited in the figures (2.12(a)) - (2.12(d)). From figures (2.12(a)) and (2.12(b)), it is observed that both the velocities are increasing with an increase in the value of R. Applying the thermal radiation accumulates the momentum boundary layer thickness and hence, velocity rises. It is seen from the figure (2.12(c)) that the temperature increases with the increasing values of the thermal radiation, which in turn, intensifies the thermal boundary layer thickness. Figure (2.12(d)) shows that concentration is decreasing with an increase in the thermal radiation.

The influence of Ri, β_h, H_a, R, γ and λ on the heat transfer $-(1+\frac{4R}{3})T'(0)$ coefficient against S are presented in the figures (2.13(a)) - (2.13(d)) and (2.14(a)) - (2.14(b)), respectively. It is observed from the Figs. (2.13(a)) and (2.13(b)) that the heat transfer coefficient is increasing with the increase in the values of the mixed convection parameter Ri and the Hall parameter β_h. The rate of heat transfer decreases with an increase in the value of the magnetic parameter H_a, as shown in the Fig. (2.13(c)). It is evident from Fig. (2.13(d)) that, the heat transfer rate is increasing with an increase in the value of the radiation parameter R. The heat transfer rate is decreasing with an increase in the values of the chemical reaction parameter γ as presented in the Fig. (2.14(a)). It is seen from Fig. (2.14(b)) that heat transfer is decreasing with an increase in the values of λ. This is due to the fact that, the slipperiness enhances the thermal boundary layer thickness. Further, it is understood

from the figures that heat transfer rate is increasing with increasing the fluid suction on the boundary of the stretching sheet.

The variation mass transfer ($-C'(0)$) coefficient against S is presented in the Figs. (2.15(a)) - (2.15(b)) and (2.16(a)) - (2.16(d)), respectively. Figures (2.15(a)) and (2.15(b)) show the variation of the mass transfer coefficient for different values of the chemical reaction parameter γ and the slip parameter λ. It is evident from these figures that the increase in the value of the chemical reaction parameter the mass transfer rate increases. An increase in the slipperiness reduces the rate of mass transfer. Figures (2.16(a)), (2.16(b)) and (2.16(d)) show that the mass transfer rate is increasing with the increase in the values of the mixed convection, Hall and thermal radiation parameters, respectively. While an increase in the magnetic parameter decreases the rate of mass transfer as shown in the Fig. (2.16(c)). It is clear from the figures that the mass transfer rate is increasing with an increase in the fluid suction at the boundary.

The behaviour of non-dimensional skin-friction in $\tilde{x}$ and $\tilde{z}$-directions, $\sqrt{(2\tilde{x}/L)Re_x}C_{F\tilde{x}}$ and $\sqrt{(2\tilde{x}/L)Re_x}C_{F\tilde{z}}$, respectively, for different values of λ, β_h, H_a, Ri, R and γ are tabulated in Table (2.3). It is evident from the table that $F''(0)$ is raising and $W'(0)$ reducing with the slipperiness. In the presence of Hall parameter both the skin-frictions are increasing. It is also observed that when $\beta_h = 0$, then there is no secondary flow velocity and hence there is no skin-friction in the direction. Table (2.3) illustrates that, $F''(0)$ is decreasing and $W'(0)$ is increasing with the magnetic parameter. It is also seen that the skin-friction in $\tilde{z}$ -direction is zero when $H_a = 0$. The positive values of Ri increases both the skin-frictions. In addition to this, $F''(0)$ in $\tilde{x}$-direction is increases with the positive values of Ri. Furthermore, it is also identified that a unique value of $F''(0) = -0.61660061$ and $W'(0) = 0.15023781$ is attained when $Ri = 0$ (the case of forced convection flow) and for all values of the radiation parameter R. Because (2.31) and (2.33) are uncoupled when $Ri = 0$. As a result, the flow and the thermal fields are independent. Hence, there is no effect of the thermal field parameters on the flow filed. The radiation parameter increases both the skin-frictions. It is noticed from the table that, $F''(0)$ is increasing and $W'(0)$ is decreasing with $\gamma < 0$ (destructive chemical reaction) and both are decreasing with $\gamma > 0$ (constructive chemical reaction).

Table 2.3: *Variation of skin friction in $\tilde{x}$- and $\tilde{z}$-directions for varying values of slip parameter λ, Hall parameter β_h, magnetic parameter H_a, mixed convection parameter Ri, radiation parameter R and chemical reaction parameter γ.*

λ	β_h	H_a	Ri	R	γ	$F''(0)$	$W'(0)$
0.0	1.0	2.0	1.0	0.5	0.5	-0.84854024	0.48354636
0.5	1.0	2.0	1.0	0.5	0.5	-0.37218224	0.44456698
1.0	1.0	2.0	1.0	0.5	0.5	-0.23963767	0.43303045
2.0	1.0	2.0	1.0	0.5	0.5	-0.14018654	0.42415295
1.0	0.0	2.0	1.0	0.5	0.5	-0.30883545	0.00000000
1.0	0.1	2.0	1.0	0.5	0.5	-0.30771879	0.06607727
1.0	1.0	2.0	1.0	0.5	0.5	-0.23963767	0.43303045
1.0	2.0	2.0	1.0	0.5	0.5	-0.17666970	0.43597489
1.0	1.0	0.0	1.0	0.5	0.5	-0.11322710	0.00000001
1.0	1.0	0.1	1.0	0.5	0.5	-0.11970192	0.03314271
1.0	1.0	1.0	1.0	0.5	0.5	-0.17852309	0.26727093
1.0	1.0	2.0	1.0	0.5	0.5	-0.23963767	0.43303045
1.0	1.0	2.0	0.0	0.5	0.5	-0.61660061	0.15023781
1.0	1.0	2.0	0.5	0.5	0.5	-0.39839663	0.33594925
1.0	1.0	2.0	1.5	0.5	0.5	-0.10565609	0.50306747
1.0	1.0	2.0	3.0	0.5	0.5	0.22147847	0.64645130
1.0	1.0	2.0	1.0	0.0	0.5	-0.26780778	0.40671604
1.0	1.0	2.0	1.0	0.5	0.5	-0.23963767	0.43303045
1.0	1.0	2.0	1.0	1.0	0.5	-0.22203919	0.45200184
1.0	1.0	2.0	1.0	2.0	0.5	-0.20024593	0.47826014
1.0	1.0	2.0	1.0	0.5	-1.0	-0.22103672	0.45452242
1.0	1.0	2.0	1.0	0.5	-0.5	-0.22876207	0.45510319
1.0	1.0	2.0	1.0	0.5	0.0	-0.23497509	0.44256653
1.0	1.0	2.0	1.0	0.5	1.0	-0.23963767	0.43303045
1.0	1.0	2.0	1.0	0.5	2.0	-0.24325520	0.42672253

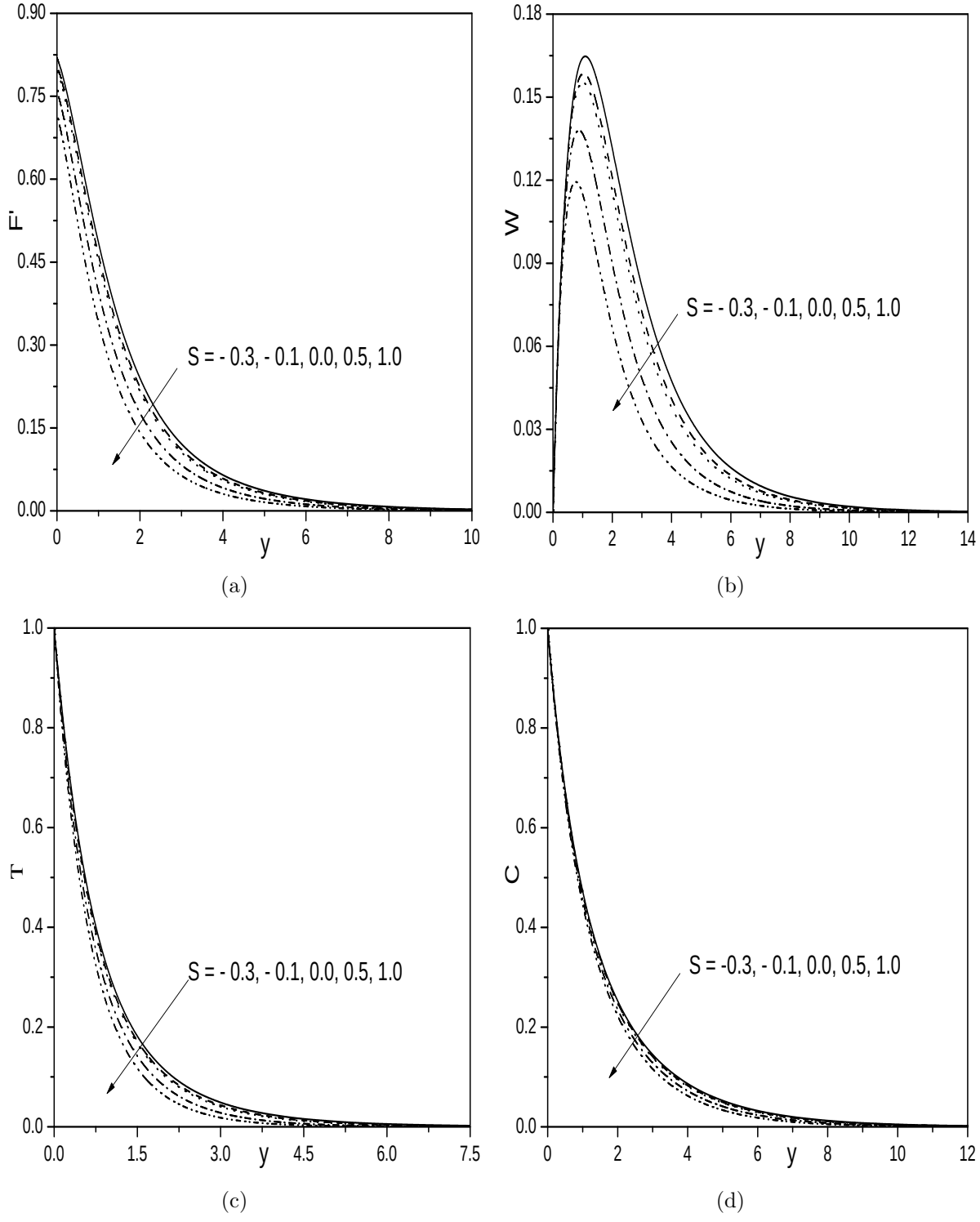

Figure 2.9: *"Effect of S on (a)Velocity, (b)transverse velocity, (c)Temperature, and (d)Concentration profiles".*

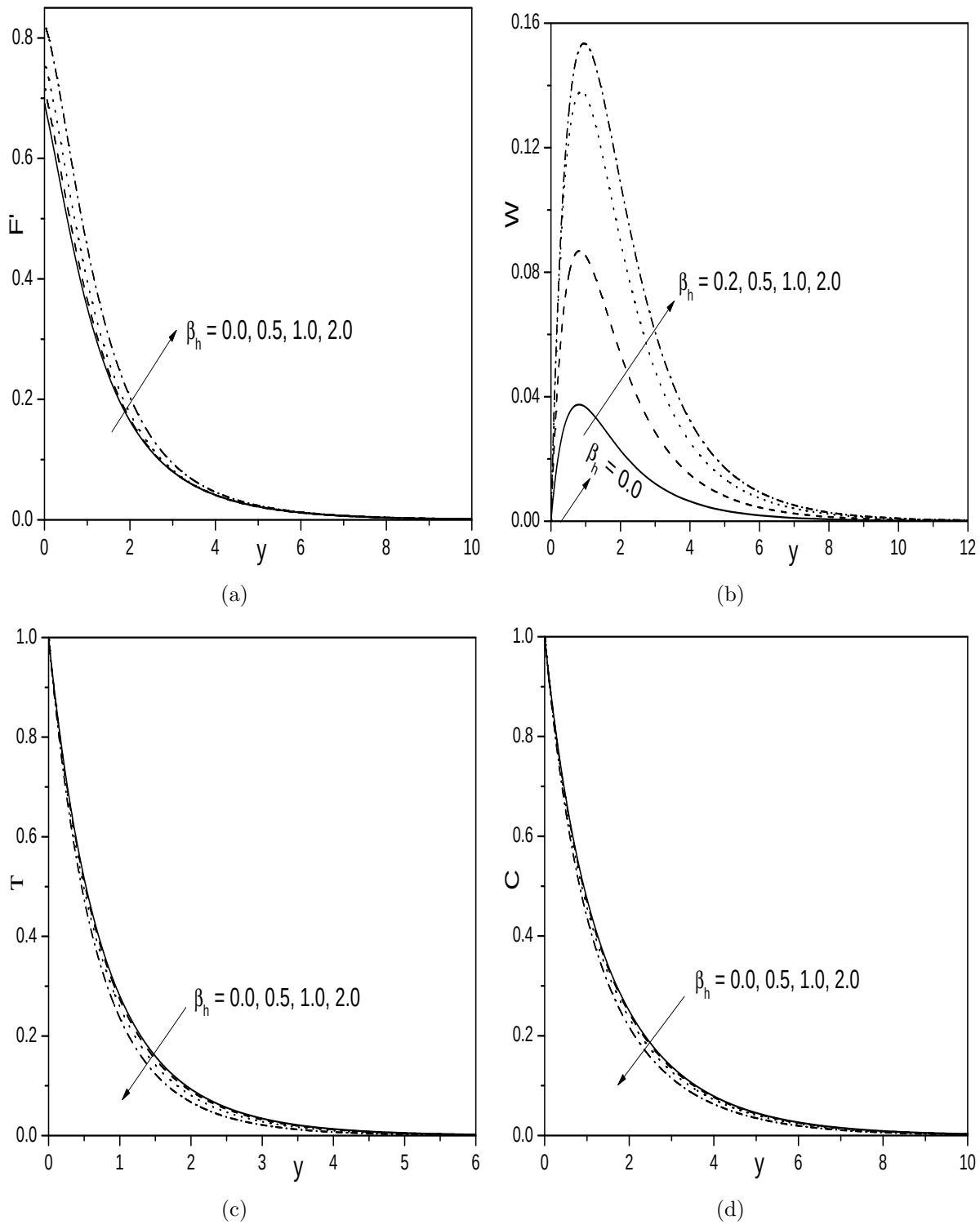

Figure 2.10: *"Effect of β_h on (a)Velocity, (b)transverse velocity, (c)Temperature, and (d)Concentration profiles".*

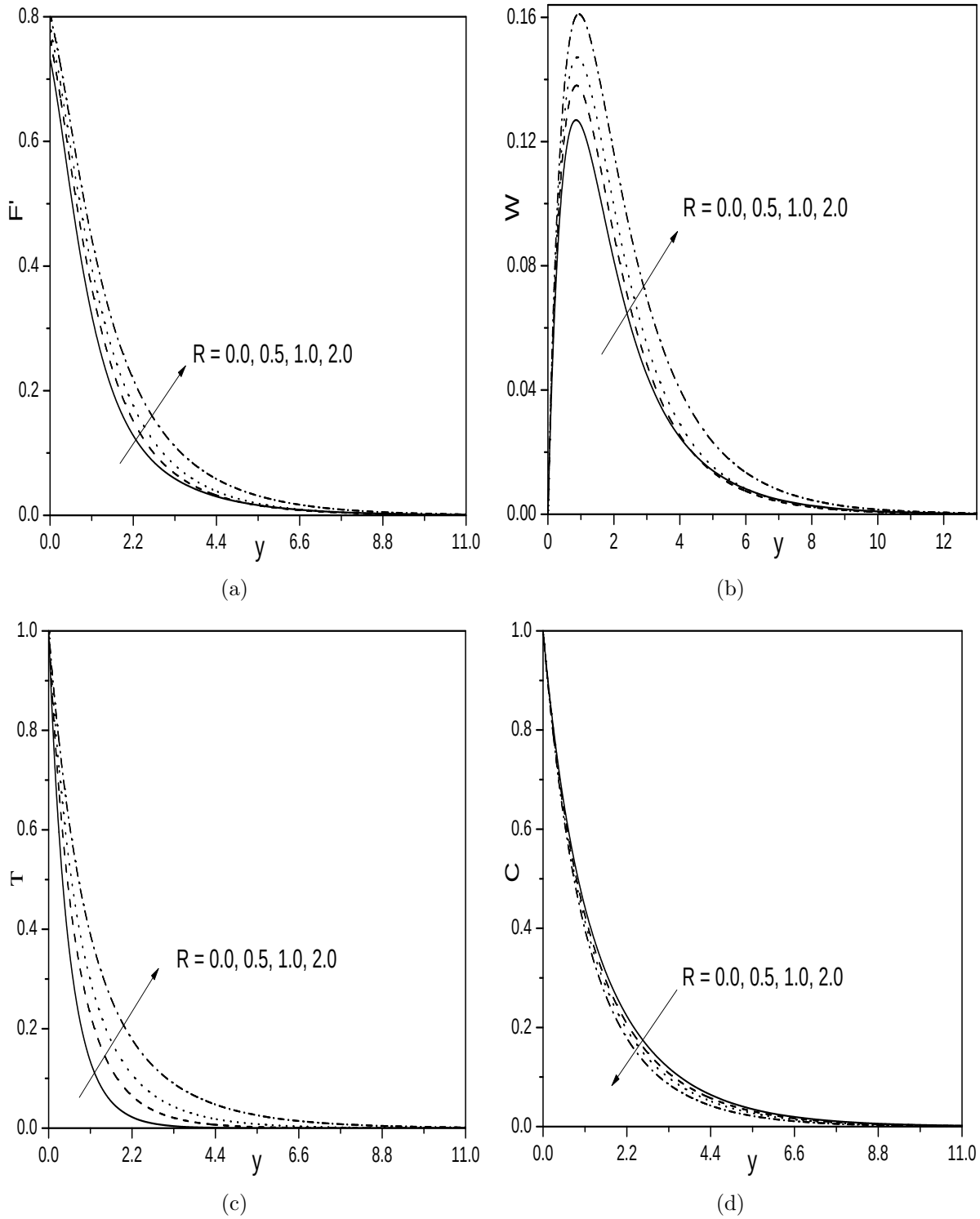

Figure 2.11: *"Effect of R on (a)Velocity, (b)transverse velocity, (c)Temperature, and (d)Concentration profiles."*

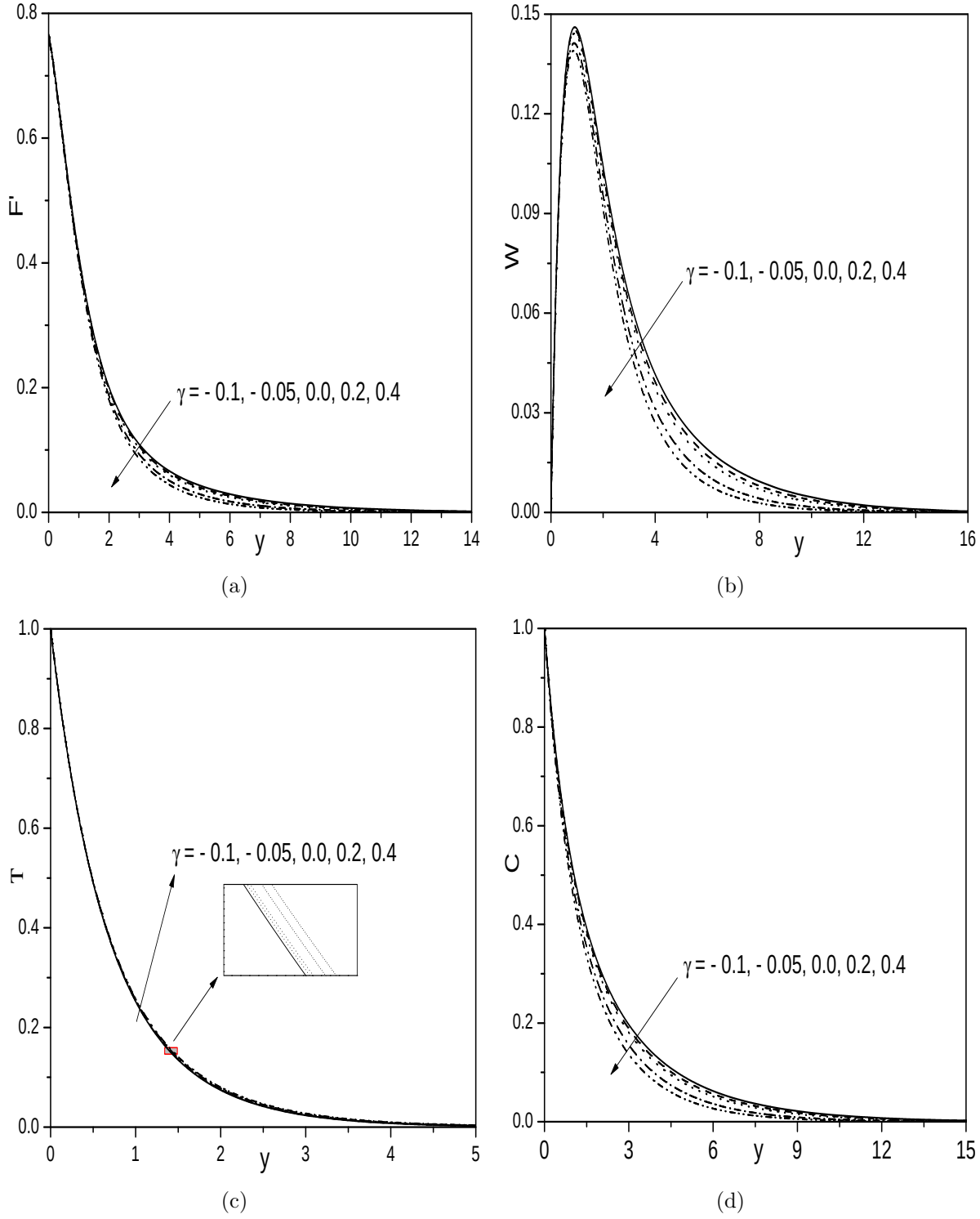

Figure 2.12: *"Effect of γ on (a)Velocity, (b)transverse velocity, (c)Temperature, and (d)Concentration" profiles.*

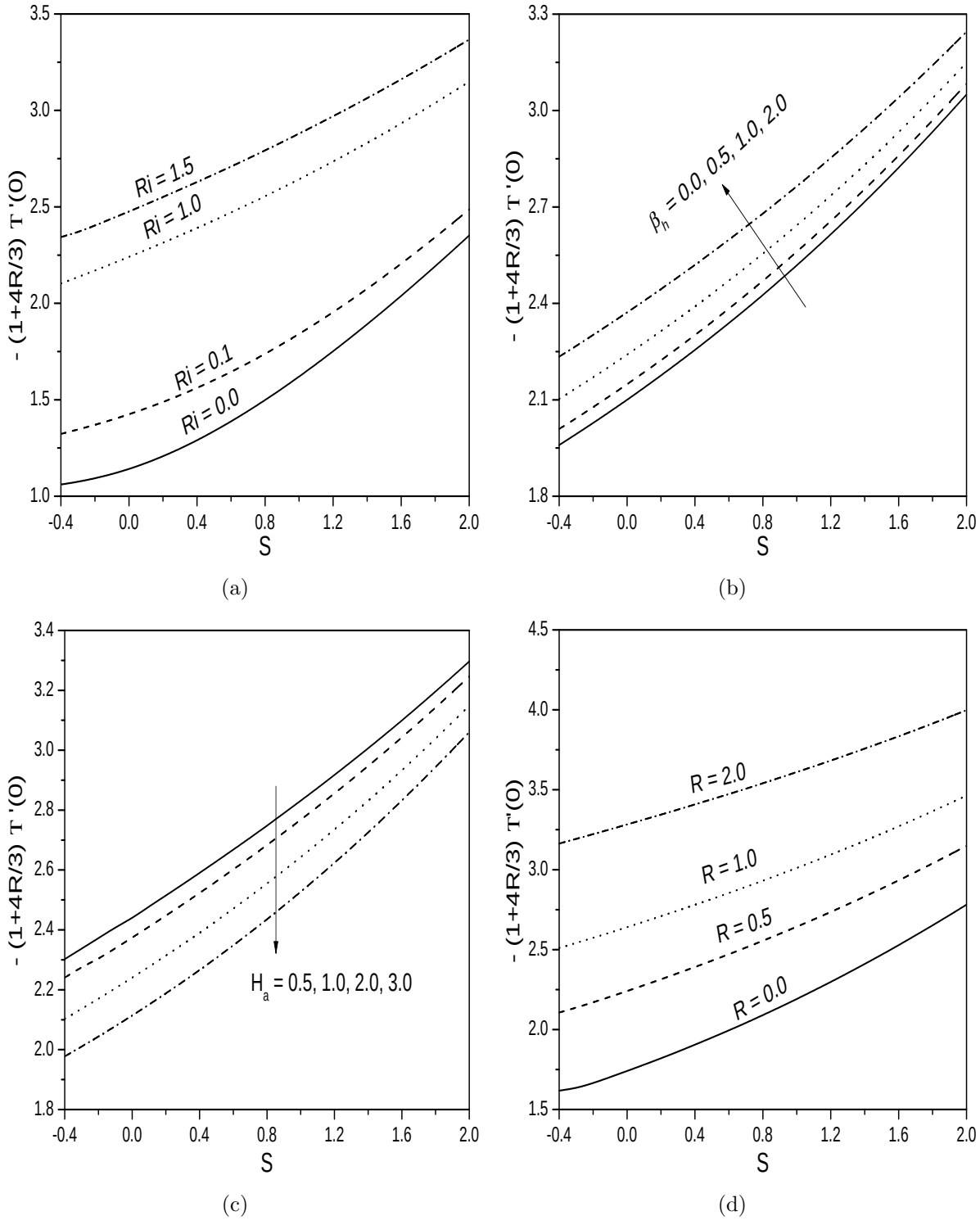

Figure 2.13: *"Effect of (a)Ri, (b)β_h, (c)H_a, and (d)R on $-(1+\frac{4R}{3})T'(0)$".*

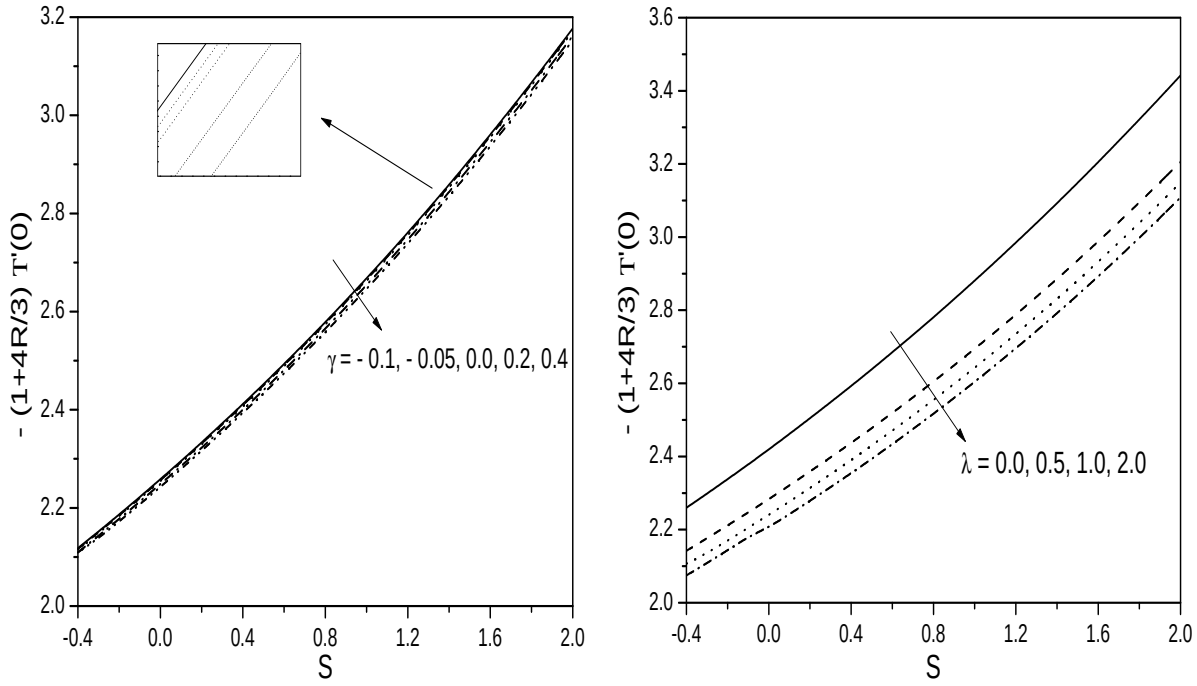

(a) (b)

Figure 2.14: *"Effect of (a)γ, and (b)λ on $-(1+\frac{4R}{3})T'(0)$".*

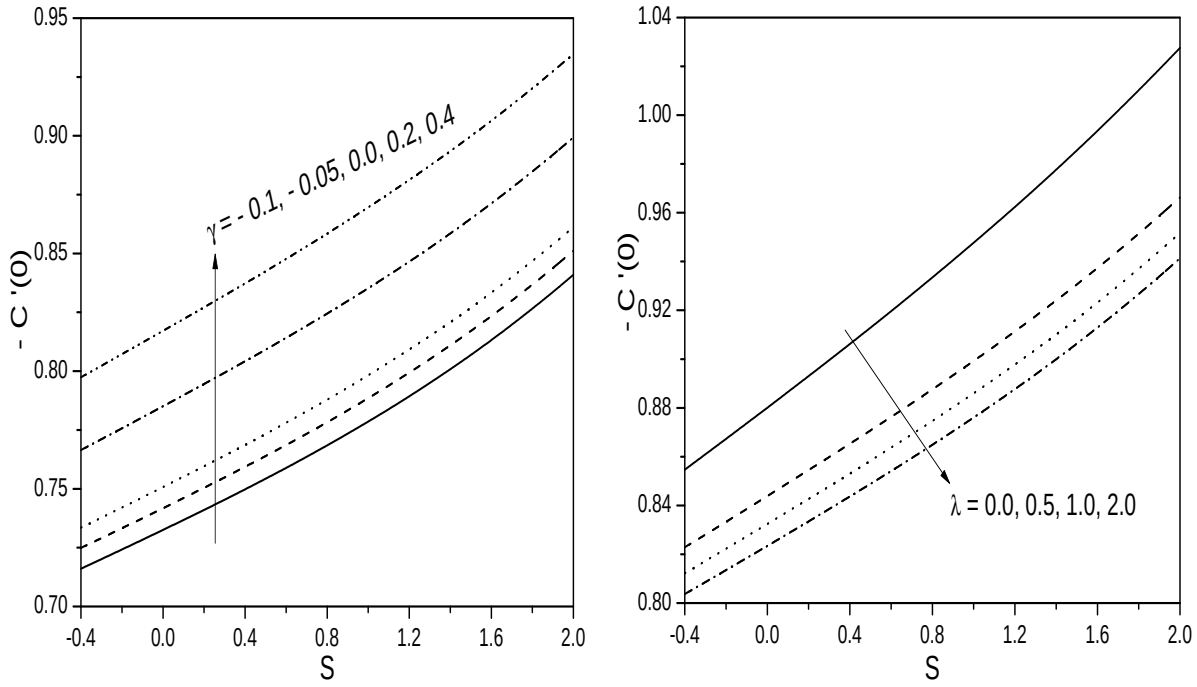

(a) (b)

Figure 2.15: *"Effect of (a)γ, and (b)λ on $-C'(0)$".*

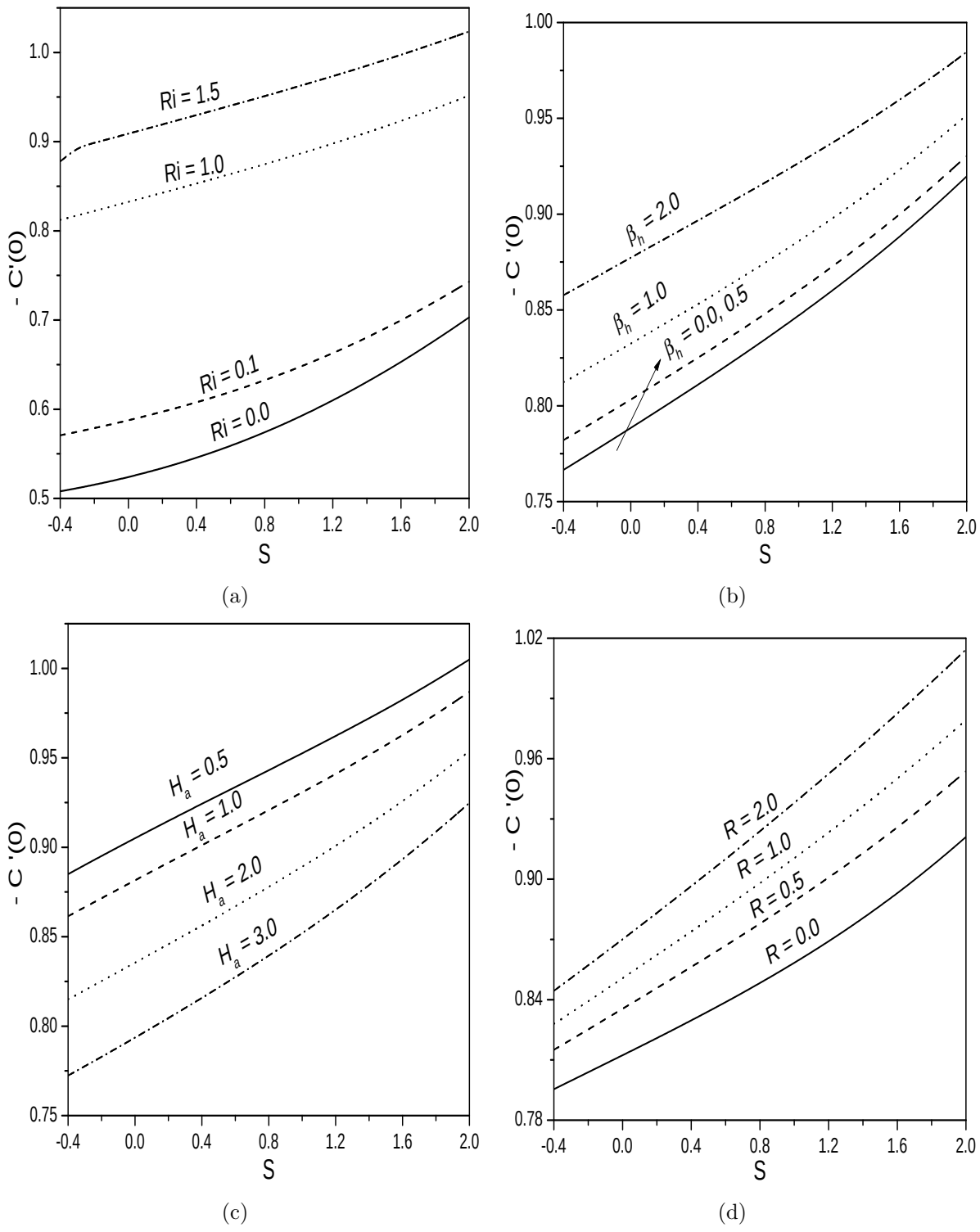

Figure 2.16: *"Effect of (a)Ri, (b)β_h, (c)H_a, and (d)R on $-C'(0)$".*

2.3 Conclusions

In this chapter, the heat and mass transfer due to laminar slip flow of electrically conducting incompressible viscous fluid over an exponentially stretching permeable sheet is studied with the thermal radiation and the chemical reaction effects. From this study the following conclusions are drawn for two cases:

The fluid suction reduces the velocity of the fluid for both the cases (a) and (b). In case (b), both the velocities increase with an increase in the Hall and the thermal radiation parameters while the opposite trend is observed with the increase in the chemical reaction parameter and suction parameter. The temperature of the fluid increases with an increase in the thermal radiation parameter in both the cases. But, an increase in the temperature is more in case (a) than in case (b). An increase in the Biot number increases the temperature in case (a). In both the cases, the concentration decreases with the increase in the chemical reaction parameter and the fluid suction. The skin-friction in $\tilde{x}$-direction increases with the fluid slippage at the boundary and decreases in $\tilde{z}$-direction. While, for case (a), the skin-friction decreases with the fluid suction. The rate of heat transfer increases with an increase in Hall, mixed convection, and thermal radiation parameters. Whereas, the opposite trend is observed with the increase in the chemical reaction parameter. While, in both the cases (a) and (b), the rate of heat and mass transfers decrease with the fluid slippage at the boundary of the stretching surface. In case (a), the rate of heat transfer increases with the increase in the thermal radiation parameter and Biot number. In both the cases, increase in the chemical reaction parameter increases the rate of mass transfer.

Chapter 3

Effect of Joule heating on the flow over an exponentially stretching sheet[1]

3.1 Introduction

A good number of investigations have been carried out to study the Joule heating effect on the flow, heat and mass transfer along difference surfaces in view of thier applications in nuclear engineering and allied engineering areas. Jat and Gopi [44] investigated the effect of Joule heating on a laminar flow over an exponentially stretching surface in presence of thermal radiation and viscous dissipation effects. Hayat *et al.* [39] reported the MHD flow of Jeffrey liquid due to a nonlinear radially stretched sheet in presence of Joule heating.

This chapter explores the effect of Joule heating on the flow of a viscous fluid over a permeable exponentially stretching surface. In addition to Joule heating, the present study explains the effects of velocity slip parameter, mixed convection parameter, Hall parameter and Biot number parameter on the physical quantities of the flow for both the suction and

[1]Case(a):Communicated to "**Mathematical Sciences**",
Case(b):Published in "**Nonlinear Engineering - Modeling and Application**" 6(2) (2017) 101–114

injection. In addition, the numerical data for skin-friction is shown in tabular form.

3.2 Formulation of the Problem

Consider a stretching sheet in a laminar slip flow of incompressible viscous fluid with a temperature T_∞ and concentration C_∞. Apart from the assumptions made in case (a) of Chapter-2, here, we assume that a magnetic field of strength $B(\tilde{x}) = B_0 e^{\frac{\tilde{x}}{2L}}$, where B_0 is the constant magnetic field, is applied orthogonal to the sheet and the induced magnetic field is neglected. Hence, the following are the equations which governs the present flow

$$\frac{\partial \tilde{u}_x}{\partial \tilde{x}} + \frac{\partial \tilde{u}_y}{\partial \tilde{y}} = 0 \tag{3.1}$$

$$\tilde{u}_x \frac{\partial \tilde{u}_x}{\partial \tilde{x}} + \tilde{u}_y \frac{\partial \tilde{u}_x}{\partial \tilde{y}} = \nu \frac{\partial^2 \tilde{u}_x}{\partial \tilde{y}^2} - \frac{\sigma B^2}{\rho} \tilde{u}_x \tag{3.2}$$

$$\tilde{u}_x \frac{\partial \tilde{T}}{\partial \tilde{x}} + \tilde{u}_y \frac{\partial \tilde{T}}{\partial \tilde{y}} = \alpha \frac{\partial^2 \tilde{T}}{\partial \tilde{y}^2} + \frac{\sigma B^2}{\rho c_p} \tilde{u}_x^2 \tag{3.3}$$

$$\tilde{u}_x \frac{\partial \tilde{C}}{\partial \tilde{x}} + \tilde{u}_y \frac{\partial \tilde{C}}{\partial \tilde{y}} = D \frac{\partial^2 \tilde{C}}{\partial \tilde{y}^2} \tag{3.4}$$

3.2.1 Case(a): Convective Thermal Condition

Assume that the sheet is either cooled or heated convectively through a fluid with temperature T_f and which induces a heat transfer coefficient h_f, where $h_f = h\sqrt{\frac{U_0}{2L}} e^{\frac{\tilde{x}}{2L}}$.

Hence, the conditions on the surface of the sheet are

$$\left.\begin{array}{l} \tilde{u}_x = U_* + N_* \nu \frac{\partial \tilde{u}_x}{\partial \tilde{y}},\ \tilde{u}_y = -V_*(\tilde{x}),\ h_f(T_f - \tilde{T}) = -\kappa \frac{\partial \tilde{T}}{\partial \tilde{y}},\ \tilde{C} = C_w \quad \text{at} \quad \tilde{y} = 0 \\ \tilde{u}_x \to 0,\ \tilde{T} \to T_\infty,\ \tilde{C} \to C_\infty \ \text{ as } \quad \tilde{y} \to \infty \end{array}\right\} \tag{3.5}$$

Introducing the stream functions through $\tilde{u}_x = -\frac{\partial \psi}{\partial \tilde{y}}$ and $\tilde{u}_y = \frac{\partial \psi}{\partial \tilde{x}}$ and then the following

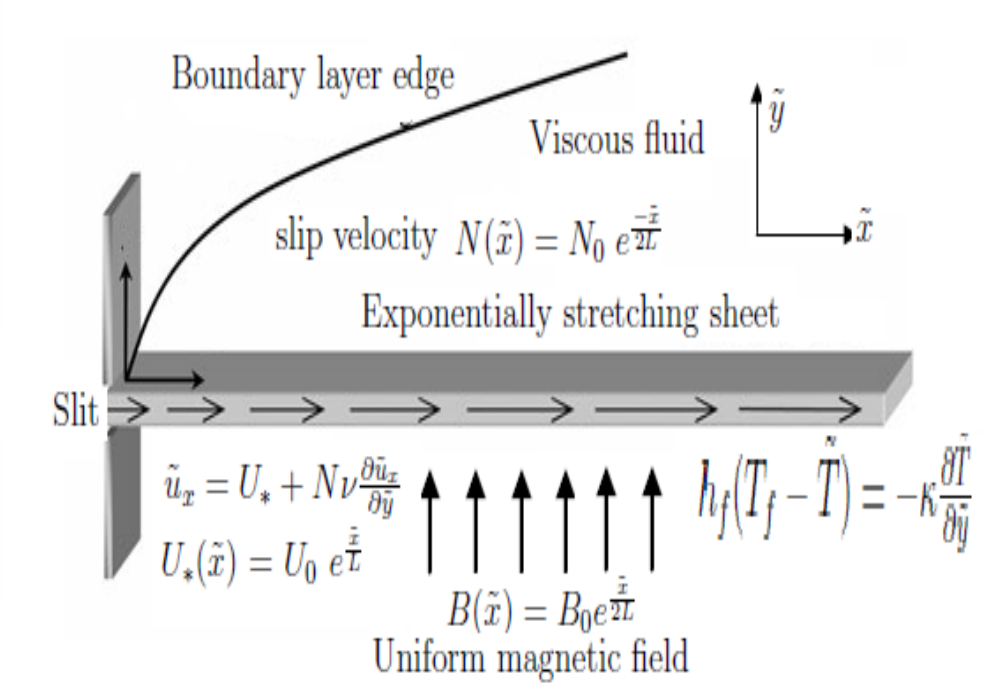

Figure 3.1: Schematic diagram with coordinate system

dimensionless variables

$$\left.\begin{aligned} &\tilde{x} = xL, \quad \tilde{y} = y\sqrt{\tfrac{2\nu L}{U_0}}e^{\frac{\tilde{x}}{2L}}, \quad \psi = \sqrt{2\nu L U_0}e^{\frac{\tilde{x}}{2L}}F(x,y), \\ &\tilde{T} = T_\infty + (T_f - T_\infty)T(x,y), \quad \tilde{C} = C_\infty + (C_w - C_\infty)C(x,y) \end{aligned}\right\} \tag{3.6}$$

into Eqs. (3.1) - (3.4), we obtain

$$F''' + FF'' - 2F'^2 - H_aF' + 2\left(F''\frac{\partial F}{\partial x} - F'\frac{\partial F'}{\partial x}\right) = 0 \tag{3.7}$$

$$\frac{1}{Pr}T'' + FT' + 2\left(T'\frac{\partial F}{\partial x} - F'\frac{\partial T}{\partial x}\right) = 0 \tag{3.8}$$

$$\frac{1}{Sc}C'' + FC' + 2\left(C'\frac{\partial F}{\partial x} - F'\frac{\partial C}{\partial x}\right) = 0 \tag{3.9}$$

The conditions at the boundary reduces to

$$\left.\begin{aligned} &F(x,0)+2\tfrac{\partial F}{\partial x}(x,0)=S,\ F'(x,0)=1+\lambda F''(x,0),\\ &T'(x,0)=-Bi(1-T(x,0)),\ C(x,0)=1,\\ &F'(x,y)\to 0,\ T(x,y)\to 0,\ C(x,y)\to 0\ \text{ as }\ y\to\infty \end{aligned}\right\} \tag{3.10}$$

where $H_a = \frac{2L\sigma B_0^2}{\rho U_0}$ is the magnetic parameter and $J = \frac{2L\sigma B_0^2 U_0}{\rho c_p(T_f - T_\infty)}$ is the Joule heating parameter.

3.2.2 Skin Friction, Heat and Mass Transfer Coefficients

The non-dimensional skin friction C_f, the local Nusselt number $Nu_{\tilde{x}}$ and the local Sherwood number $Sh_{\tilde{x}}$, are given by

$$\left.\frac{\sqrt{Re_x}\ C_f}{\sqrt{2x/L}} = F''(0),\ \frac{Nu_x}{\sqrt{x/2L}\sqrt{Re_x}} = -T'(0),\ \text{and}\ \frac{Sh_x}{\sqrt{x/2L}\sqrt{Re_x}} = -C'(0)\ \right\} \tag{3.11}$$

where $Re_x = \dfrac{xU_*(x)}{\nu}$ is the local Reynold's number.

3.2.3 Solution of the problem

To solve the system of Eqs. (3.7) - (3.9) along with the boundary conditions (3.10), a local similarity and non-similarity method([103], [67]) has been applied. The boundary value problems obtained from this method are linearized by the successive linearisation method and then solved using the Chebyshev spectral collocation method.

The local similarity and non-similarity method includes three levels of truncations which are explained as follows:

In the first level of truncation, the initial approximate solution can be obtained from the local similarity equations for a particular case $x << 1$ by suppressing the terms $x(\frac{\partial}{\partial x})$. As

there are no terms accompanied with $x\frac{\partial}{\partial x}$ in (3.7) - (3.9), there is no change in the governing equations and boundary conditions.

For the second level of truncation, we introduce $G = \frac{\partial F}{\partial x}$, $H = \frac{\partial T}{\partial x}$ and $K = \frac{\partial C}{\partial x}$ to get back the suppressed terms in the first level of truncation. Thus the governing equations at the second level truncation reduce to

$$F''' + FF'' - 2F'^2 + 2\left(F''G - F'G'\right) - H_aF' = 0 \tag{3.12}$$

$$\frac{1}{Pr}T'' + FT' + J\ e^{2x}F'^2 + 2\left(T'G - F'H\right) = 0 \tag{3.13}$$

$$\frac{1}{Sc}C'' + FC' + 2\left(C'G - F'K\right) = 0 \tag{3.14}$$

The corresponding conditions on the boundary are

$$\left.\begin{array}{l} F(x,0) + 2G(x,0) = S,\ F'(x,0) = 1 + \lambda F''(x,0), \\ T'(x,0) = -Bi(1 - T(x,0)),\ C(x,0) = 1, \\ F'(x,\infty) \to 0,\ T(x,\infty) \to 0,\ C(x,\infty) \to 0 \end{array}\right\} \tag{3.15}$$

At the third level of truncation, we differentiate Eqs. (3.12) - (3.14) with respect to x and neglect terms accompanied with $\frac{\partial G}{\partial x}$, $\frac{\partial H}{\partial x}$ and $\frac{\partial K}{\partial x}$, then we get

$$G''' + FG'' + GF'' - 4F'G' + 2\left(GG'' - G'^2\right) - H_aG' = 0 \tag{3.16}$$

$$\frac{1}{Pr}H'' + (FH' + GT') + 2J\ e^{2x}\left(F'^2 + F'G'\right) + 2\left(H'G - G'H\right) = 0 \tag{3.17}$$

$$\frac{1}{Sc}K'' + (FK' + GC') + 2\left(K'G - G'K\right) = 0 \tag{3.18}$$

The associated conditions on the surface of the stretching sheet are

$$\left.\begin{array}{l} G(x,0) = 0,\ G'(x,0) = \lambda\ G''(x,0),\ H'(x,0) = Bi\ H(x,0),\ K(x,0) = 0 \\ G'(x,\infty) \to 0,\ H(x,\infty) \to 0,\ K(x,\infty) \to 0 \end{array}\right\} \tag{3.19}$$

The set of differential equations (3.12) - (3.14) and (3.16) - (3.18) together with the boundary conditions (3.15) and (3.19) are now solved using successive linearisation method ([68], [60]) and Chebyshev spectral collocation method [12].

Proceeding as in Chapter-2, we obtain the following matrix equation

$$\mathbf{A}_{i-1}\mathbf{X}_i = \mathbf{R}_{i-1}, \tag{3.20}$$

In Eq.(3.20), $\mathbf{A}_{i-1}$ is a (6N + 6)×(6N + 6) square matrix and $\mathbf{X}_i$ and $\mathbf{R}_{i-1}$ are (6N + 6)×1 column vectors defined by

$$\mathbf{A}_{i-1} = [A_{rs}], r, s = 1, 2, \cdots, 6, \quad \mathbf{X}_i = \begin{bmatrix} \mathbf{F}_i \\ \mathbf{\Theta}_i \\ \mathbf{\Phi}_i \\ \mathbf{G}_i \\ \mathbf{H}_i \\ \mathbf{K}_i \end{bmatrix}, \quad \mathbf{R}_{i-1} = \begin{bmatrix} \mathbf{E}_{1,i-1} \\ \mathbf{E}_{2,i-1} \\ \mathbf{E}_{3,i-1} \\ \mathbf{E}_{4,i-1} \\ \mathbf{E}_{5,i-1} \\ \mathbf{E}_{6,i-1} \end{bmatrix} \tag{3.21}$$

where

$\mathbf{F}_i = [F_i(\xi_0), F_i(\xi_1), F_i(\xi_2), ..., F_i(\xi_{N-1}), F_i(\xi_N)]^T,$
$\mathbf{\Theta}_i = [T_i(\xi_0), T_i(\xi_1), T_i(\xi_2), ..., T_i(\xi_{N-1}), T_i(\xi_N)]^T,$
$\mathbf{\Phi}_i = [C_i(\xi_0), C_i(\xi_1), C_i(\xi_2), ..., C_i(\xi_{N-1}), C_i(\xi_N)]^T,$
$\mathbf{G}_i = [G_i(\xi_0), G_i(\xi_1), G_i(\xi_2), ..., G_i(\xi_{N-1}), G_i(\xi_N)]^T,$
$\mathbf{H}_i = [H_i(\xi_0), H_i(\xi_1), H_i(\xi_2), ..., H_i(\xi_{N-1}), H_i(\xi_N)]^T,$
$\mathbf{K}_i = [K_i(\xi_0), K_i(\xi_1), K_i(\xi_2), ..., K_i(\xi_{N-1}), K_i(\xi_N)]^T,$
$\mathbf{E}_{j,i-1} = [\zeta_{j,i-1}(\xi_0), \zeta_{j,i-1}(\xi_1), \zeta_{j,i-1}(\xi_2), ..., \zeta_{j,i-1}(\xi_{N-1}), \zeta_{j,i-1}(\xi_N)]^T, j = 1, 2, 3, 4, 5, 6$
$A_{11} = \mathbf{D}^3 + \chi_{11,i-1}\mathbf{D}^2 + \chi_{12,i-1}\mathbf{D} + \chi_{13,i-1}, \quad A_{12} = \mathbf{0}, \quad A_{13} = \mathbf{0},$
$A_{14} = \chi_{14,i-1}\mathbf{D} + \chi_{15,i-1}, \quad A_{15} = \mathbf{0}, \quad A_{16} = \mathbf{0},$
$A_{21} = \chi_{21,i-1}\mathbf{D} + \chi_{22,i-1}, \quad A_{22} = \frac{1}{Pr}\mathbf{D}^2 + \chi_{23,i-1}\mathbf{D}, \quad A_{23} = \mathbf{0},$
$A_{24} = \chi_{24,i-1}, \quad A_{25} = \chi_{25,i-1}, \quad A_{26} = \mathbf{0},$

$$A_{31} = \chi_{31,i-1}\mathbf{D} + \chi_{32,i-1}, \quad A_{32} = \mathbf{0}, \quad A_{33} = \tfrac{1}{Sc}\mathbf{D}^2 + \chi_{33,i-1}\mathbf{D},$$
$$A_{34} = \chi_{34,i-1}, \quad A_{35} = \mathbf{0}, \quad A_{36} = \chi_{35,i-1},$$
$$A_{41} = \chi_{41,i-1}\mathbf{D}^2 + \chi_{42,i-1}\mathbf{D} + \chi_{43,i-1}, \quad A_{42} = \mathbf{0}, \quad A_{43} = \mathbf{0},$$
$$A_{44} = \mathbf{D}^3 + \chi_{44,i-1}\mathbf{D}^2 + \chi_{45,i-1}\mathbf{D} + \chi_{46,i-1}, \quad A_{45} = \mathbf{0}, \quad A_{46} = \mathbf{0},$$
$$A_{51} = \chi_{51,i-1}\mathbf{D} + \chi_{52,i-1}, \quad A_{52} = \chi_{53,i-1}\mathbf{D}, \quad A_{53} = \mathbf{0},$$
$$A_{54} = \chi_{54,i-1}\mathbf{D} + \chi_{55,i-1}, \quad A_{55} = \tfrac{1}{Pr}\mathbf{D}^2 + \chi_{56,i-1}\mathbf{D} + \chi_{57,i-1}, \quad A_{56} = \mathbf{0},$$
$$A_{61} = \chi_{61,i-1}, \quad A_{62} = \mathbf{0}, \quad A_{63} = \chi_{62,i-1}\mathbf{D},$$
$$A_{64} = \chi_{63,i-1}\mathbf{D} + \chi_{64,i-1}, \quad A_{65} = \mathbf{0}, \quad A_{66} = \tfrac{1}{Sc}\mathbf{D}^2 + \chi_{65,i-1}\mathbf{D} + \chi_{66,i-1},$$

Here $\mathbf{I}$ is an identity matrix of size (N +1)×(N +1). After modifying the matrix system (3.20) to incorporate boundary conditions, the solution is obtained as

$$\mathbf{X}_i = \mathbf{A}_{i-1}^{-1}\mathbf{R}_{i-1} \tag{3.22}$$

3.2.4 Result and Discussion

The results of the present problem have been compared with works of Magyari and Keller [56] as a special case by taking $S = 0$, $J = 0$, $\lambda = 0$, $H_a = 0$, $x = 0$, and $Bi \to \infty$ and found that they are in good agreement, as shown in Table. (3.1). To study the effects of Joule heating parameter J, suction/injection parameter S, Biot number Bi, magnetic parameter H_a and velocity slip parameter λ, computations have been carried out taking $S = 0.5$, $J = 0.2$, $\lambda = 1.0$, $H_a = 1.0$, $x = 0.3$, and $Bi = 1.0$ unless otherwise mentioned.

The influence of slip parameter λ on the velocity, skin-friction, temperature, concentration and the rate of heat and mass transfer is portrayed through the (3.2(a)) - (3.2(f)) by taking $S = 0.5$, $J = 0.2$, $H_a = 1.0$, $x = 0.3$, and $Bi = 1.0$. It is evident from the Figs. (3.2(a)) and (3.2(b)) that raise in the slip parameter diminishes the fluid velocity and enhanaces the skin-friction. From figures (3.2(c)) and (3.2(d)), it is witnessed that the temperature and rate of heat transfer are increasing with λ. The concentration of the fluid is increasing and the rate of mass transfer is diminishing with the enhancement in λ as shown in the Figs.

Table 3.1: *Comparative analysis for* $\frac{Nu_x}{\sqrt{Lx/2}\sqrt{Re_x}}$ *by the current method for* $\lambda = 0$, $J = 0$, $H_a = 0$, $x = 0$, $S = 0$ *and* $Bi \to \infty$.

Nusselt number $\frac{Nu_x}{\sqrt{Lx/2}\sqrt{Re_x}}$		
Pr	Magyari and Keller [56]	Present
0.5	0.330493	0.33053766
1	0.549643	0.54964345
3	1.122188	1.12208577
5	1.521243	1.52123668
8	1.991847	1.99183375
10	2.257429	2.25741862

(3.2(e)) and (3.2(f)). The mass transfer rate is maximum, in the absence of slip parameter. Further, the impact of x on the skin-friction and the mass transfer rate is negligible.

The changes of the velocity, the skin-friction, the temperature, the rate of heat transfer, the concentration and the rate of mass transfer for fixed values of $S = 0.5$, $J = 0.2$, $\lambda = 1.0$, $x = 0.3$, and $Bi = 1.0$ and varying magnetic parameter H_a are presented in the Figs. (3.3(a)) - (3.3(f)) f. Due to magnetic field effect both the velocity and skin-friction are decreasing as shown in the Figs. (3.3(a)) and (3.3(b)). Applying the uniform magnetic field normal to the flow direction gives rise to Lorentz force. This force has the tendency to slow down the velocity of the fluid in the boundary layer. Hence, the velocity and skin-friction diminish with the enhancement in H_a. It is seen from the figure (3.3(c)) and (3.3(d)) that the temperature enhances slightly and the rate of heat transfer reduces with an increase in the value of H_a. Further, in the absence of magnetic field maximum heat exchange is taking place. Figures (3.3(e)) and (3.3(f)) depict that the concentration is enhancing and the rate of mass transfer is reducing with an increase in the value of H_a. Finally, it is noticed that, the rate of heat transfer is reducing with an increase in x.

For fixed values of $J = 0.2$, $\lambda = 1.0$, $H_a = 1.0$, $x = 0.3$, and $Bi = 1.0$, the variations of F', $F''(x, 0)$, T, $-T'(x, 0)$, C and $-C'(x, 0)$ with suction/injection parameter S are displayed in the Figs. (3.4(a)) - (3.4(f)). It is demonstrated from the Fig. (3.4(a)) that F' is diminishing with a rise in S. It is depicted from the Fig. (3.4(b)) that $F''(x, 0)$ decreases with an enhancement in the value of suction parameter. Figure (3.4(c)) displays that the temperature

profile reduces with an increment in the value of the suction parameter and increases with an increase in the value of injection parameter. While, a reverse trend is observed on the rate of heat transfer as shown in the Fig. (3.4(d)). Therefore, there is a maximum, heat transfer from the sheet to the fluid. Figures (3.4(e)) and (3.4(f)) narrate the variation of the concentration and rate of mass transfer. It is obvious from the figures that the same observations may be seen as that of the temperature and rate of heat transfer.

The effect of Joule heating parameter J taking the fixed values for $S = 0.5$, $\lambda = 1.0$, $H_a = 1.0$, $x = 0.3$, and $Bi = 1.0$ on the temperature and the rate of heat transfer is presented in the Figs. (3.5(a)) and (3.5(b)). As the effect of J on velocity, skin-friction, concentration and mass transfer are almost negligible, the corresponding graphs are not presented for brevity. The temperature is slightly increased and the rate of heat transfer is decreased with an increase in the value of J. It is observed that, in the absence of Joule heating parameter ($J = 0$), the effect of non-similar variable x on the rate of heat transfer is minimal and heat transfer rate is maximum.

Figures (3.6(a)) and (3.6(b)) show the variation of temperature and rate of heat transfer with Biot number Bi by taking $S = 0.5$, $J = 0.2$, $\lambda = 1.0$, $H_a = 1.0$ and $x = 0.3$. It is obvious that the temperature is increasing with the increase in Biot number. For larger values of Bi, equation (3.10) implies $T(0) \to 1$ which is clearly shown in the Fig. (3.6(a)). Increasing the value of Biot number, the heat transfer coefficient is enhanced predominantly on the surface due to the strong convection as shown in the Fig. (3.6(b)). Further, the rate of heat transfer is slightly reduced with x.

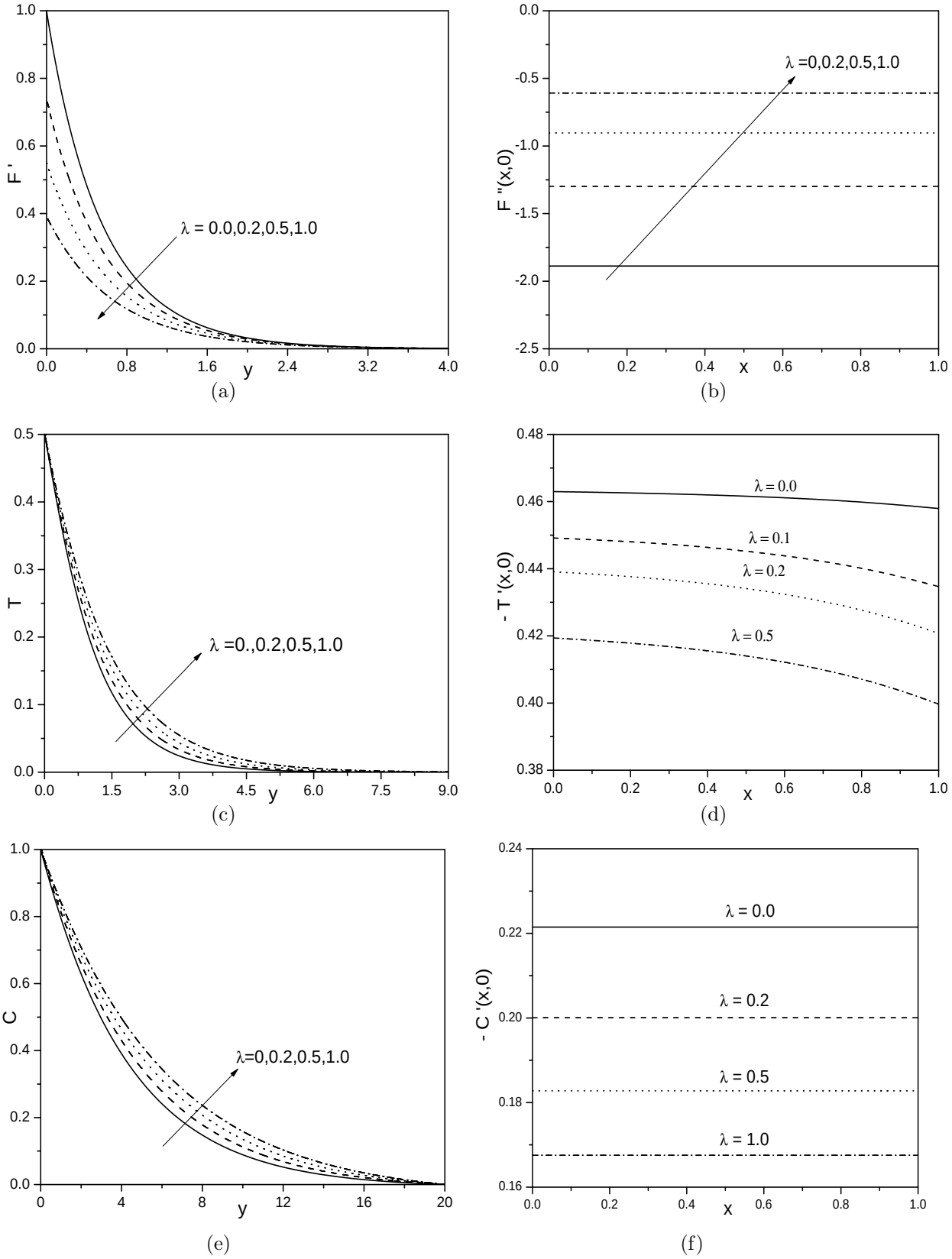

Figure 3.2: *Effect of* λ *on (a)* F'*, (b)* $F''(x,0)$*, (c)* T*, (d)* $-T'(x,0)$*, (e)* C *and (f)* $-C'(x,0)$

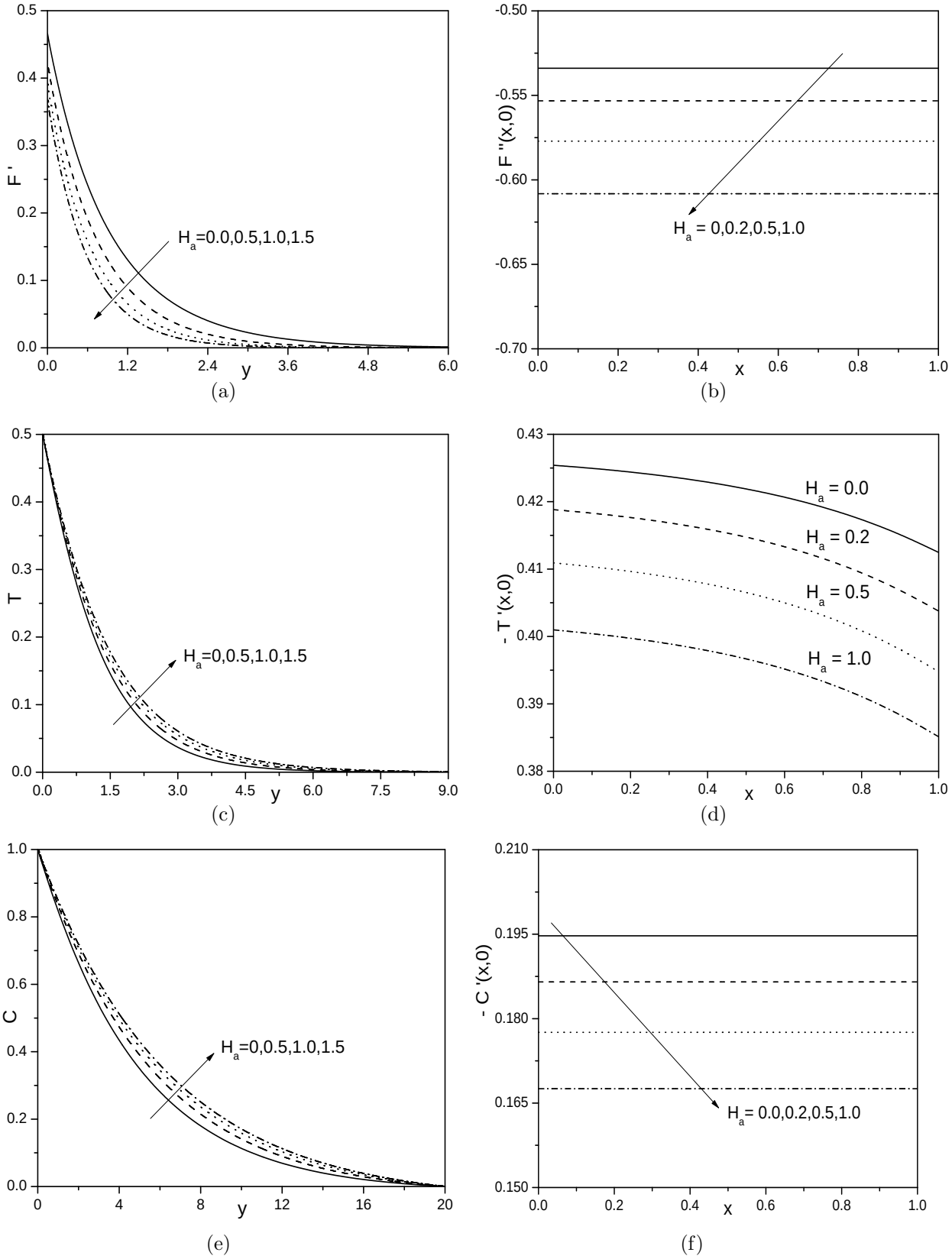

Figure 3.3: *Effect of H_a on (a) F', (b) $F''(x,0)$, (c) T, (d) $-T'(x,0)$, (e) C and (f) $-C'(x,0)$*

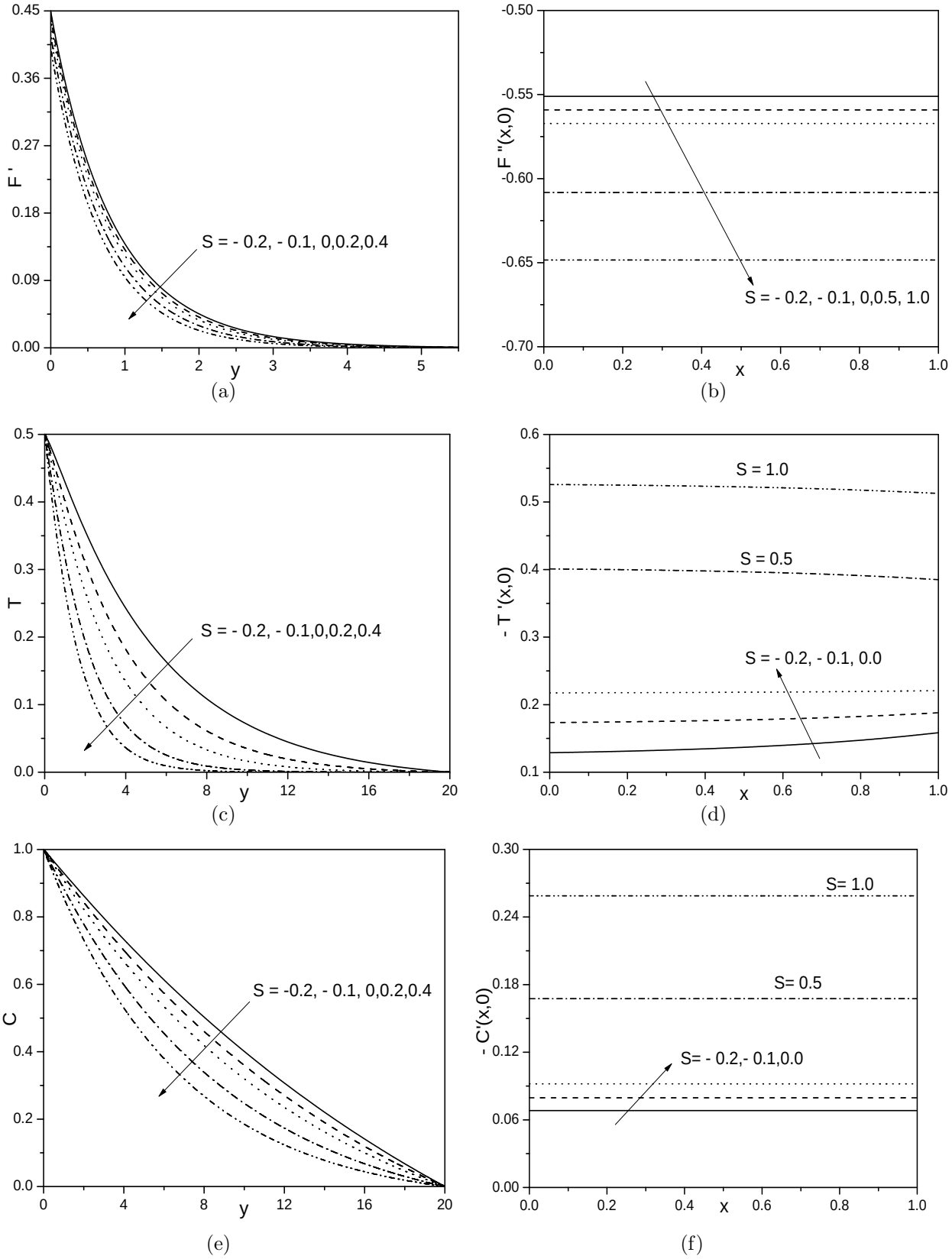

Figure 3.4: *Effect of S on (a) F', (b) $F''(x,0)$, (c) T, (d) $-T'(x,0)$, (e) C and (f) $-C'(x,0)$*

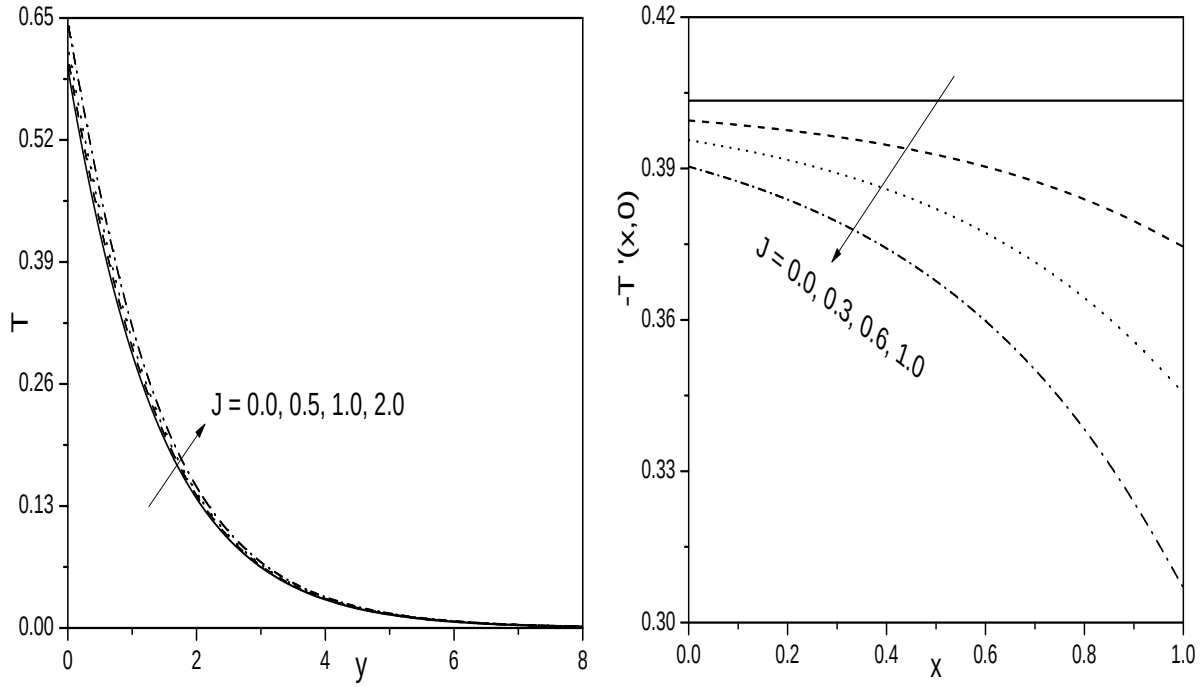

(a) (b)

Figure 3.5: *Effect of J on (a) T and (b) $-T'(x,0)$*

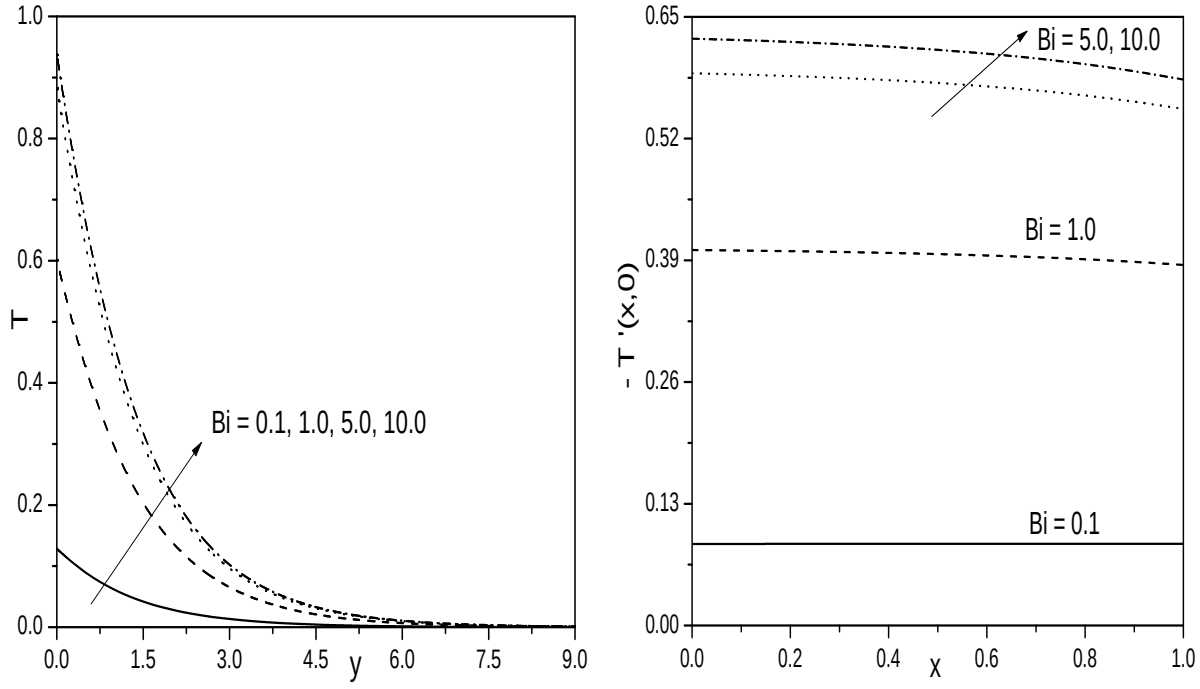

(a) (b)

Figure 3.6: *Effect of Bi on (a) T, and (b) $-T'(x,0)$*

3.2.5 Case(b): Uniform wall temperature with Hall effect

In addition to the applied magnetic field of strength $B(\tilde{x})$, here we consider the Hall current in view of relatively high electron-atom collision frequency. This assumption causes a cross flow in the $\tilde{z}$-direction, therefore the flow becomes three dimensional. Further, it is assumed that the sheet is maintained at uniform wall temperature and concentration $T_w(\tilde{x})$ and $C_w(\tilde{x})$, respectively. Under the Boussinesq approximation, the flow is governed by the equations (3.1), (3.4) along with the following momentum and energy equations

$$\tilde{u}_x\frac{\partial\tilde{u}_x}{\partial\tilde{x}}+\tilde{u}_y\frac{\partial\tilde{u}_x}{\partial\tilde{y}}=\nu\frac{\partial^2\tilde{u}_x}{\partial\tilde{y}^2}+g\ \beta_T(\tilde{T}-T_\infty)+g\ \beta_C(\tilde{C}-C_\infty)-\frac{\sigma B^2}{\rho(1+\beta_h^2)}(\tilde{u}_x+\beta_h\tilde{u}_z) \quad (3.23)$$

$$\tilde{u}_x\frac{\partial\tilde{u}_z}{\partial\tilde{x}}+\tilde{u}_y\frac{\partial\tilde{u}_z}{\partial\tilde{y}}=\nu\frac{\partial^2\tilde{u}_z}{\partial\tilde{y}^2}+\frac{\sigma B^2}{\rho(1+\beta_h^2)}(\beta_h\tilde{u}_x-\tilde{u}_z) \quad (3.24)$$

$$\tilde{u}_x\frac{\partial\tilde{T}}{\partial\tilde{x}}+\tilde{u}_y\frac{\partial\tilde{T}}{\partial\tilde{y}}=\alpha\frac{\partial^2\tilde{T}}{\partial\tilde{y}^2}+\frac{\sigma B^2}{\rho c_p(1+\beta_h^2)}(\tilde{u}_x^2+\tilde{u}_z^2) \quad (3.25)$$

$\tilde{u}_z$ is the velocity in $\tilde{z}$-direction.

The boundary conditions are

$$\left.\begin{array}{l}\tilde{u}_x=U_*+N_*\nu\frac{\partial\tilde{u}_x}{\partial\tilde{y}},\ \tilde{u}_y=-V_*(\tilde{x}),\ \tilde{u}_z=0,\\ T_w=T_\infty+T_0e^{\frac{2\tilde{x}}{L}},\ C_w=C_\infty+C_0e^{\frac{2\tilde{x}}{L}}\quad\text{at}\quad\tilde{y}=0\\ \tilde{u}_x\to0,\ \tilde{u}_z\to0,\ \tilde{T}\to T_\infty,\ \tilde{C}\to C_\infty\ \text{ as }\ \tilde{y}\to\infty\end{array}\right\} \quad (3.26)$$

Substituting the following similarity transformations

$$\left.\begin{array}{l}\tilde{y}=y\sqrt{\frac{2\nu L}{U_0}}e^{\frac{-\tilde{x}}{2L}},\ \psi=\sqrt{2\nu LU_0}e^{\frac{\tilde{x}}{2L}}F,\\ \tilde{u}_x=U_0e^{\frac{\tilde{x}}{L}}F',\quad\tilde{u}_y=-\sqrt{\frac{\nu U_0}{2L}}\ e^{\frac{\tilde{x}}{2L}}(F+yF'),\quad\tilde{u}_z=U_0e^{\frac{\tilde{x}}{L}}W\\ \tilde{T}=T_\infty+T_0\ e^{\frac{2\tilde{x}}{L}}T,\ \tilde{C}=C_\infty+C_0\ e^{\frac{2\tilde{x}}{L}}C\end{array}\right\} \quad (3.27)$$

into the Eqs. (3.1), (3.23), (3.24), (3.25), and (3.4)

$$F''' + FF'' - 2F'^2 + 2Ri(T + \mathbb{B}C) - \frac{H_a}{1+\beta_h^2}(F' + \beta_h W) = 0 \tag{3.28}$$

$$W'' - 2F'W + FW' + \frac{H_a}{1+\beta_h^2}(\beta_h F' - W) = 0 \tag{3.29}$$

$$\frac{1}{Pr}T'' + FT' - 4F'T + \frac{J}{1+\beta_h^2}\left(F'^2 + W^2\right) = 0 \tag{3.30}$$

$$\frac{1}{Sc}C'' + FC' - 4F'C = 0 \tag{3.31}$$

The conditions (3.26) reduce to

$$\left.\begin{array}{l} F(y) = S,\ F'(y) = 1 + \lambda F''(y),\ W(y) = 0,\ T(y) = 1,\ C(y) = 1 \ \text{ at } \ y = 0 \\ F'(y) \to 0,\ W(y) \to 0,\ T(y) \to 0,\ C(y) \to 0 \ \text{ as } \ y \to \infty \end{array}\right\} \tag{3.32}$$

where $J = \frac{2L\sigma B_0^2 U_0}{\rho c_p T_0}$ is the Joule heating parameter.

3.2.6 Skin Friction in $\tilde{x}$ and $\tilde{z}$-directions, Heat and Mass Transfer Coefficients

The non-dimensional skin friction in $\tilde{x}-$direction $C_{F\tilde{x}}$, local skin-friction in $\tilde{z}-$direction $C_{F\tilde{z}}$, the local Nusselt number $Nu_{\tilde{x}}$ and the local Sherwood number $Sh_{\tilde{x}}$, are given by

$$\left.\begin{array}{l} \frac{\sqrt{Re_x}}{\sqrt{2\tilde{x}/L}}C_{F\tilde{x}} = F''(0), \quad \frac{\sqrt{Re_x}}{\sqrt{2\tilde{x}/L}}C_{F\tilde{z}} = W'(0), \\ \frac{Nu_{\tilde{x}}}{\sqrt{\tilde{x}/2L}\sqrt{Re_{\tilde{x}}}} = -T'(0), \quad \text{and} \quad \frac{Sh_{\tilde{x}}}{\sqrt{\tilde{x}/2L}\sqrt{Re_{\tilde{x}}}} = -C'(0). \end{array}\right\} \tag{3.33}$$

where $Re_{\tilde{x}} = \dfrac{\tilde{x}U_*(\tilde{x})}{\nu}$ is the local Reynold's number.

3.2.7 Solution of the Problem

The system of Eqs. (3.28) - (3.31) along with the boundary conditions (3.32), is solved numerically, using the successive linearisation method as explained in Chapter-2.

Proceeding as in Chapter-2, we obtain the following matrix equation

$$\mathbf{A}_{i-1}\mathbf{X}_i = \mathbf{R}_{i-1}, \tag{3.34}$$

subject to the boundary conditions

$$F_i(\xi_N) = \sum_{k=0}^{N} \mathbf{D}_{0k} F_i(\xi_k) = \sum_{k=0}^{N} (\lambda \mathbf{D}2_{Nk} - \mathbf{D}_{Nk}) F_i(\xi_k) = 0 \tag{3.35a}$$

$$W_i(\xi_N) = W_i(\xi_0) = T_i(\xi_N) = T_i(\xi_0) = C_i(\xi_N) = C_i(\xi_0) = 0 \tag{3.35b}$$

In Eq.(3.34), $\mathbf{A}_{i-1}$ is a (4N + 4)×(4N + 4) square matrix and $\mathbf{X}_i$ and $\mathbf{R}_{i-1}$ are (4N + 4)×1 column vectors defined by

$$\mathbf{A}_{i-1} = [A_{rs}], r, s = 1, 2, 3, 4, \quad \mathbf{X}_i = \begin{bmatrix} \mathbf{F}_i \\ \mathbf{W}_i \\ \mathbf{\Theta}_i \\ \mathbf{\Phi}_i \end{bmatrix}, \quad \mathbf{R}_{i-1} = \begin{bmatrix} \mathbf{E}_{1,i-1} \\ \mathbf{E}_{2,i-1} \\ \mathbf{E}_{3,i-1} \\ \mathbf{E}_{4,i-1} \end{bmatrix} \tag{3.36}$$

where

$$\mathbf{F}_i = [F_i(\xi_0), F_i(\xi_1), F_i(\xi_2), ..., F_i(\xi_{N-1}), F_i(\xi_N)]^T,$$
$$\mathbf{W}_i = [W_i(\xi_0), W_i(\xi_1), W_i(\xi_2), ..., W_i(\xi_{N-1}), W_i(\xi_N)]^T,$$
$$\mathbf{\Theta}_i = [T_i(\xi_0), T_i(\xi_1), T_i(\xi_2), ..., T_i(\xi_{N-1}), T_i(\xi_N)]^T,$$
$$\mathbf{\Phi}_i = [C_i(\xi_0), C_i(\xi_1), C_i(\xi_2), ..., C_i(\xi_{N-1}), C_i(\xi_N)]^T,$$
$$\mathbf{E}_{1,i-1} = [\zeta_{1,i-1}(\xi_0), \zeta_{1,i-1}(\xi_1), \zeta_{1,i-1}(\xi_2), ..., \zeta_{1,i-1}(\xi_{N-1}), \zeta_{1,i-1}(\xi_N)]^T$$
$$\mathbf{E}_{2,i-1} = [\zeta_{2,i-1}(\xi_0), \zeta_{2,i-1}(\xi_1), \zeta_{2,i-1}(\xi_2), ..., \zeta_{2,i-1}(\xi_{N-1}), \zeta_{2,i-1}(\xi_N)]^T$$
$$\mathbf{E}_{3,i-1} = [\zeta_{3,i-1}(\xi_0), \zeta_{3,i-1}(\xi_1), \zeta_{3,i-1}(\xi_2), ..., \zeta_{3,i-1}(\xi_{N-1}), \zeta_{3,i-1}(\xi_N)]^T$$
$$\mathbf{E}_{4,i-1} = [\zeta_{4,i-1}(\xi_0), \zeta_{4,i-1}(\xi_1), \zeta_{4,i-1}(\xi_2), ..., \zeta_{4,i-1}(\xi_{N-1}), \zeta_{4,i-1}(\xi_N)]^T$$

Table 3.2: *Comparison of* $-F''(0)$ *and* $F(\infty)$ *calculated by the present method for* $S = 0$, $\lambda = 0$, $H_a = 0$, *and* $Ri = 0$.

	Magyari and Keller [56]	Present
$-F''(0)$	1.281808	1.28180856
$F(\infty)$	0.905639	0.90564370

$$A_{11} = \mathbf{D}^3 + \chi_{11,i-1}\mathbf{D}^2 + \chi_{12,i-1}\mathbf{D} + \chi_{13,i-1}, \quad A_{12} = -\tfrac{H_a\beta_h}{1+\beta_h^2}\mathbf{I}, \quad A_{13} = 2Ri\mathbf{I}, \quad A_{14} = 2\mathbb{B}Ri\mathbf{I}$$
$$A_{21} = \chi_{21,i-1}\mathbf{D} + \chi_{22,i-1}, \quad A_{22} = \mathbf{D}^2 + \chi_{23,i-1}\mathbf{D} + \chi_{24,i-1}, \quad A_{23} = \mathbf{0}, \quad A_{24} = \mathbf{0}$$
$$A_{31} = \chi_{31,i-1}\mathbf{D} + \chi_{32,i-1}, \quad A_{32} = \chi_{33,i-1}, \quad A_{33} = \tfrac{1}{Pr}\mathbf{D}^2 + \chi_{34,i-1}\mathbf{D} + \chi_{35,i-1}, \quad A_{34} = \mathbf{0}$$
$$A_{41} = \chi_{41,i-1}\mathbf{D} + \chi_{42,i-1}, \quad A_{42} = \mathbf{0}, \quad A_{43} = \mathbf{0}, \quad A_{44} = \tfrac{1}{Sc}\mathbf{D}^2 + \chi_{43,i-1}\mathbf{D} + \chi_{44,i-1}$$

Here $\mathbf{I}$ is an identity matrix of size (N +1)×(N +1). After modifying the matrix system (3.34) to incorporate boundary conditions (3.35), the solution is obtained as

$$\mathbf{X}_i = \mathbf{A}_{i-1}^{-1}\mathbf{R}_{i-1} \tag{3.37}$$

3.2.8 Results and Discussion

The results of the present problem are compared with that of the results obtained by Magyari and Keller [56] as a special case by taking $Ri = 0$, $H_a = 0$, $S = 0$, $\lambda = 0$, and $J = 0$ and found that they are in good agreement, as presented in Table (3.2). The computations have been carried out in the cases of $Ri = 1.0$, $\mathbb{B} = 0.5$, $S = 0.5$, $\lambda = 1.0$, $\beta_h = 2.0$, $H_a = 1.0$, and $J = 0.3$.

Figures (3.7(a)) - (3.7(d)) indicate the effect of the suction/injection parameter S on both the velocity components $F'(y)$ and $W(y)$, temperature $T(y)$ and concentration $C(y)$. From these figures it is noticed that all the physical quantities are decreasing with an enhancement in S. It is known that applying the wall suction have the propensity to lessen both the momentum and thermal boundary layer thickness.

The influence of the Hall parameter β_h on both the velocities, temperature and concentration is depicted in Figs. (3.8(a)) - (3.8(d)). From Fig. (3.8(a)), it is observed that the tangential velocity increases with the increasing values of the Hall parameter β_h. Figure (3.8(c)) reveals that the temperature decreases with the increasing values of β_h. As the Hall parameter β_h increases, the effective conductivity reduces which in turn reduces the magnetic damping force on the tangential velocity. Hence, the tangential velocity increases and temperature decreases with an increase in the Hall parameter. Figure (3.8(b)) shows that the cross flow velocity increases with an increase in the value of β_h. Further, it is observed that the cross flow velocity first increases gradually with β_h, attaining an extreme value and then drops to zero. From Fig. (3.8(d)), it is noticed that the concentration decreases with the increasing values of β_h.

Figures (3.9(a)) - (3.9(d)) exhibit the influence of the magnetic parameter H_a on both the velocities, the temperature and the concentration. It is seen from Fig. (3.9(a)) that the tangential velocity is decreasing with an increase in the value of the magnetic parameter H_a. Applying the uniform magnetic field normal to the flow direction gives rise to Lorentz force. This force has the tendency to slow down the velocity of the fluid in the boundary layer. Hence, the velocity diminishes with an enhancement in H_a. From Fig. (3.9(b)), it is seen that there is no cross flow velocity in the absence of the magnetic field ($H_a = 0$) and it increases gradually with an increase of H_a. Hence, for large values of H_a, a cross-flow is generated due to the Hall effect. This is clearly depicted in the Fig. (3.9(b)). From Figs. (3.9(c)) and (3.9(d)), it is evident that the temperature and concentration are increasing with the increasing values of H_a.

The impact of the mixed convection parameter Ri on $F'(y)$, $W(y)$, $T(y)$ and $C(y)$ is depicted in the Figs.(3.10(a)) (3.10(d)). From the Fig. (3.10(a)), it is seen that the tangential velocity increases with an increase in the values of Ri. This is because, the positive values of Ri induces a favorable pressure gradient which, in turn, increases the fluid flow in the boundary layer. The same trend is observed for the cross-flow velocity component as shown in Fig. (3.10(b)). From the Figs. (3.10(c)) and (3.10(d)), it is noticed that both the temperature and concentration are decreasing with the increasing the values of Ri. This is

due to the fact that positive values of Ri accelerate the fluid and which results in decreasing both the thermal and concentration boundary layers.

The variation of the heat and mass transfer rates with varying values of the Joule heating parameter J is presented in the Figs. (3.11(a)) and (3.11(b)). Due to Joule heating, the heat transfer from the sheet to the fluid is decreasing and the mass transfer at the surface of stretching is increasing. The effect of Hall parameter β_h on the rate of heat and mass transfers are shown in the Figs. (3.12(a)) and (3.12(b)). It is noticed from the figures that, the rate of heat and mass transfers are increasing with an increase in β_h, The increase in the rate of mass transfer is more than the increase in the rate of heat transfer. The variation of heat and mass transfer rates with the magnetic parameter H_a is presented in the Figs. (3.13(a)) and (3.13(b)). These figures describe that the heat transfer rate is reducing with the increasing values of H_a. The same trend is observed for the mass transfer rate also. The decrease in the mass transfer rate is low when compared to that heat transfer rate as shown in the Fig. (3.13(b)). The effect of the mixed convection parameter Ri on both the heat and mass transfer coefficients is shown in the Figs. (3.14(a)) and (3.14(b)). These figures indicate that the heat and mass transfer rates are rising with the increasing values of the Ri.

The values of local skin-friction coefficients in $\tilde{x}$-direction ($F''(0)$) and $\tilde{z}$-direction ($W'(0)$) are presented in Table (3.3) for various values of β_h, H_a, Ri, and J. It is seen from the table that, both the skin-friction increase with an increase the Hall parameter β_h. Further, it is observed that there is no transverse velocity and hence no skin-friction in $\tilde{z}$-direction in the absence of Hall parameter. The skin-friction in $\tilde{x}$-direction reduces and in $\tilde{z}$-direction enhances as H_a increase. In the absence of magnetic field, there is no cross flow velocity and in turn, there is no skin-friction in $\tilde{z}$-direction. Further, It is noticed that both the skin-friction increase as the values of the mixed convection parameter Ri and the Joule heating parameter J increases.

Table 3.3: *Variation of skin friction in $\tilde{x}$- and $\tilde{z}$-directions for varying values of Hall parameter β_h, magnetic parameter H_a, mixed convection parameter Ri, and Joule heating parameter J.*

β_h	H_a	Ri	J	$F''(0)$	$W'(0)$
0.0	1.0	1.0	0.3	-0.24296611	0.00000000
0.1	1.0	1.0	0.3	-0.24222539	0.04374048
0.5	1.0	1.0	0.3	-0.22726487	0.18816680
2.0	1.0	1.0	0.3	-0.16656763	0.24358744
2.0	0.0	1.0	0.3	-0.13678548	0.00000001
2.0	0.1	1.0	0.3	-0.13940455	0.02720645
2.0	1.0	1.0	0.3	-0.16656763	0.24358744
2.0	3.0	1.0	0.3	-0.23488654	0.56845554
2.0	1.0	-0.1	0.3	-0.63795469	0.02350794
2.0	1.0	-0.05	0.3	-0.59542168	0.05461319
2.0	1.0	0.0	0.3	-0.55832267	0.10101136
2.0	1.0	1.0	0.3	-0.16656763	0.24358744
2.0	1.0	3.0	0.3	0.28412908	0.32157171
2.0	1.0	1.0	0.0	-0.16781391	0.24316904
2.0	1.0	1.0	0.2	-0.16698415	0.24344783
2.0	1.0	1.0	0.5	-0.16573129	0.24386710
2.0	1.0	1.0	1.0	-0.16362106	0.24456874

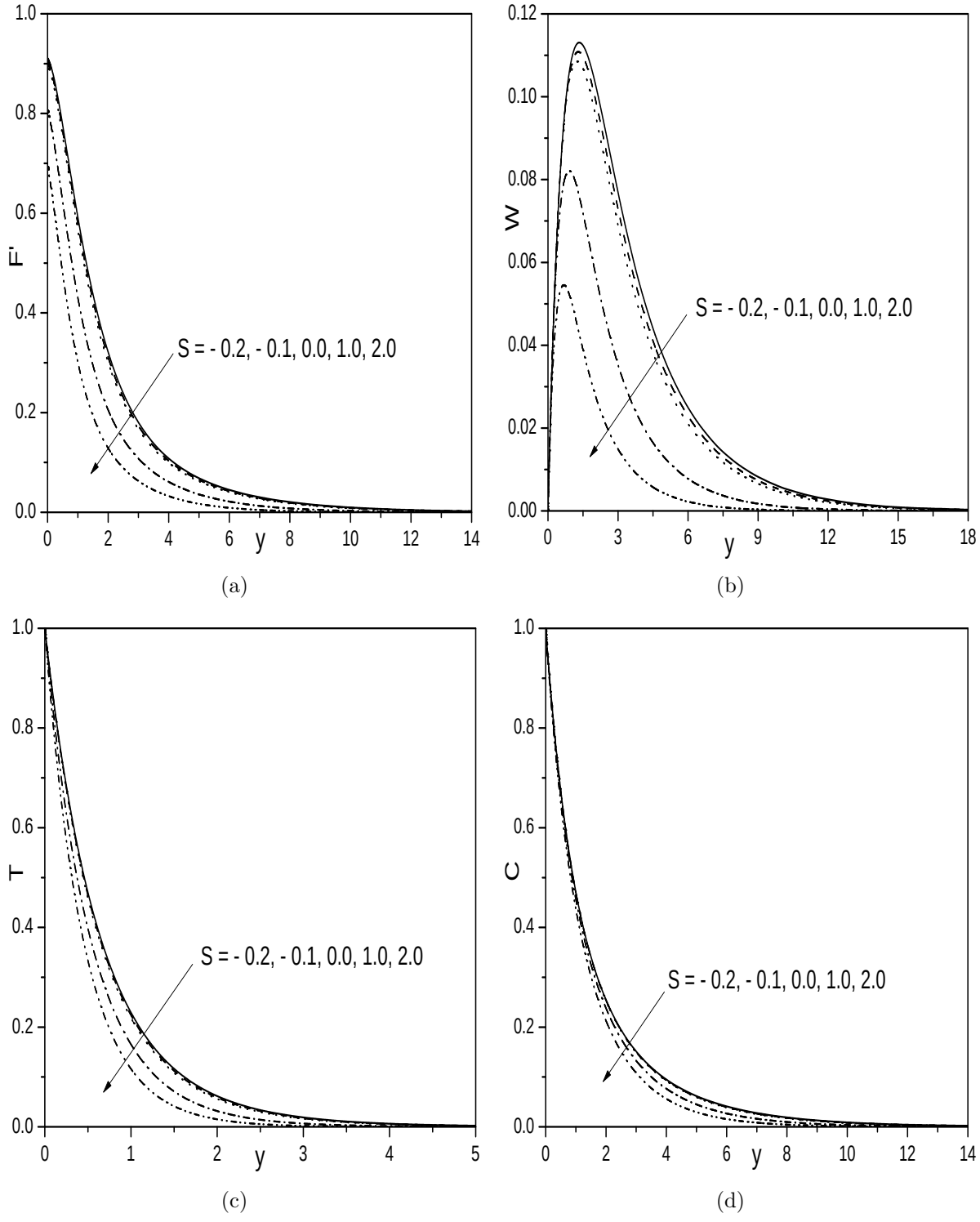

Figure 3.7: *Effect of S on (a)Velocity, (b)transverse velocity, (c)Temperature, and (d)Concentration profiles.*

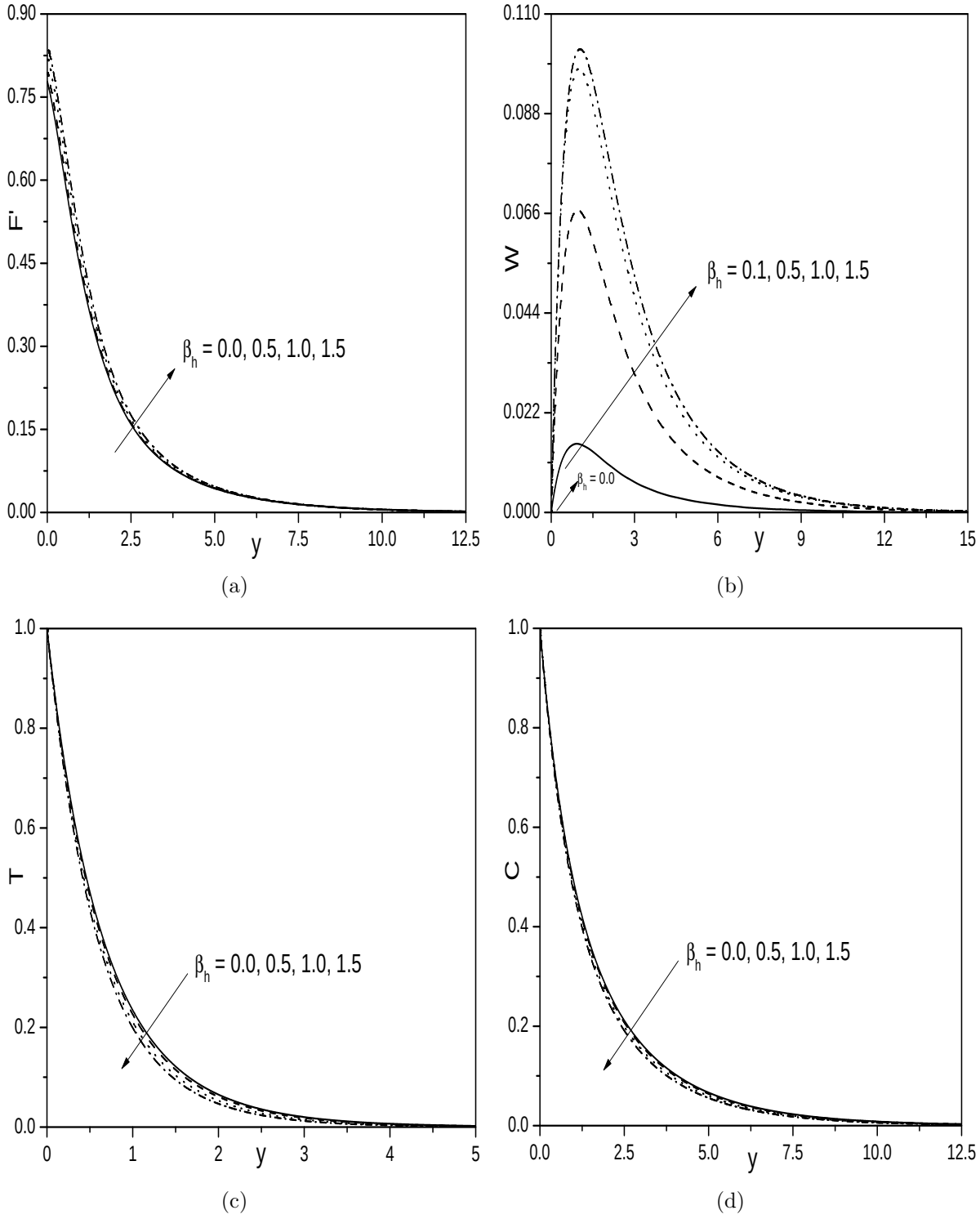

Figure 3.8: *Effect of β_h on (a)Velocity, (b)transverse velocity, (c)Temperature, and (d)Concentration profiles.*

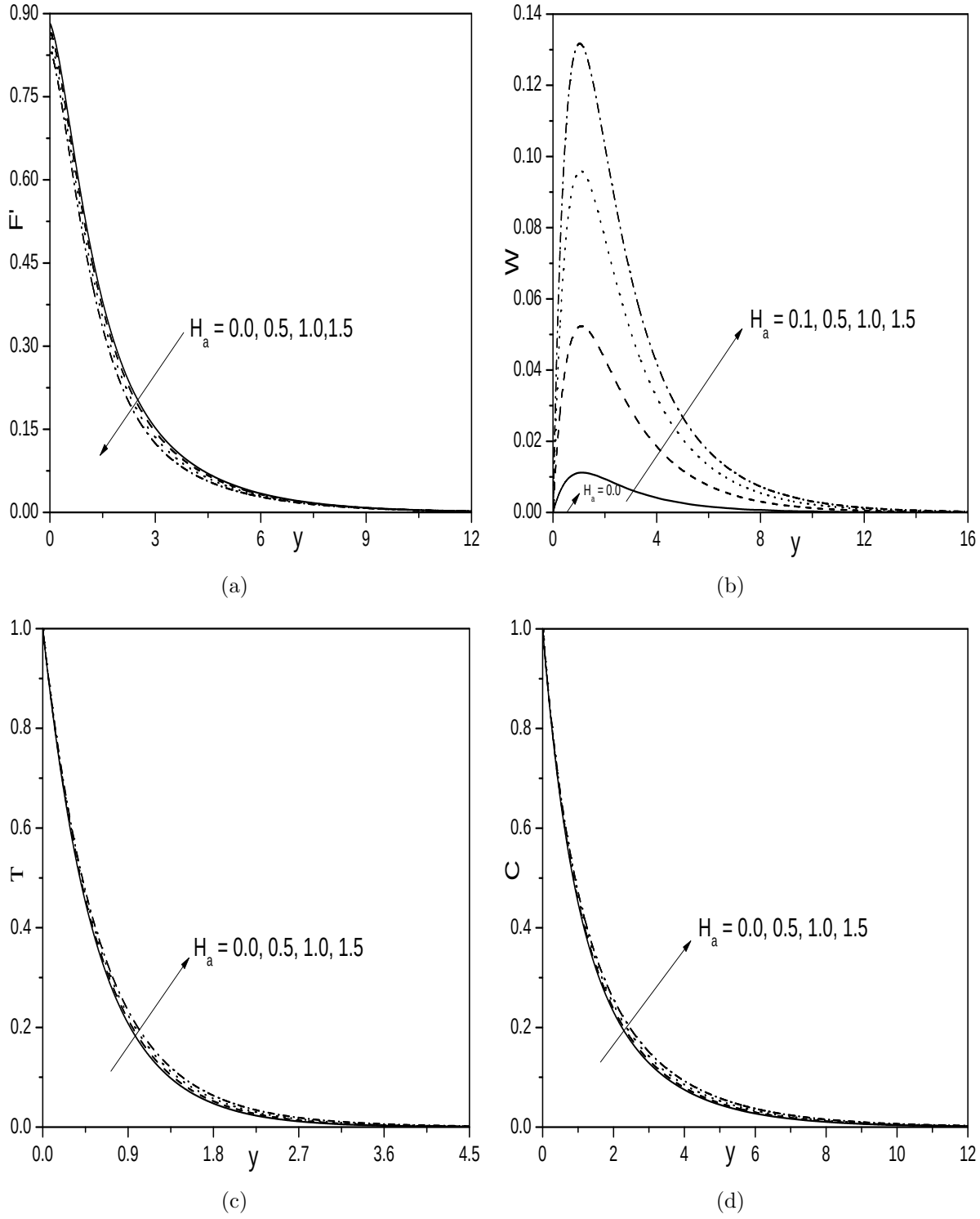

Figure 3.9: *Effect of H_a on (a)Velocity, (b)transverse velocity, (c)Temperature, and (d)Concentration profiles.*

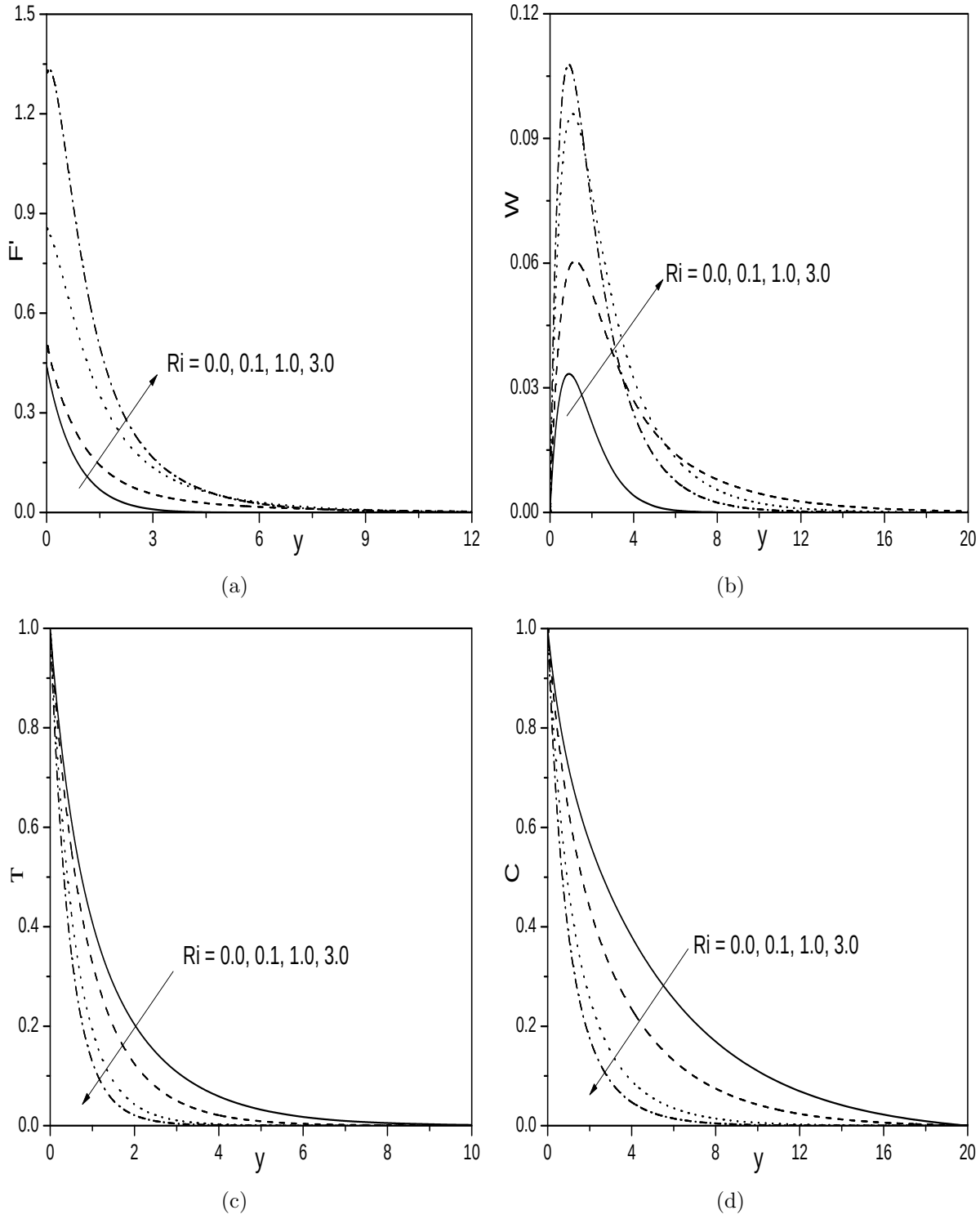

Figure 3.10: *Effect of Ri on (a)Velocity, (b)transverse velocity, (c)Temperature, and (d)Concentration profiles.*

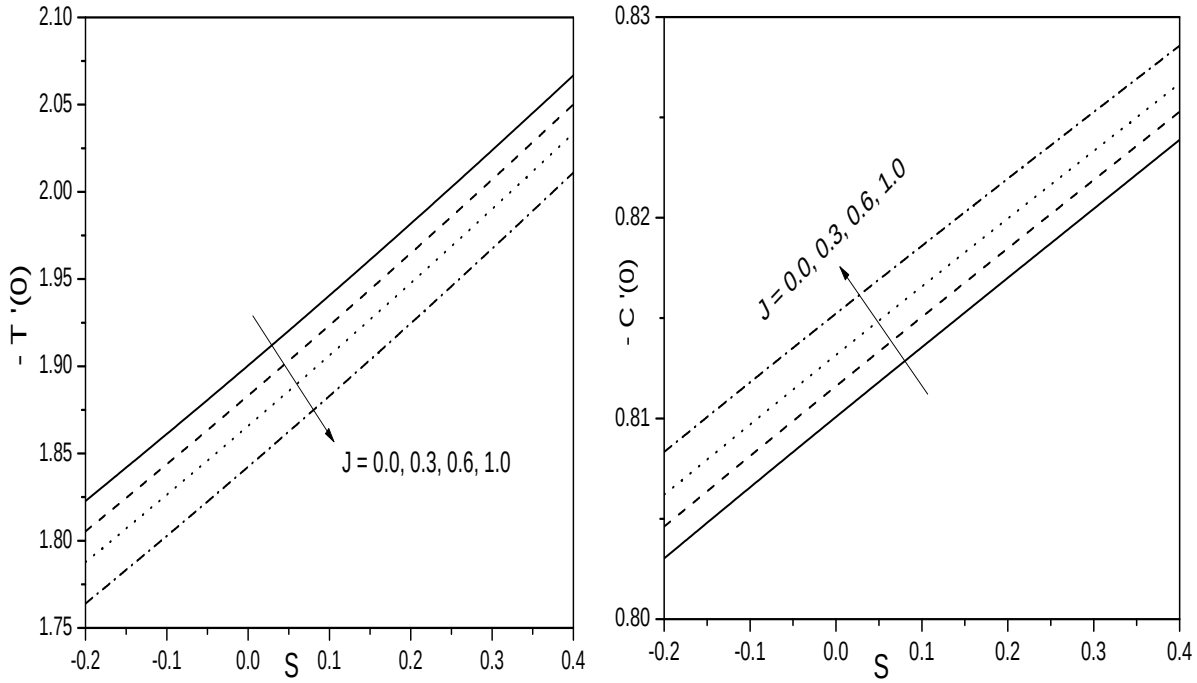

(a) (b)

Figure 3.11: *Effect of J on (a) $-T'(0)$, and (b) $-C'(0)$.*

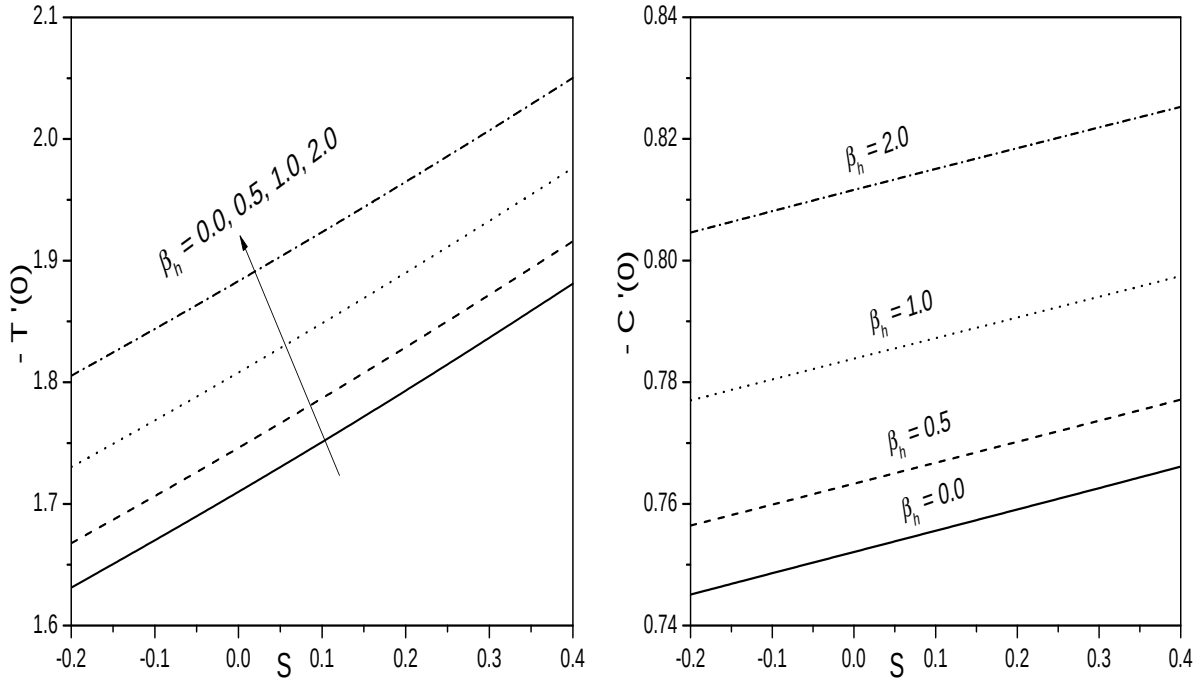

(a) (b)

Figure 3.12: *Effect of β_h on (a) $-T'(0)$, and (b) $-C'(0)$.*

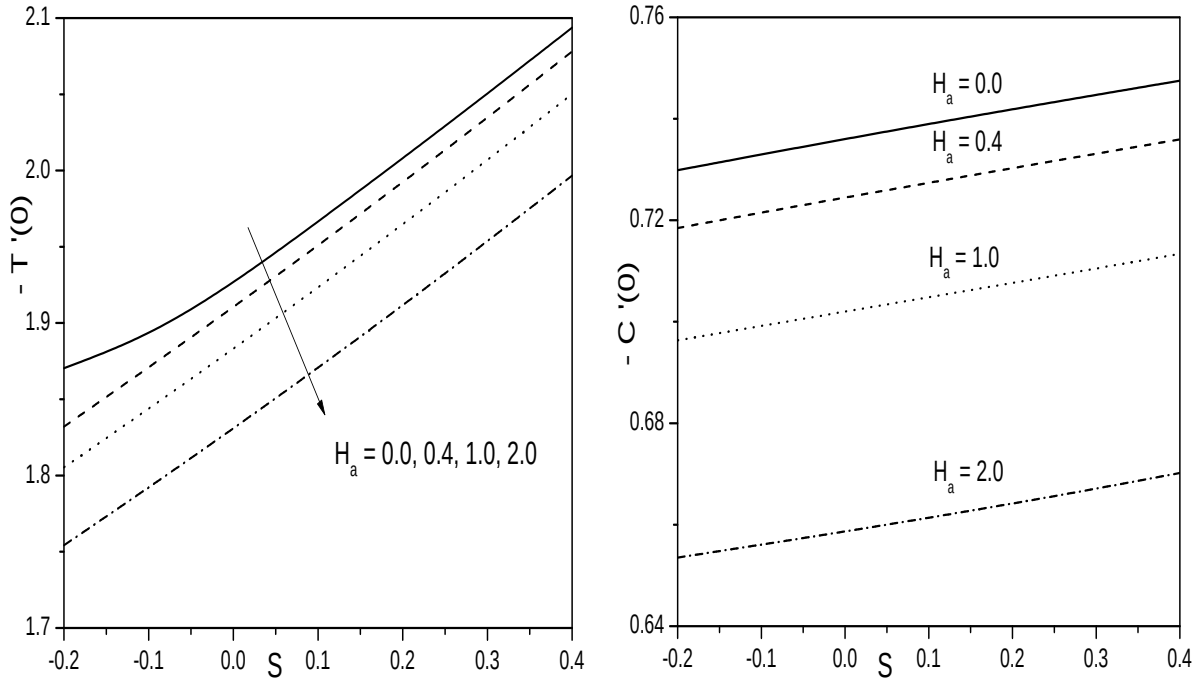

(a) (b)

Figure 3.13: *Effect of H_a on (a) $-T'(0)$, and (b) $-C'(0)$.*

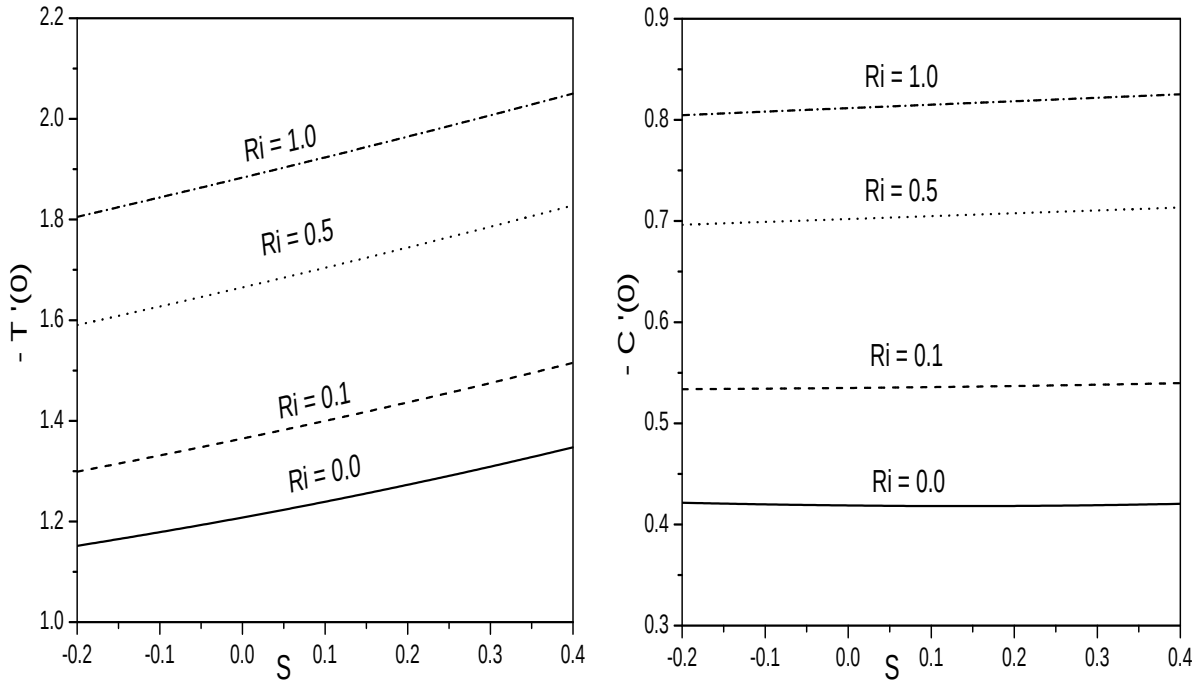

(a) (b)

Figure 3.14: *Effect of Ri on (a) $-T'(0)$, and (b) $-C'(0)$.*

3.3 Conclusions

In this chapter, the effect of Joule heating on the heat and mass transfer process due to laminar slip flow of electrically conducting incompressible viscous fluid over an exponentially stretching permeable sheet is studied for two cases namely (a) subjected to thermal convective boundary condition and (b) uniform wall temperature with Hall effect.

The velocity, temperature, and concentration of the fluid decrease for both the cases (a) and (b) with an increase in the fluid suction. Also, in case (b), the transverse velocity decreases with an increase in the suction. In both the cases, an increase in the value of the magnetic parameter H_a, the velocity reduces and temperature and concentration increases. While the transverse velocity of the fluid in case (b) enhances with an increase in the value of H_a. In case (b) both the velocities increases and temperature and concentration decreases with an increase in the value of the Hall parameter. The temperature of the fluid in case (a) increases with an increase in the Joule heating parameter and there is negligible effect on the temperature in case (b). Increasing the value of the mixed convection parameter, both the velocities increase and the temperature and the concentration decreases in case (b). On the other hand, in case (a) the same trend is observed with an increase in the value of the velocity slip parameter. Both the skin-friction in case (b) increase with the increase in the Hall and Joule heating parameter. Whereas, in case (a), the skin-friction reduces with an increase in the magnetic parameter. Both the heat and mass transfer rates increase in both the cases with the increase in fluid suction. An increase in the Biot number increases the temperature as well as the rate of heat transfer in case (a). In both the cases, the rate of heat transfer reduces with an increase in the Joule heating parameter. While mass transfer in case (b) increase with the increase in the Joule parameter. In case (b), both the heat and mass transfer rates increase with the increase in Hall and mixed convection parameters and in both the cases decreases with an increase in the value of the magnetic parameter.

Chapter 4

Cross diffusion effects on the flow due to exponentially stretching sheet [1]

4.1 Introduction

The Soret and Dufour effects on the heat and mass transfer in a viscous fluid are very important, in view of its applications engineering technology. Inspite of engineering and industrial applications of these flows, a little attention (Srinivasacharya and Ramreddy [107], Khidir and Sibanda [49], Patil *et al.* [79] etc.,) is focussed on the flow over the sheets stretching exponentially including the soret and dufour effects. This chapter presents the significance of Soret and Dufour effects in an incompressible viscous fluid flow along a sheet, which is stretching exponentially. The influence of pertinent parameters on velocity, temperature, concentration and heat and mass transfer rates are exhibited through graphs and salient features are discussed. The numerical values of the skin friction for different values of governing parameters are also tabulated.

[1] Case(a):Published in "**International Journal of Engineering, TRANSACTIONS A**" 31(1) (2018) 120–127,
Case(b):Communicated to "**Propulsion and Power Research**"

4.2 Formulation of the Problem

Consider a stretching sheet in a laminar slip flow of incompressible viscous fluid with a temperature T_∞ and concentration C_∞. The stretching velocity, suction/injection velocity and slip velocity are taken as in case(a) of Chapter-2. The equations which governs the flow in the presence of cross-diffusion effects are:

$$\frac{\partial \tilde{u}_x}{\partial \tilde{x}} + \frac{\partial \tilde{u}_y}{\partial \tilde{y}} = 0 \tag{4.1}$$

$$\tilde{u}_x \frac{\partial \tilde{u}_x}{\partial \tilde{x}} + \tilde{u}_y \frac{\partial \tilde{u}_x}{\partial \tilde{y}} = \nu \frac{\partial^2 \tilde{u}_x}{\partial \tilde{y}^2} \tag{4.2}$$

$$\tilde{u}_x \frac{\partial \tilde{T}}{\partial \tilde{x}} + \tilde{u}_y \frac{\partial \tilde{T}}{\partial \tilde{y}} = \alpha \frac{\partial^2 \tilde{T}}{\partial \tilde{y}^2} + \frac{DK_T}{c_s\ c_p} \frac{\partial^2 \tilde{C}}{\partial \tilde{y}^2} \tag{4.3}$$

$$\tilde{u}_x \frac{\partial \tilde{C}}{\partial \tilde{x}} + \tilde{u}_y \frac{\partial \tilde{C}}{\partial \tilde{y}} = D \frac{\partial^2 \tilde{C}}{\partial \tilde{y}^2} + \frac{DK_T}{T_m} \frac{\partial^2 \tilde{T}}{\partial \tilde{y}^2} \tag{4.4}$$

where K_T is thermal diffusion ratio and T_m is mean fluid temperature.

4.2.1 Case(a): Convective Thermal Condition

Assume that the sheet is either cooled or heated convectively through a fluid with temperature T_f and which induces a heat transfer coefficient h_f, where $h_f = h\sqrt{\frac{U_0}{2L}} e^{\frac{\tilde{x}}{2L}}$.

Hence, the conditions on the surface of the stretching sheet are

$$\left.\begin{array}{l} \tilde{u}_x = U_* + N_* \nu \frac{\partial \tilde{u}_x}{\partial \tilde{y}},\ \tilde{u}_y = -V_*(\tilde{x}),\ h_f(T_f - \tilde{T}) = -\kappa \frac{\partial \tilde{T}}{\partial \tilde{y}},\ \tilde{C} = C_w \quad \text{at} \quad \tilde{y} = 0 \\ \tilde{u}_x \to 0,\ \tilde{T} \to T_\infty,\ \tilde{C} \to C_\infty \ \text{ as } \quad \tilde{y} \to \infty \end{array}\right\} \tag{4.5}$$

Introducing the stream functions through $\tilde{u}_x = -\frac{\partial \psi}{\partial \tilde{y}}$ and $\tilde{u}_y = \frac{\partial \psi}{\partial \tilde{x}}$ and then the following dimensionless variables

$$\left.\begin{array}{l} y = \tilde{y}\sqrt{\frac{U_0}{2\nu L}} e^{\frac{\tilde{x}}{2L}}, \quad \psi = \sqrt{2\nu L U_0} e^{\frac{\tilde{x}}{2L}} F(x,y), \\ \tilde{T} = T_\infty + (T_f - T_\infty) T(x,y), \quad \tilde{C} = C_\infty + (C_w - C_\infty) C(x,y) \end{array}\right\} \tag{4.6}$$

into Eqs. (4.1) - (4.4), we obtain

$$F''' + FF'' - 2F'^2 = 0 \tag{4.7}$$

$$\frac{1}{Pr}T'' + FT' + D_f\ C'' = 0 \tag{4.8}$$

$$\frac{1}{Sc}C'' + FC' + S_r\ T'' = 0 \tag{4.9}$$

The conditions (4.5) at the boundary reduces to

$$\left.\begin{array}{l} F(0) = S, \quad F'(0) = 1 + \lambda F''(0), \quad T'(0) = -Bi(1 - T(0)), \quad C(0) = 1 \ \text{ at } \quad y = 0 \\ F'(\infty) \to 0, \quad T(\infty) \to 0, \quad C(\infty) \to 0 \ \text{ as } \quad y \to \infty \end{array}\right\} \tag{4.10}$$

where $S_r = \frac{D\ K_T\ (T_f - T_\infty)}{\nu\ T_m(C_w - C_\infty)}$ is the Soret number, and $D_f = \frac{D\ K_T\ (C_w - C_\infty)}{\nu c_s\ c_p\ (T_f - T_\infty)}$ is the Dufour number.

4.2.2 Skin Friction, Heat and Mass Transfer Coefficients

The non-dimensional skin friction C_f, the local Nusselt number $Nu_{\tilde{x}}$ and the local Sherwood number $Sh_{\tilde{x}}$, are given by

$$\left.\frac{\sqrt{Re_{\tilde{x}}}\ C_f}{\sqrt{2\tilde{x}/L}} = F''(0),\ \frac{Nu_{\tilde{x}}}{\sqrt{\tilde{x}/2L}\sqrt{Re_{\tilde{x}}}} = -T'(0),\ \text{and}\ \frac{Sh_{\tilde{x}}}{\sqrt{\tilde{x}/2L}\sqrt{Re_{\tilde{x}}}} = -C'(0)\ \right\} \tag{4.11}$$

where $Re_{\tilde{x}} = \dfrac{\tilde{x}U_*(\tilde{x})}{\nu}$ is the local Reynold's number.

4.2.3 Solution of the problem

The system of Eqs. (4.7) - (4.9) along with the boundary conditions (4.10), is solved numerically, using the successive linearisation method as explained in Chapter-2.

Proceeding as in Chapter-2, we obtain the following matrix equation

$$\mathbf{A}_{i-1}\mathbf{X}_i = \mathbf{R}_{i-1}, \tag{4.12}$$

subject to the boundary conditions

$$F_i(\xi_N) = \sum_{k=0}^{N} \mathbf{D}_{0k} F_i(\xi_k) = \sum_{k=0}^{N} (\lambda \mathbf{D}2_{Nk} - \mathbf{D}_{Nk}) F_i(\xi_k) = 0 \tag{4.13a}$$

$$\sum_{k=0}^{N} \mathbf{D}_{Nk} T_i(\xi_k) - BiT_i(\xi_N) = T_i(\xi_0) = C_i(\xi_0) = C_i(\xi_N) = 0 \tag{4.13b}$$

In Eq.(4.12), $\mathbf{A}_{i-1}$ is a (3N + 3)×(3N + 3) square matrix and $\mathbf{X}_i$ and $\mathbf{R}_{i-1}$ are (3N + 3)×1 column vectors defined by

$$\mathbf{A}_{i-1} = \begin{bmatrix} A_{11} & A_{12} & A_{13} \\ A_{21} & A_{22} & A_{23} \\ A_{31} & A_{32} & A_{33} \end{bmatrix}, \quad \mathbf{X}_i = \begin{bmatrix} \mathbf{F}_i \\ \mathbf{\Theta}_i \\ \mathbf{\Phi}_i \end{bmatrix}, \quad \mathbf{R}_{i-1} = \begin{bmatrix} \mathbf{E}_{1,i-1} \\ \mathbf{E}_{2,i-1} \\ \mathbf{E}_{3,i-1} \end{bmatrix} \tag{4.14}$$

where

$$\mathbf{F}_i = [F_i(\xi_0), F_i(\xi_1), F_i(\xi_2), ..., F_i(\xi_{N-1}), F_i(\xi_N)]^T,$$
$$\mathbf{\Theta}_i = [T_i(\xi_0), T_i(\xi_1), T_i(\xi_2), ..., T_i(\xi_{N-1}), T_i(\xi_N)]^T,$$
$$\mathbf{\Phi}_i = [C_i(\xi_0), C_i(\xi_1), C_i(\xi_2), ..., C_i(\xi_{N-1}), C_i(\xi_N)]^T,$$
$$\mathbf{E}_{1,i-1} = [\zeta_{1,i-1}(\xi_0), \zeta_{1,i-1}(\xi_1), \zeta_{1,i-1}(\xi_2), ..., \zeta_{1,i-1}(\xi_{N-1}), \zeta_{1,i-1}(\xi_N)]^T$$
$$\mathbf{E}_{2,i-1} = [\zeta_{2,i-1}(\xi_0), \zeta_{2,i-1}(\xi_1), \zeta_{2,i-1}(\xi_2), ..., \zeta_{2,i-1}(\xi_{N-1}), \zeta_{2,i-1}(\xi_N)]^T$$
$$\mathbf{E}_{3,i-1} = [\zeta_{3,i-1}(\xi_0), \zeta_{3,i-1}(\xi_1), \zeta_{3,i-1}(\xi_2), ..., \zeta_{3,i-1}(\xi_{N-1}), \zeta_{3,i-1}(\xi_N)]^T$$
$$A_{11} = \mathbf{D}^3 + \chi_{11,i-1}\mathbf{D}^2 + \chi_{12,i-1}\mathbf{D} + \chi_{13,i-1}, \quad A_{12} = \mathbf{0}, \quad A_{13} = \mathbf{0}$$
$$A_{21} = \chi_{21,i-1}, \quad A_{22} = \tfrac{1}{Pr}\mathbf{D}^2 + \chi_{22,i-1}\mathbf{D}, \quad A_{23} = D_f\mathbf{D}^2$$
$$A_{31} = \chi_{31,i-1}, \quad A_{32} = S_r\mathbf{D}^2, \quad A_{33} = \tfrac{1}{Sc}\mathbf{D}^2 + \chi_{32,i-1}\mathbf{D}$$

Here $\mathbf{I}$ is an identity matrix of size (N +1)×(N +1). After modifying the matrix system (4.12) to incorporate boundary conditions (4.13), the solution is obtained as

$$\mathbf{X}_i = \mathbf{A}_{i-1}^{-1}\mathbf{R}_{i-1} \tag{4.15}$$

Table 4.1: *Comparative analysis for* $\frac{Nu_{\tilde{x}}}{\sqrt{\tilde{x}/2L}\sqrt{Re_{\tilde{x}}}}$ *by the current method for* $\lambda = 0$, $S_r = 0$, $D_f = 0$, $S = 0$ *and* $Bi \to \infty$.

Nusselt number $\frac{Nu_{\tilde{x}}}{\sqrt{\tilde{x}/2L}\sqrt{Re_{\tilde{x}}}}$		
Pr	Magyari and Keller [56]	Present
0.5	0.330493	0.33053766
1	0.549643	0.54964345
3	1.122188	1.12208577
5	1.521243	1.52123668
8	1.991847	1.99183375
10	2.257429	2.25741862

4.2.4 Result and Discussion

In order to validate the code generated, the results of the present problem have been compared with works of Magyari and Keller [56] as a special case by taking $S = 0$, $D_f = 0$, $S_r = 0$, $\lambda = 0$, and $Bi \to \infty$ and found that they are in good agreement, as shown in Table. (4.1). The computations have been carried out by taking $S = 0.5$, $S_r = 0.5$, $D_f = 0.03$, $\lambda = 1.0$, and $Bi = 1.0$ unless otherwise mentioned.

The influence of the slip and the suction/injection parameters on the velocity is portrayed in the Figs. (4.1(a)) - (4.1(b)). It is evident from the Figs. 4.1(a) and (4.1(b)) that the rise in the slipperiness and the fluid suction diminishes the fluid velocity while the injection enhances the velocity. The skin-friction is enhancing with the slipperiness and reducing with the suction of the fluid as depicted in the Fig. (4.2).

The variation of temperature distribution with Bi, λ, S, D_f, and S_r is plotted in the Figures (4.3(a)) - (4.3(e)). Figure (4.3(a)) illustrates that the temperature is enhancing with the rise in the value of Bi and gain in the thickness of thermal boundary. Further, for a large value of the Biot number, the convective thermal condition from (4.10) transforms to $T(0) \to 1$, which signifies the constant wall condition. It is evident from the Figure (4.3(b)) that temperature is enhancing with the rise in the slipperiness. It is well-known fact that the suction reduces the thickness of thermal boundary layer and hence, reduction in temperature arises. This phenomenon is graphically presented in the Figure (4.3(c)).

However, the injection produces an exactly contradictory nature. It is observed from the figures that the thickness of the thermal boundary layer is increasing with the increasing values of Dufour number as shown in the Figure (4.3(d)). But, there is no dominance of Soret number on the temperature distribution as shown in the Fig. (4.3(e)).

The influence of λ, S, S_r, Bi, and D_f on the concentration is shown graphically in Figures (4.4(a)) - (4.4(e)). It is clear from the Figure (4.4(a)) that the increase in slipperiness rises the concentration. While the injection is enhancing the concentration and suction reducing the concentration as shown in the Figure (4.4(b)). The impact of the Soret number on the concentration profile is presented in the Figure (4.4(c)). It is apparent from this figure that the concentration is increasing with the increase in S_r. Figure (4.4(d)) illustrates that the concentration is enhancing with the rise in the value of Bi and hence gain in thickness of the concentration boundary. But, the enhancement in concentration is less compared to that of temperature with the rise in Biot number as shown in the Figure (4.3(a)). Further, there is no dominance of D_f on fluid's concentration distribution as shown in the Fig. (4.4(e)).

The influence of Bi, Df, λ, and S_r on the rate of heat transfer against S are depicted through the Figures (4.5(a)) - (4.5(d)). Figure (4.5(a)) demonstrates that the rate of heat transfer is increasing with a rise in Bi. On the other hand, Figures (4.5(b)) and (4.5(c)) depict the behavior of the rate of heat transfer for different values of the Dufour number and the slip parameter. It is clear from these figures that the rate of heat transfer decreases with the increase in the values of Dufour number and slip parameter. It is evidenced from the Fig. (4.5(d)), that the rate of heat transfer increasing with an increase in the value of Soret number S_r.

The rate of mass transfer under the influence of Dufour, Soret, Biot numbers and velocity slip parameter is represented in Figures (4.6(a)) - (4.6(d)). It is noticed from the Figure (4.6(a)) that the rate of mass transfer is enhanced with an enhancement in the value of D_f. While the reduction in the rate of mass transfer is observed with the rise in S_r as portrayed in Figure (4.6(b)). Figures (4.6(c)) and (4.6(d)) depict that the rate of mass transfer is diminishing with the rise in Biot number and slip parameter. Further, the rate of heat and mass transfers increasing with fluid suction.

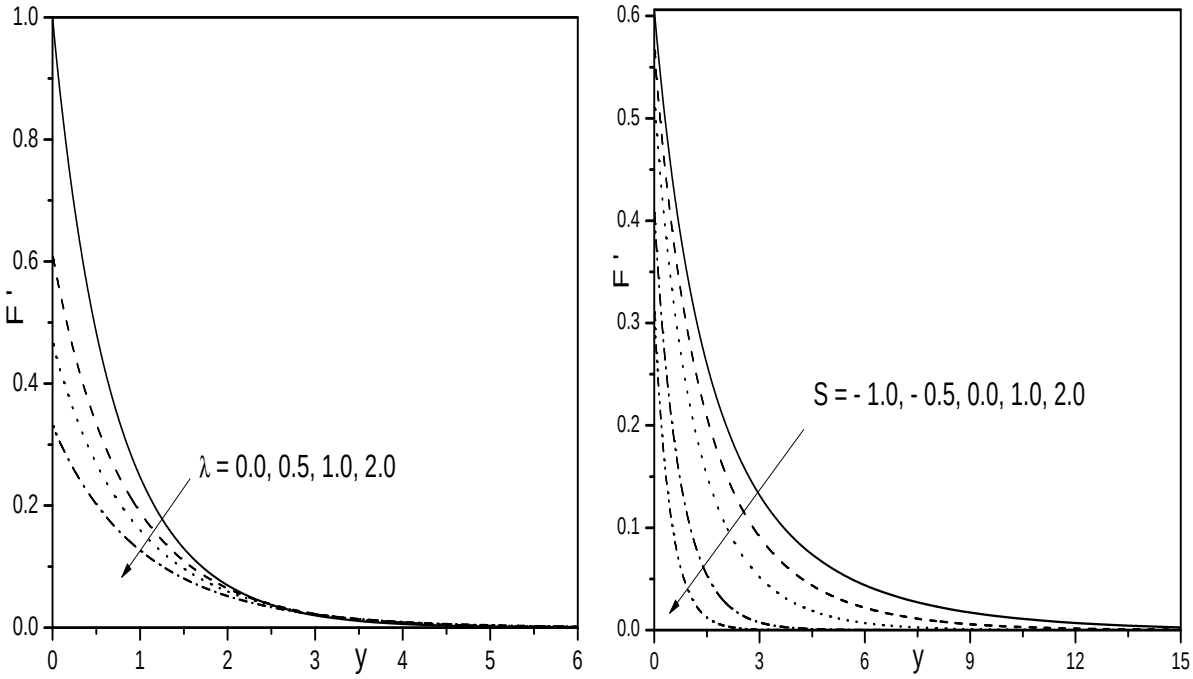

(a) (b)

Figure 4.1: *Effect of (a)λ and (b)S on Velocity*

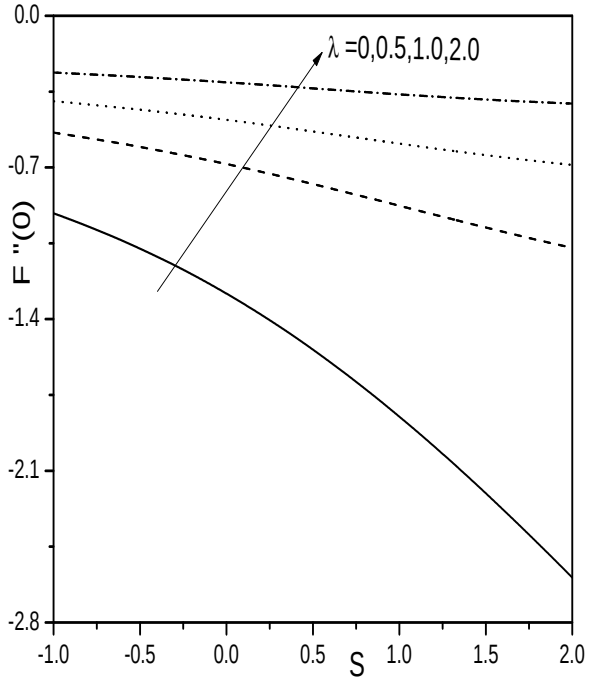

Figure 4.2: *Effect of* λ *on* $F''(0)$ *against* S

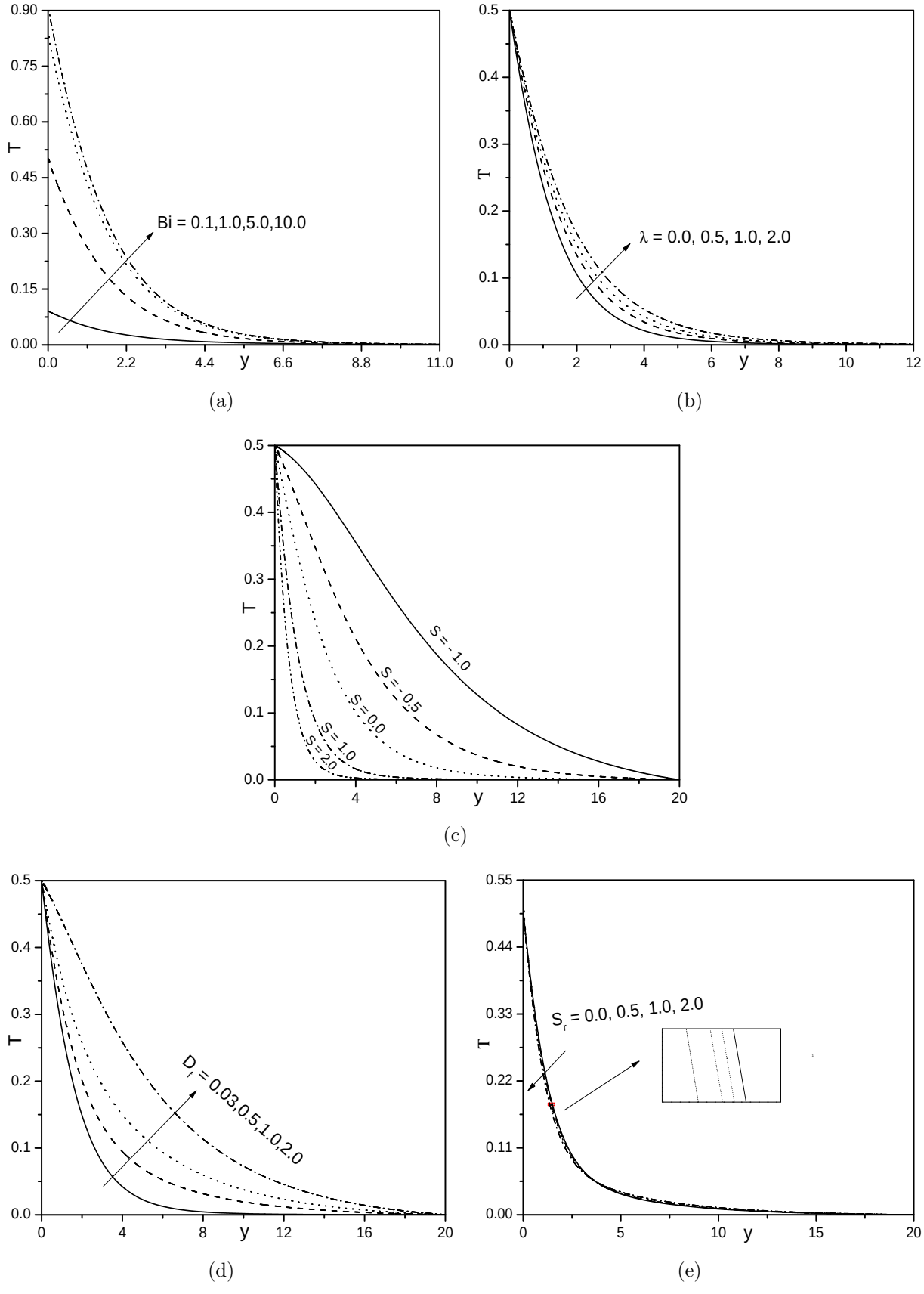

Figure 4.3: *Effect of (a)Bi, (b)λ, (c)S, (d)D_f and (e) S_r on T*

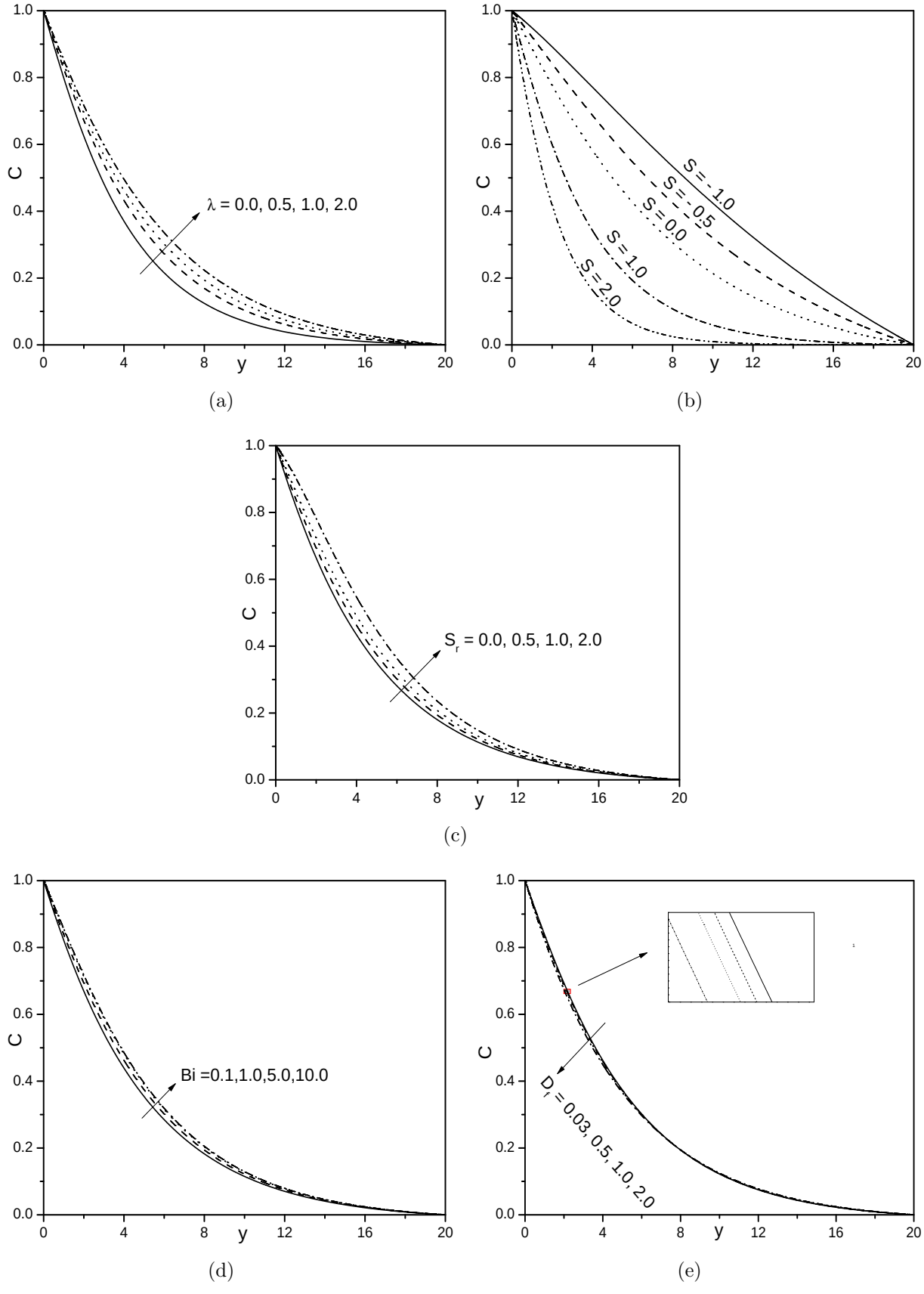

Figure 4.4: *Effect of (a)λ, (b)S, (c)S_r, (d)Bi and (e)D_f on C*

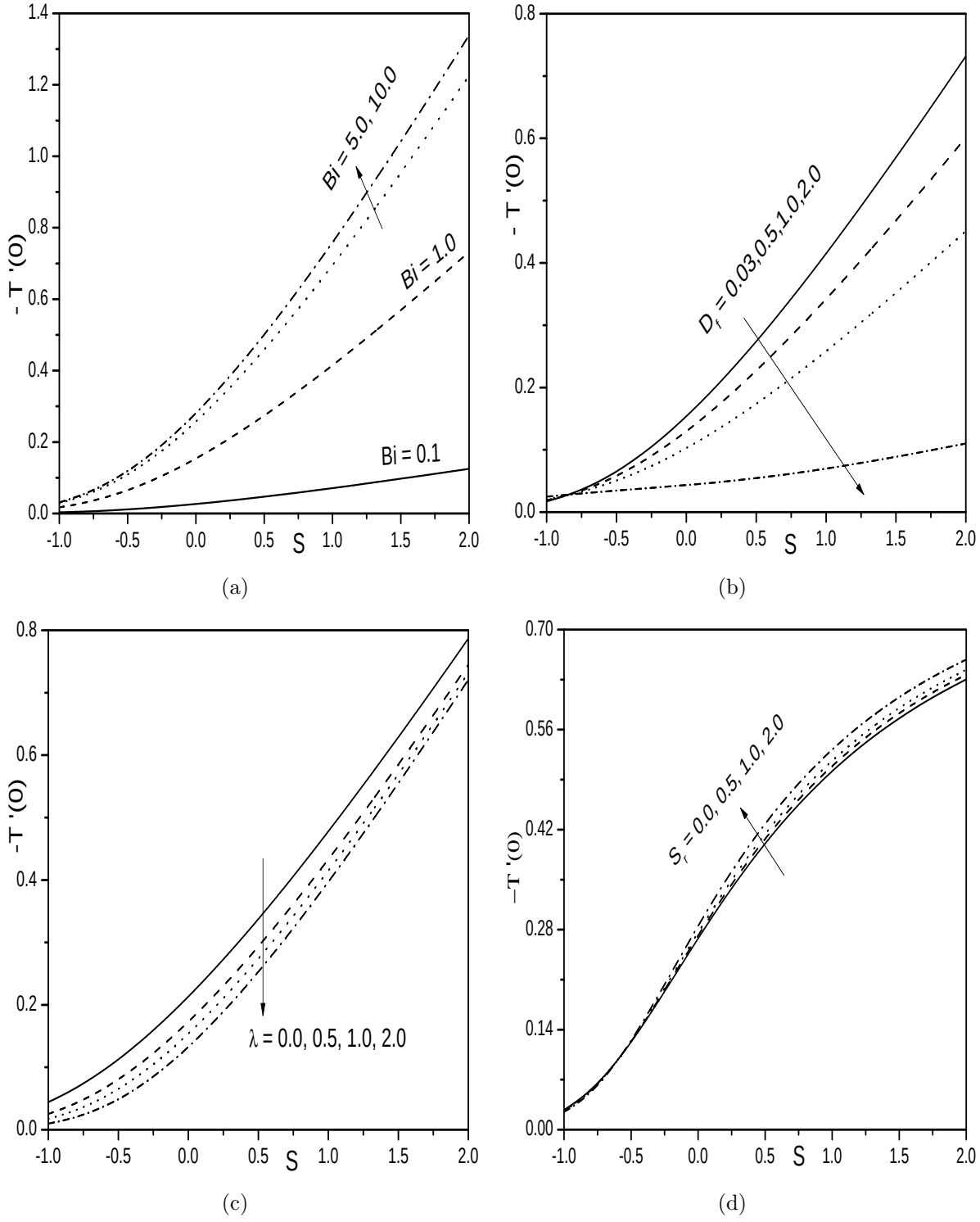

Figure 4.5: *Effect of (a)Bi, (b)D_f, (c)λ and S_r on $-T'(0)$*

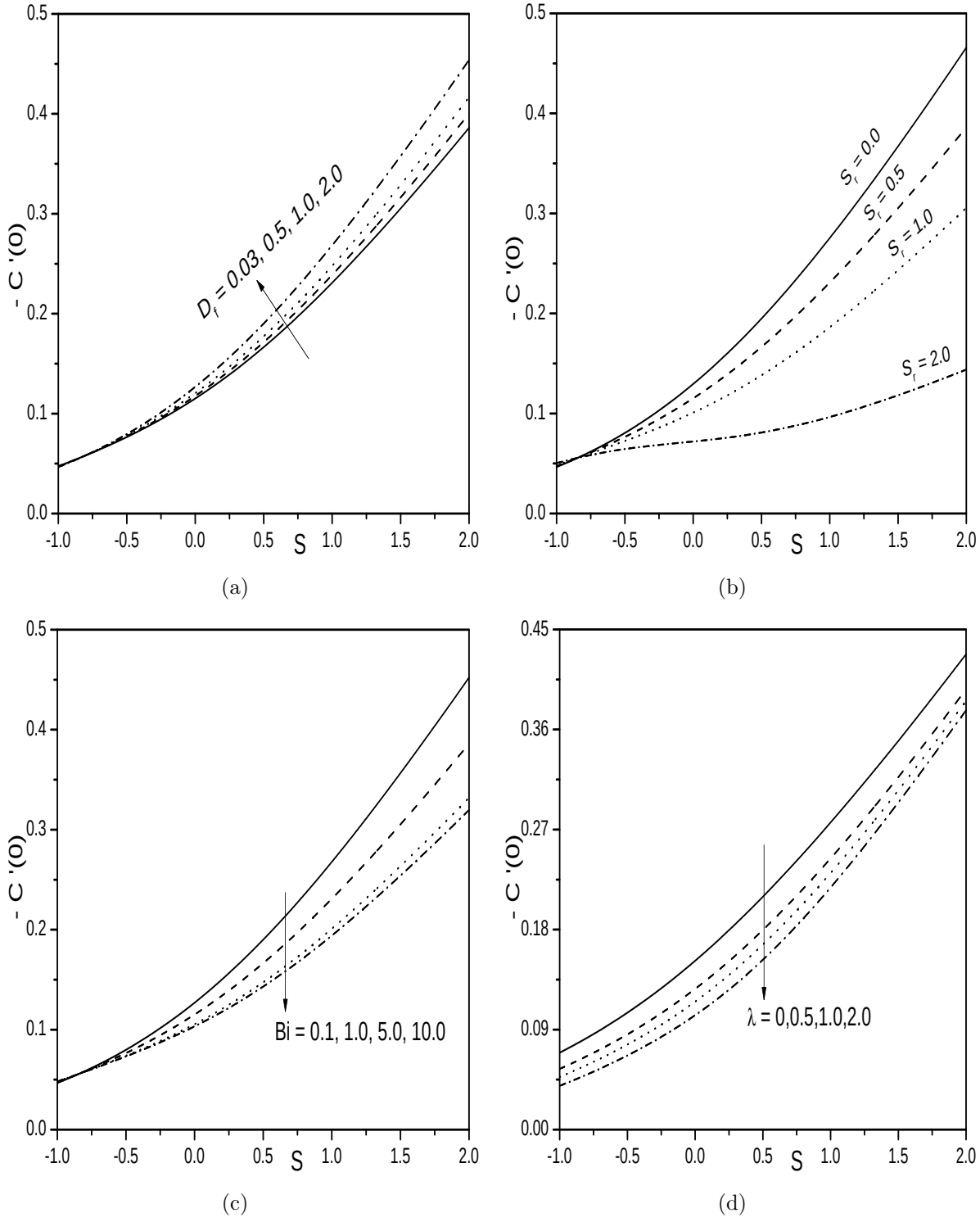

Figure 4.6: *Effect of (a)D_f, (b)S_r, (c)Bi and (d)λ on $-C'(0)$*

4.2.5 Case(b): Uniform wall temperature with Hall effect

Assume that, a strong magnetic field of strength $B(\tilde{x}) = B_0 e^{\frac{\tilde{x}}{2L}}$ is applied in $\tilde{y}-$direction and the influence of Hall current is not neglected. Assume that magnetic Reynolds number is very small so that the induced magnetic field is negligible in comparison to applied magnetic field. The presence of Hall current induces a cross flow in $\tilde{z}$-direction and hence the flow becomes three-dimensional. Under the Boussinesq approximation, the equations governing the flow in non-dimensional form are

$$F''' + FF'' - 2F'^2 + 2Ri(T + \mathbb{B}C) - \frac{H_a}{1+\beta_h^2}(F' + \beta_h W) = 0 \tag{4.16}$$

$$W'' - 2F'W + FW' + \frac{H_a}{1+\beta_h^2}(\beta_h F' - W) = 0 \tag{4.17}$$

$$\frac{1}{Pr}T'' + FT' - 4F'T + D_f\ C'' = 0 \tag{4.18}$$

$$\frac{1}{Sc}C'' + FC' - 4F'C + S_r\ T'' = 0 \tag{4.19}$$

The non-dimensional boundary conditions are

$$\left.\begin{array}{l} F(y) = S,\ F'(y) = 1 + \lambda F''(y),\ W(y) = 0,\ T(y) = 1,\ C(y) = 1 \quad \text{at} \quad y = 0 \\ F'(y) \to 0,\ W(y) \to 0,\ T(y) \to 0,\ C(y) \to 0 \quad \text{as} \quad y \to \infty \end{array}\right\} \tag{4.20}$$

where $S_r = \frac{D\ K_T\ T_0}{\nu T_m\ C_0}$ is the Soret number, and $D_f = \frac{D\ K_T\ C_0}{\nu c_s\ c_p\ T_0}$ is the Dufour number.

4.2.6 Skin Friction in $\tilde{x}$ and $\tilde{z}$-directions, Heat and Mass Transfer Coefficients

The non-dimensional skin friction in $\tilde{x}-$direction $C_{F\tilde{x}}$, local skin-friction in $\tilde{z}-$direction $C_{F\tilde{z}}$, the local Nusselt number $Nu_{\tilde{x}}$ and the local Sherwood number $Sh_{\tilde{x}}$, are given by

$$\left.\begin{array}{ll} \frac{\sqrt{Re_{\tilde{x}}}}{\sqrt{2\tilde{x}/L}}C_{F\tilde{x}} = F''(0), & \frac{\sqrt{Re_{\tilde{x}}}}{\sqrt{2\tilde{x}/L}}C_{F\tilde{z}} = W'(0), \\ \frac{Nu_{\tilde{x}}}{\sqrt{\tilde{x}/2L}\sqrt{Re_{\tilde{x}}}} = -T'(0), \quad \text{and} & \frac{Sh_{\tilde{x}}}{\sqrt{\tilde{x}/2L}\sqrt{Re_{\tilde{x}}}} = -C'(0). \end{array}\right\} \tag{4.21}$$

where $Re_{\tilde{x}} = \dfrac{\tilde{x}U_*(\tilde{x})}{\nu}$ is the local Reynold's number.

4.2.7 Solution of the Problem

The system of Eqs. (4.16) - (4.19) along with the boundary conditions (4.20), is solved numerically, using the successive linearisation method as explained in Chapter-2.

Proceeding as in Chapter-2, we obtain the following matrix equation

$$\mathbf{A}_{i-1}\mathbf{X}_i = \mathbf{R}_{i-1}, \tag{4.22}$$

subject to the boundary conditions

$$F_i(\xi_N) = \sum_{k=0}^{N} \mathbf{D}_{0k}F_i(\xi_k) = \sum_{k=0}^{N}(\lambda\mathbf{D}2_{Nk} - \mathbf{D}_{Nk})F_i(\xi_k) = 0 \tag{4.23a}$$

$$W_i(\xi_N) = W_i(\xi_0) = T_i(\xi_N) = T_i(\xi_0) = C_i(\xi_N) = C_i(\xi_0) = 0 \tag{4.23b}$$

In Eq.(4.22), $\mathbf{A}_{i-1}$ is a (4N + 4)×(4N + 4) square matrix and $\mathbf{X}_i$ and $\mathbf{R}_{i-1}$ are (4N + 4)×1

column vectors defined by

$$\mathbf{A}_{i-1} = [A_{rs}], r, s = 1, 2, 3, 4, \quad \mathbf{X}_i = \begin{bmatrix} \mathbf{F}_i \\ \mathbf{W}_i \\ \mathbf{\Theta}_i \\ \mathbf{\Phi}_i \end{bmatrix}, \quad \mathbf{R}_{i-1} = \begin{bmatrix} \mathbf{E}_{1,i-1} \\ \mathbf{E}_{2,i-1} \\ \mathbf{E}_{3,i-1} \\ \mathbf{E}_{4,i-1} \end{bmatrix} \tag{4.24}$$

where

$\mathbf{F}_i = [F_i(\xi_0), F_i(\xi_1), F_i(\xi_2), ..., F_i(\xi_{N-1}), F_i(\xi_N)]^T,$
$\mathbf{W}_i = [W_i(\xi_0), W_i(\xi_1), W_i(\xi_2), ..., W_i(\xi_{N-1}), W_i(\xi_N)]^T,$
$\mathbf{\Theta}_i = [T_i(\xi_0), T_i(\xi_1), T_i(\xi_2), ..., T_i(\xi_{N-1}), T_i(\xi_N)]^T,$
$\mathbf{\Phi}_i = [C_i(\xi_0), C_i(\xi_1), C_i(\xi_2), ..., C_i(\xi_{N-1}), C_i(\xi_N)]^T,$
$\mathbf{E}_{1,i-1} = [\zeta_{1,i-1}(\xi_0), \zeta_{1,i-1}(\xi_1), \zeta_{1,i-1}(\xi_2), ..., \zeta_{1,i-1}(\xi_{N-1}), \zeta_{1,i-1}(\xi_N)]^T$
$\mathbf{E}_{2,i-1} = [\zeta_{2,i-1}(\xi_0), \zeta_{2,i-1}(\xi_1), \zeta_{2,i-1}(\xi_2), ..., \zeta_{2,i-1}(\xi_{N-1}), \zeta_{2,i-1}(\xi_N)]^T$
$\mathbf{E}_{3,i-1} = [\zeta_{3,i-1}(\xi_0), \zeta_{3,i-1}(\xi_1), \zeta_{3,i-1}(\xi_2), ..., \zeta_{3,i-1}(\xi_{N-1}), \zeta_{3,i-1}(\xi_N)]^T$
$\mathbf{E}_{4,i-1} = [\zeta_{4,i-1}(\xi_0), \zeta_{4,i-1}(\xi_1), \zeta_{4,i-1}(\xi_2), ..., \zeta_{4,i-1}(\xi_{N-1}), \zeta_{4,i-1}(\xi_N)]^T$
$A_{11} = \mathbf{D}^3 + \chi_{11,i-1}\mathbf{D}^2 + \chi_{12,i-1}\mathbf{D} + \chi_{13,i-1}, \quad A_{12} = -\frac{H_a\beta_h}{1+\beta_h^2}\mathbf{I}, \quad A_{13} = 2Ri\mathbf{I}, \quad A_{14} = 2\mathbb{B}Ri\mathbf{I}$
$A_{21} = \chi_{21,i-1}\mathbf{D} + \chi_{22,i-1}, \quad A_{22} = \mathbf{D}^2 + \chi_{23,i-1}\mathbf{D} + \chi_{24,i-1}, \quad A_{23} = \mathbf{0}, \quad A_{24} = \mathbf{0}$
$A_{31} = \chi_{31,i-1}\mathbf{D} + \chi_{32,i-1}, \quad A_{32} = \mathbf{0}, \quad A_{33} = \frac{1}{Pr}\mathbf{D}^2 + \chi_{33,i-1}\mathbf{D} + \chi_{34,i-1}, \quad A_{34} = D_f\mathbf{D}^2$
$A_{41} = \chi_{41,i-1}\mathbf{D} + \chi_{42,i-1}, \quad A_{42} = \mathbf{0}, \quad A_{43} = S_r\mathbf{D}^2, \quad A_{44} = \frac{1}{Sc}\mathbf{D}^2 + \chi_{43,i-1}\mathbf{D} + \chi_{44,i-1}$

Here $\mathbf{I}$ is an identity matrix of size (N +1)×(N +1). After modifying the matrix system (4.22) to incorporate boundary conditions (4.23), the solution is obtained as

$$\mathbf{X}_i = \mathbf{A}_{i-1}^{-1}\mathbf{R}_{i-1} \tag{4.25}$$

4.2.8 Results and Discussion

In order to validate the code generated the results of the present problem have been compared with that of the results obtained by Magyari and Keller [56] as a special case by

Table 4.2: *Comparison of* $-F''(0)$ *and* $F(\infty)$ *calculated by the present method for* $S = 0$, $\lambda = 0$, $H_a = 0$, $S_r = 0$, $D_f = 0$, *and* $Ri = 0$.

	Magyari and Keller [56]	Present
$-F''(0)$	1.281808	1.28180856
$F(\infty)$	0.905639	0.90564370

taking $Ri = 0$, $H_a = 0$, $S = 0$, $\lambda = 0$, $S_r = 0$, and $D_f = 0$ and found that they are in good agreement, as presented in Table (4.2). To study the effects of Hall parameter β_h, suction/injection parameter S, Soret number S_r, Dufour number D_f, and magnetic parameter H_a, computations have been carried out in the cases of $Ri = 1.0$, $\mathbb{B} = 0.5$, $S = 0.5$, $\lambda = 1.0$, $\beta_h = 1.0$, $H_a = 2.0$, $S_r = 0.5$, and $D_f = 0.03$.

Figures (4.7(a)) - (4.7(d)) depict the effect of S on both the velocities, the temperature and the concentration. It is evident from the figures that both the velocities, the temperature and the concentration are increasing with the rise in the values (magnitude) of the injection ($S < 0$) parameter. Further, the imposition of wall suction ($S > 0$) lowers the thickness of the momentum, thermal and concentration boundary layers which, in turn, decrease both the tangential and cross flow velocities, temperature and concentration of the fluid.

The effect of the Hall parameter β_h on the velocity profiles, the temperature, and the concentration is shown graphically through the Figs. (4.8(a)) - (4.8(d)). As the value of the Hall parameter increases, the primary velocity increases as shown in the Fig. (4.8(a)). Due to the Hall effect, the secondary flow increases as depicted in the Fig. (4.8(b)). Further, it is identified from the Figs. (4.8(c)) and (4.8(d)) that in the presence of the Hall parameter, the temperature and the concentration of the fluid decreases.

The Soret (S_r) effect on both the velocities, the temperature and concentration profiles are depicted in the Figs. (4.9(a)) - (4.9(d)). In the presence of Soret parameter, both the velocity components are increasing as shown in the Figs. (4.9(a)) and (4.9(b)). The temperature of the fluid is severely affected by the Soret effect, especially thickness of the concentration boundary layer escalates and thickness of the thermal boundary layer decreases with rising in the value of the Soret number. Hence, the temperature of the fluid decreases and the fluid

concentration increases with an increase in the value of the Soret parameter as presented in the Fig. (4.9(c)) and (4.9(d)). Figs. (4.10(a)) - (4.10(d)), exhibit the influence of the Dufour (D_f) effect on both the velocities, the temperature and the concentration. Figures (4.10(a)) and (4.10(b)) show that both the tangential and transverse velocities are increasing as the value of the Dufour number increasing. Further, it is observed from the figures that the thickness of the thermal boundary layer increases and concentration boundary layer decreases with the increasing value of the Dufour number as shown in the Figs (4.10(c)) and (4.10(d)). Thus, in mixed convection flow problems the influence of diffusion-thermal and the thermal-diffusion effects is very important.

The effect of Soret number S_r on $-T'(0)$ and $-C'(0)$ is graphically presented through the Figs. (4.11(a)) - (4.11(b)). It is known that in the presence of the Soret parameter, the temperature reduces and the concentration increases. As a result, $-T'(0)$ increases and $-C'(0)$ decreases. Figs. (4.12(a)) - (4.12(b)) exhibit the influence of the Dufour D_f parameter on the heat and mass transfer rates. It is for the same reason under the influence of Dufour parameter, the temperature increases, and the concentration decreases. The heat transfer rate decreases and mass transfer rate increases as shown in the Fig. (4.12(a)) and Fig. (4.12(b)). It is also observed that the heat transfer rate is increasing and mass transfer rate is reducing with the suction/injection parameter S. The fluctuations of $-T'(0)$ and $-C'(0)$ for various values of the Hall parameter β_h, against S, is presented via the Figs. (4.13(a)) - (4.13(b)). It is clearly evident from the Fig. (4.13(a)) that the rate of heat transfer is increasing with an increase in the value of the Hall parameter β_h. Figure (4.13(b)) reveals that mass transfer rate is escalated with an increase in the value of Hall parameter β_h. Further, it is observed from the figures that $-T'(0)$ is increasing and $-C'(0)$ is reducing with the suction/injection parameter S. The behavior of heat transfer and mass transfer coefficients for distinct values of the slip parameter λ against the suction/injection parameter S is presented through the Figs. (4.14(a)) - (4.14(b)). It is inferred from the Fig. (4.14(a)) that, the rate of heat transfer is decreasing with the slip parameter λ for both suction ($S > 0$) and injection ($S < 0$) cases. Furthermore, it is reducing with the injection parameter and increasing with the suction parameter. While from Fig. (4.14(b)),

it is deduced that the mass transfer rate is decreasing with the rise in slip parameter and increasing with an increase in the injection parameter. It is noticed from the figures that, the mass transfer rate is drastically falling down when compared with the heat transfer rate against S.

The variations of local skin-friction coefficient $F''(0)$ in $\tilde{x}$-direction and local skin-friction coefficient $W'(0)$ in $\tilde{z}$-direction for diverse values of pertinent parameters are tabulated in Table (4.3). It is noticeable from the table that the $F''(0)$ is raising and $W'(0)$ reducing with slip parameter. As the Hall parameter increase, both the skin frictions are increasing. It is also observed that when $\beta_h = 0$, then there is no cross flow and hence there is no skin-friction in $\tilde{z}$-direction. The fluid suction reduces the skin-friction in $\tilde{x}$-direction and increases in $\tilde{z}$-direction. The positive values of Ri increase both the skin frictions. In addition to this, skin-friction in $\tilde{x}$-direction is greatly increased with the positive values of Ri. As mentioned earlier, the positive buoyancy forces act as a favorable pressure gradient and which in turn, accelerates the fluid velocity in the boundary layer. Due to which, the thickness of the boundary layer reduces and higher velocity gradient at the surface. Furthermore, it is also identified that a unique value of $F''(0) = -0.616601$ and $W'(0) = 0.150238$ is attained for all values of Soret (S_r) and Dufour (D_f) parameters when $Ri = 0$ (forced convection). This is due to the fact that equations (4.16) and (4.18) are uncoupled when $Ri = 0$. As a result, the obtained solutions for flow and thermal fields are independent. Hence, there is no effect of thermal field parameters on the flow field. At the end of the table, the influence of the Soret and Dufour parameters on the skin-friction is presented. It is obvious from the table that, both the skin-friction is increasing with the Soret and Dufour parameters, and which, rises the fluid velocity in the boundary layer.

Table 4.3: *Variation of skin friction in $\tilde{x}$- and $\tilde{z}$-directions for varying values of suction/injection parameter S, slip parameter λ, Hall parameter β_h, Dufour number S_r, mixed convection parameter Ri, and Soret number S_r.*

λ	β_h	S	Ri	S_r	D_f	$F''(0)$	$W'(0)$
0.0	1.0	0.5	1.0	0.5	0.03	-0.906158	0.480939
0.5	1.0	0.5	1.0	0.5	0.03	-0.397836	0.438572
1.0	1.0	0.5	1.0	0.5	0.03	-0.256311	0.425975
2.0	1.0	0.5	1.0	0.5	0.03	-0.150026	0.416256
1.0	0.0	0.5	1.0	0.5	0.03	-0.323340	0.000000
1.0	0.1	0.5	1.0	0.5	0.03	-0.322259	0.064472
1.0	0.5	0.5	1.0	0.5	0.03	-0.299899	0.285576
1.0	2.0	0.5	1.0	0.5	0.03	-0.194722	0.435495
1.0	1.0	-0.5	1.0	0.5	0.03	-0.177965	0.389593
1.0	1.0	-0.3	1.0	0.5	0.03	-0.192026	0.399476
1.0	1.0	0.0	1.0	0.5	0.03	-0.214672	0.412193
1.0	1.0	0.5	1.0	0.5	0.03	-0.256311	0.425975
1.0	1.0	1.0	1.0	0.5	0.03	-0.302077	0.428199
1.0	1.0	0.5	0.0	0.5	0.03	-0.616601	0.150238
1.0	1.0	0.5	0.1	0.5	0.03	-0.564879	0.205253
1.0	1.0	0.5	1.0	0.5	0.03	-0.256311	0.425975
1.0	1.0	0.5	3.0	0.5	0.03	0.185927	0.635549
1.0	1.0	0.5	1.0	0.0	0.03	-0.261722	0.419414
1.0	1.0	0.5	1.0	0.5	0.03	-0.256311	0.425975
1.0	1.0	0.5	1.0	1.0	0.03	-0.250931	0.432281
1.0	1.0	0.5	1.0	2.0	0.03	-0.240264	0.444231
1.0	1.0	0.5	1.0	0.5	0.0	-0.256822	0.425276
1.0	1.0	0.5	1.0	0.5	0.03	-0.256311	0.425975
1.0	1.0	0.5	1.0	0.5	0.5	-0.248220	0.436555
1.0	1.0	0.5	1.0	0.5	2.0	-0.221230	0.467005

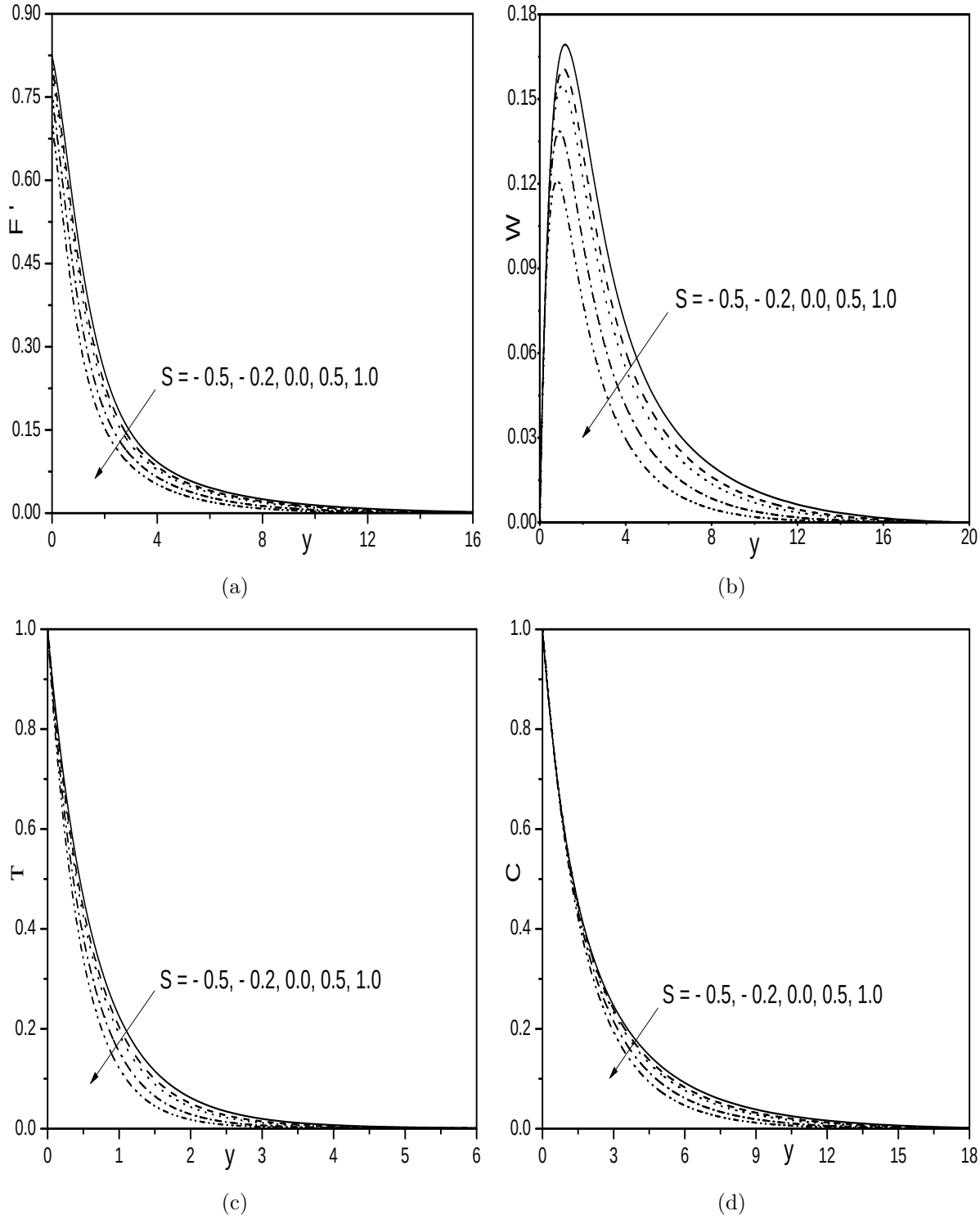

Figure 4.7: *Effect of S on (a)Velocity, (b)transverse velocity, (c)Temperature, and (d)Concentration profiles.*

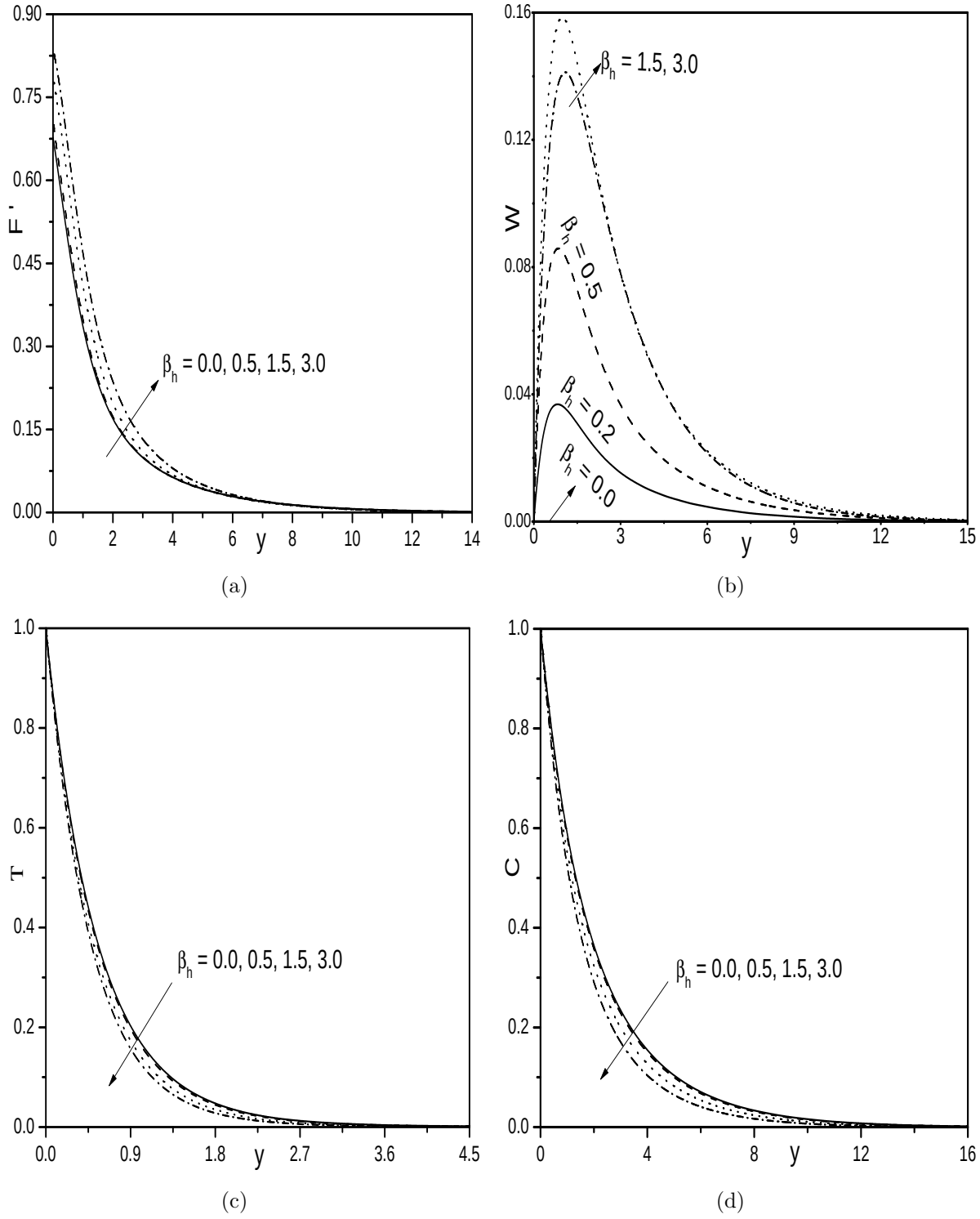

Figure 4.8: *Effect of β_h on (a)Velocity, (b)transverse velocity, (c)Temperature, and (d)Concentration profiles.*

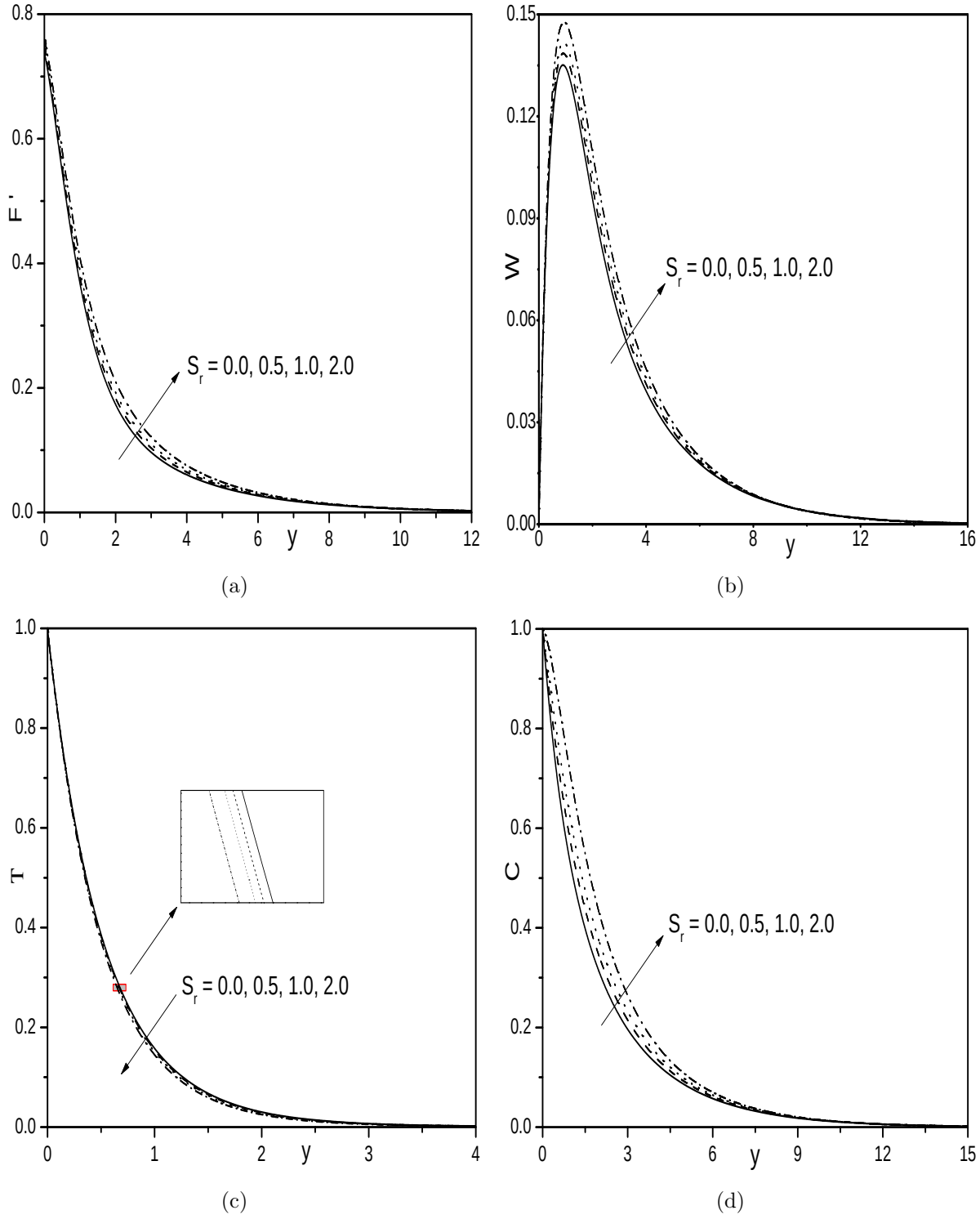

Figure 4.9: *Effect of S_r on (a)Velocity, (b)transverse velocity, (c)Temperature, and (d)Concentration profiles.*

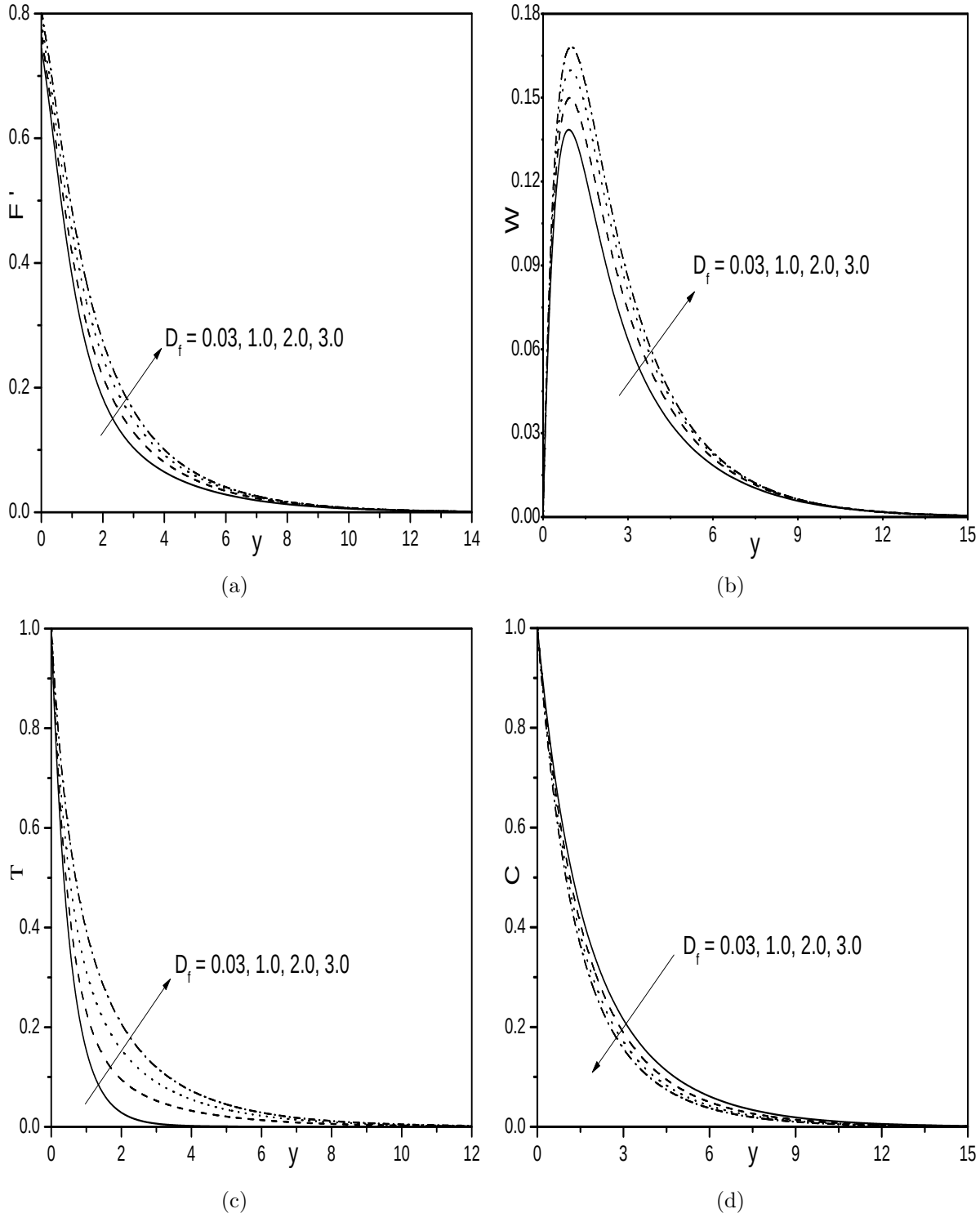

Figure 4.10: *Effect of D_f on (a)Velocity, (b)transverse velocity, (c)Temperature, and (d)Concentration profiles.*

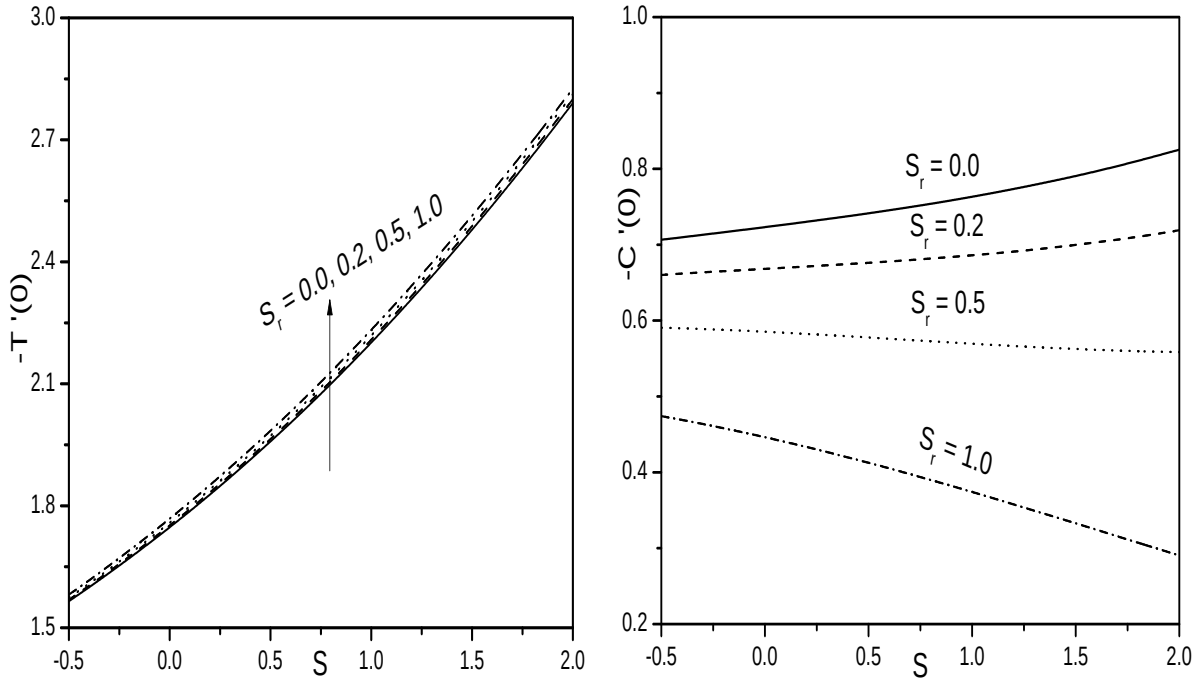

(a) (b)

Figure 4.11: *Effect of S_r on (a) $-T'(0)$, and (b) $-C'(0)$.*

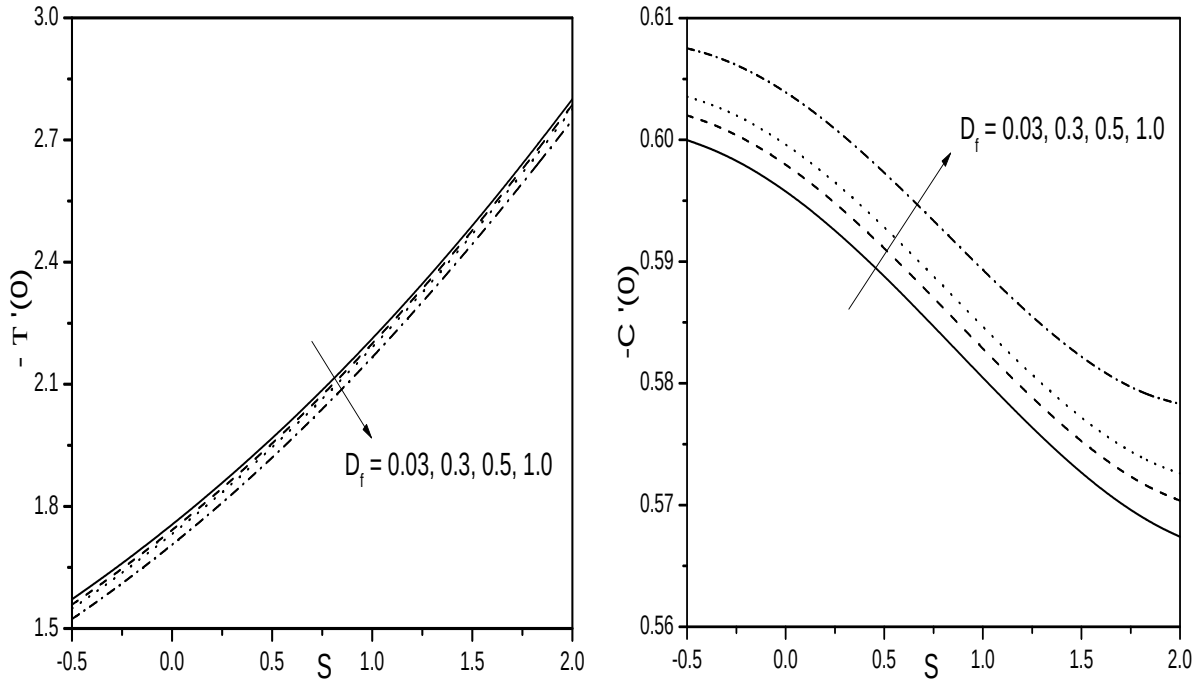

(a) (b)

Figure 4.12: *Effect of D_f on (a) $-T'(0)$, and (b) $-C'(0)$.*

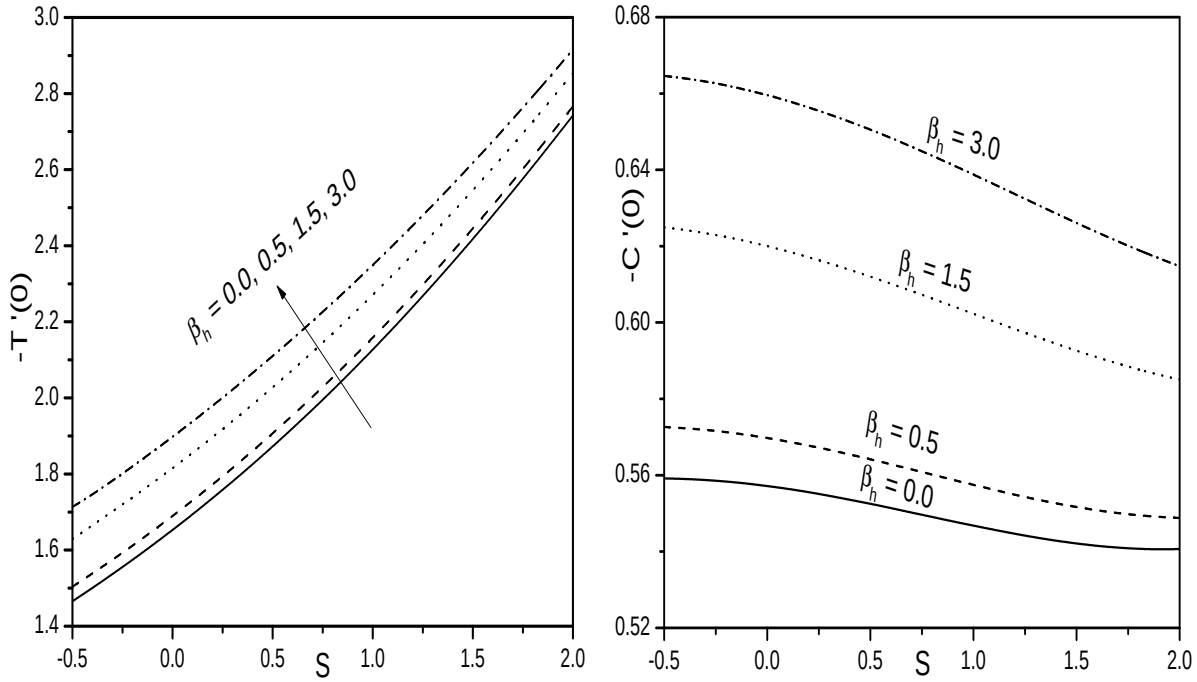

(a) (b)

Figure 4.13: *Effect of β_h on (a) $-T'(0)$, and (b) $-C'(0)$.*

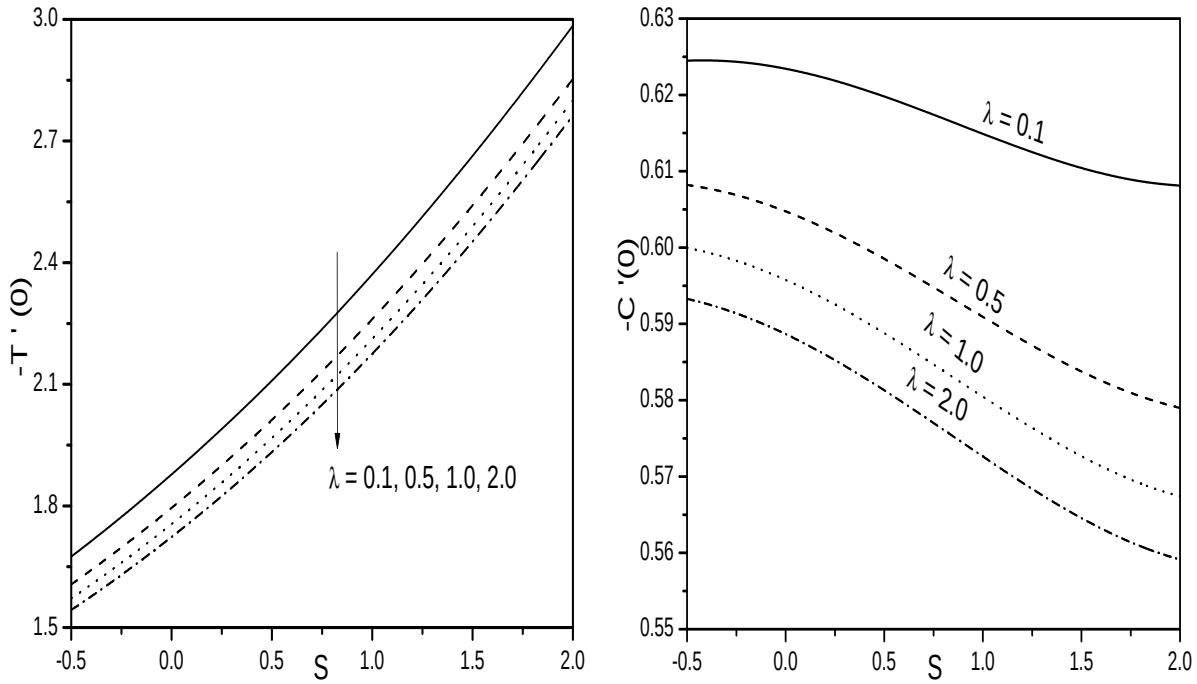

(a) (b)

Figure 4.14: *Effect of λ on (a) $-T'(0)$, and (b) $-C'(0)$.*

4.3 Conclusions

This chapter investigates the influence of cross-diffusion effects on the slip viscous fluid flow over a porous sheet, stretching exponentially From this study the following conclusions are drawn for two cases:

The fluid suction reduces the velocity the for both cases (a) and (b). In case (b), the transverse velocity decreases with the fluid suction, while, it reduces with an increase in the values of the Hall parameter, Soret and Dufour numbers. In both the cases (a) and (b), the temperature increases with an increase in the Soret number and decreases with the increase in the Dufour number. But, in both cases, an opposite trend is witnessed for the concentration. In case (a), it is observed that both the temperature and concentration of the fluid increase with an increase in the Biot number and the velocity slip parameter. Skin-friction in both the cases increase with an increase in the value of the velocity slip parameter and decrease with the fluid suction. In both cases, the rate of heat transfer is increasing with the increase in the Soret number and decreasing with an increase in Dufour number. But, an opposite impact is observed for the mass transfer. In case (a), the heat transfer rate increases and the mass transfer rate decreases with an increase in the value of the Biot number. It is observed that an increase in the value of velocity slip parameter reduces the heat and mass transfer rates for both the cases. Further, it is identified that the heat and mass transfer rates are increasing with the fluid suction, except for the mass transfer rate in case (b) when the Hall and slip parameters increase.

Chapter 5

Viscous flow over an exponentially stretching sheet with variable fluid properties [1]

5.1 Introduction

In many of the flow problems the thermo physical properties of fluid were assumed to be constant. However, it is known that these properties, especially for fluid viscosity and fluid thermal conductivity, may change with temperature. To predict the heat transfer rate accurately, it is necessary to take into account the variation of viscosity. Singh and Agarwal [99] studied the effects of variable viscosity and variable thermal conductivity on the steady flow and heat transfer of Maxwell fluid over an exponentially stretching sheet. Hazarika and Goswami [41] investigated the influence of variable viscosity and thermal conductivity on the MHD boundary layer flow over an exponentially stretching sheet with viscous dissipation and Joule heating effects. Mahmoud [58] reported the laminar flow of viscous, electrically conducting fluid past an exponentially stretching permeable sheet with variable viscosity and

[1] Case(a):Accepted for publication in "**Modelling, Measurement and Control B**" 87(1) (2018) 7–14, Case(b):Published in "**International Journal of Energy for a Clean Environment** " 19(1-2) (2018) 67–83

thermal conductivity in the presence of non-uniform magnetic field and non-uniform heat generation/absorption.

This chapter presents the influence of variable viscosity and thermal conductivity in an incompressible viscous fluid flow along a sheet, stretching exponentially. The influence of pertinent parameters on velocity, temperature, concentration and heat and mass transfer rates are exhibited through graphs and salient features are discussed. The numerical values of the skin friction for different values of governing parameters are also tabulated.

5.2 Formulation of the Problem

Consider a laminar slip flow of viscous incompressible fluid over an exponentially stretching sheet with variable viscosity and thermal conductivity. The heat source is assumed as $Q(\tilde{x}) = Q_0\ e^{\frac{\tilde{x}}{L}}$, where Q_0 is the constant. The stretching velocity and suction/injection velocity are taken as in case(a) of Chapter-2, the equations governing the flow are

$$\frac{\partial \tilde{u}_x}{\partial \tilde{x}} + \frac{\partial \tilde{u}_y}{\partial \tilde{y}} = 0 \tag{5.1}$$

$$\tilde{u}_x \frac{\partial \tilde{u}_x}{\partial \tilde{x}} + \tilde{u}_y \frac{\partial \tilde{u}_x}{\partial \tilde{y}} = \frac{1}{\rho}\ \frac{\partial}{\partial \tilde{y}} \left(\mu\ \frac{\partial \tilde{u}_x}{\partial \tilde{y}} \right) \tag{5.2}$$

$$\tilde{u}_x \frac{\partial \tilde{T}}{\partial \tilde{x}} + \tilde{u}_y \frac{\partial \tilde{T}}{\partial \tilde{y}} = \frac{1}{\rho\ c_p}\ \frac{\partial}{\partial \tilde{y}} \left(\kappa\ \frac{\partial \tilde{T}}{\partial \tilde{y}} \right) + \frac{Q}{\rho\ c_p} (\tilde{T} - T_\infty) \tag{5.3}$$

$$\tilde{u}_x \frac{\partial \tilde{C}}{\partial \tilde{x}} + \tilde{u}_y \frac{\partial \tilde{C}}{\partial \tilde{y}} = D \frac{\partial^2 \tilde{C}}{\partial \tilde{y}^2} \tag{5.4}$$

where μ is the viscosity of the fluid, κ is the thermal conductivity, and ρ is fluid density(assumed constant).

Assue that the temperature dependent coefficient of viscosity $\mu(\tilde{T})$ vary as inverse function of temperature [51] and temperature dependent thermal conductivity $\kappa(\tilde{T})$ vary as the

linear function of temperature [13] such as

$$\frac{1}{\mu} = b(\tilde{T} - T_r), \quad \kappa = \kappa_\infty \left[1 + \epsilon \left(\frac{\tilde{T} - T_\infty}{T_w - T_\infty}\right)\right] \tag{5.5}$$

where $T_r = T_\infty - 1/\delta$, $b = \delta/\mu_\infty$, b and T_r are the constants and their values depend on the reference state, δ is the thermal property of the fluid, ϵ is the variable conductivity parameter and κ_∞ is the conductivity of the fluid far away from the sheet. Generally for the liquids $b > 0$ and for gases $b < 0$.

The relation between constant viscosity and variable viscosity is $\mu = \mu_\infty \left(1 - \frac{T}{\theta_r}\right)^{-1}$

Prandtl number depends on variable viscosity and variable thermal conductivity [84], therefore, Prandtl number also varies

$$Pr = \frac{\mu c_p}{\kappa} = \frac{(\mu_\infty c_p/\kappa_\infty)}{(1 + \epsilon T)(1 - \frac{T}{\theta_r})} \tag{5.6}$$

where $Pr_\infty = \frac{\mu_\infty c_p}{\kappa_\infty}$ is the Prandtl number related to constant viscosity. From equation (5.6) it is clear that as $\theta_r \to \infty$ and $\epsilon \to 0$, $Pr \to Pr_\infty$.

5.2.1 Case(a): Convective Thermal Condition

Assume that the sheet is either cooled or heated convectively through a fluid with temperature T_f and which induces a heat transfer coefficient h_f, where $h_f = h\sqrt{\frac{U_0}{2L}} e^{\frac{\tilde{x}}{2L}}$.

The conditions on the surface of the sheet are

$$\left.\begin{aligned} &\tilde{u}_x = U_*,\ \tilde{u}_y = -V_*(\tilde{x}),\ h_f(T_f - \tilde{T}) = -\kappa \tfrac{\partial \tilde{T}}{\partial \tilde{y}},\ \tilde{C} = C_w \quad \text{at} \quad \tilde{y} = 0 \\ &\tilde{u}_x \to 0,\ \tilde{T} \to T_\infty,\ \tilde{C} \to C_\infty \ \text{ as } \quad \tilde{y} \to \infty \end{aligned}\right\} \tag{5.7}$$

The non-dimensional form of the governing equations (5.1) - (5.4), are

$$\left(1-\frac{T}{\theta_r}\right)F'''+\frac{1}{\theta_r}T'F''+\left(1-\frac{T}{\theta_r}\right)^2\left(FF''-2F'^2\right)=0 \tag{5.8}$$

$$\left(1+\epsilon T\right)T''+\epsilon T'^2+Pr\left(1-\frac{T}{\theta_r}\right)\left(1+\epsilon T\right)\left(FT'+q_1T\right)=0 \tag{5.9}$$

$$\frac{1}{Sc}C''+FC'=0 \tag{5.10}$$

The conditions (5.7) at the boundary reduces to

$$\left.\begin{array}{l} F(0)=S,\quad F'(0)=1,\quad T'(0)=-Bi(1-T(0)),\quad C(0)=1\ \text{ at }\ y=0 \\ F'(\infty)\to 0,\quad T(\infty)\to 0,\quad C(\infty)\to 0\ \text{ as }\ y\to\infty \end{array}\right\} \tag{5.11}$$

where ν_∞ is the kinematic viscosity of the fluid in the free stream, $Bi=\frac{h}{\kappa}\sqrt{\nu_\infty}$ is the Biot number, $\theta_r=\frac{-1}{\delta(T_f-T_\infty)}$ is the fluid viscosity parameter, $q_1=\frac{2LQ_0}{\rho c_p\ U_0}$ is the heat source parameter, and $S=V_0\sqrt{\frac{2L}{\nu_\infty U_0}}$ is the suction($S>0$) or injection($S<0$) parameter.

5.2.2 Skin Friction, Heat and Mass Transfer Coefficients

The non-dimensional skin friction C_f, the local Nusselt number $Nu_{\tilde{x}}$ and the local Sherwood number $Sh_{\tilde{x}}$, are given by

$$\left.\begin{array}{l} \frac{\sqrt{Re_{\tilde{x}}}\ C_f}{\sqrt{2\tilde{x}/L}}=\left(\frac{\theta_r}{\theta_r-T(0)}\right)F''(0),\ \dfrac{Nu_{\tilde{x}}}{\sqrt{\tilde{x}/2L}\sqrt{Re_{\tilde{x}}}}=-T'(0),\ \text{and}\ \dfrac{Sh_{\tilde{x}}}{\sqrt{\tilde{x}/2L}\sqrt{Re_{\tilde{x}}}}=-C'(0) \end{array}\right\} \tag{5.12}$$

where $Re_{\tilde{x}}=\dfrac{\tilde{x}U_*(\tilde{x})}{\nu_\infty}$ is the local Reynold's number.

5.2.3 Solution of the Problem

The system of Eqs. (5.8) - (5.10) along with the boundary conditions (5.11), is solved numerically, using the successive linearisation method as explained in Chapter-2.

Proceeding as in Chapter-2, we obtain the following matrix equation

$$\mathbf{A}_{i-1}\mathbf{X}_i = \mathbf{R}_{i-1}, \tag{5.13}$$

subject to the boundary conditions

$$F_i(\xi_N) = \sum_{k=0}^{N} \mathbf{D}_{0k} F_i(\xi_k) = \sum_{k=0}^{N} \mathbf{D}_{Nk} F_i(\xi_k) = 0 \tag{5.14a}$$

$$\sum_{k=0}^{N} \mathbf{D}_{Nk} T_i(\xi_k) - BiT_i(\xi_N) = T_i(\xi_0) = C_i(\xi_0) = C_i(\xi_N) = 0 \tag{5.14b}$$

In Eq.(5.13), $\mathbf{A}_{i-1}$ is a (3N + 3)×(3N + 3) square matrix and $\mathbf{X}_i$ and $\mathbf{R}_{i-1}$ are (3N + 3)×1 column vectors defined by

$$\mathbf{A}_{i-1} = \begin{bmatrix} A_{11} & A_{12} & A_{13} \\ A_{21} & A_{22} & A_{23} \\ A_{31} & A_{32} & A_{33} \end{bmatrix}, \quad \mathbf{X}_i = \begin{bmatrix} \mathbf{F}_i \\ \mathbf{\Theta}_i \\ \mathbf{\Phi}_i \end{bmatrix}, \quad \mathbf{R}_{i-1} = \begin{bmatrix} \mathbf{E}_{1,i-1} \\ \mathbf{E}_{2,i-1} \\ \mathbf{E}_{3,i-1} \end{bmatrix} \tag{5.15}$$

where

$\mathbf{F}_i = [F_i(\xi_0), F_i(\xi_1), F_i(\xi_2), ..., F_i(\xi_{N-1}), F_i(\xi_N)]^T,$

$\mathbf{\Theta}_i = [T_i(\xi_0), T_i(\xi_1), T_i(\xi_2), ..., T_i(\xi_{N-1}), T_i(\xi_N)]^T,$

$\mathbf{\Phi}_i = [C_i(\xi_0), C_i(\xi_1), C_i(\xi_2), ..., C_i(\xi_{N-1}), C_i(\xi_N)]^T,$

$\mathbf{E}_{1,i-1} = [\zeta_{1,i-1}(\xi_0), \zeta_{1,i-1}(\xi_1), \zeta_{1,i-1}(\xi_2), ..., \zeta_{1,i-1}(\xi_{N-1}), \zeta_{1,i-1}(\xi_N)]^T$

$\mathbf{E}_{2,i-1} = [\zeta_{2,i-1}(\xi_0), \zeta_{2,i-1}(\xi_1), \zeta_{2,i-1}(\xi_2), ..., \zeta_{2,i-1}(\xi_{N-1}), \zeta_{2,i-1}(\xi_N)]^T$

$\mathbf{E}_{3,i-1} = [\zeta_{3,i-1}(\xi_0), \zeta_{3,i-1}(\xi_1), \zeta_{3,i-1}(\xi_2), ..., \zeta_{3,i-1}(\xi_{N-1}), \zeta_{3,i-1}(\xi_N)]^T$

$A_{11} = \chi_{11,i-1}\mathbf{D}^3 + \chi_{12,i-1}\mathbf{D}^2 + \chi_{13,i-1}\mathbf{D} + \chi_{14,i-1}, \quad A_{12} = \chi_{15,i-1}\mathbf{D} + \chi_{16,i-1}, \quad A_{13} = \mathbf{0}$

$A_{21} = \chi_{21,i-1}, \quad A_{22} = \chi_{22,i-1}\mathbf{D}^2 + \chi_{23,i-1}\mathbf{D} + \chi_{24,i-1}, \quad A_{23} = \mathbf{0}$

$A_{31} = \chi_{31,i-1}, \quad A_{32} = \mathbf{0}, \quad A_{33} = \frac{1}{Sc}\mathbf{D}^2 + \chi_{32,i-1}\mathbf{D}$

Here $\mathbf{I}$ is an identity matrix of size (N +1)×(N +1). After modifying the matrix system

Table 5.1: *Comparative analysis for* $\frac{Nu_{\tilde{x}}}{\sqrt{\tilde{x}/2L}\sqrt{Re_{\tilde{x}}}}$ *by the current method for* $\lambda = 0$, $\theta_r \to \infty$, $\epsilon = 0$, $q_1 = 0$, $S = 0$ *and* $Bi \to \infty$.

Nusselt number $\frac{Nu_{\tilde{x}}}{\sqrt{\tilde{x}/2L}\sqrt{Re_{\tilde{x}}}}$		
Pr	Magyari and Keller [56]	Present
0.5	0.330493	0.33053741
1	0.549643	0.54964317
3	1.122188	1.12208592
5	1.521243	1.52123757
8	1.991847	1.99183597
10	2.257429	2.25742182

(5.13) to incorporate boundary conditions (5.14), the solution is obtained as

$$\mathbf{X}_i = \mathbf{A}_{i-1}^{-1}\mathbf{R}_{i-1} \tag{5.16}$$

5.2.4 Result and Discussion

As in the previous Chapters, the results of the present problem are compared with works of Magyari and Keller [56] as a special case by taking $S = 0$, $q_1 = 0$, $\epsilon = 0$, $\theta_r \to \infty$, $\lambda = 0$, and $Bi \to \infty$ and presetned in Table. (5.1). In order to study the effects of viscosity parameter θ_r, suction/injection parameter S, Biot number Bi, thermal conductivity parameter ϵ, heat source parameter q_1, velocity slip parameter λ, computations have been carried out taking $S = 0.5$, $q_1 = 0.1$, $\epsilon = 0.1$, $\theta_r = 3.0$, $\lambda = 1.0$, and $Bi = 1.0$ unless otherwise mentioned.

The variation of the velocity profile for diverse values of θ_r, q_1, Bi and S is presented in the Figs. (5.1(a)) - (5.1(d)). It is obvious that fluid velocity is decreasing with the enhancement in the value of θ_r as shown in the Fig. (5.1(a)). Heat source parameter q_1 has an almost negligible influence on velocity. Figure (5.1(b)) depicts that the velocity is increasing, but negligible as the value of that q_1 is increasing. Biot number Bi has a considerable effect on the fluid velocity as shown in the Fig. (5.1(c)). It is seen that the velocity is enhanced with the rise in the value of Bi. From Fig. (5.1(d)), it is clear that velocity is rising with the injection ($S < 0$) and reducing with the suction ($S > 0$).

The effect of the parameters ϵ, q_1, Bi and S on temperature is shown in the Figs. (5.2(a)) - (5.2(d)). It is observed that the temperature increases as the value of thermal conductivity parameter ϵ increases as shown in the Fig. (5.2(a)). An increase in the values of heat source parameter and Biot number, the temperature increases as shown in the Figs. (5.2(b)) and (5.2(c)). Reduction in the temperature is observed with an increase in the suction and enhancement with the blowing as shown in the Fig. (5.2(d)). This is due to the fact that the wall suction, reduces thermal boundary layer thickness.

The behavior of the concentration profile for various values of the parameters θ_r, q_1, Bi and S is depicted in the Figs. (5.3(a)) - (5.3(d)). Rising the value of θ_r, the concentration of the fluid is increased as shown in the Fig. (5.3(a)). It is noticed from the Figs. (5.3(b)) and (5.3(c)) that an increase in the values of q_1 and Bi increases the concentration. It is observed that the effect of heat source parameter q_1 on concentration is almost negligible. From the Fig. (5.3(d)), it is observed that an increase in the value of suction/injection parameter S reduces the concentration. Therefore, the concentration of the fluid decreases with the suction and increases with the injection as depicted in the Fig. (5.3(d)).

The variation of the skin-friction coefficient with varying values of θ_r, Bi, q_1 and ϵ against S is presented in the Figs. (5.4(a)) - (5.4(d)). It is evident from the Fig. (5.4(a)) that increase in the value of viscosity parameter increases the skin-friction. Hence, decrease in the fluid velocity. An increase in the value of Bi diminishes the skin-friction and increases the fluid velocity as shown in the Fig. (5.4(b)). While there is a negligible effect of q_1 and ϵ on the skin-friction as depicted in the Figs. (5.4(c)) and (5.4(d)). It is obvious from these figures that the skin-friction is reducing slightly with an increase in the value of heat source and thermal conductivity parameters. Further, it is identified that the skin-friction is reducing with the increase in the value of S.

The behaviour of rate of heat transfer for several values of θ_r, Bi, q_1 and ϵ against S is portrayed in the Figs. (5.5(a)) - (5.5(d)). The rate of heat transfer is diminishing with the rise in θ_r as shown in the Fig. (5.5(a)). Further, it is noticed that the trend is reversed from $S = 0.15$ onwards. ie., heat transfer is increasing with an increase in the values of S and θ_r ($S > 0.15$). Figure (5.5(b)) narrates the rise in Bi enhances the rate of heat transfer.

The rate of heat transfer is reducing with the rise in the values of q_1 and ϵ as shown in the Figs. (5.5(c)) and (5.5(d)). While it is clear from the figures that the rate of heat transfer increasing with the suction.

For distinct values of θ_r, Bi, q_1 and ϵ, the variations of the rate of mass transfer is graphitized against S through the Figs. (5.6(a)) - (5.6(d)). Increasing the value of the viscosity parameter θ_r, the rate of mass transfer is diminishing as shown in the Fig. (5.6(a)). From the Fig. (5.6(b)), it is obvious that the rate of mass transfer is reducing with the rise in Bi. There is a mild effect of the heat source and thermal conductivity parameters on the rate of mass transfer as depicted in the Figs. (5.6(c)) and (5.6(d)). It is obvious from these figures that the rate of mass transfer is slightly enhanced with the rise in q_1 and ϵ. Further, it is noticed that the suction increases the rate of mass transfer.

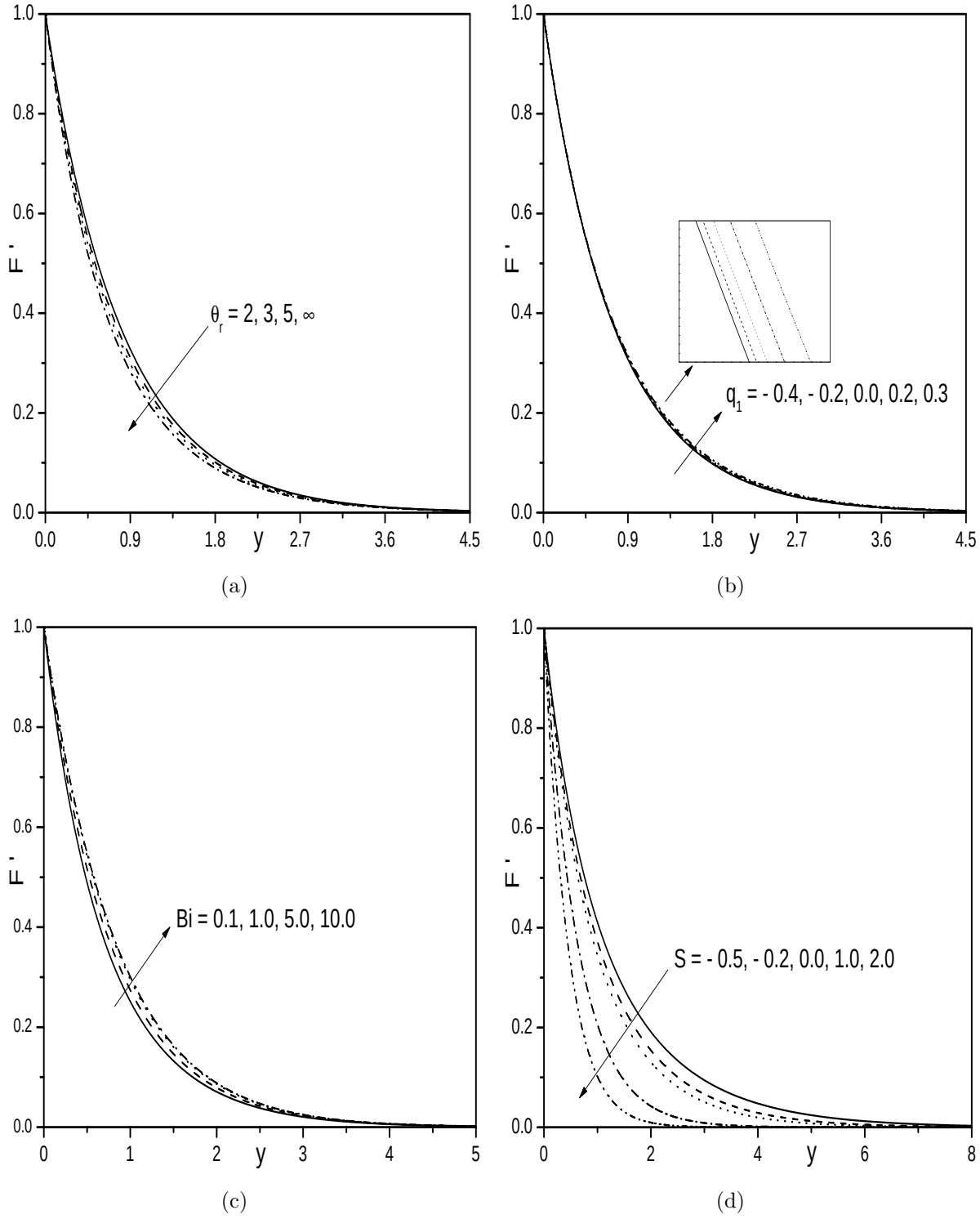

Figure 5.1: *Effect of (a) θ_r, (b) q_1, (c) Bi, and (d) S on velocity profile.*

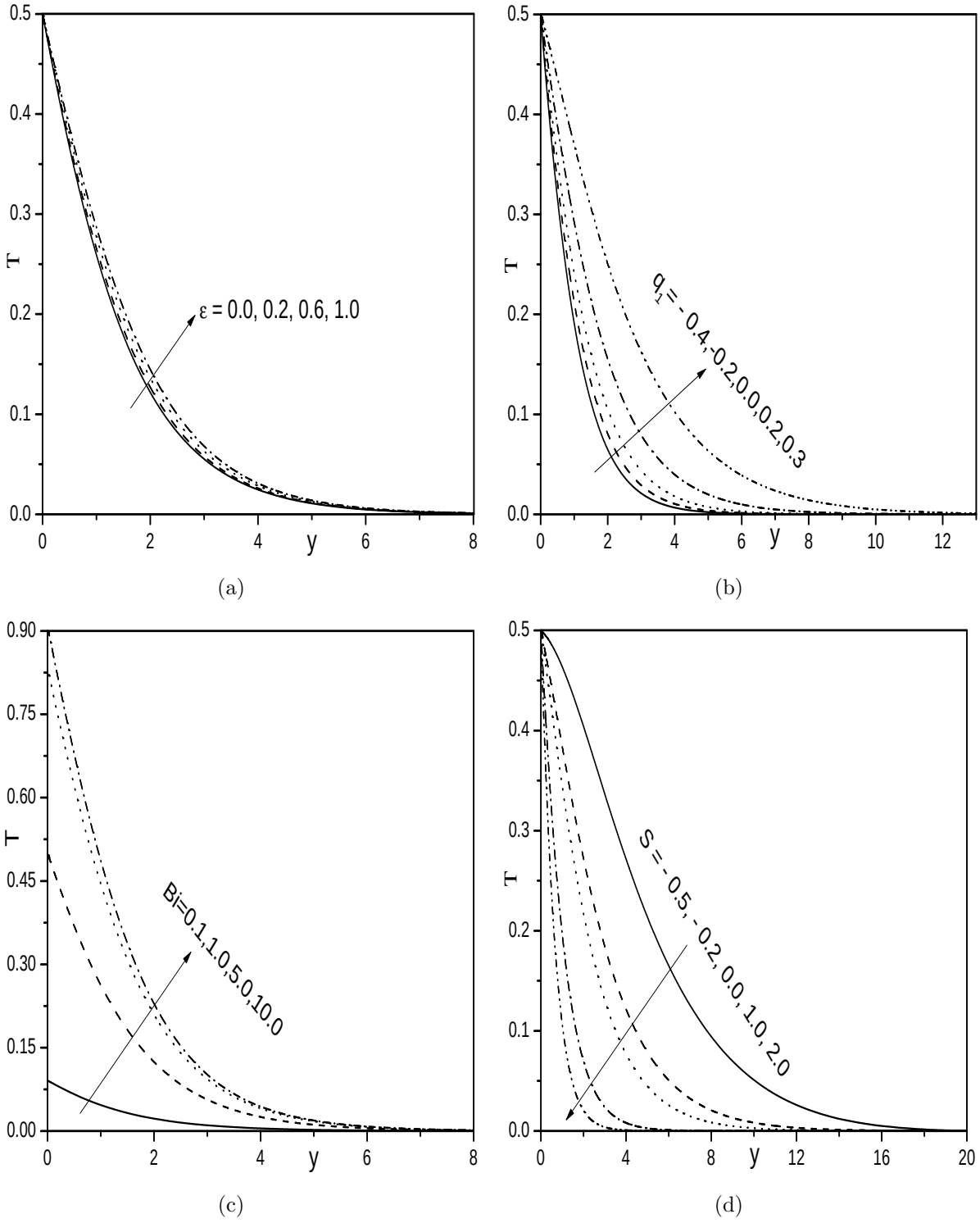

Figure 5.2: *Effect of (a) ϵ, (b) q_1, (c) Bi, and (d) S on temperature profile.*

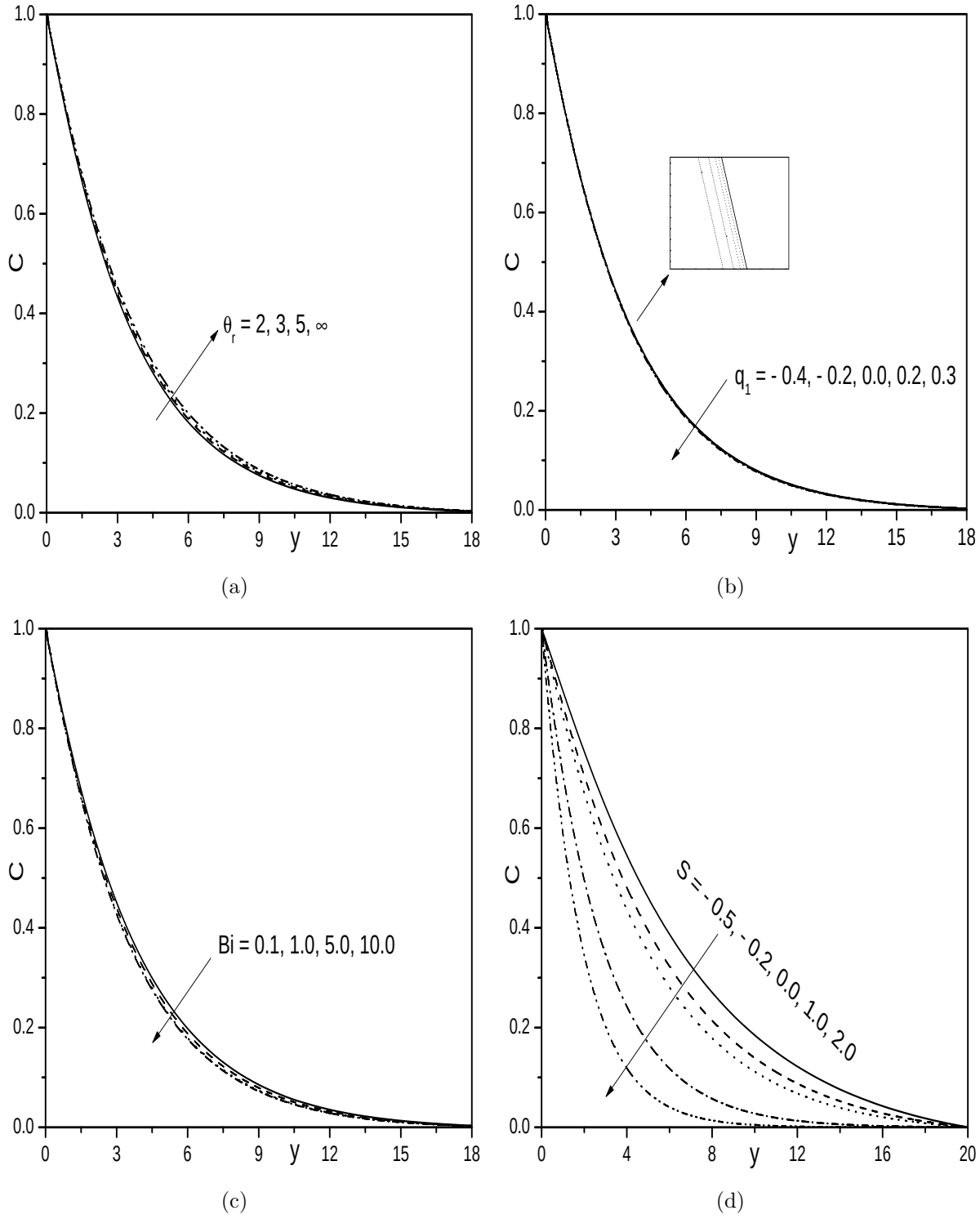

Figure 5.3: *Effect of (a) θ_r, (b) q_1, (c) Bi, and (d) S on concentration profile.*

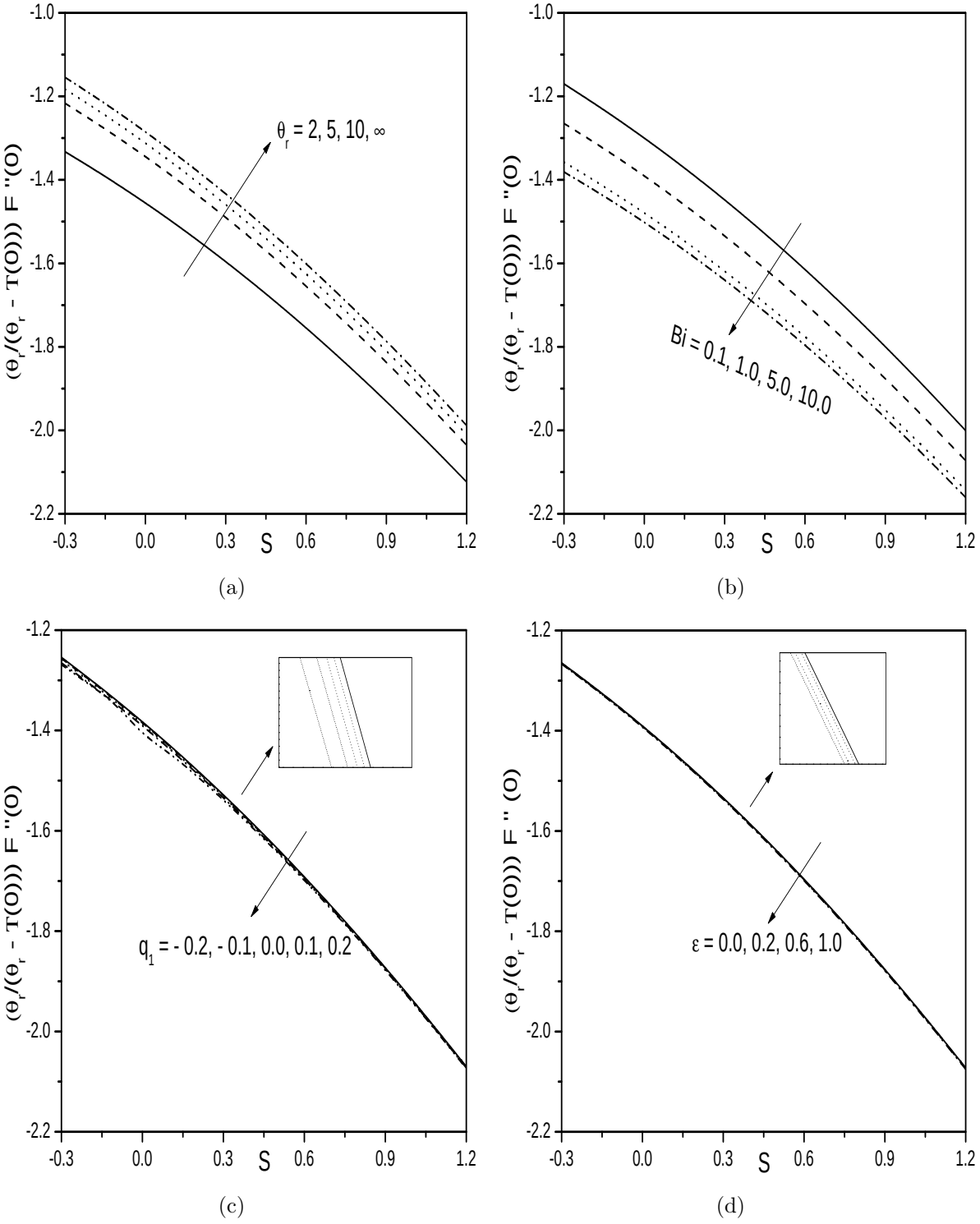

Figure 5.4: *Effect of (a) θ_r, (b) Bi, (c) q_1, and (d) ϵ on skin-friction coefficient.*

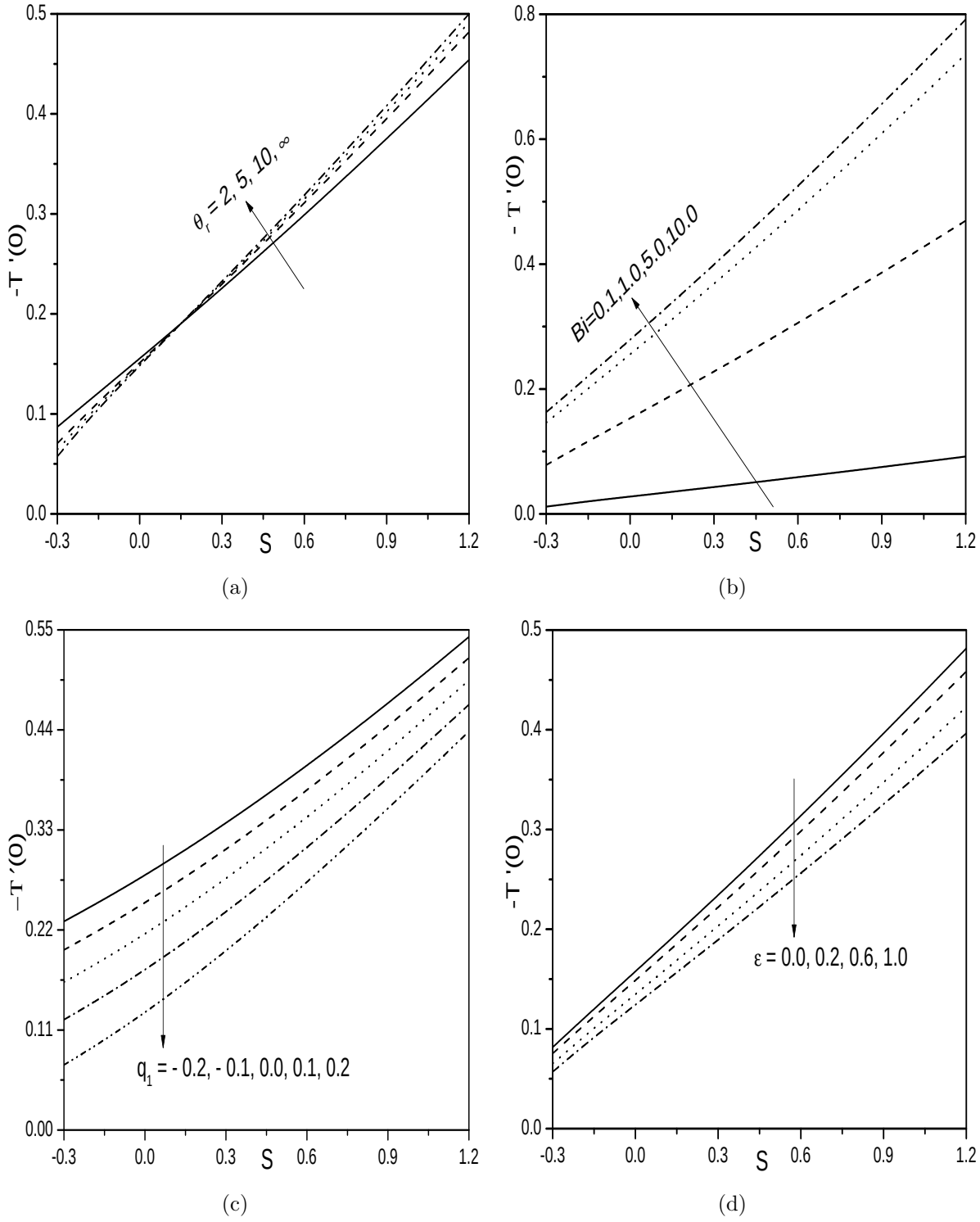

Figure 5.5: *Effect of (a) θ_r, (b) Bi, (c) q_1, and (d) ϵ on -T'(0).*

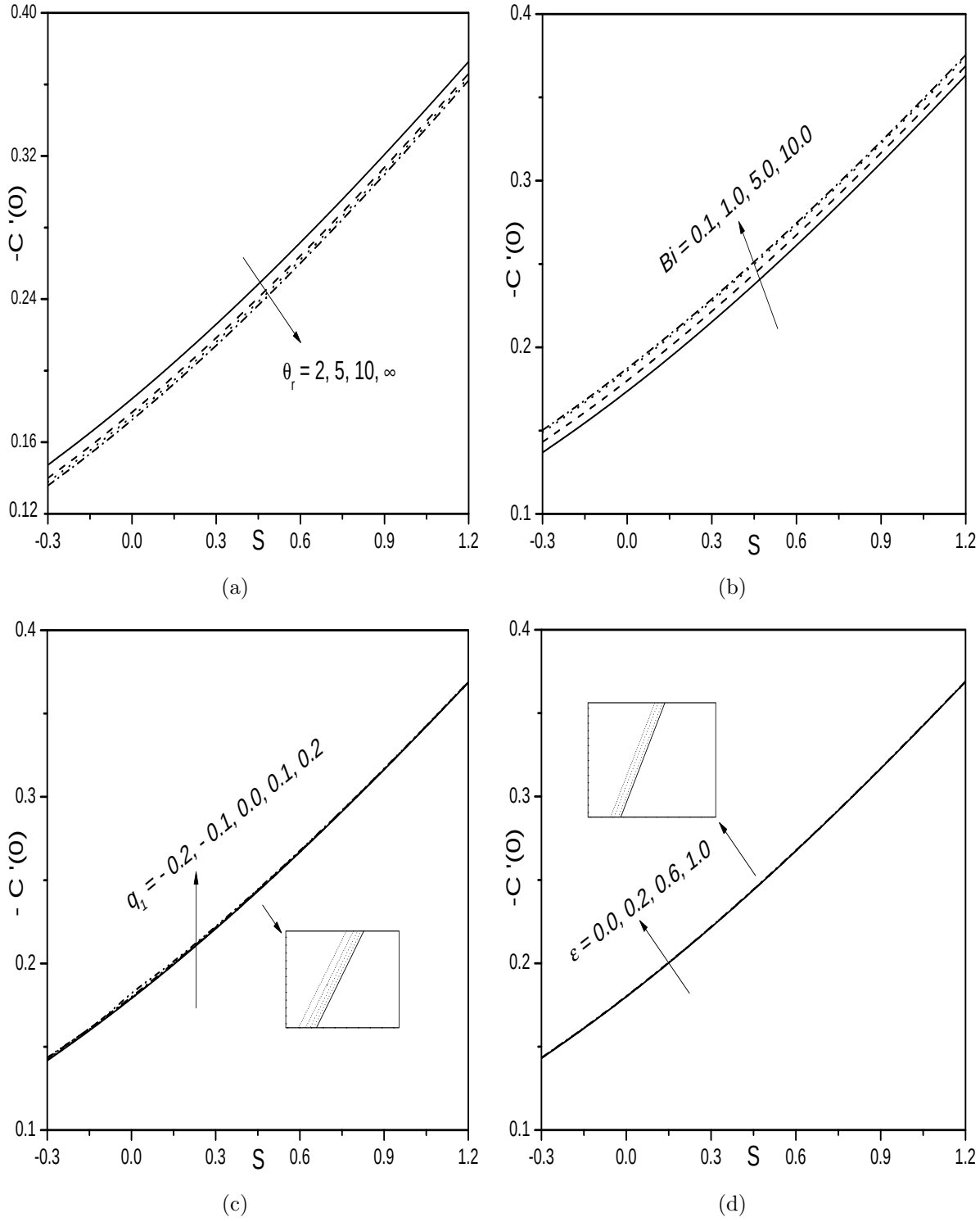

Figure 5.6: *Effect of (a) θ_r, (b) Bi, (c) q_1, and (d) ϵ on -C'(0).*

5.2.5 Case(b): Uniform wall temperature with Hall effect

Assume that, a strong magnetic field of strength $B(\tilde{x}) = B_0 e^{\frac{\tilde{x}}{2L}}$ is applied in $\tilde{y}-$direction and the influence of Hall current is not neglected. Assume that magnetic Reynolds number is very small so that the induced magnetic field is negligible in comparison to applied magnetic field. The presence of Hall current induces a cross flow in $\tilde{z}$-direction and hence the flow becomes three-dimensional. Further, the slip velocity of the fluid is assumed as $N_*(\tilde{x}) = N_0\, e^{\frac{-\tilde{x}}{2L}}$, where N_0 is the velocity slip factor. Under the Boussinesq approximation, the non-dimensional form of the governing equations are

$$\left(1-\frac{T}{\theta_r}\right)F'''+\frac{1}{\theta_r}T'F''+\left(1-\frac{T}{\theta_r}\right)^2\left(FF''-2F'^2+2Ri(T+\mathbb{B}C)-\frac{H_a}{1+\beta_h^2}(F'+\beta_h W)\right)=0 \tag{5.17}$$

$$\left(1-\frac{T}{\theta_r}\right)W''+\frac{1}{\theta_r}T'W'+\left(1-\frac{T}{\theta_r}\right)^2\left(FW'-2F'W+\frac{H_a}{1+\beta_h^2}(\beta_h F'-W)\right)=0 \tag{5.18}$$

$$(1+\epsilon T)\,T''+\epsilon T'^2+Pr\left(1-\frac{T}{\theta_r}\right)(1+\epsilon T)\,(FT'-4F'T+q_1T)=0 \tag{5.19}$$

$$\frac{1}{Sc}C''+FC'-4F'C=0 \tag{5.20}$$

The boundary conditions, in dimensionless form, are

$$\left.\begin{array}{l} F(y)=S,\ F'(y)=1+\left(\frac{\theta_r}{\theta_r-1}\right)\lambda F''(y),\ W(y)=0,\ T(y)=1,\ C(y)=1 \ \text{ at } \ y=0 \\ F'(y)\to 0,\ W(y)\to 0,\ T(y)\to 0,\ C(y)\to 0 \ \text{ as } \ y\to\infty \end{array}\right\} \tag{5.21}$$

5.2.6 Skin Friction in $\tilde{x}$ and $\tilde{z}$-directions, Heat and Mass Transfer Coefficients

The non-dimensional skin friction in $\tilde{x}-$direction $C_{F\tilde{x}}$, local skin-friction in $\tilde{z}-$direction $C_{F\tilde{z}}$, the local Nusselt number $Nu_{\tilde{x}}$ and the local Sherwood number $Sh_{\tilde{x}}$, are given by

$$\left.\begin{aligned} &\frac{\sqrt{Re_{\tilde{x}}}}{\sqrt{2\tilde{x}/L}}C_{F\tilde{x}} = \left(\frac{\theta_r}{\theta_r-1}\right)F''(0), \quad \frac{\sqrt{Re_{\tilde{x}}}}{\sqrt{2\tilde{x}/L}}C_{F\tilde{z}} = \left(\frac{\theta_r}{\theta_r-1}\right)W'(0), \\ &\frac{Nu_{\tilde{x}}}{\sqrt{\tilde{x}/2L}\sqrt{Re_{\tilde{x}}}} = -T'(0), \quad \text{and} \quad \frac{Sh_{\tilde{x}}}{\sqrt{\tilde{x}/2L}\sqrt{Re_{\tilde{x}}}} = -C'(0). \end{aligned}\right\} \tag{5.22}$$

5.2.7 Solution of the Problem

The system of Eqs. (5.17) - (5.20) along with the boundary conditions (5.21), is solved numerically, using the successive linearisation method as explained in Chapter-2.

Proceeding as in Chapter-2, we obtain the following matrix equation

$$\mathbf{A}_{i-1}\mathbf{X}_i = \mathbf{R}_{i-1}, \tag{5.23}$$

subject to the boundary conditions

$$F_i(\xi_N) = \sum_{k=0}^{N}\mathbf{D}_{0k}F_i(\xi_k) = \sum_{k=0}^{N}(\lambda\mathbf{D}2_{Nk} - \mathbf{D}_{Nk})F_i(\xi_k) = 0 \tag{5.24a}$$

$$W_i(\xi_N) = W_i(\xi_0) = T_i(\xi_N) = T_i(\xi_0) = C_i(\xi_N) = C_i(\xi_0) = 0 \tag{5.24b}$$

In Eq.(5.23), $\mathbf{A}_{i-1}$ is a (4N + 4)×(4N + 4) square matrix and $\mathbf{X}_i$ and $\mathbf{R}_{i-1}$ are (4N + 4)×1 column vectors defined by

$$\mathbf{A}_{i-1} = [A_{rs}], r, s = 1, 2, 3, 4, \quad \mathbf{X}_i = \begin{bmatrix} \mathbf{F}_i \\ \mathbf{W}_i \\ \mathbf{\Theta}_i \\ \mathbf{\Phi}_i \end{bmatrix}, \quad \mathbf{R}_{i-1} = \begin{bmatrix} \mathbf{E}_{1,i-1} \\ \mathbf{E}_{2,i-1} \\ \mathbf{E}_{3,i-1} \\ \mathbf{E}_{4,i-1} \end{bmatrix} \tag{5.25}$$

where

$$\mathbf{F}_i = [F_i(\xi_0), F_i(\xi_1), F_i(\xi_2), ..., F_i(\xi_{N-1}), F_i(\xi_N)]^T,$$
$$\mathbf{W}_i = [W_i(\xi_0), W_i(\xi_1), W_i(\xi_2), ..., W_i(\xi_{N-1}), W_i(\xi_N)]^T,$$
$$\mathbf{\Theta}_i = [T_i(\xi_0), T_i(\xi_1), T_i(\xi_2), ..., T_i(\xi_{N-1}), T_i(\xi_N)]^T,$$
$$\mathbf{\Phi}_i = [C_i(\xi_0), C_i(\xi_1), C_i(\xi_2), ..., C_i(\xi_{N-1}), C_i(\xi_N)]^T,$$
$$\mathbf{E}_{1,i-1} = [\zeta_{1,i-1}(\xi_0), \zeta_{1,i-1}(\xi_1), \zeta_{1,i-1}(\xi_2), ..., \zeta_{1,i-1}(\xi_{N-1}), \zeta_{1,i-1}(\xi_N)]^T$$
$$\mathbf{E}_{2,i-1} = [\zeta_{2,i-1}(\xi_0), \zeta_{2,i-1}(\xi_1), \zeta_{2,i-1}(\xi_2), ..., \zeta_{2,i-1}(\xi_{N-1}), \zeta_{2,i-1}(\xi_N)]^T$$
$$\mathbf{E}_{3,i-1} = [\zeta_{3,i-1}(\xi_0), \zeta_{3,i-1}(\xi_1), \zeta_{3,i-1}(\xi_2), ..., \zeta_{3,i-1}(\xi_{N-1}), \zeta_{3,i-1}(\xi_N)]^T$$
$$\mathbf{E}_{4,i-1} = [\zeta_{4,i-1}(\xi_0), \zeta_{4,i-1}(\xi_1), \zeta_{4,i-1}(\xi_2), ..., \zeta_{4,i-1}(\xi_{N-1}), \zeta_{4,i-1}(\xi_N)]^T$$
$$A_{11} = \chi_{11,i-1}\mathbf{D}^3 + \chi_{12,i-1}\mathbf{D}^2 + \chi_{13,i-1}\mathbf{D} + \chi_{14,i-1}, \quad A_{12} = \chi_{15,i-1},$$
$$A_{13} = \chi_{16,i-1}\mathbf{D} + \chi_{17,i-1}, \quad A_{14} = \chi_{18,i-1}$$
$$A_{21} = \chi_{21,i-1}\mathbf{D} + \chi_{22,i-1}, \quad A_{22} = \chi_{23,i-1}\mathbf{D}^2 + \chi_{24,i-1}\mathbf{D} + \chi_{25,i-1},$$
$$A_{23} = \chi_{26,i-1}\mathbf{D} + \chi_{27,i-1}, \quad A_{24} = \mathbf{0}$$
$$A_{31} = \chi_{31,i-1}\mathbf{D} + \chi_{32,i-1}, \quad A_{32} = \mathbf{0}, \quad A_{33} = \chi_{33,i-1}\mathbf{D}^2 + \chi_{34,i-1}\mathbf{D} + \chi_{35,i-1}, \quad A_{34} = \mathbf{0}$$
$$A_{41} = \chi_{41,i-1}\mathbf{D} + \chi_{42,i-1}, \quad A_{42} = \mathbf{0}, \quad A_{43} = \mathbf{0}, \quad A_{44} = \frac{1}{Sc}\mathbf{D}^2 + \chi_{43,i-1}\mathbf{D} + \chi_{44,i-1}$$

Here $\mathbf{I}$ is an identity matrix of size (N +1)×(N +1). After modifying the matrix system (5.23) to incorporate boundary conditions (5.24), the solution is obtained as

$$\mathbf{X}_i = \mathbf{A}_{i-1}^{-1}\mathbf{R}_{i-1} \tag{5.26}$$

5.2.8 Results and Discussion

The comparison of the results with the results obtained by Magyari and Keller [56] as a special case by taking $Ri = 0$, $H_a = 0$, $S = 0$, $\lambda = 0$, $\theta_r \to \infty$, $q_1 = 0$, and $\epsilon = 0$ is presented in Table (5.2).

The variation of both the velocities, temperature and concentration under the influence of Hall parameter β_h, is demonstrated in the Figs. (5.7(a)) - (5.7(d)). The Hall parameter increases the tangential velocity as shown in the Fig. (5.7(a)). In the absence of the hall

Table 5.2: *Comparison of* $-F''(0)$ *and* $F(\infty)$ *calculated by the present method for* $S = 0$, $\lambda = 0$, $H_a = 0$, $\theta_r \to \infty$, $\epsilon = 0$, $q_1 = 0$, *and* $Ri = 0$.

	Magyari and Keller [56]	Present
$-F''(0)$	1.281808	1.28180856
$F(\infty)$	0.905639	0.90564382

parameter ($\beta_h = 0$) there is no transverse flow velocity as shown in Fig. (5.7(b)).

The effect of the viscosity parameter θ_r ($\theta_r = 2.0, 3.0, 5.0, \infty$) on the velocities, the temperature and the concentration is presented in the Figs. (5.8(a)) - (5.8(d)). The tangential velocity decreases as the viscosity parameter $\theta_r \to \infty$ as shown in the Fig. (5.8(a)). This is due to the fact that an increase in the viscosity parameter θ_r decreases the boundary layer thickness which results in decrease of the tangential velocity. Further, the transverse flow increases as the the viscosity parameter $\theta_r \to \infty$ as shown in the Fig. (5.8(b)). There is a slightly decrease in the temperature and an increase in the fluid concentration as the value of the viscosity parameter $\theta_r \to \infty$ as demonstrated through the Figs. (5.8(c)) - (5.8(d)).

The variation of both velocities, the temperature and the concentration for diverse values of the thermal conductivity parameter ϵ is shown graphically through the Figs. (5.9(a)) - (5.9(b)). The fluid velocity is increasing with the increase in the values of the thermal conductivity parameter ϵ as depicted in the Fig. (5.9(a)). Fig. (5.9(b)) shows that the secondary velocity increases first reaching to a maximum with ϵ for every profile slightly, and then gradually decreases with the increasing boundary layer thickness and about from $\eta = 3.8$, the trend is reversed with the rising values of ϵ. From Figs. (5.9(c)) - (5.9(d)), it is evident that the temperature is increasing and the concentration is decreasing with the increasing values of the thermal conductivity parameter ϵ. It is also observed that the increase in the temperature is more when compared that of the decrease in the concentration with ϵ.

The effect of heat source parameter q_1 on both the velocities, temperature and concentration is presented in the Figs. (5.10(a)) - (5.10(b)). Both the fluid velocities are increasing with the increase in the value of heat source parameter q_1 as presented in the Figs. (5.10(a))

and (5.10(b)). Figs. (5.10(c)) and (5.10(d)), demonstrate that the fluid temperature increases and the concentration decreases as the value of the heat source parameter q_1 is increasing.

The behavior of the rate of heat and mass transfers against suction/injection parameter S are presented in the Figs. (5.11(a)) - (5.14(b)) for different values of β_h, θ_r, ϵ, and q_1. Figures (5.11(a)) and (5.11(b)) demonstrates the variation of the rate of heat and mass transfers for different values of Hall parameter β_h. It is clear from the figures that both the heat and mass transfers are increasing with an increase in the value of Hall parameter β_h. It is evident from the figures that the rate of heat transfer is increasing and the rate of mass transfer is decreasing with θ_r as shown in the Figs. (5.12(a)) and (5.12(b)). From the Figs. (5.13(a)) and (5.13(b)), it is observed an opposite trend, on the rate of heat and mass transfer transfers when θ_r is replaced by thermal conductivity parameter ϵ. From figures (5.14(a)) and (5.14(b)), it is seen that the rate of heat transfer is decreasing and the rate of mass transfer is increasing with an increase in the value of heat source parameter q_1. Further, It is observed from these figures that both the rate of heat and mass transfers are increasing with an increase in the fluid suction. The influence of the velocity slip parameter λ on the rate of heat and mass transfers is depicted in the Figs. (5.15(a)) and (5.15(b)). It is evident from these figures that both the heat and mass transfer rates are reducing with the fluid slippage at the boundary. Moreover, both the heat and mass transfer rates are increasing with the fluid suction.

The variations of the local skin-friction coefficient in $\tilde{x}$ and $\tilde{z}$-directions for diverse values of pertinent parameters are tabulated in Table (5.3). The effect of the slip parameter on both the skin-friction is depicted numerically in the table (5.3) and it is noticeable from the table that the skin-friction in $\tilde{x}$-direction is increasing and $\tilde{z}$-direction is decreasing with the fluid slippage at the boundary. Table (5.3) shows that in the presence of Hall parameter both the skin-friction increase which results in reducing the boundary layer and therefore, higher velocity gradient at the surface. It is also observed that when $\beta_h = 0$, then there is no cross flow velocity and hence there is no skin-friction in $\tilde{z}$-direction. Table (5.3) illustrates that, the fluid suction at the boundary reduces the skin-friction in $\tilde{x}$ and $\tilde{z}$-directions. It is

identified from the table that the skin-friction in $\tilde{x}$-direction is increasing with an increase in the magnitude of the value of θ_r. But, an opposite trend is observed for the skin-friction in $\tilde{z}$-direction. At the end of the table, the influence thermal conductivity and heat source parameters are presented. It is obvious from the table that, both the skin-friction increase with an increase in the value of the thermal conductivity and heat source parameters and hence, fluid velocity enhances in the boundary layer.

Table 5.3: *Variation of skin friction in $\tilde{x}$- and $\tilde{z}$-directions for varying values of suction/injection parameter S, slip parameter λ, Hall parameter β_h, viscosity parameter θ_r, thermal conductivity parameter Ri, and heat source parameter q_1.*

λ	β_h	S	θ_r	ϵ	q_1	$\left(\frac{\theta_r}{\theta_r-1}\right) F''(0)$	$\left(\frac{\theta_r}{\theta_r-1}\right) W'(0)$
0.0	1.0	0.5	2.0	0.1	0.1	-1.782612	0.501525
0.5	1.0	0.5	2.0	0.1	0.1	-0.728843	0.391008
1.0	1.0	0.5	2.0	0.1	0.1	-0.463473	0.358577
2.0	1.0	0.5	2.0	0.1	0.1	-0.269148	0.333299
1.0	0.0	0.5	2.0	0.1	0.1	-0.521005	0.000000
1.0	0.1	0.5	2.0	0.1	0.1	-0.520091	0.053623
1.0	0.5	0.5	2.0	0.1	0.1	-0.501077	0.238343
1.0	2.0	0.5	2.0	0.1	0.1	-0.408879	0.375312
1.0	1.0	-0.4	2.0	0.1	0.1	-0.402515	0.366976
1.0	1.0	-0.2	2.0	0.1	0.1	-0.414789	0.369755
1.0	1.0	0.0	2.0	0.1	0.1	-0.427883	0.368949
1.0	1.0	0.5	2.0	0.1	0.1	-0.463473	0.358577
1.0	1.0	1.0	2.0	0.1	0.1	-0.502533	0.336370
1.0	1.0	0.5	-5.0	0.1	0.1	-0.430670	0.287220
1.0	1.0	0.5	-3.0	0.1	0.1	-0.426055	0.278507
1.0	1.0	0.5	-1.0	0.1	0.1	-0.407420	0.245875
1.0	1.0	0.5	2.0	0.1	0.1	-0.463473	0.358577
1.0	1.0	0.5	3.0	0.1	0.1	-0.453923	0.335858
1.0	1.0	0.5	2.0	0.0	0.1	-0.464558	0.356664
1.0	1.0	0.5	2.0	0.1	0.1	-0.463473	0.358577
1.0	1.0	0.5	2.0	0.5	0.1	-0.460092	0.364618
1.0	1.0	0.5	2.0	1.0	0.1	-0.457247	0.369831
1.0	1.0	0.5	2.0	0.1	-0.2	-0.467421	0.350981
1.0	1.0	0.5	2.0	0.1	-0.1	-0.466202	0.353284
1.0	1.0	0.5	2.0	0.1	0.0	-0.464892	0.355799
1.0	1.0	0.5	2.0	0.1	0.2	-0.462039	0.360916
1.0	1.0	0.5	2.0	0.1	0.4	-0.458192	0.369602

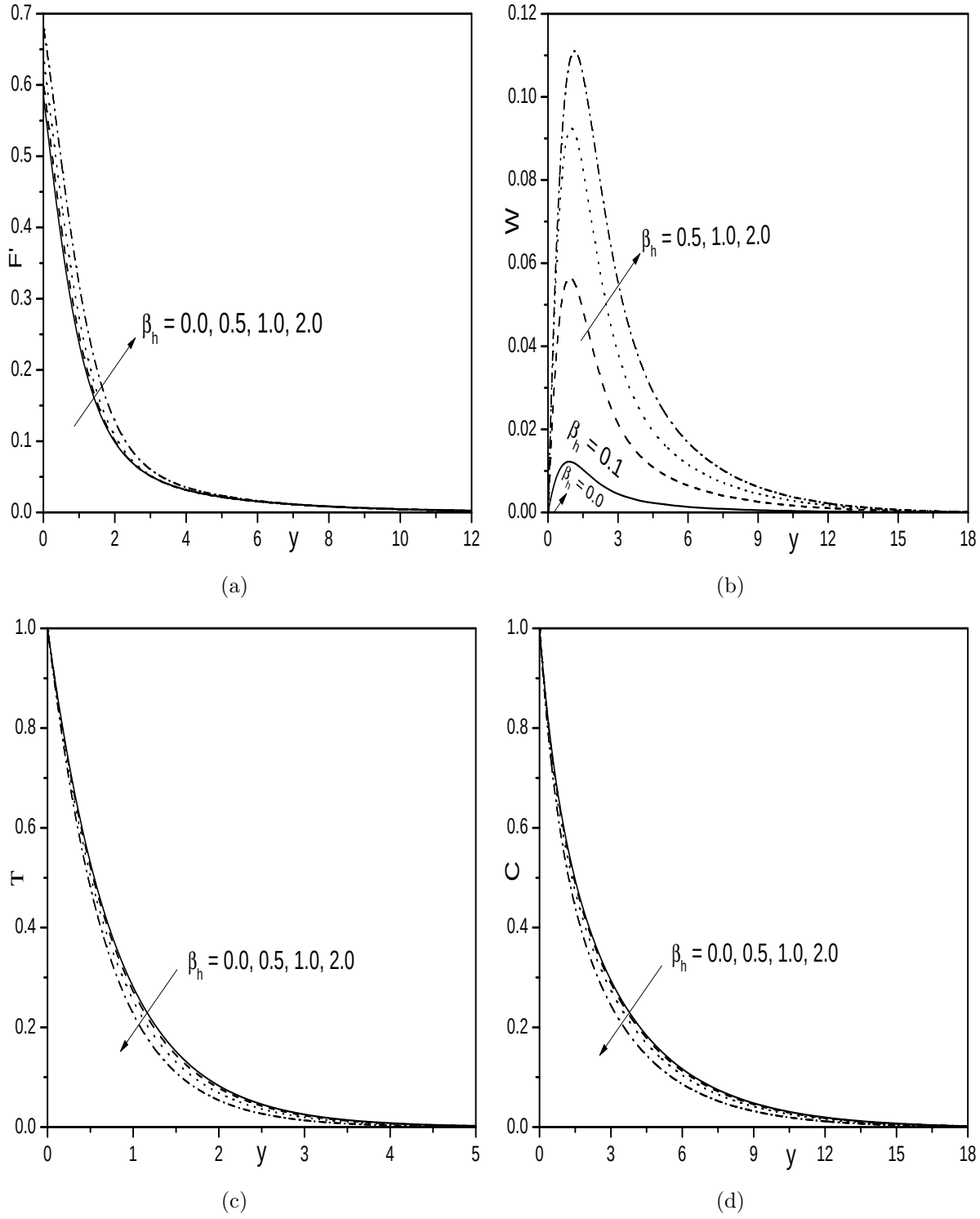

Figure 5.7: *Effect of β_h on (a)Velocity, (b)transverse velocity, (c)Temperature, and (d)Concentration profiles.*

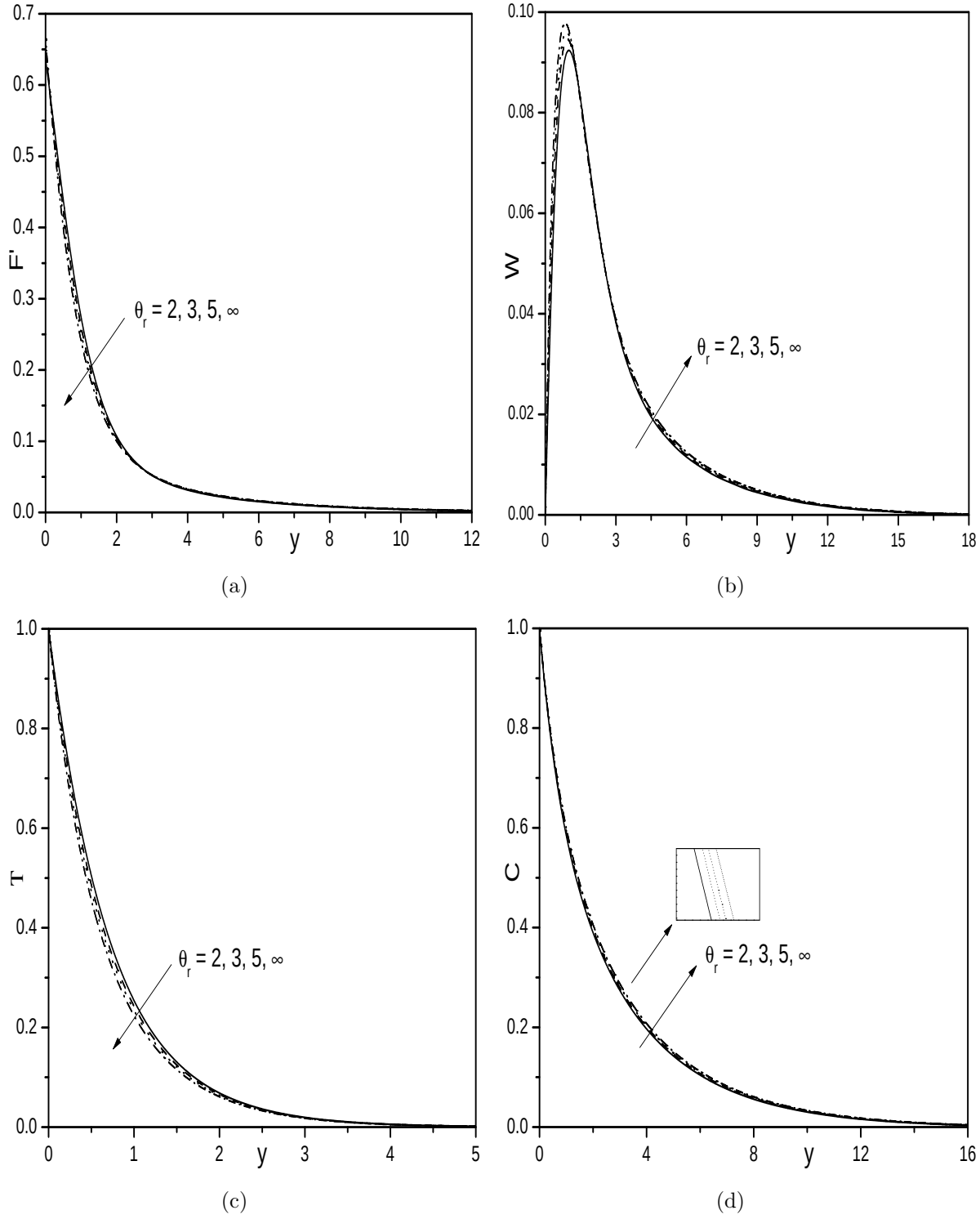

Figure 5.8: *Effect of θ_r on (a)Velocity, (b)transverse velocity, (c)Temperature, and (d)Concentration profiles.*

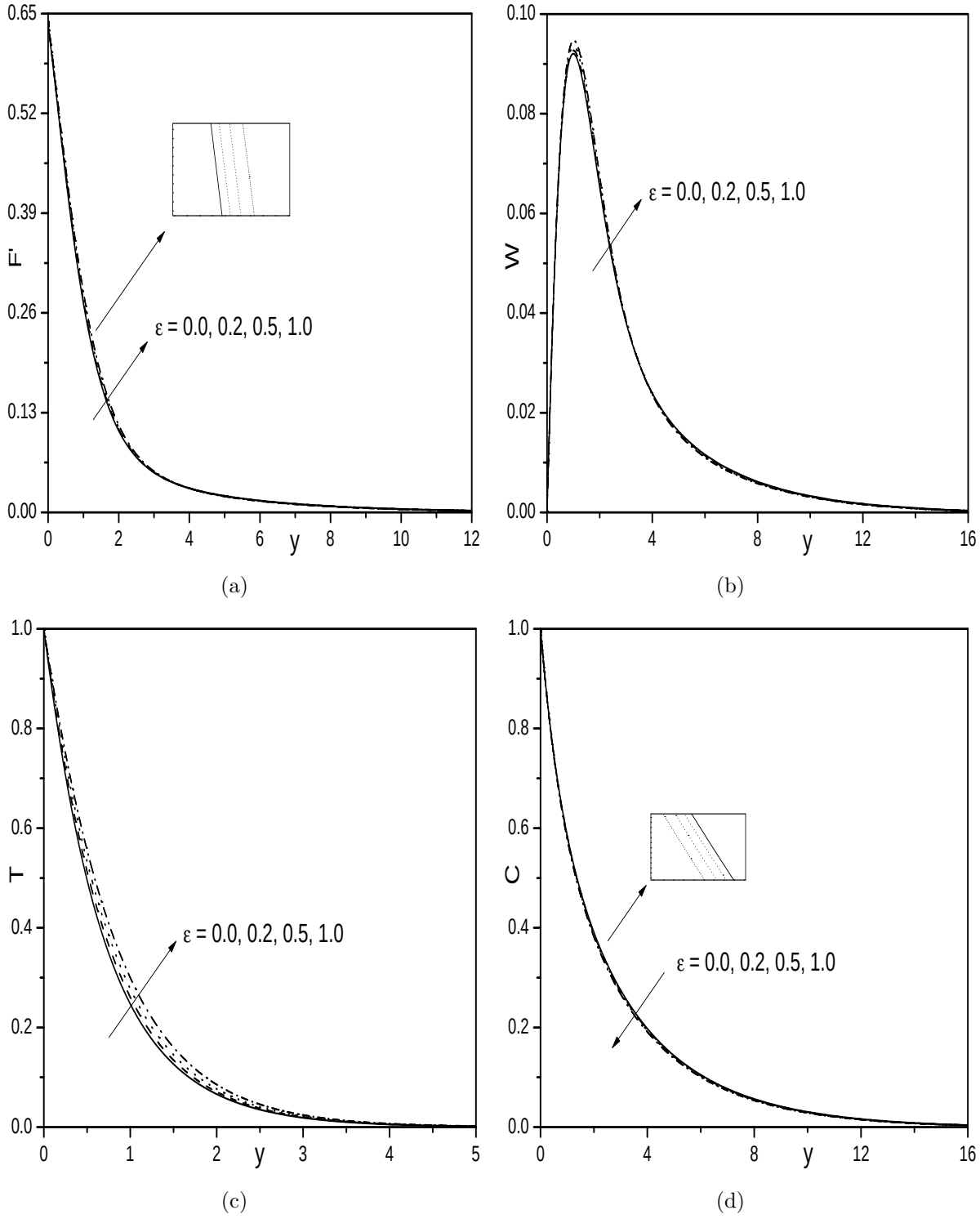

Figure 5.9: *Effect of ϵ on (a)Velocity, (b)transverse velocity, (c)Temperature, and (d)Concentration profiles.*

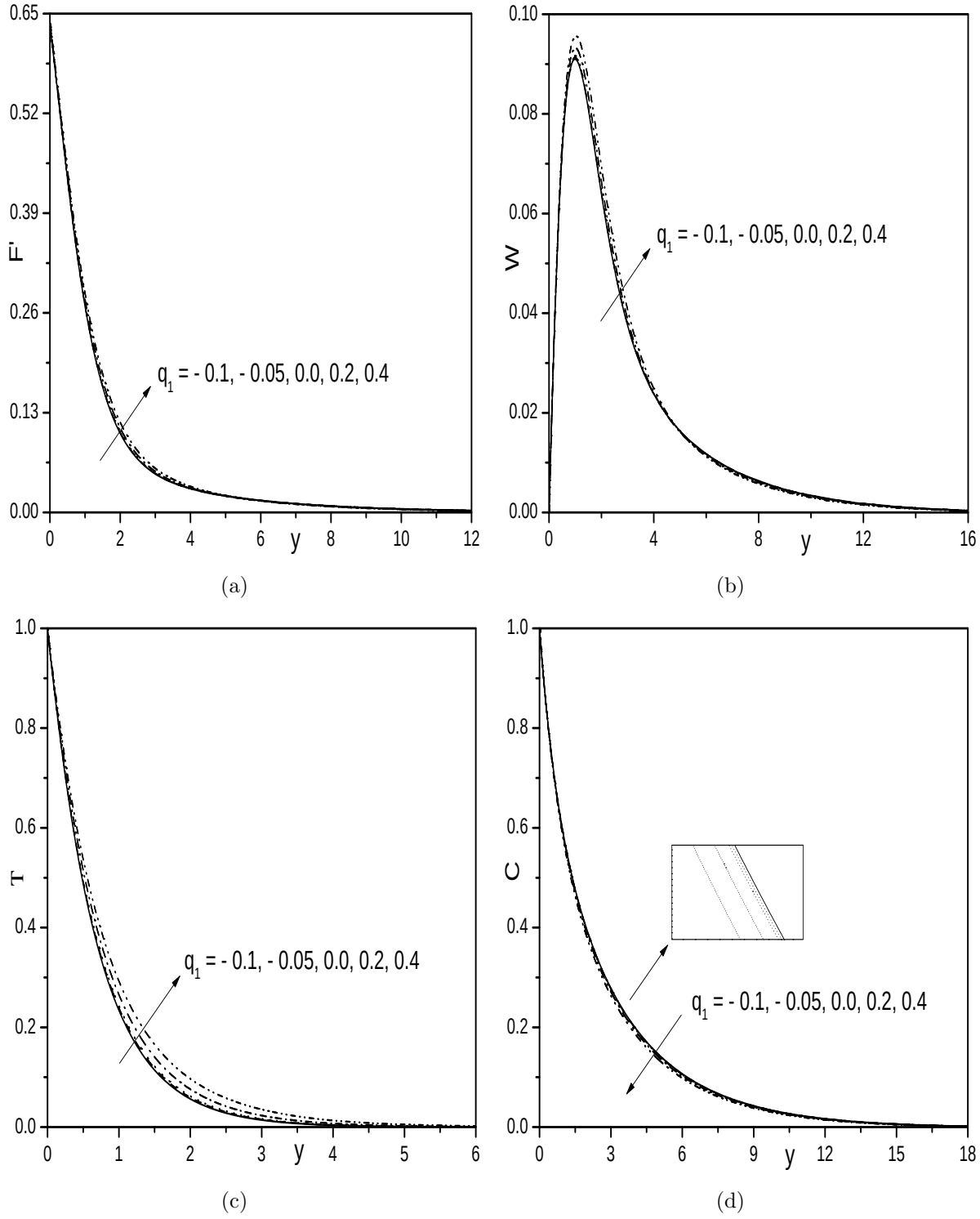

Figure 5.10: *Effect of q_1 on (a)Velocity, (b)transverse velocity, (c)Temperature, and (d)Concentration profiles.*

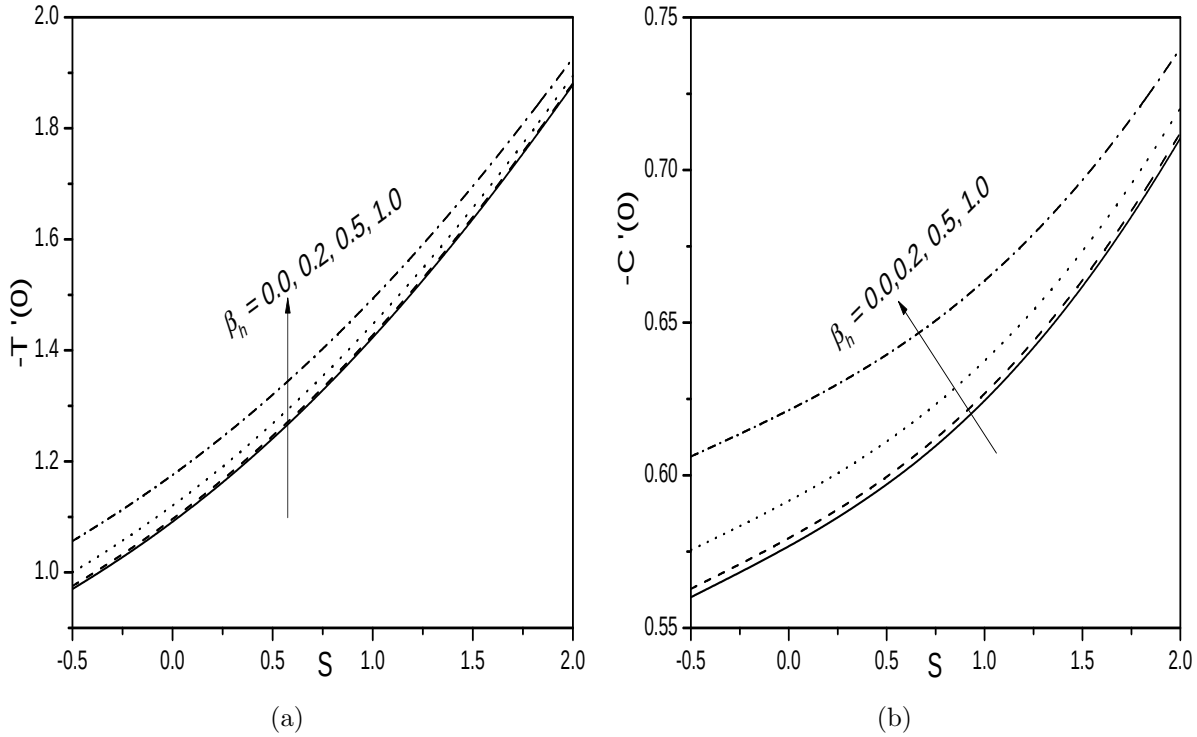

(a) (b)

Figure 5.11: *Effect of β_h on (a) $-T'(0)$, and (b) $-C'(0)$.*

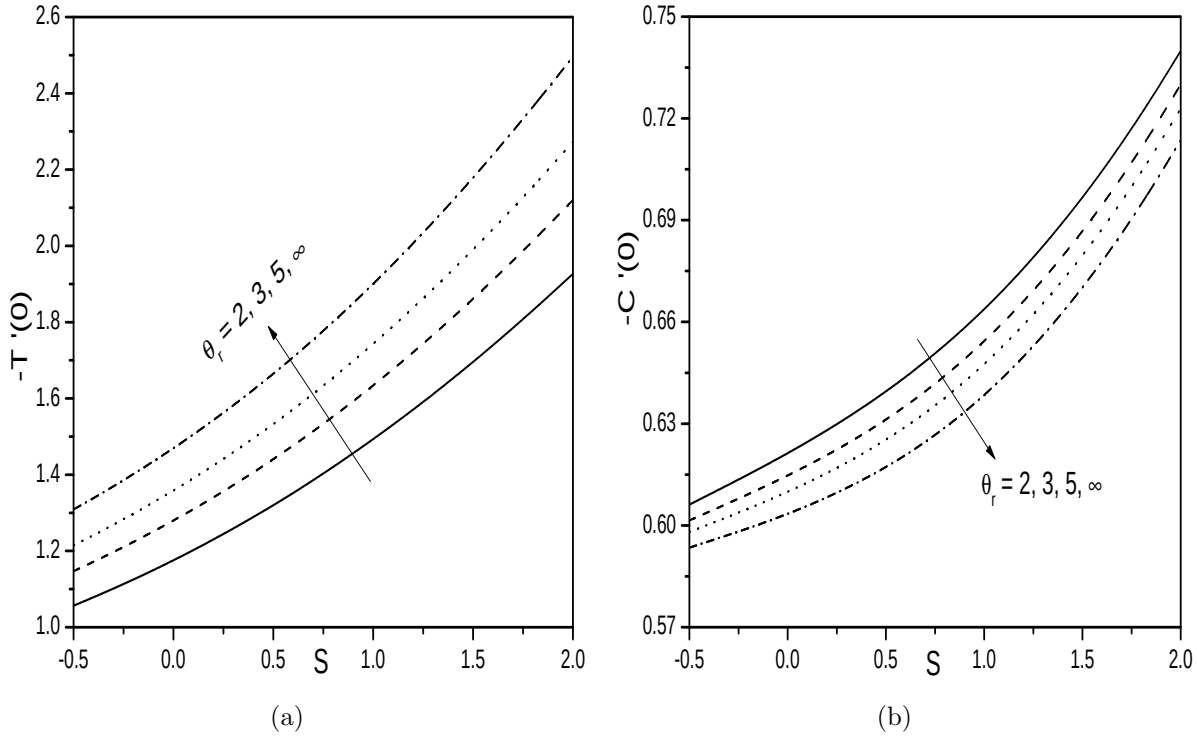

(a) (b)

Figure 5.12: *Effect of θ_r on (a) $-T'(0)$, and (b) $-C'(0)$.*

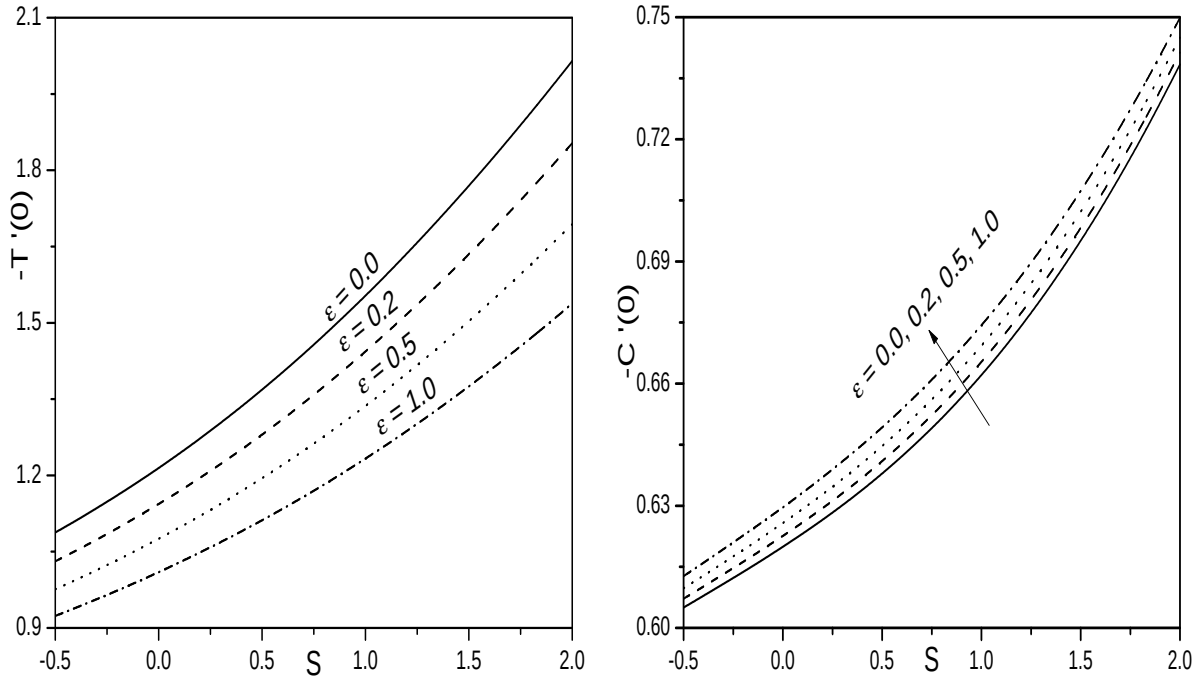

(a) (b)

Figure 5.13: *Effect of* ϵ *on (a)* $-T'(0)$*, and (b)* $-C'(0)$.

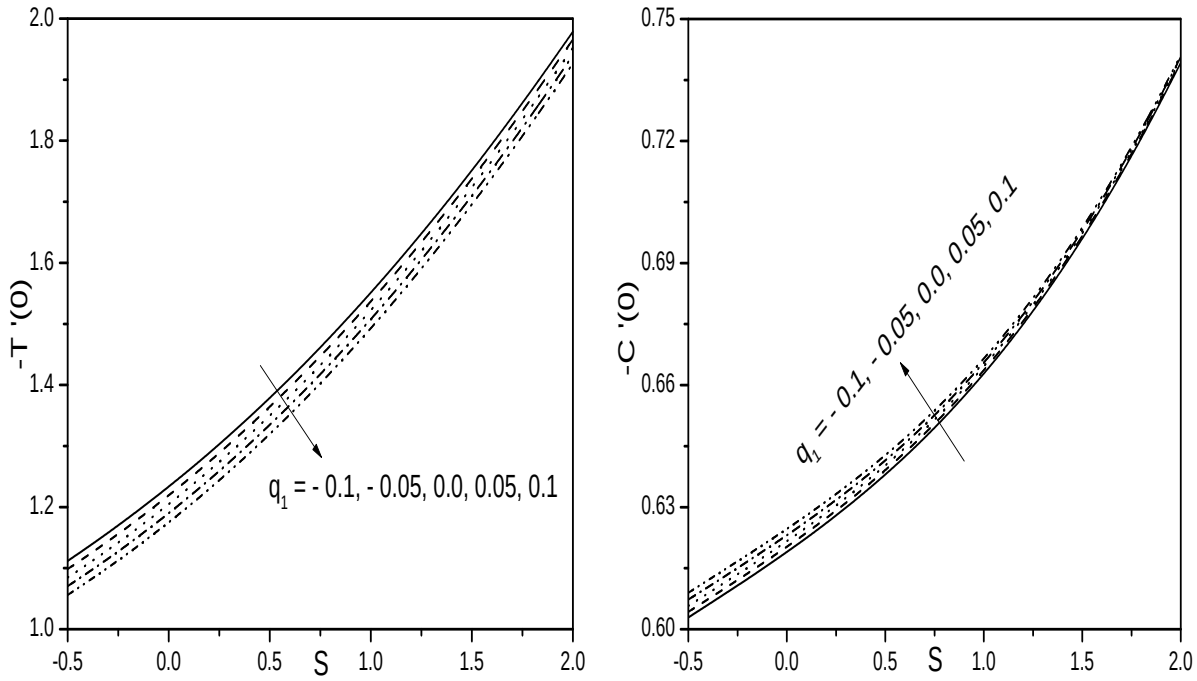

(a) (b)

Figure 5.14: *Effect of* q_1 *on (a)* $-T'(0)$*, and (b)* $-C'(0)$.

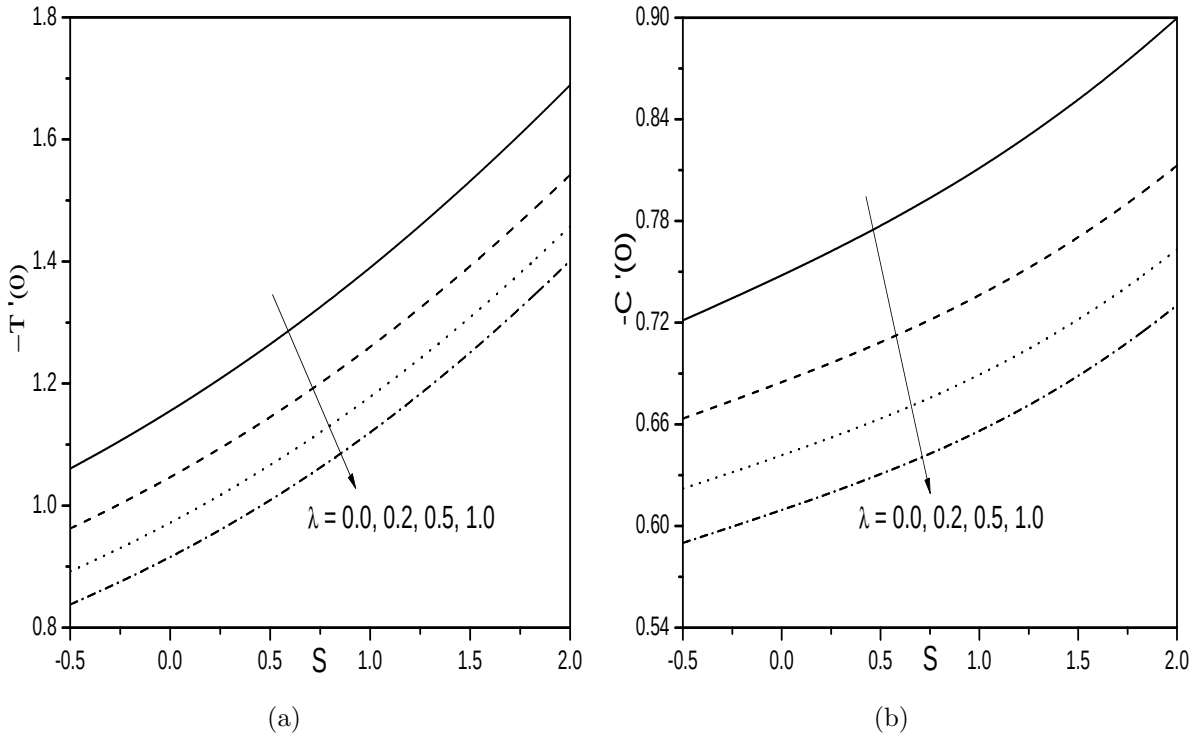

Figure 5.15: *Effect of* λ *on (a)* $-T'(0)$*, and (b)* $-C'(0)$.

5.3 Conclusions

In this chapter, the effect of variable viscosity and thermal conductivity of a viscous fluid flow over an exponentially stretching permeable sheet is considered. From this study the following conclusions are drawn for two cases:

The velocity, in both the cases, decreases with an increase in the value of viscosity parameter and increases with the increase in the thermal conductivity parameter. But, an opposite result is observed for the concentration profile. In case (b), the transverse velocity increases with the increase in the value of the Hall, viscosity, heat source, and thermal conductivity parameters. In both cases, the temperature increase with an increase in the value of thermal conductivity and heat source parameters. While, in case (a), the temperature increases with the increase in the Biot number and in case (b), the temperature decreases with the increase in the Hall parameter. In case (a), the skin-friction decreases with an increase in the value of thermal conductivity and heat source parameters. While in case (b), it increases. In both the cases, the skin-friction increase with an increase in the thermal conductivity parameter, while skin-friction in $\tilde{z}$-direction decreases. In case (a) and (b), the rate of heat transfer increases with the increase in viscosity parameter and decreases with an increase in the thermal conductivity and heat source parameters. Whereas an opposite trend is observed for the rate of mass transfer. In case (b), both the heat and mass transfer rates are decreasing with the slipperiness and increasing with the Hall parameter. Further, in both the cases, the skin-friction decrease and the rate of heat and mass transfers increase with the fluid suction.

Chapter 6

Viscous fluid flow over an exponentially stretching sheet with thermophoresis and viscous dissipation [1]

6.1 Introduction

Thermophoresis is a mechanism in which small particles migrate in the direction of decreasing thermal gradient. It is quite significant in radioactive particle deposition in nuclear reactor safety simulations, aerosol particle sampling, deposition of silicon thin films etc. Sandeep and Sulochana [92] studied the nanofluid flow over an exponentially stretching porous sheet immersed in a porous medium in the presence of thermophoresis, radiation and magnetic field. Viscous dissipation is necessary when analyzing the characteristics of fluids with low specific heat and high viscosity. It is significant in geological process, nuclear engineering and number of devices which are subjected to large deceleration or high rotational speeds. Megahed

[1] Case(a): Communicated to "**International Journal of Applied Mechanics and Engineering**", Case(b) Communicated to "**Journal of the Association of Arab Universities for Basic and Applied Sciences**"

[63] reported the flow of Casson thin film over an unsteady stretching sheet in the presence of viscous dissipation and velocity slip. Daniel [19] presented the MHD nanofluid flow and slip boundary conditions over an exponential stretching sheet in the presence of thermal radiation and thermophoresis effects. Mahantesh *et al.* [57] investigated Unsteady three-dimensional MHD flow of a nano Eyring-Powell fluid past a convectively heated stretching sheet in the presence of thermal radiation, viscous dissipation and Joule heating.

This chapter investigates the thermophoresis and viscous dissipation effects on the incompressible viscous fluid flow over an permeable exponentially stretching sheet.

6.2 Formulation of the Problem

Consider the slip flow of an incompressible viscous fluid over an exponential stretching permeable sheet with thermophoresis and viscous dissipation effects. Making use of the assumptions of case (a) of Chapter-2, the equations governing the flow are given by

$$\frac{\partial \tilde{u}_x}{\partial \tilde{x}} + \frac{\partial \tilde{u}_y}{\partial \tilde{y}} = 0 \tag{6.1}$$

$$\tilde{u}_x \frac{\partial \tilde{u}_x}{\partial \tilde{x}} + \tilde{u}_y \frac{\partial \tilde{u}_x}{\partial \tilde{y}} = \nu \frac{\partial^2 \tilde{u}_x}{\partial \tilde{y}^2} \tag{6.2}$$

$$\tilde{u}_x \frac{\partial \tilde{T}}{\partial \tilde{x}} + \tilde{u}_y \frac{\partial \tilde{T}}{\partial \tilde{y}} = \alpha \frac{\partial^2 \tilde{T}}{\partial \tilde{y}^2} + \frac{\mu}{\rho c_p} \left(\frac{\partial \tilde{u}_x}{\partial \tilde{y}} \right)^2 \tag{6.3}$$

$$\tilde{u}_x \frac{\partial \tilde{C}}{\partial \tilde{x}} + \tilde{u}_y \frac{\partial \tilde{C}}{\partial \tilde{y}} = D \frac{\partial^2 \tilde{C}}{\partial \tilde{y}^2} - \frac{\partial}{\partial y} \left[V_T (\tilde{C} - C_\infty) \right] \tag{6.4}$$

where V_T is the thermophoretic velocity.

The term V_T ([111]) in (6.4) can be written as

$$V_T = -\frac{\nu \; k_t}{T_r} \frac{\partial \tilde{T}}{\partial \tilde{y}} \tag{6.5}$$

where T_r is the reference temperature and k_t is the thermophoretic coefficient.

6.2.1 Case(a): Convective Thermal Condition

Assume that the sheet is either cooled or heated convectively through a fluid with temperature T_f and which induces a heat transfer coefficient h_f, where $h_f = h\sqrt{\frac{U_0}{2L}}e^{\frac{\tilde{x}}{2L}}$.

The non-dimensional form of the conditions at the boundary are

$$\left.\begin{aligned} &F(x,0) + 2\tfrac{\partial F}{\partial x}(x,0) = S,\ F'(x,0) = 1 + \lambda F''(x,0), \\ &T'(x,0) = -Bi(1 - T(x,0)),\ C(x,0) = 1, \\ &F'(x,y) \to 0,\ T(x,y) \to 0,\ C(x,y) \to 0 \ \text{ as } \ y \to \infty \end{aligned}\right\} \tag{6.6}$$

The dimensionless form of the equations (6.1) - (6.4) governing the flow(see case (a) of Chapter-3) are

$$F''' + FF'' - 2F'^2 + 2\left(F''\frac{\partial F}{\partial x} - F'\frac{\partial F'}{\partial x}\right) = 0 \tag{6.7}$$

$$\frac{1}{Pr}T'' + FT' + Ec\ e^{2x}\ F''^2 + 2\left(T'\frac{\partial F}{\partial x} - F'\frac{\partial T}{\partial x}\right) = 0 \tag{6.8}$$

$$\frac{1}{Sc}C'' + FC' - \tau\left(T'C' + C\ T''\right) + 2\left(C'\frac{\partial F}{\partial x} - F'\frac{\partial C}{\partial x}\right) = 0 \tag{6.9}$$

where $Ec = \frac{U_0^2}{c_p(T_f - T_\infty)}$ is the Eckert number and $\tau = -\frac{k_t}{T_r}(T_f - T_\infty)$ is the thermophoretic parameter (The surface is cold for $\tau > 0$ and hot for $\tau < 0$ [66, 114]).

6.2.2 Skin Friction, Heat and Mass Transfer Coefficients

The non-dimensional skin friction C_f, the local Nusselt number $Nu_{\tilde{x}}$ and the local Sherwood number $Sh_{\tilde{x}}$, are given by

$$\left.\frac{\sqrt{Re_x}\ C_f}{\sqrt{2x/L}} = F''(0),\ \frac{Nu_x}{\sqrt{x/2L}\sqrt{Re_x}} = -T'(0),\ \text{and}\ \frac{Sh_x}{\sqrt{x/2L}\sqrt{Re_x}} = -C'(0)\ \right\} \tag{6.10}$$

6.2.3 Solution of the Problem

The system of Eqs. (6.7) - (6.9) along with the boundary conditions (6.6), is solved numerically, as explained in case (a) of Chapter-3.

Proceeding in case (a) of Chapter-3, we obtain the following matrix equation

$$\mathbf{A}_{i-1}\mathbf{X}_i = \mathbf{R}_{i-1}, \tag{6.11}$$

In Eq. (6.11), $\mathbf{A}_{i-1}$ is a (6N + 6)×(6N + 6) square matrix and $\mathbf{X}_i$ and $\mathbf{R}_{i-1}$ are (6N + 6)×1 column vectors defined by

$$\mathbf{A}_{i-1} = [A_{rs}], r, s = 1, 2, \cdots, 6, \quad \mathbf{X}_i = \begin{bmatrix} \mathbf{F}_i \\ \mathbf{\Theta}_i \\ \mathbf{\Phi}_i \\ \mathbf{G}_i \\ \mathbf{H}_i \\ \mathbf{K}_i \end{bmatrix}, \quad \mathbf{R}_{i-1} = \begin{bmatrix} \mathbf{E}_{1,i-1} \\ \mathbf{E}_{2,i-1} \\ \mathbf{E}_{3,i-1} \\ \mathbf{E}_{4,i-1} \\ \mathbf{E}_{5,i-1} \\ \mathbf{E}_{6,i-1} \end{bmatrix} \tag{6.12}$$

where

$\mathbf{F}_i = [F_i(\xi_0), F_i(\xi_1), F_i(\xi_2), ..., F_i(\xi_{N-1}), F_i(\xi_N)]^T,$
$\mathbf{\Theta}_i = [T_i(\xi_0), T_i(\xi_1), T_i(\xi_2), ..., T_i(\xi_{N-1}), T_i(\xi_N)]^T,$
$\mathbf{\Phi}_i = [C_i(\xi_0), C_i(\xi_1), C_i(\xi_2), ..., C_i(\xi_{N-1}), C_i(\xi_N)]^T,$
$\mathbf{G}_i = [G_i(\xi_0), G_i(\xi_1), G_i(\xi_2), ..., G_i(\xi_{N-1}), G_i(\xi_N)]^T,$
$\mathbf{H}_i = [H_i(\xi_0), H_i(\xi_1), H_i(\xi_2), ..., H_i(\xi_{N-1}), H_i(\xi_N)]^T,$
$\mathbf{K}_i = [K_i(\xi_0), K_i(\xi_1), K_i(\xi_2), ..., K_i(\xi_{N-1}), K_i(\xi_N)]^T,$
$\mathbf{E}_{j,i-1} = [\zeta_{j,i-1}(\xi_0), \zeta_{j,i-1}(\xi_1), \zeta_{j,i-1}(\xi_2), ..., \zeta_{j,i-1}(\xi_{N-1}), \zeta_{j,i-1}(\xi_N)]^T, j = 1, 2, 3, 4, 5, 6$
$A_{11} = \mathbf{D}^3 + \chi_{11,i-1}\mathbf{D}^2 + \chi_{12,i-1}\mathbf{D} + \chi_{13,i-1}, \quad A_{12} = \mathbf{0}, \quad A_{13} = \mathbf{0},$
$A_{14} = \chi_{14,i-1}\mathbf{D} + \chi_{15,i-1}, \quad A_{15} = \mathbf{0}, \quad A_{16} = \mathbf{0},$
$A_{21} = \chi_{21,i-1}\mathbf{D}^2 + \chi_{22,i-1}\mathbf{D} + \chi_{23,i-1}, \quad A_{22} = \frac{1}{Pr}\mathbf{D}^2 + \chi_{24,i-1}\mathbf{D}, \quad A_{23} = \mathbf{0},$
$A_{24} = \chi_{25,i-1}, \quad A_{25} = \chi_{26,i-1}, \quad A_{26} = \mathbf{0},$

$$A_{31} = \chi_{31,i-1}\mathbf{D} + \chi_{32,i-1}, \quad A_{32} = \chi_{32,i-1}\mathbf{D}^2 + \chi_{34,i-1}\mathbf{D}, \quad A_{33} = \tfrac{1}{Sc}\mathbf{D}^2 + \chi_{35,i-1}\mathbf{D} + \chi_{36,i-1},$$
$$A_{34} = \chi_{37,i-1}, \quad A_{35} = \mathbf{0}, \quad A_{36} = \chi_{38,i-1},$$
$$A_{41} = \chi_{41,i-1}\mathbf{D}^2 + \chi_{42,i-1}\mathbf{D} + \chi_{43,i-1}, \quad A_{42} = \mathbf{0}, \quad A_{43} = \mathbf{0},$$
$$A_{44} = \mathbf{D}^3 + \chi_{44,i-1}\mathbf{D}^2 + \chi_{45,i-1}\mathbf{D} + \chi_{46,i-1}, \quad A_{45} = \mathbf{0}, \quad A_{46} = \mathbf{0},$$
$$A_{51} = \chi_{51,i-1}\mathbf{D}^2 + \chi_{52,i-1}, \quad A_{52} = \chi_{53,i-1}\mathbf{D}, \quad A_{53} = \mathbf{0},$$
$$A_{54} = \chi_{54,i-1}\mathbf{D}^2 + \chi_{55,i-1}\mathbf{D} + \chi_{56,i-1}, \quad A_{55} = \tfrac{1}{Pr}\mathbf{D}^2 + \chi_{57,i-1}\mathbf{D} + \chi_{58,i-1}, \quad A_{56} = \mathbf{0},$$
$$A_{61} = \chi_{61,i-1}, \quad A_{62} = \chi_{62,i-1}\mathbf{D}^2 + \chi_{63,i-1}\mathbf{D}, \quad A_{63} = \chi_{64,i-1}\mathbf{D} + \chi_{65,i-1},$$
$$A_{64} = \chi_{66,i-1}\mathbf{D} + \chi_{67,i-1}, \quad A_{65} = \chi_{68,i-1}\mathbf{D}^2 + \chi_{69,i-1}\mathbf{D}, \quad A_{66} = \tfrac{1}{Sc}\mathbf{D}^2 + \chi_{610,i-1}\mathbf{D} + \chi_{611,i-1},$$

Here $\mathbf{I}$ is an identity matrix of size (N +1)×(N +1). After modifying the matrix system (6.11) to incorporate boundary conditions, the solution is obtained as

$$\mathbf{X}_i = \mathbf{A}_{i-1}^{-1}\mathbf{R}_{i-1} \tag{6.13}$$

6.2.4 Result and Discussion

The results of the present analysis are compared with the results of the Magyari and Keller [56] as a special case and shown in Table. (6.1). In order to study the effects of Joule heating parameter J, suction/injection parameter S, Biot number Bi, magnetic parameter H_a and velocity slip parameter λ, computations have been carried out taking $S = 0.5$, $Ec = 0.2$, $\lambda = 0.5$, $\tau = 0.3$, $x = 0.2$, and $Bi = 1.0$ unless otherwise mentioned. The behavior of velocity in the presence of the velocity slip at the boundary for the exponentially stretching sheet is presented in the fig. (6.1(a)). The velocity is decreasing with an increase in the slip parameter, which in turn lessens the momentum boundary layer thickness. Figure (6.1(b)) represents the variation of the velocity profile in the presence of suction/injection parameter S. It is observed that the velocity is decreasing by the rise in the value of S. While a reverse trend is noticed for injection($S < 0$). The variation of the skin-friction coefficient $F''(x, 0)$ against non-similar variable x for distinct values of the slip and the suction/injection parameters is presented in the figures (6.2(a)) and (6.2(b)). It is noticed from these figures

Table 6.1: *Comparative analysis for* $\frac{Nu_x}{\sqrt{Lx/2}\sqrt{Re_x}}$ *by the current method for* $\lambda = 0$, $\tau = 0$, $Ec = 0$, $x = 0$, $S = 0$ *and* $Bi \to \infty$.

Nusselt number $\frac{Nu_x}{\sqrt{Lx/2}\sqrt{Re_x}}$		
Pr	Magyari and Keller [56]	Present
0.5	0.330493	0.33053766
1	0.549643	0.54964345
3	1.122188	1.12208577
5	1.521243	1.52123668
8	1.991847	1.99183375
10	2.257429	2.25741862

that the skin-friction coefficient is increasing with an increase in the value of the slip and decreasing with the rise in the suction parameter.

Figures (6.3(a)) - (6.3(d)) exhibit the behaviour of the temperature profile for diverse values of Ec, Bi, λ and S, respectively. It is evident from the figure (6.3(a)) that the temperature is increasing with an increase in the value of Ec. Figure (6.3(b)) shows that the temperature enhancing by the rise in the value of Bi. It is seen that temperature within the boundary layer increases with the increase in the Biot number. For $Bi \to \infty$, equation (6.6) implies $T(0) \to 1$, which is clearly shown in the Fig. (6.3(b)) for larger values of Bi. The figure (6.3(c)) reveals that the temperature profile increases with an increase in the value of the slip parameter λ. Figure (6.3(d)) shows that the temperature of the fluid is decreasing with an increase in the value of the suction parameter and an opposite trend is seen for injection.

The effect of thermophoretic parameter τ, Biot number Bi, slip parameter λ and suction/injection parameter S on the concentration profile is presented in the Figs. (6.4(a)) - (6.4(d)). An increase in the value of τ decreases the concentration as shown in the figure (6.4(a)). This is due to the fact that fluid particles move away from cool surroundings with the increase in the thermophoretic parameter. Figure (6.4(b)) shows that the influence of convection on concentration. It is known that a rise in the convection at the stretching sheet results in lowering thermal penetration and hence decreases the concentration boundary layer thickness. Therefore, mass transfer at the sheet increases with an increase in the value of Bi.

Further, as the value of the slip parameter increases, the concentration of the fluid increases as shown in the Fig. (6.4(c)). Due to which, mass transfer at the sheet decreases. Further, the concentration decreases with the increase in the value of the suction and increases with the increase in the value of the injection as shown in Fig. (6.4(d)).

The variation of heat transfer coefficient for different values of Eckert number, Biot number, slip and suction/injection parameters against non-similar variable x are presented through the Figs. (6.5(a)) - (6.5(d)). It is evident from the Fig. (6.5(a)) that heat transfer from the sheet to the fluid is decreasing with an increase in the value of Ec. In the absence of Eckert number($Ec = 0$), there is no effect of the non-similar variable x on the heat transfer coefficient. As the value of Ec increases, the heat transfer from the sheet to the fluid increases and for higher values of Eckert number heat absorption takes place. Increasing the values of the Biot number enhances the heat transfer coefficient predominantly on the surface due to the strong convection as shown in the Fig. (6.5(b)). Figure (6.5(c)) shows that the rate of heat transfer enhanced with an increase in the slipperiness. But, it is noticed that in the absence of the slipperiness and for small values of slipperiness heat absorption is taking place far away from the boundary. While heat transfer coefficient is increasing with increase in the value of S as depicted in the Fig. (6.5(d)).

The behavior of the mass transfer coefficient with τ against x is portrayed in the Fig. (6.6(a)). It is seen from the figure that the rate of mass transfer is increasing with an increase in the value of τ. Further, it is noticed that for higher values of τ, the mass transfer rate is slightly decreasing with x. The influence of Biot number Bi on the mass transfer rate is presented in the Fig. (6.6(b)). From this figure, it is observed that the rate of mass transfer is increasing with the increase in Bi. From Fig. (6.6(c)) it is evident that the rate of mass transfer is reducing with a rise in the value of λ. Further, in the absence of slip parameter, there is maximum mass transfer from the sheet to the fluid. But, an opposite trend is observed on the rate of mass transfer when the slip parameter is replaced by the Biot number. Finally, the variation of mass transfer coefficient for different values of S is depicted in the Fig. (6.6(d)). This figure reveals that the rate of mass transfer is increasing with an increase in the value of suction and reducing with a rise in the value of injection.

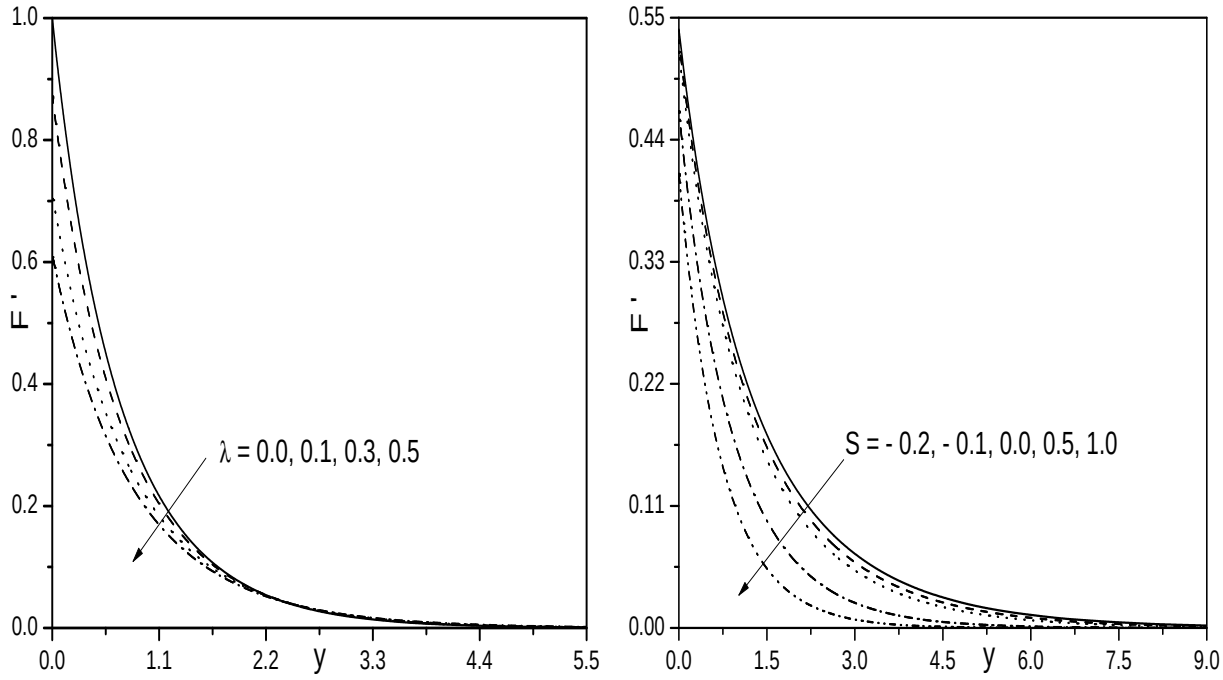

(a) (b)

Figure 6.1: *Effect of(a) λ, and (b) S on F'.*

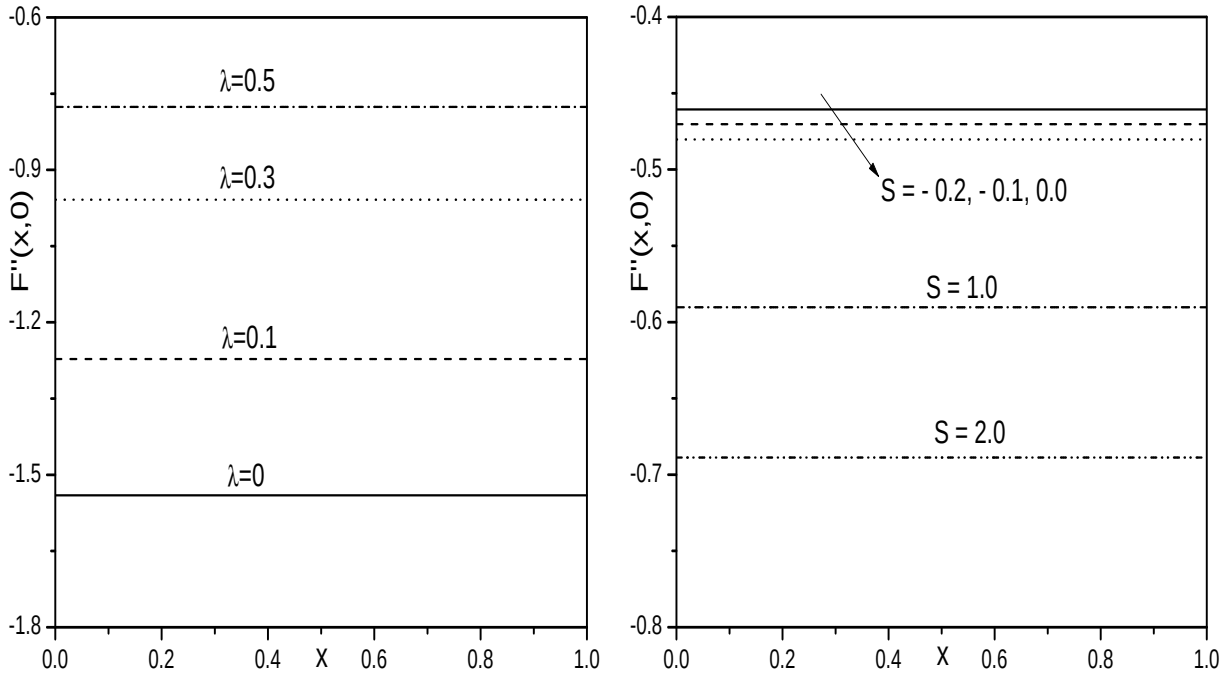

(a) (b)

Figure 6.2: *Effect of (a) λ, and (b) S on $F''(x,0)$.*

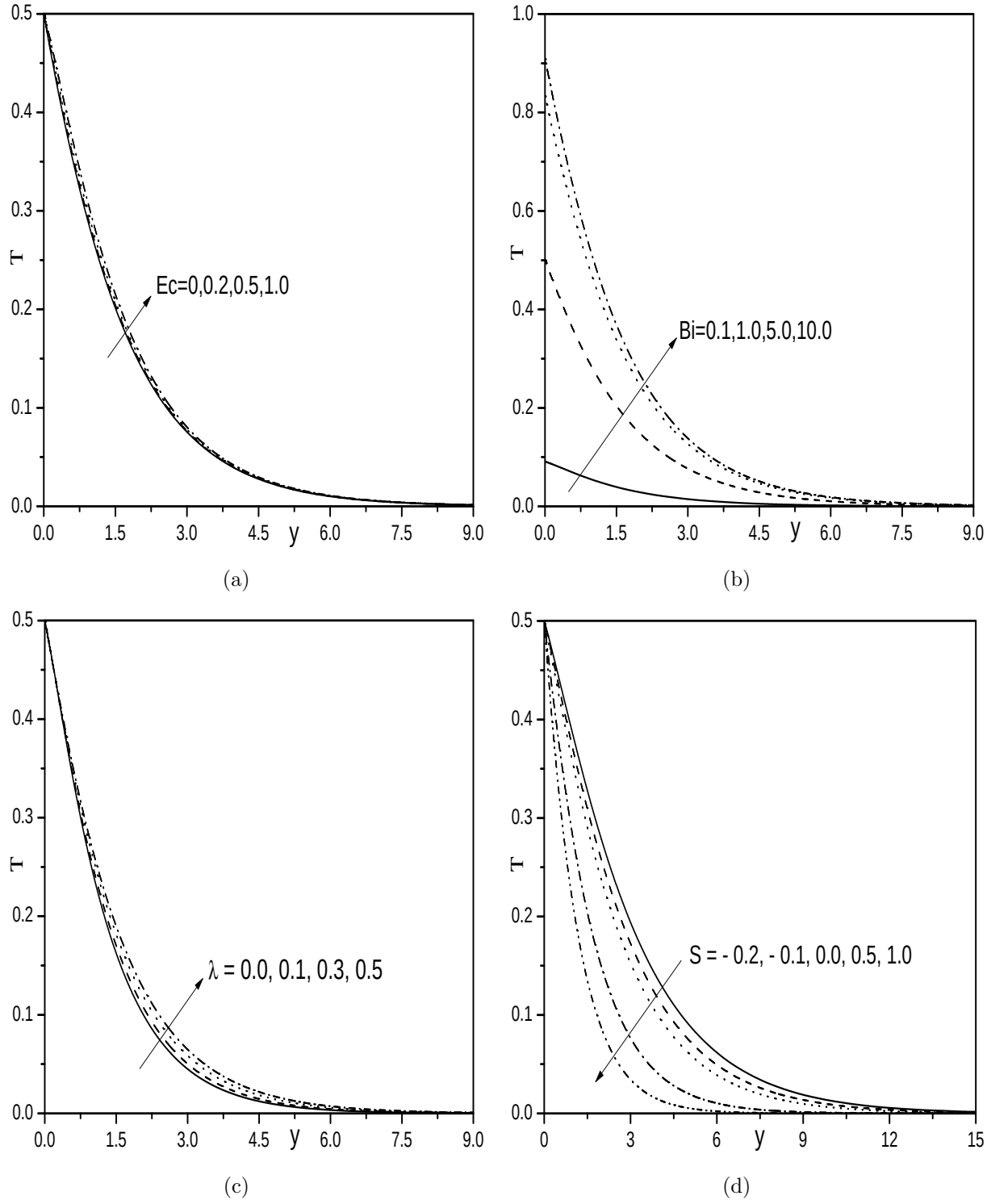

Figure 6.3: *Effect of (a) Ec, (b) Bi, (c) λ, and (d) S on T.*

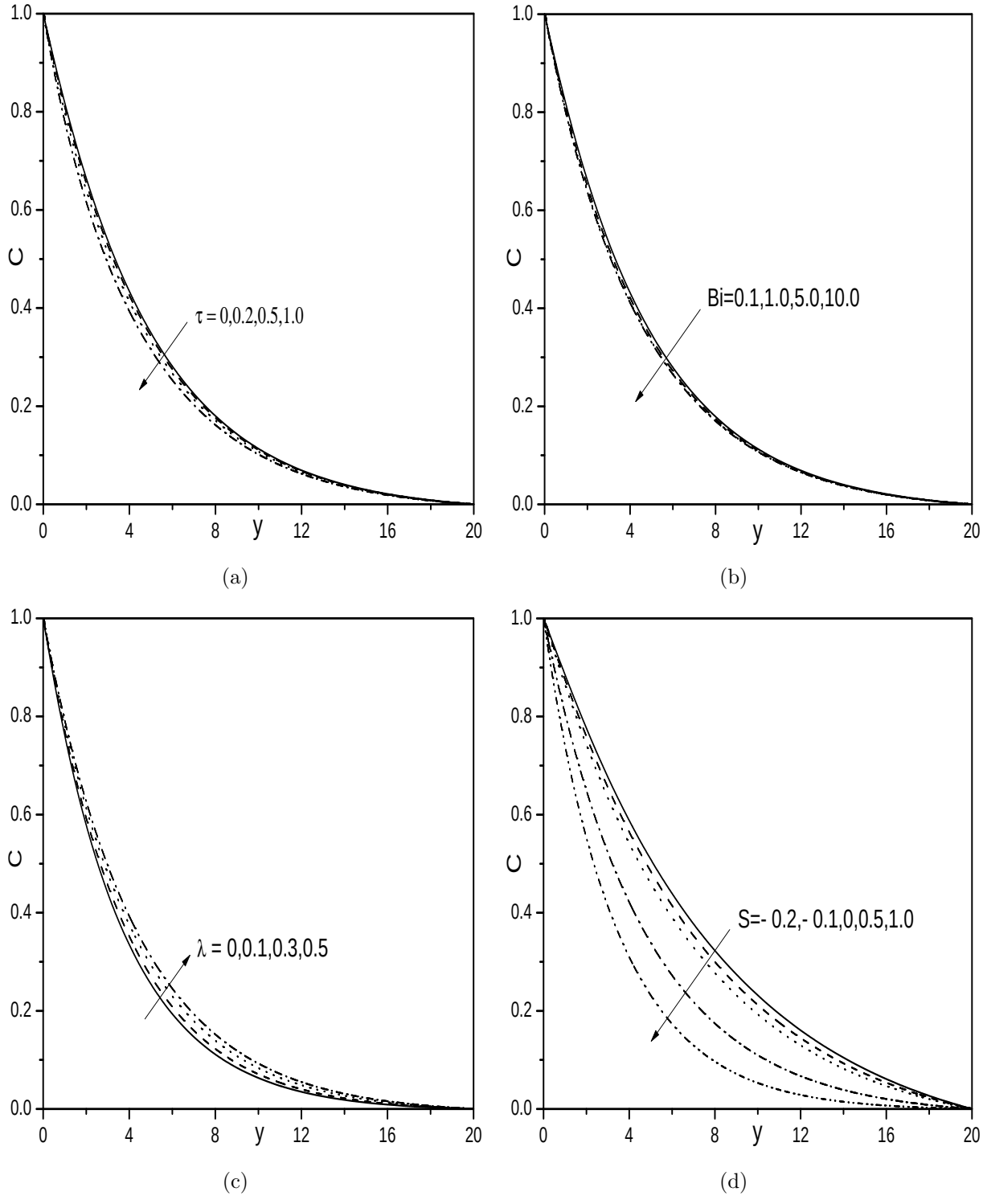

Figure 6.4: *Effect of (a) τ, (b) Bi, (c) λ, and (d) S on C.*

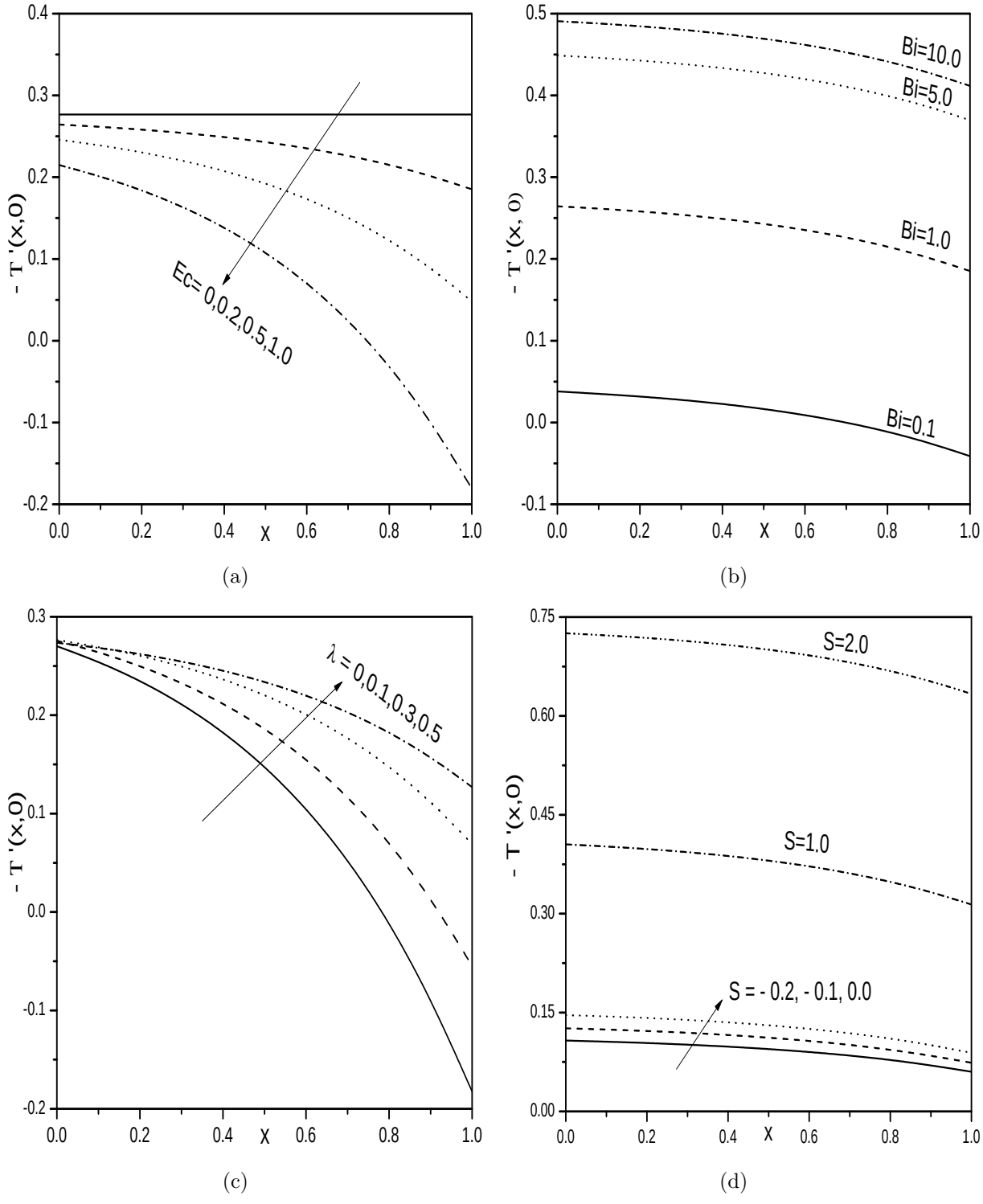

Figure 6.5: *Effect of (a) Ec, (b) Bi, (c) λ, and (d) S on $-T'(x,0)$.*

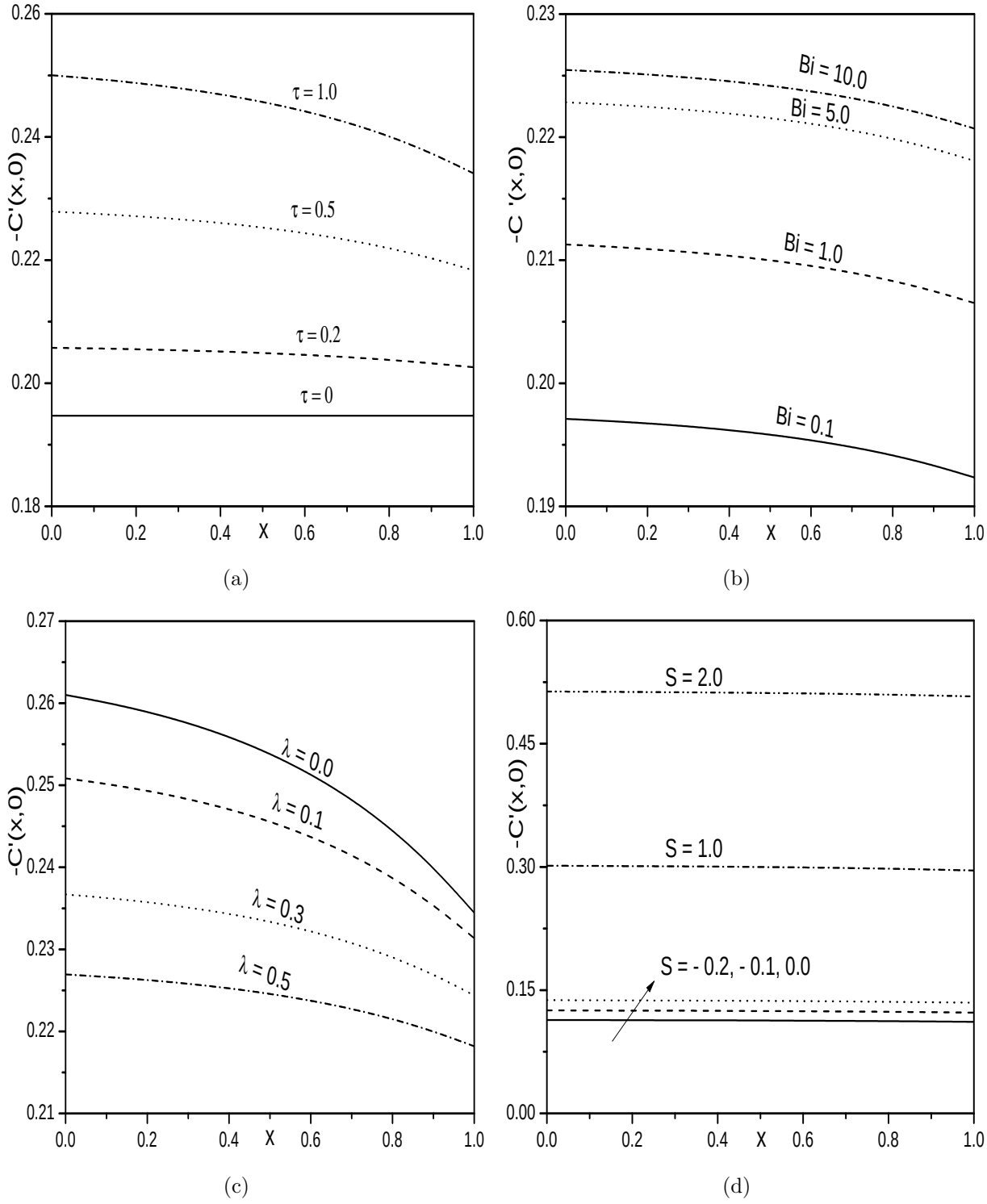

Figure 6.6: *Effect of (a) τ, (b) Bi, (c) λ, and (d) S on $-C'(x,0)$.*

6.2.5 Case(b): Uniform wall temperature with Hall effect

Assume that, a strong magnetic field of strength $B(\tilde{x}) = B_0 e^{\frac{\tilde{x}}{2L}}$ is applied in $\tilde{y}-$direction and the influence of Hall current is not neglected. Assume that magnetic Reynolds number is very small so that the induced magnetic field is negligible in comparison to applied magnetic field. The presence of Hall current induces a cross flow in $\tilde{z}$-direction and hence the flow becomes three-dimensional. Under the Boussinesq approximation, the flow is governed by the following non-dimensional equations

$$F''' + FF'' - 2F'^2 + 2Ri(T + \mathbb{B}C) - \frac{H_a}{1+\beta_h^2}(F' + \beta_h W) = 0 \tag{6.14}$$

$$W'' - 2F'W + FW' + \frac{H_a}{1+\beta_h^2}(\beta_h F' - W) = 0 \tag{6.15}$$

$$\frac{1}{Pr}T'' + FT' - 4F'T + Ec\ (F''^2 + W'^2) = 0 \tag{6.16}$$

$$\frac{1}{Sc}C'' + FC' - 4F'C - \tau\,(T'C' + C\ T'') = 0 \tag{6.17}$$

The corresponding boundary conditions are

$$\left.\begin{array}{l} F(y) = S,\ F'(y) = 1 + \lambda F''(y),\ W(y) = 0,\ T(y) = 1,\ C(y) = 1 \quad \text{at} \quad y = 0 \\ F'(y) \to 0,\ W(y) \to 0,\ T(y) \to 0,\ C(y) \to 0 \quad \text{as} \quad y \to \infty \end{array}\right\} \tag{6.18}$$

where $Ec = \frac{U_0^2}{c_p T_0}$ is the Eckert number and $\tau = -\frac{k_t}{T_r}(T_w - T_\infty)$ is the thermophoretic parameter (The surface is cold for $\tau > 0$ and hot for $\tau < 0$ [66, 114]).

6.2.6 Skin Friction in $\tilde{x}$ and $\tilde{z}$-directions, Heat and Mass Transfer Coefficients

The non-dimensional skin friction in $\tilde{x}-$direction $C_{F\tilde{x}}$, local skin-friction in $\tilde{z}-$direction $C_{F\tilde{z}}$, the local Nusselt number $Nu_{\tilde{x}}$ and the local Sherwood number $Sh_{\tilde{x}}$, are given by

$$\left.\begin{array}{ll} \frac{\sqrt{Re_{\tilde{x}}}}{\sqrt{2\tilde{x}/L}}C_{F\tilde{x}} = F''(0), & \frac{\sqrt{Re_{\tilde{x}}}}{\sqrt{2\tilde{x}/L}}C_{F\tilde{z}} = W'(0), \\ \frac{Nu_{\tilde{x}}}{\sqrt{\tilde{x}/2L}\sqrt{Re_{\tilde{x}}}} = -T'(0), \quad \text{and} & \frac{Sh_{\tilde{x}}}{\sqrt{\tilde{x}/2L}\sqrt{Re_{\tilde{x}}}} = -C'(0). \end{array}\right\} \tag{6.19}$$

where $Re_{\tilde{x}} = \dfrac{\tilde{x}U_*(\tilde{x})}{\nu}$ is the local Reynold's number.

6.2.7 Solution of the Problem

The system of Eqs. (6.14) - (6.17) along with the boundary conditions (6.18), is solved numerically using the successive linearisation method as explained in Chapter-2.

Proceeding as in Chapter-2, we obtain the following matrix equation

$$\mathbf{A}_{i-1}\mathbf{X}_i = \mathbf{R}_{i-1}, \tag{6.20}$$

subject to the boundary conditions

$$F_i(\xi_N) = \sum_{k=0}^{N} \mathbf{D}_{0k}F_i(\xi_k) = \sum_{k=0}^{N}(\lambda\mathbf{D}2_{Nk} - \mathbf{D}_{Nk})F_i(\xi_k) = 0 \tag{6.21a}$$

$$W_i(\xi_N) = W_i(\xi_0) = T_i(\xi_N) = T_i(\xi_0) = C_i(\xi_N) = C_i(\xi_0) = 0 \tag{6.21b}$$

In Eq.(6.20), $\mathbf{A}_{i-1}$ is a (4N + 4)×(4N + 4) square matrix and $\mathbf{X}_i$ and $\mathbf{R}_{i-1}$ are (4N + 4)×1

column vectors defined by

$$\mathbf{A}_{i-1} = [A_{rs}], r, s = 1, 2, 3, 4, \quad \mathbf{X}_i = \begin{bmatrix} \mathbf{F}_i \\ \mathbf{W}_i \\ \mathbf{\Theta}_i \\ \mathbf{\Phi}_i \end{bmatrix}, \quad \mathbf{R}_{i-1} = \begin{bmatrix} \mathbf{E}_{1,i-1} \\ \mathbf{E}_{2,i-1} \\ \mathbf{E}_{3,i-1} \\ \mathbf{E}_{4,i-1} \end{bmatrix} \tag{6.22}$$

where

$\mathbf{F}_i = [F_i(\xi_0), F_i(\xi_1), F_i(\xi_2), ..., F_i(\xi_{N-1}), F_i(\xi_N)]^T,$
$\mathbf{W}_i = [W_i(\xi_0), W_i(\xi_1), W_i(\xi_2), ..., W_i(\xi_{N-1}), W_i(\xi_N)]^T,$
$\mathbf{\Theta}_i = [T_i(\xi_0), T_i(\xi_1), T_i(\xi_2), ..., T_i(\xi_{N-1}), T_i(\xi_N)]^T,$
$\mathbf{\Phi}_i = [C_i(\xi_0), C_i(\xi_1), C_i(\xi_2), ..., C_i(\xi_{N-1}), C_i(\xi_N)]^T,$
$\mathbf{E}_{1,i-1} = [\zeta_{1,i-1}(\xi_0), \zeta_{1,i-1}(\xi_1), \zeta_{1,i-1}(\xi_2), ..., \zeta_{1,i-1}(\xi_{N-1}), \zeta_{1,i-1}(\xi_N)]^T$
$\mathbf{E}_{2,i-1} = [\zeta_{2,i-1}(\xi_0), \zeta_{2,i-1}(\xi_1), \zeta_{2,i-1}(\xi_2), ..., \zeta_{2,i-1}(\xi_{N-1}), \zeta_{2,i-1}(\xi_N)]^T$
$\mathbf{E}_{3,i-1} = [\zeta_{3,i-1}(\xi_0), \zeta_{3,i-1}(\xi_1), \zeta_{3,i-1}(\xi_2), ..., \zeta_{3,i-1}(\xi_{N-1}), \zeta_{3,i-1}(\xi_N)]^T$
$\mathbf{E}_{4,i-1} = [\zeta_{4,i-1}(\xi_0), \zeta_{4,i-1}(\xi_1), \zeta_{4,i-1}(\xi_2), ..., \zeta_{4,i-1}(\xi_{N-1}), \zeta_{4,i-1}(\xi_N)]^T$
$A_{11} = \mathbf{D}^3 + \chi_{11,i-1}\mathbf{D}^2 + \chi_{12,i-1}\mathbf{D} + \chi_{13,i-1}, \quad A_{12} = -\frac{H_a\beta_h}{1+\beta_h^2}\mathbf{I}, \quad A_{13} = 2Ri\mathbf{I}, \quad A_{14} = 2\mathbb{B}Ri\mathbf{I}$
$A_{21} = \chi_{21,i-1}\mathbf{D} + \chi_{22,i-1}, \quad A_{22} = \mathbf{D}^2 + \chi_{23,i-1}\mathbf{D} + \chi_{24,i-1}, \quad A_{23} = \mathbf{0}, \quad A_{24} = \mathbf{0}$
$A_{31} = \chi_{31,i-1}\mathbf{D}^2 + \chi_{32,i-1}\mathbf{D} + \chi_{33,i-1}, \quad A_{32} = \chi_{34,i-1}\mathbf{D},$
$A_{33} = \frac{1}{Pr}\mathbf{D}^2 + \chi_{35,i-1}\mathbf{D} + \chi_{36,i-1}, \quad A_{34} = \mathbf{0}$
$A_{41} = \chi_{41,i-1}\mathbf{D} + \chi_{42,i-1}, \quad A_{42} = \mathbf{0}, \quad A_{43} = \chi_{43,i-1}\mathbf{D}^2 + \chi_{44,i-1}\mathbf{D},$
$A_{44} = \frac{1}{Sc}\mathbf{D}^2 + \chi_{45,i-1}\mathbf{D} + \chi_{46,i-1}$

Here $\mathbf{I}$ is an identity matrix of size (N +1)×(N +1). After modifying the matrix system (6.20) to incorporate boundary conditions (6.21), the solution is obtained as

$$\mathbf{X}_i = \mathbf{A}_{i-1}^{-1}\mathbf{R}_{i-1} \tag{6.23}$$

Table 6.2: *Comparison of* $-F''(0)$ *and* $F(\infty)$ *calculated by the present method for* $S = 0$, $\lambda = 0$, $H_a = 0$, *and* $Ri = 0$.

	Magyari and Keller [56]	Present
$-F''(0)$	1.281808	1.28180856
$F(\infty)$	0.905639	0.90564370

6.2.8 Results and Discussion

In this case also, the results are compared with the results of Magyari and Keller [56] and presented in Table (6.2). To study the effects of Hall parameter β_h, Eckert number Ec, slip parameter λ, and thermophoresis parameter τ, computations have been carried out in the cases of $S = 0.5$, $Ri = 1.0$, $\mathbb{B} = 0.5$, $S = 0.5$, $\lambda = 1.0$, $\beta_h = 1.0$, $H_a = 2.0$, $Ec = 0.5$, and $\tau = 0.3$.

Figures (6.7(a)) - (6.7(d)) represent the behaviour of both the velocities, temperature and concentration with the Hall parameter β_h. From Fig. (6.7(a)), it is observed that the tangential velocity rises with the rise in β_h. Fig. (6.7(b)) indicates that $W(y)$ enhances with an enhancement in β_h. This is in tune with the fact that the Hall currents produce cross flow velocity. It is increasing near the plate and then gradually decreasing. Figs. (6.7(c)) and (6.7(d)) depict that the $T(y)$ and $C(y)$ are reducing with an enhancement in β_h.

The influence of τ on the tangential and transverse velocities, temperature and concentration is presented in the Figs. (6.8(a)) - (6.8(d)). Figure (6.8(a)) depicts that $F'(y)$ is diminishing with the increment in the values τ. The same trend is seen on the secondary velocity as presented in the Fig. (6.8(b)). Further, from Fig. (6.8(c)), it is observed that the temperature is enhancing with the enhancement in τ. The concentration is lessened with the increasing values of τ as portrayed in the Fig. (6.8(d)). From Figures (6.8(a)) - (6.8(d)), it is noticed that the impact is very mild.

The behavior of $F'(y)$, $W(y)$, $T(y)$ and $C(y)$ with the Eckert number Ec is exhibited in the Figs. (6.9(a)) - (6.9(d)). From Figs. (6.9(a)) and (6.9(b)), it is perceived that both the velocities are increasing with an increase in the value of Ec. Applying the viscous

dissipation effect, the momentum boundary layer thickness reduces slightly and hence, the velocity raises. It is apparent from the Fig. (6.9(c)) that the temperature increases with the increasing value of Ec, which in turn, intensifies the thermal boundary layer thickness. Figure (6.9(d)) shows that the concentration is reducing with the increase in the value of Ec. It is obvious from the figures that the impact of Ec on the profiles is not significant.

The influence of β_h, τ, Ec and λ on the heat transfer ($-T'(0)$) and mass transfer ($-C'(0)$) coefficients against S is depicted in the Figs. (6.10(a)) to (6.13(b)). It is understood from these figures that $-T'(0)$ and $-C'(0)$ are improving with the improvement in S. It is evident from Fig. (6.10(a)) and Fig. (6.10(b)) that, the heat transfer and mass transfer phenomena are increasing with a rise in the value of Hall parameter β_h. Further, it is clear from the figures that the variation in the mass transfer is more to that of heat transfer. $-T'(0)$ is decreasing with the increasing value of τ as presented in the Fig. (6.11(a)). $-C'(0)$ is increasing with the rise in the value of τ as shown in the Fig. (6.11(b)). But, the amount of the mass transfer from the sheet to the fluid is very high when compared that decrease in heat transfer from the sheet to the fluid. It is depicted from Fig. (6.12(a)) that the heat transfer coefficient is decreasing with an increase in the values of Ec. But, an opposite trend is observed for the mass transfer rate as shown in the Fig. (6.12(b)). Further, it is identified that the mass transfer rate is decreasing with the increasing values of Ec after $S = 1.4$. It is seen from the Fig. (6.13(a)) that the heat transfer rate is decreasing with an increase in λ. Further, the mass transfer rate is decreasing with an increase in the value of λ. as presented in Fig. (6.13(b)).

The behaviour of $F''(0)$ and $W'(0)$ for different values of λ, β_h, S, Ri, Ec and τ are tabulated in Table (6.3). It is evident from the table that the $F''(0)$ is increasing and $W'(0)$ is reducing with the slipperiness. In the presence of the Hall parameter both the skin-frictions are increasing. It is also observed that the transverse velocity vanishes when $\beta_h = 0$ and hence in $\tilde{z}-$direction there is no skin-friction. Table (6.3) illustrates that, $F''(0)$ is decreasing and $W'(0)$ is increasing with slip at the surface of the stretching sheet. The positive values of Ri increases both the skin-frictions. In addition to this, $F''(0)$ in $\tilde{x}-$direction is greatly increasing with the positive values of Ri. Furthermore, it is identified that a unique value of

$F''(0) = -0.61660061$ and $W'(0) = 0.15023781$ is attained when $Ri = 0$ (the case of forced convection flow) and for all values of Eckert number Ec and thermophoresis parameter τ. Because (6.14) and (6.16) are uncoupled when $Ri = 0$. As a result, the flow and thermal fields are independent. Hence, there is no effect of thermal field parameters on the flow filed. Also, both the skin-friction coefficients are increasing with an increase in the viscous dissipation parameter Ec. At the end of the table, the influence of the thermophoresis parameter τ is presented. It is noticed from the table that, both $F''(0)$ and $W'(0)$ are decreasing with the increasing value of τ.

6.3 Conclusions

A laminar slip flow of electrically conducting incompressible viscous fluid over an exponentially stretching permeable sheet in presence of thermophoresis and viscous dissipation effects is studied. The following conclusions are drawn for two cases:

In case (a), the rate of heat transfer increased with an increase in the value of Biot number. While, in case (b), the rate of heat and mass transfers are increased with an increase in the Hall parameter. In both the cases, the rate of heat transfer decreases with an increase in viscous dissipation parameter and the rate of mass transfer is increased with an increase in the thermophoresis parameter. In both cases, the rate of mass transfer is decreased with an increase in the velocity slip parameter and both the rate of heat and mass transfers are increased with an increase in the fluid suction.

Table 6.3: *Variation of skin friction in $\tilde{x}$- and $\tilde{z}$-directions for varying values of suction/injection parameter S, slip parameter λ, Hall parameter β_h, mixed convection parameter Ri, Eckert number Ec, and thermophoretic parameeter τ.*

λ	β_h	S	Ri	Ec	τ	$F''(0)$	$W'(0)$
0.0	1.0	2.0	1.0	0.5	0.3	-0.91411137	0.47617496
0.5	1.0	2.0	1.0	0.5	0.3	-0.40508974	0.43196532
1.0	1.0	2.0	1.0	0.5	0.3	-0.26159285	0.41872230
2.0	1.0	2.0	1.0	0.5	0.3	-0.15337319	0.40848340
1.0	0.0	2.0	1.0	0.5	0.3	-0.32860030	0.00000000
1.0	0.1	2.0	1.0	0.5	0.3	-0.32751833	0.06334880
1.0	0.5	2.0	1.0	0.5	0.3	-0.30513773	0.28064884
1.0	2.0	2.0	1.0	0.5	0.3	-0.20049245	0.42829099
1.0	1.0	-1.0	1.0	0.5	0.3	-0.14906795	0.35949291
1.0	1.0	-0.5	1.0	0.5	0.3	-0.18095685	0.38686966
1.0	1.0	0.0	1.0	0.5	0.3	-0.21855851	0.40771949
1.0	1.0	0.2	1.0	0.5	0.3	-0.23514661	0.41348703
1.0	1.0	0.4	1.0	0.5	0.3	-0.25257718	0.41746135
1.0	1.0	2.0	0.0	0.5	0.3	-0.61660061	0.15023781
1.0	1.0	2.0	0.5	0.5	0.3	-0.41196661	0.32493986
1.0	1.0	2.0	1.5	0.5	0.3	-0.13354694	0.48753998
1.0	1.0	2.0	3.0	0.5	0.3	0.18359188	0.63163669
1.0	1.0	2.0	1.0	0.0	0.3	-0.26528503	0.41540314
1.0	1.0	2.0	1.0	0.1	0.3	-0.26454405	0.41606772
1.0	1.0	2.0	1.0	0.6	0.3	-0.26085833	0.41938493
1.0	1.0	2.0	1.0	1.0	0.3	-0.25793402	0.42203084
1.0	1.0	2.0	1.0	0.5	0.0	-0.25881448	0.42180522
1.0	1.0	2.0	1.0	0.5	0.1	-0.25974839	0.42077008
1.0	1.0	2.0	1.0	0.5	0.5	-0.26340638	0.41670467
1.0	1.0	2.0	1.0	0.5	1.0	-0.26780688	0.41179353

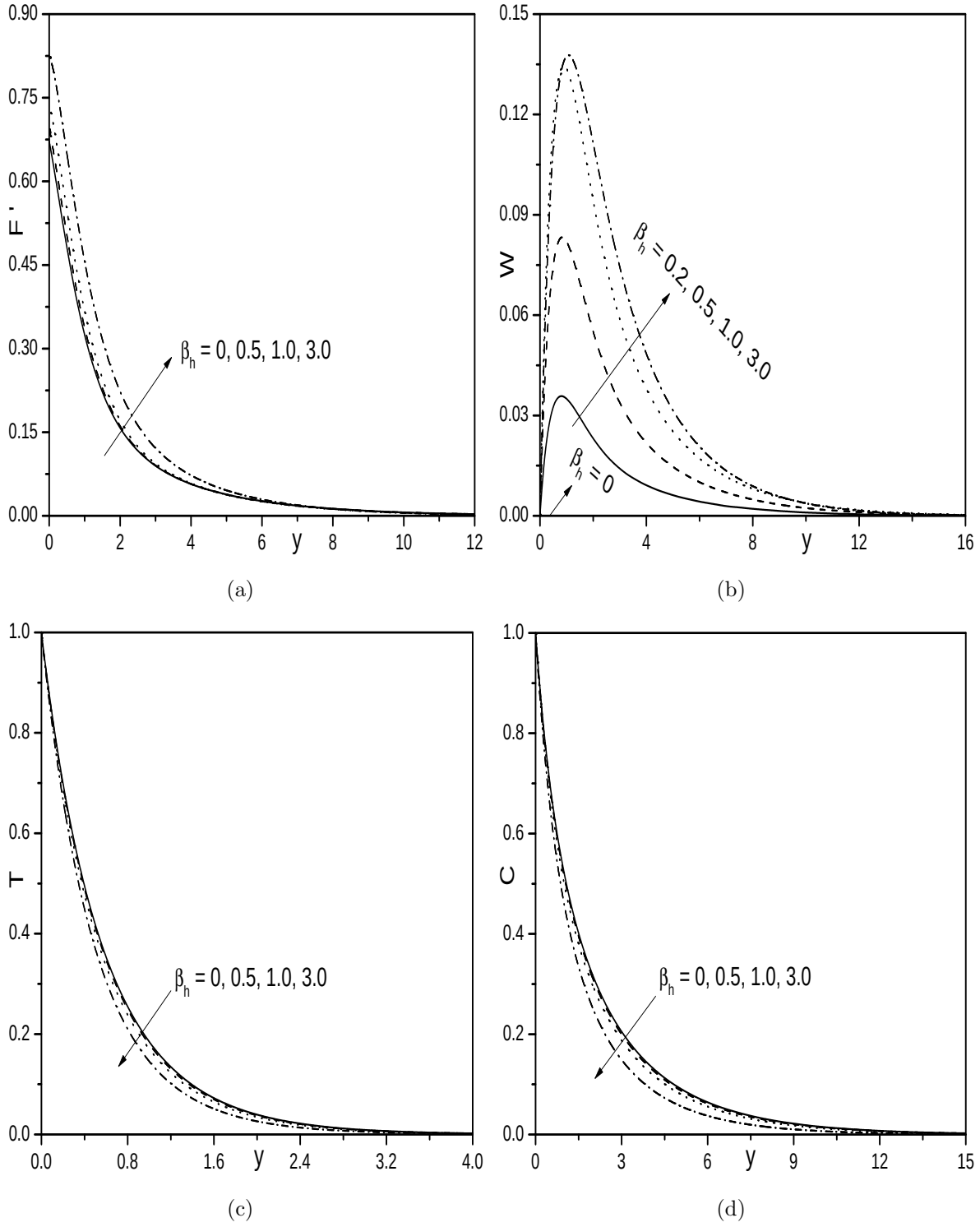

Figure 6.7: *Effect of β_h on (a)Velocity, (b)transverse velocity, (c)Temperature, and (d)Concentration profiles.*

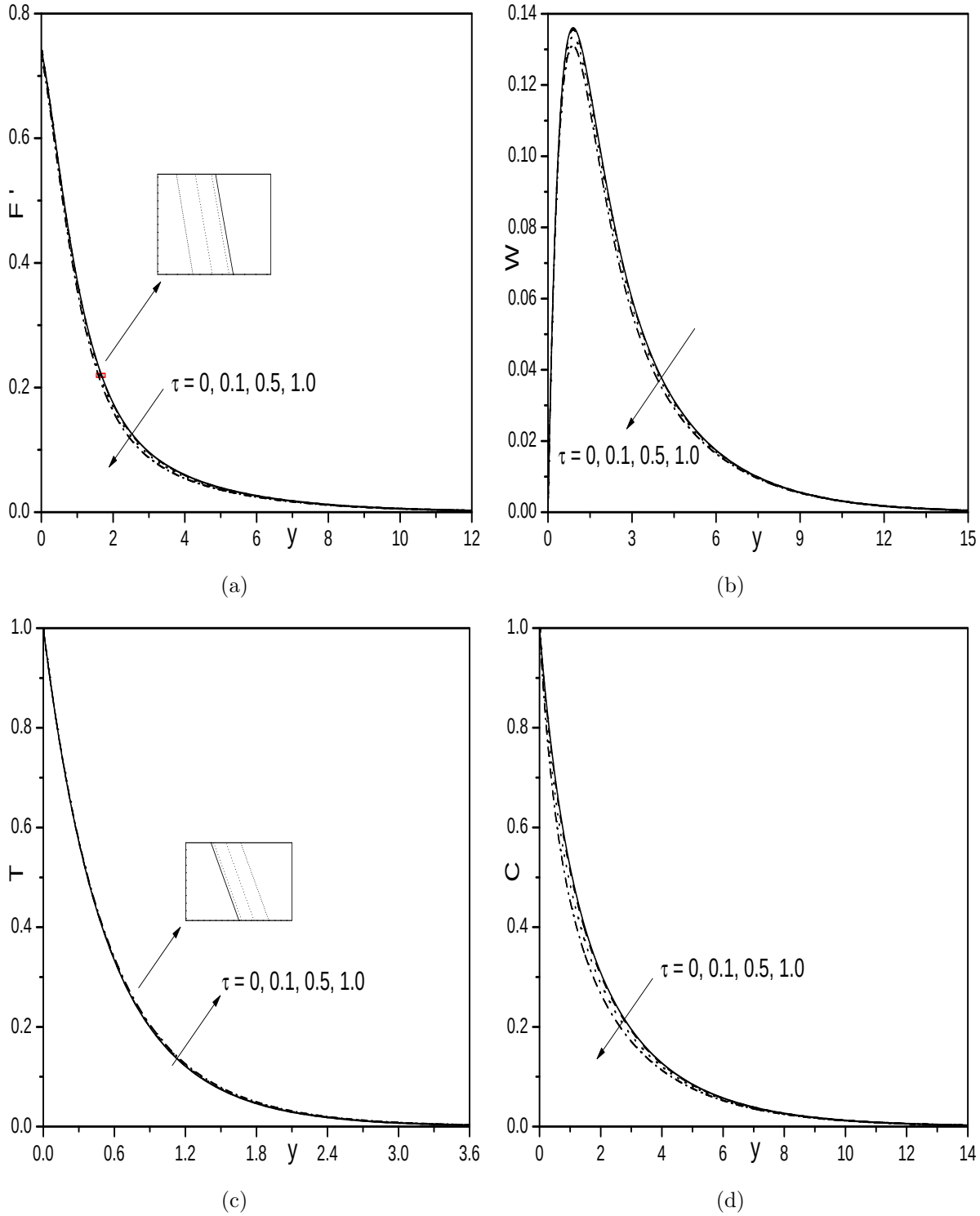

Figure 6.8: *Effect of τ on (a)Velocity, (b)transverse velocity, (c)Temperature, and (d)Concentration profiles.*

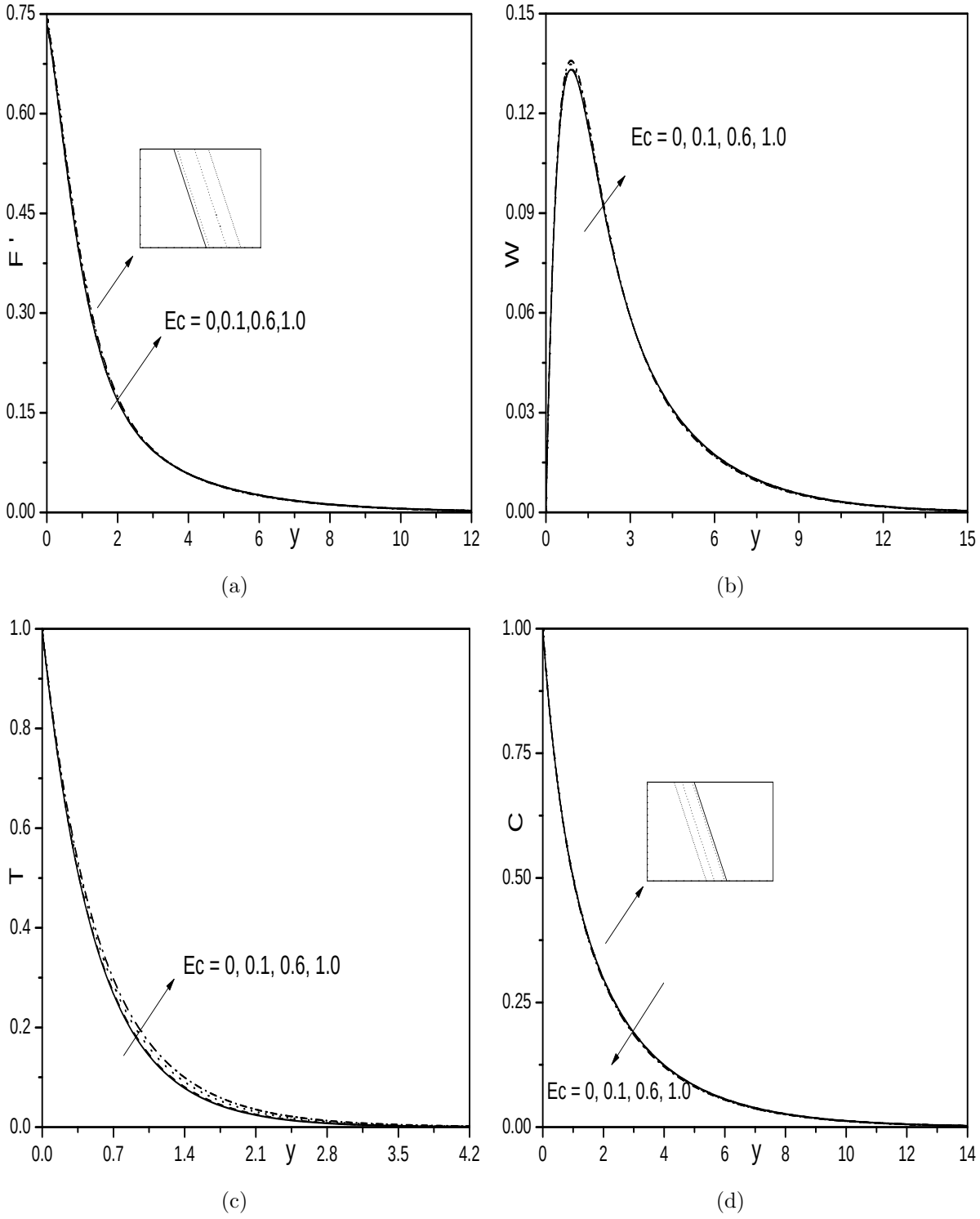

Figure 6.9: *Effect of Ec on (a)Velocity, (b)transverse velocity, (c)Temperature, and (d)Concentration profiles.*

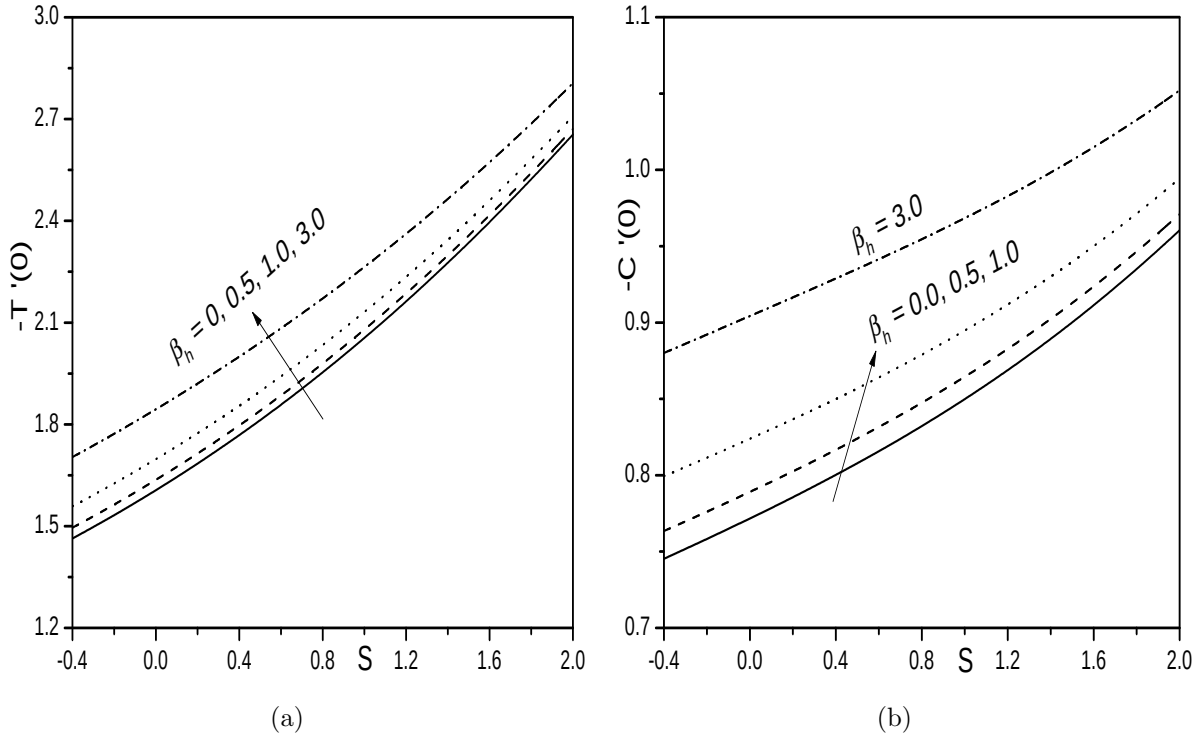

(a) (b)

Figure 6.10: *Effect of β_h on (a) $-T'(0)$, and (b) $-C'(0)$.*

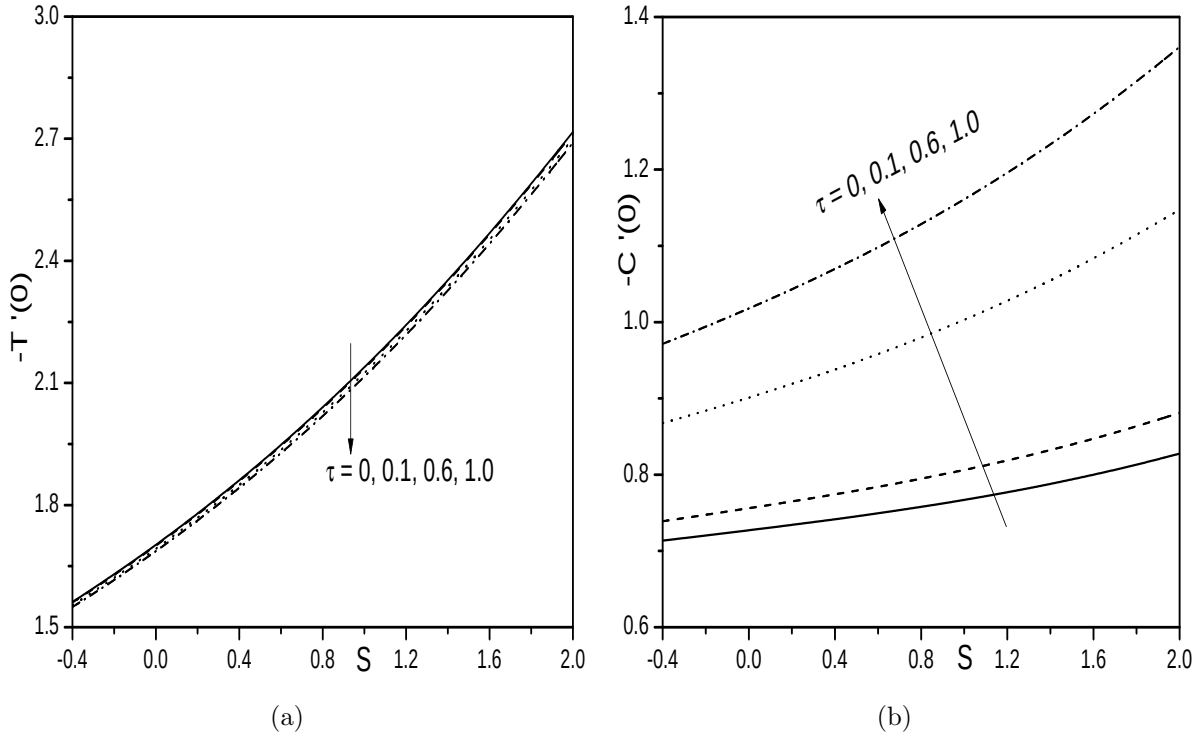

(a) (b)

Figure 6.11: *Effect of τ on (a) $-T'(0)$, and (b) $-C'(0)$.*

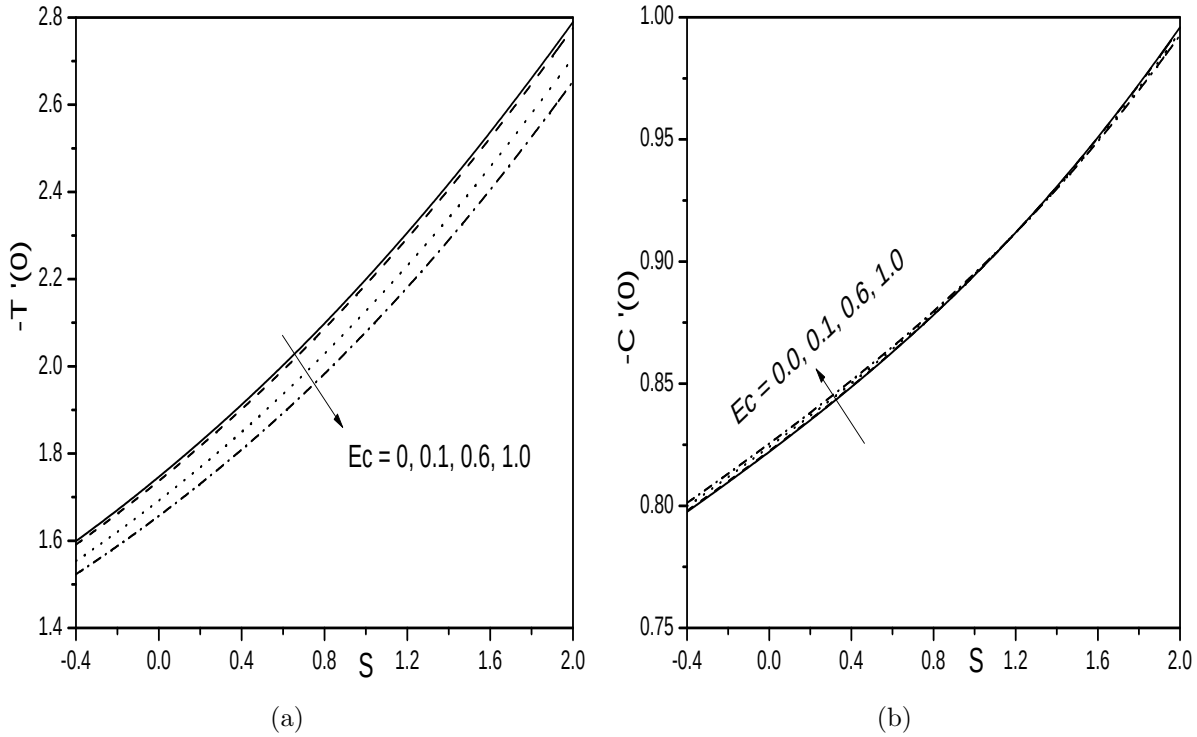

(a) (b)

Figure 6.12: *Effect of Ec on (a)* $-T'(0)$*, and (b)* $-C'(0)$.

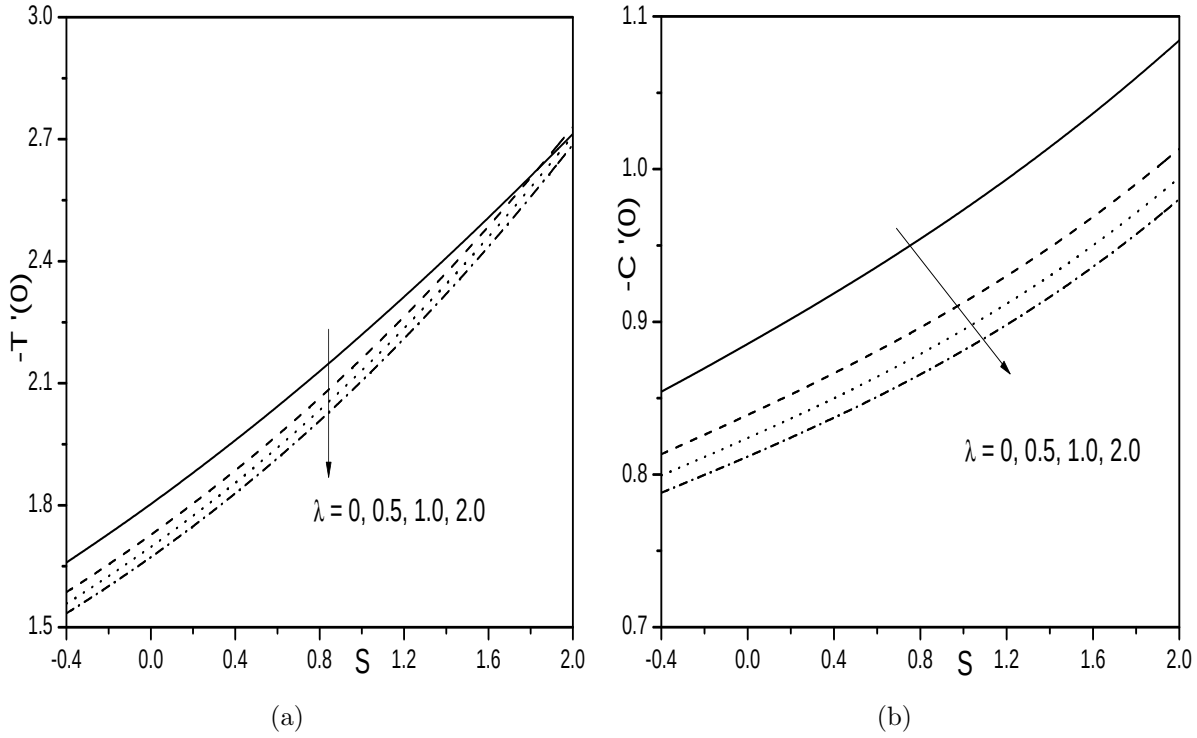

(a) (b)

Figure 6.13: *Effect of* λ *on (a)* $-T'(0)$*, and (b)* $-C'(0)$.

Chapter 7

Double dispersion effects on the flow over an exponentially stretching sheet

[1]

7.1 Introduction

Mixing and recirculation of local fluid streams occur as the fluid moves through tortuous paths in packed beds. This hydrodynamic mixing of fluid at pore level causes the dispersion effects in porous medium. This becomes more considerable for moderate and fast flows. The development of dispersion theory has been mainly related to miscible displacement and solute spreading in porous media. These areas are of major interest to secondary and tertiary oil recovery operations and to pollution control in water resources engineering. Awad *et al.* [7] investigated the nanofluid flow in a porous layer with double dispersion effects. Srinivasacharya *et al.* [106] reported the dispersion effects and variable properties on mixed convection over vertical wavy surface immersed in a fluid saturated Darcy porous medium. To the authors knowledge, no studies has been reported yet to analyse the flow, heat and

[1]Case(a): Communicated to "**International Journal of Engineering Science**",
Case(b) Communicated to "**Journal of Molecular Liquids**"

mass transfer behaviour of flow towards a permeable sheet stretching exponentially, in the presence of thermal radiation effect.

Thermal and solutal dispersion effects together with thermal radiation on laminar slip flow in a porous medium saturated with of incompressible viscous fluid over an exponentially stretching permeable sheet under two types of boundary conditions as considered in Chapter-2.

7.2 Formulation of the Problem

Consider a laminar slip flow in a Darcy-Brinkman porous medium saturated with incompressible viscous fluid over an exponentially stretching sheet with double dispersion effects. The fluid is considered to be a gray, absorbing/emitting radiation, but non-scattering medium. The Rosseland approximation [102] is used to describe the radiative heat flux in the energy equation. Hence, the equations governing the flow are given by

$$\frac{\partial \tilde{u}_x}{\partial \tilde{x}} + \frac{\partial \tilde{u}_y}{\partial \tilde{y}} = 0 \tag{7.1}$$

$$\tilde{u}_x \frac{\partial \tilde{u}_x}{\partial \tilde{x}} + \tilde{u}_y \frac{\partial \tilde{u}_x}{\partial \tilde{y}} = \nu \frac{\partial^2 \tilde{u}_x}{\partial \tilde{y}^2} - \frac{\nu}{k_p} \tilde{u}_x \tag{7.2}$$

$$\tilde{u}_x \frac{\partial \tilde{T}}{\partial \tilde{x}} + \tilde{u}_y \frac{\partial \tilde{T}}{\partial \tilde{y}} = \frac{\partial}{\partial \tilde{y}} \left(\tilde{\alpha_e} \, \frac{\partial \tilde{T}}{\partial \tilde{y}} \right) + \frac{16 T_\infty^3 \sigma^*}{3 k^* \rho c_p} \frac{\partial^2 \tilde{T}}{\partial \tilde{y}^2} \tag{7.3}$$

$$\tilde{u}_x \frac{\partial \tilde{C}}{\partial \tilde{x}} + \tilde{u}_y \frac{\partial \tilde{C}}{\partial \tilde{y}} = \frac{\partial}{\partial \tilde{y}} \left(\tilde{D}_e \, \frac{\partial \tilde{C}}{\partial \tilde{y}} \right) \tag{7.4}$$

where $\tilde{\alpha_e}$ and $\tilde{D}_e$ are the effective thermal and molecular diffusivities, respectively, and can be written as

$$\tilde{\alpha_e} = \alpha + \gamma_* \, ud, \;\; \tilde{D}_e = D + \chi \, ud \tag{7.5}$$

where k_p is the permeability of the porous medium, γ_* and χ are coefficient of thermal and molecular diffusiveness which varies between $\frac{1}{7}$ to $\frac{1}{3}$ and d is pore diameter or mean particle

diameter.

7.2.1 Case(a): Convective Thermal Condition

Assume that the sheet is either cooled or heated convectively through a fluid with temperature T_f and which induces a heat transfer coefficient h_f, where $h_f = h\sqrt{\frac{U_0}{2L}}e^{\frac{\tilde{x}}{2L}}$.

The conditions on the boundary of the stretching surface are

$$\left.\begin{array}{l} \tilde{u}_x = U_* + N_*\nu\frac{\partial \tilde{u}_x}{\partial \tilde{y}},\ \tilde{u}_y = -V_*(\tilde{x}),\ h_f(T_f - \tilde{T}) = -\kappa\frac{\partial \tilde{T}}{\partial \tilde{y}},\ \tilde{C} = C_w \quad \text{at} \quad \tilde{y} = 0 \\ \tilde{u}_x \to 0,\ \tilde{T} \to T_\infty,\ \tilde{C} \to C_\infty \ \text{ as } \quad \tilde{y} \to \infty \end{array}\right\} \tag{7.6}$$

Introducing the stream functions through $\tilde{u}_x = -\frac{\partial \psi}{\partial \tilde{y}}$ and $\tilde{u}_y = \frac{\partial \psi}{\partial \tilde{x}}$ and then the following dimensionless variables

$$\left.\begin{array}{l} \tilde{x} = xL, \quad \tilde{y} = y\sqrt{\frac{2\nu L}{U_0}}e^{\frac{-\tilde{x}}{2L}},\ \psi = \sqrt{2\nu L U_0}e^{\frac{\tilde{x}}{2L}}F(x,y), \\ \tilde{T} = T_\infty + (T_f - T_\infty)T(x,y),\ \tilde{C} = C_\infty + (C_w - C_\infty)C(x,y) \end{array}\right\} \tag{7.7}$$

into Eqs. (7.1) - (7.4), we obtain

$$F''' + FF'' - 2F'^2 - K_p\, e^{-x}F' + 2\left(F''\frac{\partial F}{\partial x} - F'\frac{\partial F'}{\partial x}\right) = 0 \tag{7.8}$$

$$\frac{1}{Pr}\left(1 + \frac{4R}{3}\right)T'' + FT' + 2\left(T'\frac{\partial F}{\partial x} - F'\frac{\partial T}{\partial x}\right) + D_\gamma e^x\left(F'T'' + F''T'\right) = 0 \tag{7.9}$$

$$\frac{1}{Sc}C'' + FC' + 2\left(C'\frac{\partial F}{\partial x} - F'\frac{\partial C}{\partial x}\right) + D_\chi e^x(F'C'' + F''C') = 0 \tag{7.10}$$

The conditions at the boundary reduces to

$$\left.\begin{array}{l} F(x,0) + 2\frac{\partial F}{\partial x}(x,0) = S,\ F'(x,0) = 1 + \lambda F''(x,0), \\ T'(x,0) = -Bi(1 - T(x,0)),\ C(x,0) = 1, \\ F'(x,y) \to 0,\ T(x,y) \to 0,\ C(x,y) \to 0 \ \text{ as } \quad y \to \infty \end{array}\right\} \tag{7.11}$$

where $K_p = \frac{2\nu L}{k_p U_0}$ is the porosity parameter, $D_\gamma = \frac{\gamma_* dU_0}{\nu}$ is the thermal dispersion parameter and $D_\chi = \frac{\chi dU_0}{\nu}$ is the solutal dispersion parameter.

7.2.2 Skin Friction, Heat and Mass Transfer Coefficients

The non-dimensional skin friction C_f, the local Nusselt number $Nu_{\tilde{x}}$ and the local Sherwood number $Sh_{\tilde{x}}$, are given by

$$\left.\begin{aligned} \frac{\sqrt{Re_x}}{\sqrt{2x/L}}\, C_f = F''(x,0),\ \frac{Nu_x}{\sqrt{Lx/2}\sqrt{Re_x}} = -\left(1+\frac{4R}{3}\right)T'(x,0),\ \text{and}\ \frac{Sh_x}{\sqrt{Lx/2}\sqrt{Re_x}} = -C'(x,0) \end{aligned}\right\} \tag{7.12}$$

where $Re_x = \dfrac{xU_*(x)}{\nu}$ is the local Reynold's number.

7.2.3 Solution of the Problem

The system of Eqs. (7.8) - (7.10) along with the boundary conditions (7.11), is solved numerically, as explained in case (a) of Chapter-3.

Proceeding in case (a) of Chapter-3, we obtain the following matrix equation

$$\mathbf{A}_{i-1}\mathbf{X}_i = \mathbf{R}_{i-1}, \tag{7.13}$$

In Eq. (7.13), $\mathbf{A}_{i-1}$ is a (6N + 6)×(6N + 6) square matrix and $\mathbf{X}_i$ and $\mathbf{R}_{i-1}$ are (6N + 6)×1 column vectors defined by

$$\mathbf{A}_{i-1} = [A_{rs}], \mathbf{R}_{i-1} = [\mathbf{E}_{r,i-1}], r, s = 1, 2, \cdots, 6, \quad \mathbf{X}_i = \begin{bmatrix} \mathbf{F}_i \\ \mathbf{\Theta}_i \\ \mathbf{\Phi}_i \\ \mathbf{G}_i \\ \mathbf{H}_i \\ \mathbf{K}_i \end{bmatrix} \tag{7.14}$$

where

$$\mathbf{F}_i = [F_i(\xi_0), F_i(\xi_1), F_i(\xi_2), ..., F_i(\xi_{N-1}), F_i(\xi_N)]^T,$$
$$\mathbf{\Theta}_i = [T_i(\xi_0), T_i(\xi_1), T_i(\xi_2), ..., T_i(\xi_{N-1}), T_i(\xi_N)]^T,$$
$$\mathbf{\Phi}_i = [C_i(\xi_0), C_i(\xi_1), C_i(\xi_2), ..., C_i(\xi_{N-1}), C_i(\xi_N)]^T,$$
$$\mathbf{G}_i = [G_i(\xi_0), G_i(\xi_1), G_i(\xi_2), ..., G_i(\xi_{N-1}), G_i(\xi_N)]^T,$$
$$\mathbf{H}_i = [H_i(\xi_0), H_i(\xi_1), H_i(\xi_2), ..., H_i(\xi_{N-1}), H_i(\xi_N)]^T,$$
$$\mathbf{K}_i = [K_i(\xi_0), K_i(\xi_1), K_i(\xi_2), ..., K_i(\xi_{N-1}), K_i(\xi_N)]^T,$$
$$\mathbf{E}_{j,i-1} = [\zeta_{j,i-1}(\xi_0), \zeta_{j,i-1}(\xi_1), \zeta_{j,i-1}(\xi_2), ..., \zeta_{j,i-1}(\xi_{N-1}), \zeta_{j,i-1}(\xi_N)]^T, j = 1, 2, 3, 4, 5, 6$$
$$A_{11} = \mathbf{D}^3 + \chi_{11,i-1}\mathbf{D}^2 + \chi_{12,i-1}\mathbf{D} + \chi_{13,i-1}, \quad A_{12} = \mathbf{0}, \quad A_{13} = \mathbf{0},$$
$$A_{14} = \chi_{14,i-1}\mathbf{D} + \chi_{15,i-1}, \quad A_{15} = \mathbf{0}, \quad A_{16} = \mathbf{0},$$
$$A_{21} = \chi_{21,i-1}\mathbf{D}^2 + \chi_{22,i-1}\mathbf{D} + \chi_{23,i-1}, \quad A_{22} = \chi_{24,i-1}\mathbf{D}^2 + \chi_{25,i-1}\mathbf{D}, \quad A_{23} = \mathbf{0},$$
$$A_{24} = \chi_{26,i-1}, \quad A_{25} = \chi_{27,i-1}, \quad A_{26} = \mathbf{0},$$
$$A_{31} = \chi_{31,i-1}\mathbf{D}^2 + \chi_{32,i-1}\mathbf{D} + \chi_{33,i-1}, \quad A_{32} = \mathbf{0}, \quad A_{33} = \chi_{34,i-1}\mathbf{D}^2 + \chi_{35,i-1}\mathbf{D},$$
$$A_{34} = \chi_{36,i-1}, \quad A_{35} = \mathbf{0}, \quad A_{36} = \chi_{37,i-1},$$
$$A_{41} = \chi_{41,i-1}\mathbf{D}^2 + \chi_{42,i-1}\mathbf{D} + \chi_{43,i-1}, \quad A_{42} = \mathbf{0}, \quad A_{43} = \mathbf{0},$$
$$A_{44} = \mathbf{D}^3 + \chi_{44,i-1}\mathbf{D}^2 + \chi_{45,i-1}\mathbf{D} + \chi_{46,i-1}, \quad A_{45} = \mathbf{0}, \quad A_{46} = \mathbf{0},$$
$$A_{51} = \chi_{51,i-1}\mathbf{D}^2 + \chi_{52,i-1}\mathbf{D} + \chi_{53,i-1}, \quad A_{52} = \chi_{54,i-1}\mathbf{D} + \chi_{55,i-1}, \quad A_{53} = \mathbf{0},$$
$$A_{54} = \chi_{56,i-1}\mathbf{D}^2 + \chi_{57,i-1}\mathbf{D} + \chi_{58,i-1}, \quad A_{55} = \chi_{59,i-1}\mathbf{D}^2 + \chi_{510,i-1}\mathbf{D} + \chi_{511,i-1},$$
$$A_{56} = \mathbf{0}, \quad A_{61} = \chi_{61,i-1}\mathbf{D}^2 + \chi_{62,i-1}\mathbf{D} + \chi_{63,i-1}, \quad A_{62} = \mathbf{0},$$
$$A_{63} = \chi_{64,i-1}\mathbf{D}^2 + \chi_{65,i-1}\mathbf{D}, \quad A_{64} = \chi_{66,i-1}\mathbf{D}^2 + \chi_{67,i-1}\mathbf{D} + \chi_{68,i-1},$$
$$A_{65} = \mathbf{0}, \quad A_{66} = \chi_{69,i-1}\mathbf{D}^2 + \chi_{610,i-1}\mathbf{D} + \chi_{611,i-1},$$

where the coefficients $\chi_{lk,n-1}$ and $\zeta_{l,i-1}$, $(l = 1, 2, 3, ..., 6, k = 1, 2, 3, ..., 11)$ are approximations in terms of F_i, T_i and C_i, $(i = 1, 2, 3, ..., n-1)$ and their derivatives, $\mathbf{0}$ and $\mathbf{I}$ are null and identity matrices of size (N +1)×(N +1).

After modifying the matrix system (7.13) to incorporate boundary conditions, the solution is obtained as

$$\mathbf{X}_i = \mathbf{A}_{i-1}^{-1}\mathbf{R}_{i-1} \tag{7.15}$$

Table 7.1: *Comparative analysis for* $\frac{Nu_x}{\sqrt{Lx/2}\sqrt{Re_x}}$ *by the current method for* $\lambda = 0$, $D_\chi = 0$, $D_\gamma = 0$, $K_p = 0$, $R = 0$, $x = 0$, $S = 0$ *and* $Bi \to \infty$.

Nusselt number $\frac{Nu_x}{\sqrt{Lx/2}\sqrt{Re_x}}$		
Pr	Magyari and Keller [56]	Present
0.5	0.330493	0.33053766
1	0.549643	0.54964345
3	1.122188	1.12208577
5	1.521243	1.52123668
8	1.991847	1.99183375
10	2.257429	2.25741862

7.2.4 Result and Discussion

The results of the present problem are compared with works of Magyari and Keller [56] as a special case and shown in Table. (7.1). Further, the computations have been carried out taking $\lambda = 1.0$, $Sc = 0.22$, $Pr = 1.0$, $K_p = 0.0$, $R = 0.5$, $Bi = 1.0$, $D_\gamma = 0.3$, $S = 0.5$, $D_\chi = 0.3$ and $x = 0.2$ unless otherwise mentioned.

The variation of the velocity with the slip parameter, suction/injection and porosity parameters is portrayed through the Figures (7.1(a)) - (7.1(c)). It is known that as the slipperiness escalates the thickness of the momentum boundary layer reduces. As a result, the velocity reduces as shown in the Figure (7.1(a)). Figure (7.1(b)) depicts the variation of the velocity in the presence of S. It is evident from the figure that the velocity reduces with the suction and escalates with the injection. This is due to the fact that the suction has the tendency to reduce the momentum boundary. While the velocity of the fluid is reducing with an increase in the value of porosity parameter as shown in the Fig. (7.1(c)).

Figures (7.2(a)) - (7.2(c)) represent the fluctuation of skin-friction against x for distinct values of λ, S and K_p, respectively. It is obvious from these figures that the skin-friction escalates with the slipperiness and falls down with the fluid suction. Further, it is noticed that the non-similar variable has no effect on the skin-friction coefficient in the presence of velocity slip and fluid suction/injection as shown in the Figs. (7.2(a)) and (7.2(b)). In the presence of the porosity parameter K_p, the skin-friction reduces and increases with an

increase in x as depicted in the Fig. (7.2(c)). The effect of the other parameters on the velocity and skin-friction are not much significant and hence graphs are not included.

Figures (7.3(a)) - (7.3(e)) exhibit the behaviour of the temperature for different values of D_γ, R, Bi, λ and K_p. The temperature rises with an increase in the value D_γ as shown in the Figure (7.3(a)). It is seen from the Figure (7.3(b)) that the temperature increases with the increasing values of thermal radiation, which in turn, intensifies the thermal boundary layer thickness. Figure (7.3(c)) illustrates that the temperature is enhancing with the rise in the value of Bi and hence gain in the thickness of thermal boundary. Further, for large value of Biot number Bi, the convective thermal condition from (7.11) transforms to $T(0) \to 1$, which signifies the constant wall condition. Due to slipperiness, thermal boundary intensifies, and hence, the temperature escalates with an increase in the value of λ as portrayed in the Figure (7.3(d)). Further, Fig. (7.3(e)) explores that the temperature increases with an increase in the value of porosity parameter K_p.

The influence of D_γ, R, Bi, λ and K_p on the rate of heat transfer against non-similar variable x is explored in the Figures (7.4(a)) - (7.4(e)). It is evident from the Fig. (7.4(a)), that the rate of heat transfer is decreasing with an increase in the value of D_γ. In the absence of D_γ, i.e.,$(D_\gamma = 0)$, there is no effect of the non-similar variable x on the rate of heat transfer. As expected, enhancing the value of D_γ, the rate of heat transfer reduces. While the rate of heat transfer escalates with an increase in the value of thermal radiation parameter R as depicted in the Fig. (7.4(b)). Figure (7.4(c)) narrates the behaviour of the rate of heat transfer for different values of Biot number Bi. As Biot number enhances, the rate of heat transfer escalates predominantly on the surface due to the strong convection. Figures (7.4(d)) and (7.4(e)) show that the rate of heat transfer reduces with an increase in the values of velocity slip and porosity parameters.

The variation of concentration profile for distinct values of D_χ, λ and K_p is shown in the Figures (7.5(a)) - (7.5(c)). An enhancement in the value of D_χ increases the concentration of the fluid as shown in the Fig. (7.5(a)). It is noticed from the Figs. (7.5(b)) and (7.5(c)) that, as the value of the slip parameter and the porosity parameter increases, the concentration of the fluid increases. Hence, mass transfer at the sheet decreases.

Figures (7.6(a)) - (7.6(c)) depict the behaviour of the rate of mass transfer for different values of D_χ, λ and K_p against the non-similar variable x. Enhancing the solute dispersion parameter D_χ, the rate of mass transfer from the sheet to the fluid is falling down. In the absence of D_χ, i.e., $(D_\chi = 0)$, there is no effect of the non-similar variable x on the rate of mass transfer. As the value of D_χ escalates, the rate of mass transfer reduces as shown in the Fig. (7.6(a)). Figures (7.6(b)) and (7.6(c)), it is identified that the rate of mass transfer at the sheet reduces with an increase in the values of velocity and porosity parameters. Further, it is identified that in the presence of porosity parameter K_p the rate of mass transfer increases gradually as $x \to 1$.

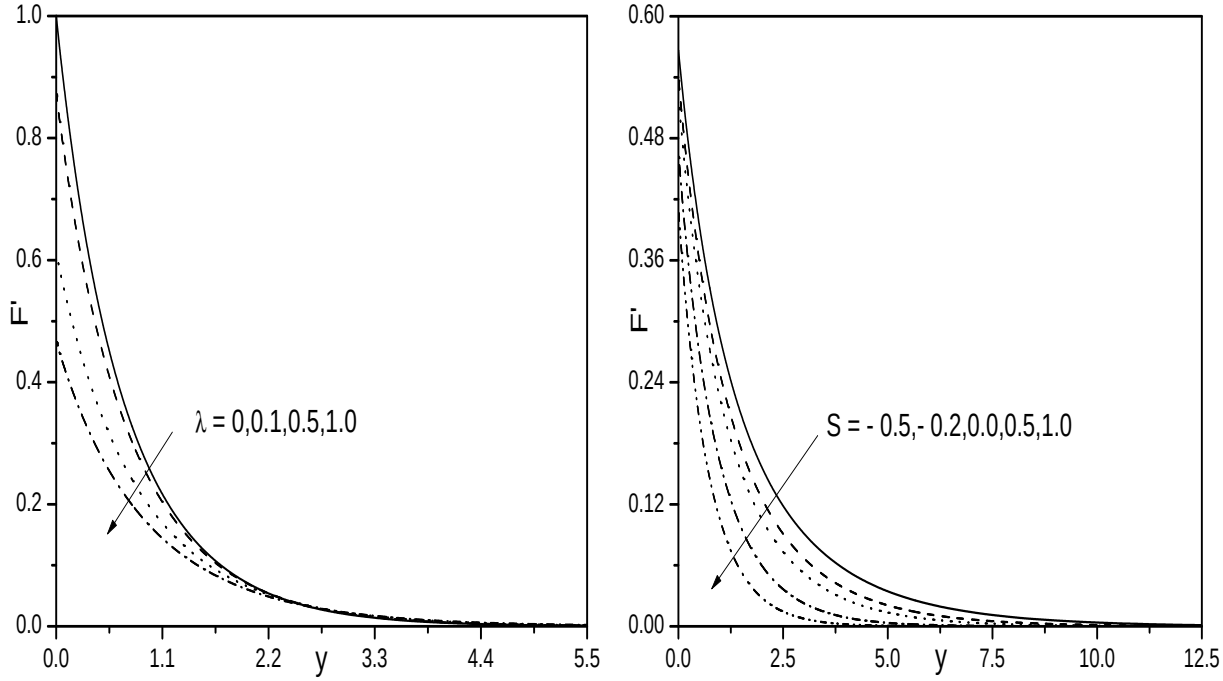

(a)

(b)

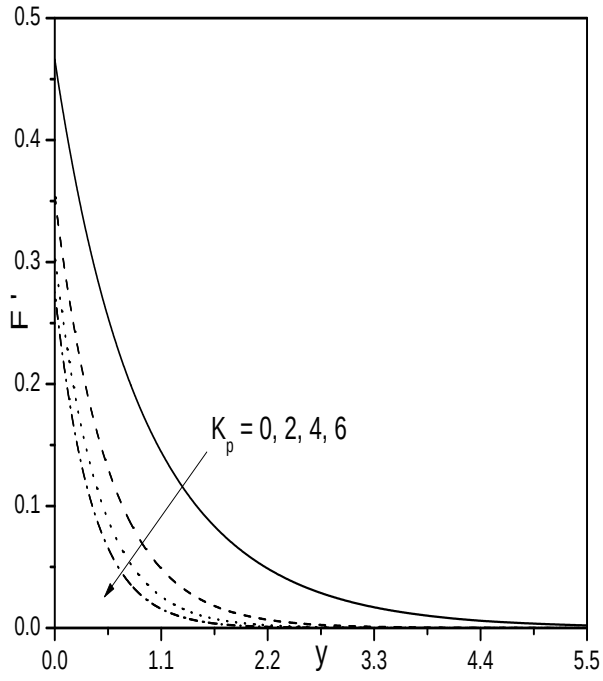

(c)

Figure 7.1: *Effect of (a) λ, (b) S and (c) K_p on F'.*

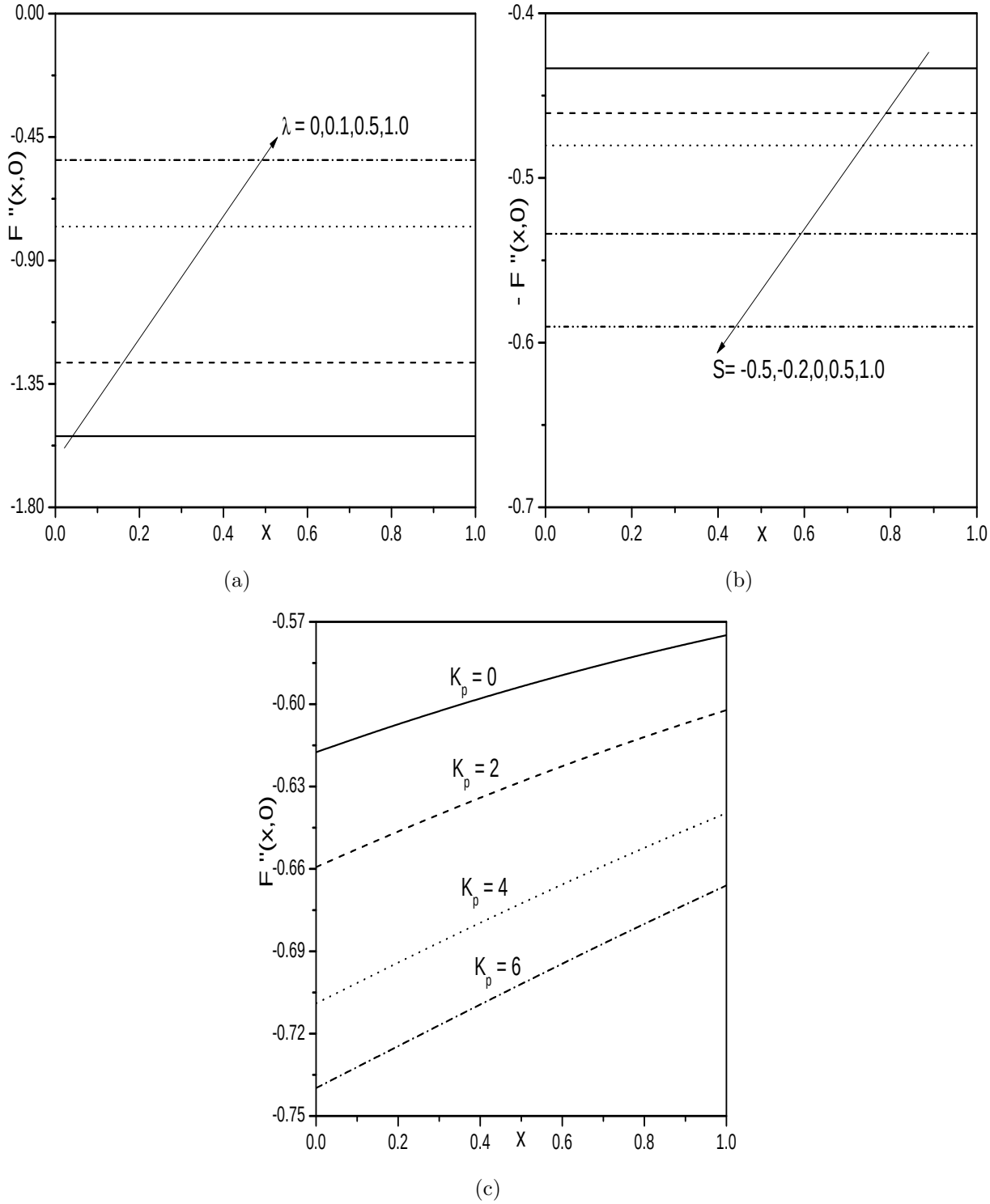

Figure 7.2: *Effect of (a) λ, (b) S and (c) K_p on $F''(x,0)$.*

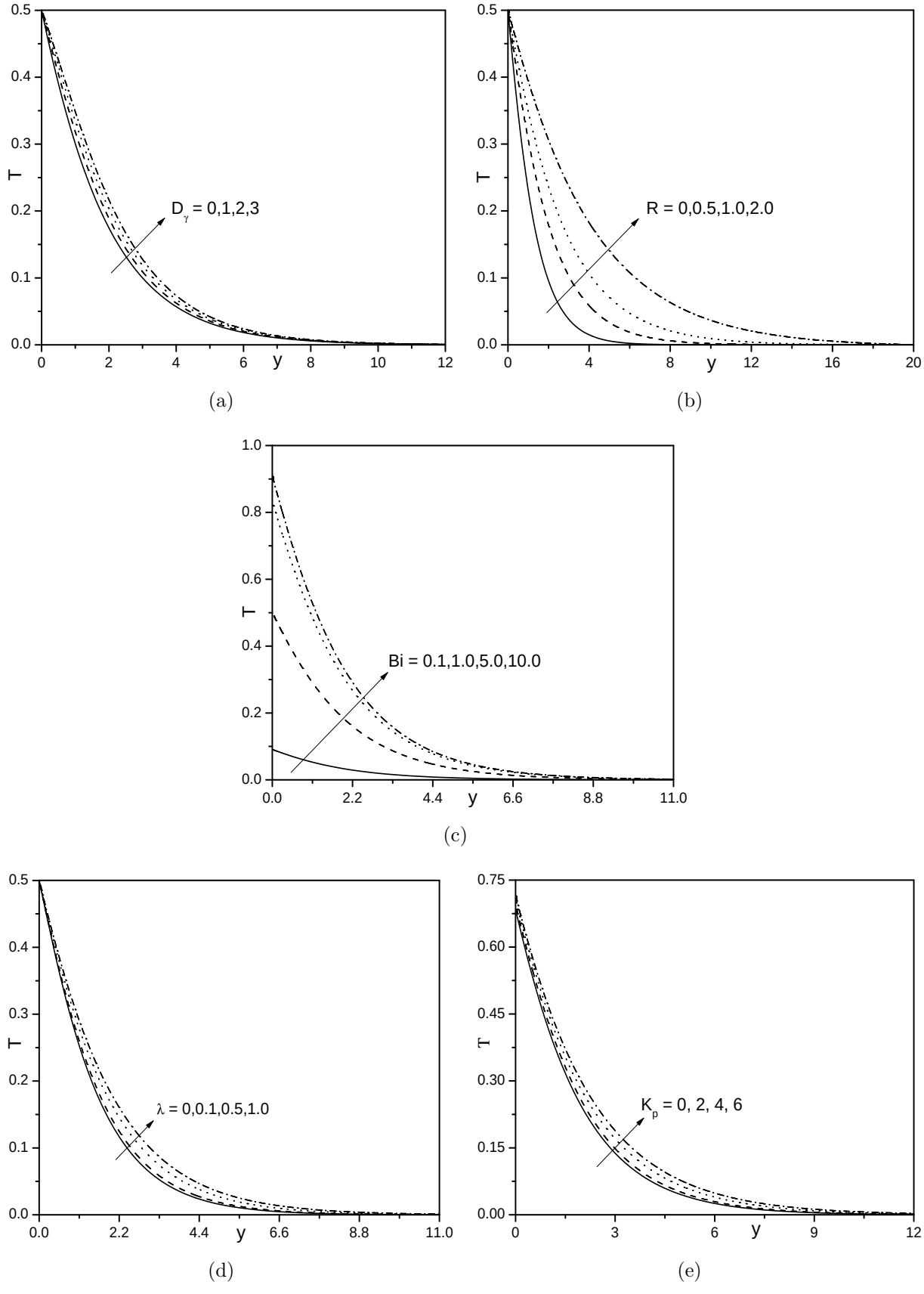

Figure 7.3: *Effect of (a)D_γ, (b)R, (c)Bi, (d)λ and (e) K_p on T.*

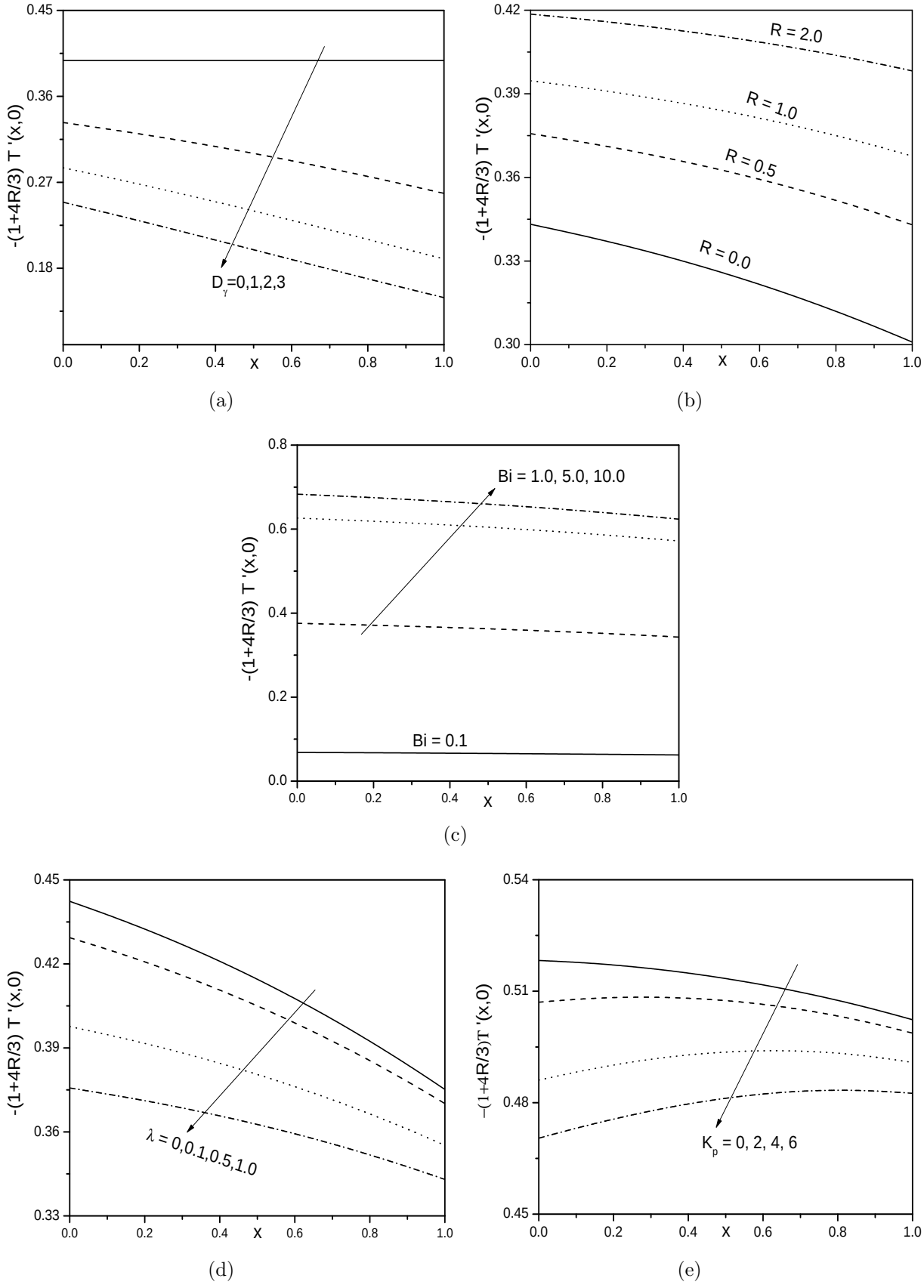

Figure 7.4: *Effect of (a)D_γ, (b)R, (c)Bi, (d)λ and (e) K_p on* $-\left(1+\frac{4R}{3}\right)T'(x,0)$.

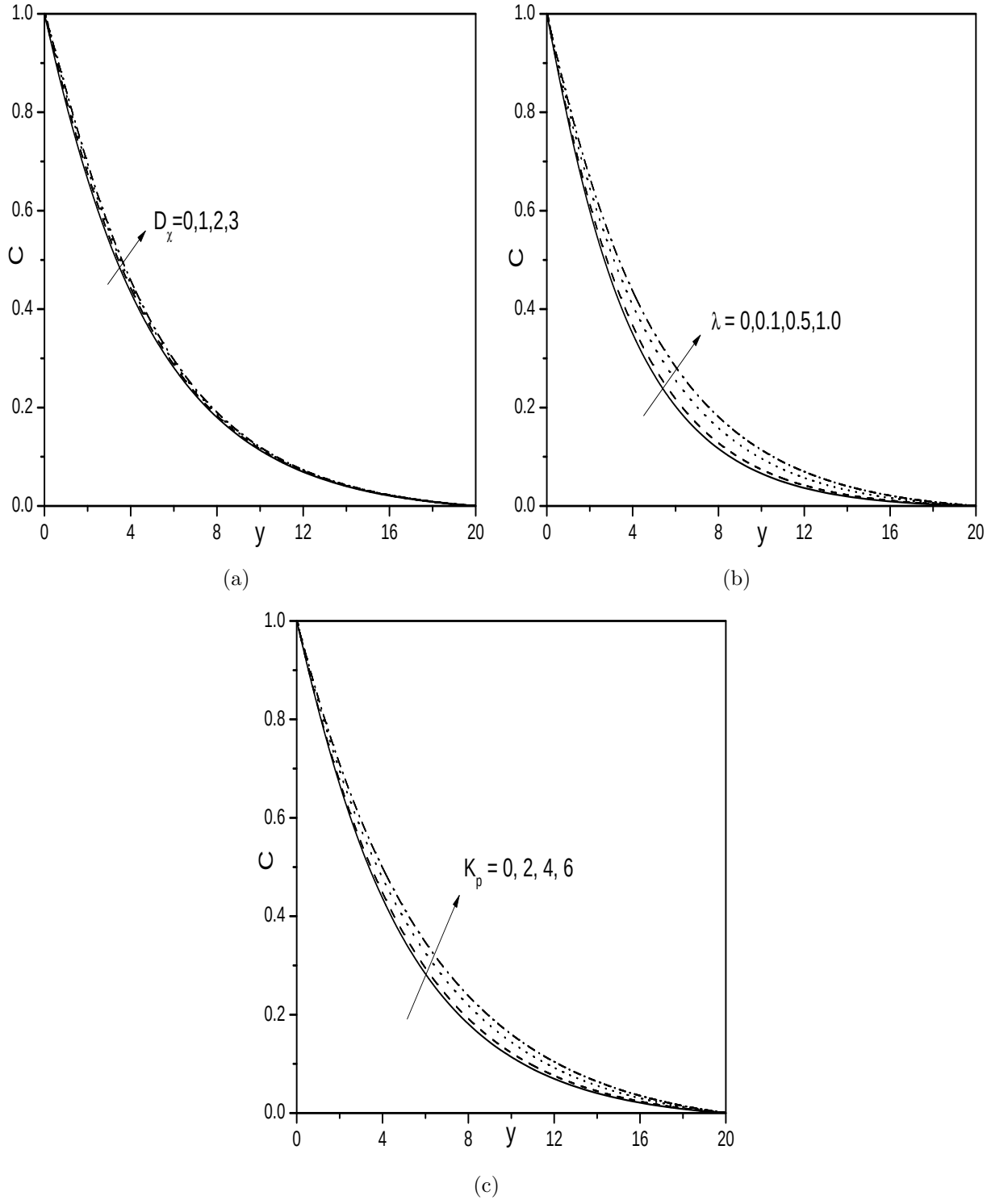

Figure 7.5: *Effect of(a)* D_χ*, (b)* λ *and (c)* K_p *on* F'*.*

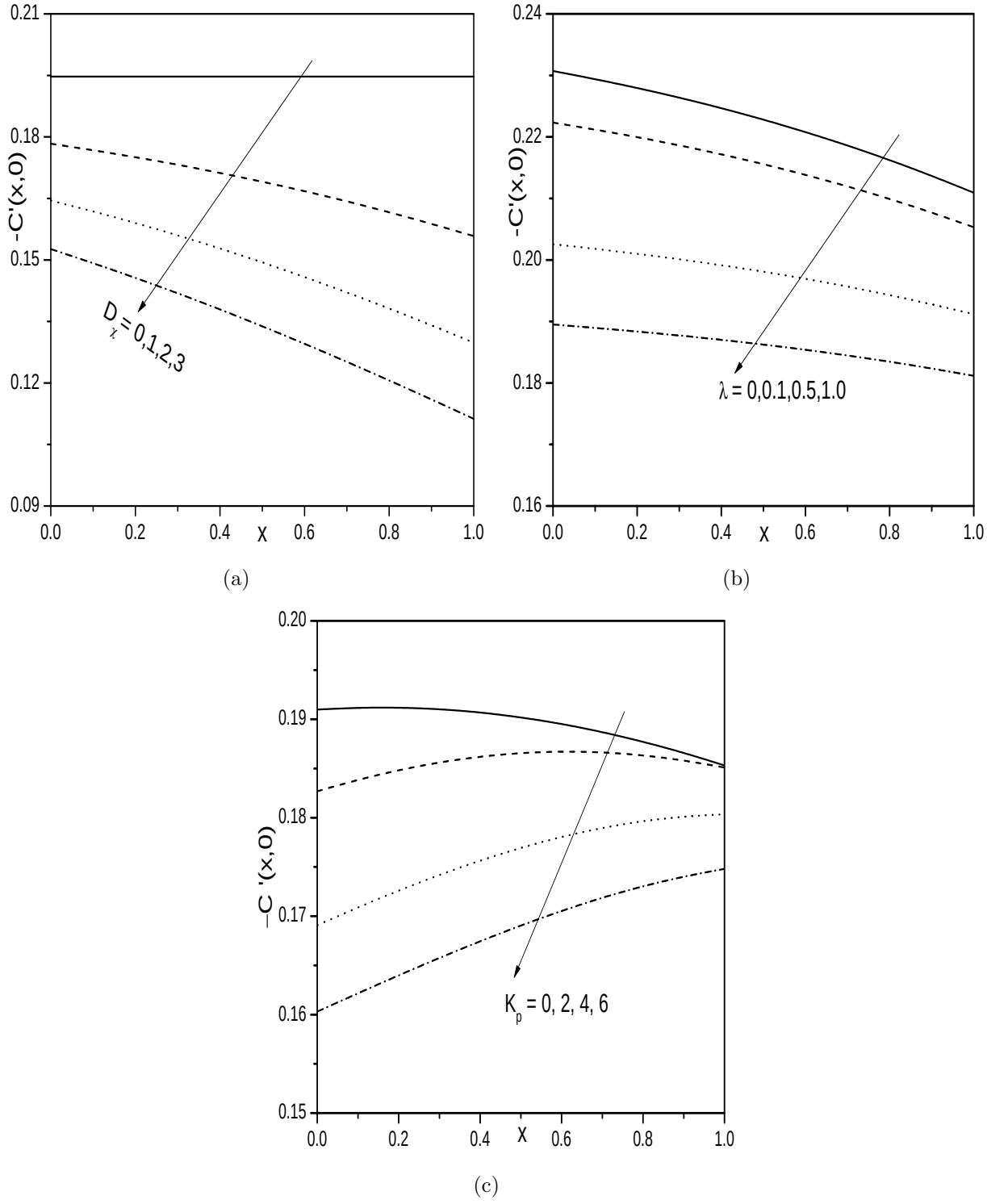

Figure 7.6: *Effect of (a) D_χ, (b) λ and (c) K_p on $F''(x,0)$.*

7.2.5 Case(b): Uniform wall temperature with Hall effect

Assume that, a strong magnetic field of strength $B(\tilde{x}) = B_0 e^{\frac{\tilde{x}}{2L}}$ is applied in $\tilde{y}-$direction and the influence of Hall current is not neglected. Assume that magnetic Reynolds number is very small so that the induced magnetic field is negligible in comparison to applied magnetic field. The presence of Hall current induces a cross flow in $\tilde{z}$-direction and hence the flow becomes three-dimensional. Under the Boussinesq approximation, the flow is governed by the equations (7.1), (7.4) along with the following momentum and energy equations

$$\tilde{u}_x\frac{\partial\tilde{u}_x}{\partial\tilde{x}}+\tilde{u}_y\frac{\partial\tilde{u}_x}{\partial\tilde{y}}=\nu\frac{\partial^2\tilde{u}_x}{\partial\tilde{y}^2}+g\,\beta_T(\tilde{T}-T_\infty)+g\,\beta_C(\tilde{C}-C_\infty)-\frac{\sigma B^2}{\rho(1+\beta_h^2)}(\tilde{u}_x+\beta_h\tilde{u}_z)-\frac{\nu}{k_p}\tilde{u}_x \quad (7.16)$$

$$\tilde{u}_x\frac{\partial\tilde{u}_z}{\partial\tilde{x}}+\tilde{u}_y\frac{\partial\tilde{u}_z}{\partial\tilde{y}}=\nu\frac{\partial^2\tilde{u}_z}{\partial\tilde{y}^2}+\frac{\sigma B^2}{\rho(1+\beta_h^2)}(\beta_h\tilde{u}_x-\tilde{u}_z)-\frac{\nu}{k_p}\tilde{u}_z \quad (7.17)$$

$\tilde{u}_z$ is the velocity in $\tilde{z}$-direction.

The conditions on the boundary of the sheet are

$$\left.\begin{array}{l}\tilde{u}_x=U_*+N_*\nu\frac{\partial\tilde{u}_x}{\partial\tilde{y}},\ \tilde{u}_y=-V_*(\tilde{x}),\ \tilde{u}_z=0,\\ T_w=T_\infty+T_0e^{\frac{2\tilde{x}}{L}},\ C_w=C_\infty+C_0e^{\frac{2\tilde{x}}{L}}\quad\text{at}\quad\tilde{y}=0\\ \tilde{u}_x\to0,\ \tilde{u}_z\to0,\ \tilde{T}\to T_\infty,\ \tilde{C}\to C_\infty\ \text{ as }\ \tilde{y}\to\infty\end{array}\right\} \quad (7.18)$$

Introducing the following dimensionless variables

$$\left.\begin{array}{l}\tilde{x}=xL,\quad\tilde{y}=y\sqrt{\frac{2\nu L}{U_0}}e^{\frac{-\tilde{x}}{2L}},\ \psi=\sqrt{2\nu LU_0}e^{\frac{\tilde{x}}{2L}}F,\\ \tilde{u}_x=U_0e^{\frac{\tilde{x}}{L}}F',\quad\tilde{u}_y=-\sqrt{\frac{\nu U_0}{2L}}\,e^{\frac{\tilde{x}}{2L}}(F+yF'),\quad\tilde{u}_z=U_0e^{\frac{\tilde{x}}{L}}W\\ \tilde{T}=T_\infty+T_0\,e^{\frac{2\tilde{x}}{L}}T,\ \tilde{C}=C_\infty+C_0\,e^{\frac{2\tilde{x}}{L}}C\end{array}\right\} \quad (7.19)$$

into the Eqs. (7.1), (7.16), (7.17), (7.3), (7.4)

$$F'''+FF''-2F'^2-K_p\,e^{-x}F'+2Ri(T+\mathbb{B}C)-\frac{H_a}{1+\beta_h^2}(F'+\beta_hW)+2\left(F''\frac{\partial F}{\partial x}-F'\frac{\partial F'}{\partial x}\right)=0 \quad (7.20)$$

$$W''-2F'W+FW'-K_p\,e^{-x}W+\frac{H_a}{1+\beta_h^2}(\beta_hF'-W)+2\left(W'\frac{\partial F}{\partial x}-F'\frac{\partial W}{\partial x}\right)=0 \quad (7.21)$$

$$\frac{1}{Pr}\left(1+\frac{4R}{3}\right)T''+FT'-4F'T+2\left(T'\frac{\partial F}{\partial x}-F'\frac{\partial T}{\partial x}\right)+D_\gamma e^x\left(F'T''+F''T'\right)=0 \quad (7.22)$$

$$\frac{1}{Sc}C''+FC'-4F'C+2\left(C'\frac{\partial F}{\partial x}-F'\frac{\partial C}{\partial x}\right)+D_\chi e^x(F'C''+F''C')=0 \quad (7.23)$$

The conditions (7.18) reduce to

$$\left.\begin{array}{l} F'(x,0)=1+\lambda F''(x,0),\ F(x,0)+2\frac{\partial F}{\partial x}(x,0)=S, \\ W(x,0)=0,\quad T(x,0)=1,\quad C(x,0)=1, \\ F'(x,y)\to 0,\ W(x,y)\to 0,\ T(x,y)\to 0,\ C(x,y)\to 0 \ \text{ as } \ y\to\infty \end{array}\right\} \quad (7.24)$$

7.2.6 Skin Friction in $\tilde{x}$ and $\tilde{z}$-directions, Heat and Mass Transfer Coefficients

The non-dimensional skin friction in $\tilde{x}-$direction $C_{F\tilde{x}}$, local skin-friction in $\tilde{z}-$direction $C_{F\tilde{z}}$, the local Nusselt number $Nu_{\tilde{x}}$ and the local Sherwood number $Sh_{\tilde{x}}$, are given by

$$\left.\begin{array}{l} \frac{\sqrt{Re_x}}{\sqrt{2x/L}}C_{F\tilde{x}}=F''(x,0), \quad \frac{\sqrt{Re_x}}{\sqrt{2x/L}}C_{F\tilde{z}}=W'(x,0), \\ \frac{Nu_x}{\sqrt{x/2L}\sqrt{Re_x}}=-\left(1+\frac{4R}{3}\right)T'(x,0), \quad \text{and} \quad \frac{Sh_x}{\sqrt{x/2L}\sqrt{Re_x}}=-C'(x,0). \end{array}\right\} \quad (7.25)$$

where $Re_x=\frac{xU_*(x)}{\nu}$ is the local Reynold's number.

7.2.7 Solution of the Problem

To solve the system of Eqs. (7.20) - (7.23) along with the boundary conditions (7.24), is solved numerically, as explained in case (a) of Chapter-3.

Proceeding in case (a) of Chapter-3, we obtain the following matrix equation

$$\mathbf{A}_{i-1}\mathbf{X}_i=\mathbf{R}_{i-1}, \quad (7.26)$$

In Eq. (7.26), $\mathbf{A}_{i-1}$ is a (8N + 8)×(8N + 8) square matrix and $\mathbf{X}_i$ and $\mathbf{R}_{i-1}$ are (8N + 8)×1 column vectors defined by

$$\mathbf{A}_{i-1} = [A_{rs}], \mathbf{R}_{i-1} = [\mathbf{E}_{r,i-1}], r, s = 1, 2, \cdots, 8, \ \mathbf{X}_i = \begin{bmatrix} \mathbf{F}_i \\ \mathbf{W}_i \\ \mathbf{\Theta}_i \\ \mathbf{\Phi}_i \\ \mathbf{G}_i \\ \mathbf{H}_i \\ \mathbf{J}_i \\ \mathbf{K}_i \end{bmatrix} \tag{7.27}$$

where

$\mathbf{F}_i = [F_i(\xi_0), F_i(\xi_1), F_i(\xi_2), ..., F_i(\xi_{N-1}), F_i(\xi_N)]^T,$
$\mathbf{W}_i = [W_i(\xi_0), W_i(\xi_1), W_i(\xi_2), ..., W_i(\xi_{N-1}), W_i(\xi_N)]^T,$
$\mathbf{\Theta}_i = [T_i(\xi_0), T_i(\xi_1), T_i(\xi_2), ..., T_i(\xi_{N-1}), T_i(\xi_N)]^T,$
$\mathbf{\Phi}_i = [C_i(\xi_0), C_i(\xi_1), C_i(\xi_2), ..., C_i(\xi_{N-1}), C_i(\xi_N)]^T,$
$\mathbf{G}_i = [G_i(\xi_0), G_i(\xi_1), G_i(\xi_2), ..., G_i(\xi_{N-1}), G_i(\xi_N)]^T,$
$\mathbf{H}_i = [H_i(\xi_0), H_i(\xi_1), H_i(\xi_2), ..., H_i(\xi_{N-1}), H_i(\xi_N)]^T,$
$\mathbf{J}_i = [J_i(\xi_0), J_i(\xi_1), J_i(\xi_2), ..., J_i(\xi_{N-1}), J_i(\xi_N)]^T,$
$\mathbf{K}_i = [K_i(\xi_0), K_i(\xi_1), K_i(\xi_2), ..., K_i(\xi_{N-1}), K_i(\xi_N)]^T,$
$\mathbf{E}_{j,i-1} = [\zeta_{j,i-1}(\xi_0), \zeta_{j,i-1}(\xi_1), \zeta_{j,i-1}(\xi_2), ..., \zeta_{j,i-1}(\xi_{N-1}), \zeta_{j,i-1}(\xi_N)]^T, j = 1, 2, 3, ..., 8$
$A_{11} = \mathbf{D}^3 + \chi_{11,i-1}\mathbf{D}^2 + \chi_{12,i-1}\mathbf{D} + \chi_{13,i-1}, \quad A_{12} = -\frac{H_a\beta_h}{1+\beta_h^2}\mathbf{I}, \quad A_{13} = 2Ri\mathbf{I},$
$A_{14} = 2\mathbb{B}Ri\mathbf{I}, \quad A_{15} = \chi_{14,i-1}\mathbf{D} + \chi_{15,i-1}, \quad A_{16} = \mathbf{0}, \quad A_{17} = \mathbf{0}, \quad A_{18} = \mathbf{0},$
$A_{21} = \chi_{21,i-1}\mathbf{D} + \chi_{22,i-1}, \quad A_{22} = \mathbf{D}^2 + \chi_{23,i-1}\mathbf{D} + \chi_{24,i-1}, \quad A_{23} = \mathbf{0},$
$A_{24} = \mathbf{0}, \quad A_{25} = \chi_{25,i-1}, \quad A_{26} = \chi_{26,i-1}, \quad A_{27} = \mathbf{0}, \quad A_{28} = \mathbf{0}$
$A_{31} = \chi_{31,i-1}\mathbf{D}^2 + \chi_{32,i-1}\mathbf{D} + \chi_{33,i-1}, \quad A_{32} = \mathbf{0}, \quad A_{33} = \chi_{34,i-1}\mathbf{D}^2 + \chi_{35,i-1}\mathbf{D} + \chi_{36,i-1},$
$A_{34} = \mathbf{0}, \quad A_{35} = \chi_{37,i-1}, \quad A_{36} = \mathbf{0}, \quad A_{37} = \chi_{38,i-1}, \quad A_{38} = \mathbf{0}$
$A_{41} = \chi_{41,i-1}\mathbf{D}^2 + \chi_{42,i-1}\mathbf{D} + \chi_{43,i-1}, \quad A_{42} = \mathbf{0}, \quad A_{43} = \mathbf{0},$

$A_{44} = \chi_{44,i-1}\mathbf{D}^2 + \chi_{45,i-1}\mathbf{D} + \chi_{46,i-1}, \quad A_{45} = \chi_{47,i-1}, \quad A_{46} = \mathbf{0}, \quad A_{47} = \mathbf{0},$

$A_{48} = \chi_{48,i-1}, \quad A_{51} = \chi_{51,i-1}\mathbf{D}^2 + \chi_{52,i-1}\mathbf{D} + \chi_{53,i-1}, \quad A_{52} = \mathbf{0}, \quad A_{53} = \mathbf{0}, \quad A_{54} = \mathbf{0},$

$A_{55} = \mathbf{D}^3 + \chi_{54,i-1}\mathbf{D}^2 + \chi_{55,i-1}\mathbf{D} + \chi_{56,i-1}, \quad A_{56} = -\frac{H_a\beta_h}{1+\beta_h^2}\mathbf{I}, \quad A_{57} = 2Ri\mathbf{I},$

$A_{58} = 2\mathbb{B}Ri\mathbf{I}, \quad A_{61} = \chi_{61,i-1}\mathbf{D} + \chi_{62,i-1}, \quad A_{62} = \chi_{63,i-1}\mathbf{D} + \chi_{64,i-1}, \quad A_{63} = \mathbf{0}, \quad A_{64} = \mathbf{0},$

$A_{65} = \chi_{65,i-1}\mathbf{D} + \chi_{66,i-1}, \quad A_{66} = \mathbf{D}^2 + \chi_{67,i-1}\mathbf{D} + \chi_{68,i-1}, \quad A_{67} = \mathbf{0}, \quad A_{68} = \mathbf{0},$

$A_{71} = \chi_{71,i-1}\mathbf{D}^2 + \chi_{72,i-1}\mathbf{D} + \chi_{73,i-1}, \quad A_{72} = \mathbf{0}, \quad A_{73} = \chi_{74,i-1}\mathbf{D}^2 + \chi_{75,i-1}\mathbf{D} + \chi_{76,i-1},$

$A_{74} = \mathbf{0}, \quad A_{75} = \chi_{77,i-1}\mathbf{D}^2 + \chi_{78,i-1}\mathbf{D} + \chi_{79,i-1}, \quad A_{76} = \mathbf{0},$

$A_{77} = \chi_{710,i-1}\mathbf{D}^2 + \chi_{711,i-1}\mathbf{D} + \chi_{712,i-1}, \quad A_{78} = \mathbf{0},$

$A_{81} = \chi_{81,i-1}\mathbf{D}^2 + \chi_{82,i-1}\mathbf{D} + \chi_{83,i-1}, \quad A_{82} = \mathbf{0}, \quad A_{83} = \mathbf{0},$

$A_{84} = \chi_{84,i-1}\mathbf{D}^2 + \chi_{85,i-1}\mathbf{D} + \chi_{86,i-1}, \quad A_{85} = \chi_{87,i-1}\mathbf{D}^2 + \chi_{88,i-1}\mathbf{D} + \chi_{89,i-1},$

$A_{86} = \mathbf{0}, \quad A_{87} = \mathbf{0}, \quad A_{88} = \chi_{810,i-1}\mathbf{D}^2 + \chi_{811,i-1}\mathbf{D} + \chi_{812,i-1},$

where the coefficients $\chi_{lk,n-1}$ and $\zeta_{l,i-1}$, $(l = 1, 2, 3, ..., 8, k = 1, 2, 3, ..., 12)$ are approximations in terms of F_i, W_i, T_i and C_i, $(i = 1, 2, 3, ..., n-1)$ and their derivatives, $\mathbf{0}$ and $\mathbf{I}$ are null and identity matrices of size (N +1)×(N +1).

After modifying the matrix system (7.26) to incorporate boundary conditions, the solution is obtained as

$$\mathbf{X}_i = \mathbf{A}_{i-1}^{-1}\mathbf{R}_{i-1} \tag{7.28}$$

7.2.8 Results and Discussion

The variation of the tangential velocity for distinct values of β_h, R, D_γ and K_p is exhibited through the Figs. (7.7(a)) - (7.7(d)). An increase in the Hall parameter, the tangential velocity of the fluid enhances as depicted in the Fig. (7.7(a)). It is witnessed from the Fig. (7.7(b)) that, an increase in the thermal radiation, the velocity of the fluid escalated. It is seen from the Fig. (7.7(c)) that the fluid velocity is less in the absence of thermal dispersion and more in the presence of thermal dispersion. This is because conduction over convection occurs by considering the thermal dispersion effect into the energy equation. As a

result, more dominance of the thermal conduction. Therefore, increase in thermal dispersion enhances the fluid velocity. An increase in the value of K_p reduces the fluid velocity in the boundary layer as portrayed in the Fig. (7.7(d)).

Figures (7.8(a)) - (7.8(d)) represents the fluctuation of transverse velocity for distinct values of β_h, D_γ, R and K_p, respectively. It is noticed from the Fig. (7.8(a)) that there is no secondary flow velocity in the absence of the Hall parameter. As the value of β_h increased, the cross flow is generated As expected, an increase in the thermal dispersion the transverse velocity reduces as shown in the Fig. (7.8(b)). Figs. (7.8(c)) and (7.8(d)) depict that the cross flow generated due to Hall effect, escalates with an enhance in the values of R and K_p.

Figures (7.9(a)) - (7.9(d)) are due to the variation of temperature profile for distinct values of β_h, R, D_γ and K_p. Enhance in the value of β_h, the effective thermal conductivity of the fluid reduces and hence temperature diminishes as shown in the Fig. (7.9(a)). It is seen from the Fig. (7.9(b)) that the temperature escalates with the increasing values of the thermal radiation, which in turn, intensifies the thermal boundary layer thickness. The temperature rises with enhancing the value D_γ as shown in the Fig. (7.9(c)). Increase in the value of porosity parameter K_p results in the reduction of the thermal boundary layer. ie., temperature reduces with the rise in K_p as shown in the Fig. (7.9(d)).

Variation of concentration profile for distinct values of β_h, R, D_χ and K_p is portrayed in the Figs. (7.10(a)) - (7.10(d)). Figure (7.10(a)) exhibits that concentration reduces with the rise in the value of β_h. As the values of the radiation and porosity parameter escalates, the concentration boundary layer reduces and hence, fluid concentration reduces as shown in the Figs. (7.10(b)) and (7.10(d)), respectively. It is observed from the Fig. (7.10(c)) that, the concentration is less in the absence of D_χ and more in the presence of D_χ. ie., the concentration of the fluid enhances with the rise in D_χ, which in turn, intensifies the concentration boundary layer thickness.

The influence of β_h, D_γ, R, D_χ, S and K_p on the rate of heat transfer against non-similar variable x is explored in the Figures (7.11(a)) - (7.11(f)). It is observed from the Fig. (7.11(a)) that the rate of heat transfer reduces with enhancing the value of β_h. It is

portrayed in the Fig. (7.11(b)) that the rate of heat transfer reduces with the enhancement in the value of D_γ. In the absence of D_γ, i.e.,($D_\gamma = 0$), there's no effect of non-similar variable x on the rate of heat transfer. As expected, enhancing the value of D_γ, the rate of heat transfer reduces. While the rate of heat transfer escalates with an increase in the value of thermal radiation parameter R as depicted in the Fig. (7.11(c)). It is noticed that in the absence of solutal dispersion maximum rate of heat transfer occurs and as strengthening the solutal dispersion rate of mass transfer escalated as shown in the Fig. (7.11(d)). It is also noticed that the decrease in the rate of heat transfer is more in the presence of the thermal dispersion than that of increase in the presence of the solutal dispersion. The effect of S on the rate of heat transfer is presented in the Fig. (7.11(e)) and it is evident from the figure that the rate of heat transfer enhances with the suction. Figure (7.11(f)) shows that the rate of heat transfer reduces with the rising the slipperiness. Further, it is seen that the rate of heat transfer is reducing gradually as $x \to 1$.

Figures (7.12(a)) - (7.12(f)) depict the behaviour of rate of mass transfer for different values of β_h, R, D_χ, D_γ, S and K_p against non-similar variable x. Increase in the values of β_h and R the rate of mass transfer escalated as portrayed in the Figs. (7.12(a)) and (7.12(b)). Enhancing the solutal dispersion parameter D_χ, the rate of mass transfer is falling down. In the absence of D_χ, i.e., ($D_\chi = 0$), there is no effect of the non-similar variable x on the rate of mass transfer. As the value of D_χ escalates, the rate of mass transfer reduces as shown in the Fig. (7.12(c)). It is evident from the Fig. (7.12(d)) that the rate mass transfer escalates by strengthening the thermal dispersion. While the rate of mass transfer enhances with an increase in fluid suction and opposite trend is observed with an increase in porosity parameter as shown in the Figs. (7.12(e)) and (7.12(f)). Further, it is identified that the rate of mass transfer is reducing gradually as $x \to 1$ except in presence of porosity parameter K_p.

The behaviour of $F''(x,0)$ and $W'(x,0)$ for different values of λ, β_h, R, Ri, D_γ and D_χ are tabulated in Table (7.2). It is evident from the table that the $F''(x,0)$ is increasing and $W'(x,0)$ is reducing with slipperiness. In the presence of Hall parameter both the skin-frictions are increasing. It is also observed that the transverse velocity vanishes when $\beta_h = 0$

Table 7.2: *Variation of skin friction in $\tilde{x}$- and $\tilde{z}$-directions for varying values of slip parameter λ, Hall parameter β_h, radiation parameter R, mixed convection parameter Ri, thermal dispersion parameter D_γ, and solutal dispersion parameeter D_χ.*

λ	β_h	R	Ri	D_γ	D_χ	$F''(0)$	$W'(0)$
0.0	0.5	1.0	0.5	0.2	0.3	-1.311129	0.186076
0.5	0.5	1.0	0.5	0.2	0.3	-0.602602	0.157860
1.0	0.5	1.0	0.5	0.2	0.3	-0.395690	0.148450
2.0	0.5	1.0	0.5	0.2	0.3	-0.235600	0.140698
1.0	0.0	1.0	0.5	0.2	0.3	-0.409960	0.000000
1.0	0.1	1.0	0.5	0.2	0.3	-0.409293	0.034153
1.0	0.5	1.0	0.5	0.2	0.3	-0.395690	0.148450
1.0	2.0	1.0	0.5	0.2	0.3	-0.337632	0.201963
1.0	0.5	0.0	0.5	0.2	0.3	-0.427562	0.131475
1.0	0.5	0.5	0.5	0.2	0.3	-0.408048	0.141353
1.0	0.5	1.0	0.5	0.2	0.3	-0.395690	0.148450
1.0	0.5	3.0	0.5	0.2	0.3	-0.370626	0.164738
1.0	0.5	1.0	0.0	0.2	0.3	-0.598768	0.070074
1.0	0.5	1.0	0.5	0.2	0.3	-0.395690	0.148450
1.0	0.5	1.0	1.0	0.2	0.3	-0.252741	0.184808
1.0	0.5	1.0	3.0	0.2	0.3	0.162148	0.262885
1.0	0.5	1.0	0.5	0.0	0.3	-0.396671	0.148266
1.0	0.5	1.0	0.5	1.0	0.3	-0.391956	0.149278
1.0	0.5	1.0	0.5	2.0	0.3	-0.387727	0.150419
1.0	0.5	1.0	0.5	3.0	0.3	-0.383945	0.151588
1.0	0.5	1.0	0.5	0.2	0.0	-0.395823	0.148420
1.0	0.5	1.0	0.5	0.2	1.0	-0.395387	0.148529
1.0	0.5	1.0	0.5	0.2	2.0	-0.394971	0.148662
1.0	0.5	1.0	0.5	0.2	3.0	-0.394579	0.148807

and hence in $\tilde{z}-$direction there is no skin-friction. Table (7.2) illustrates that, $F''(x,0)$ and $W'(x,0)$ are enhancing with a rise in the thermal radiation. The positive values of Ri increases both the skin-frictions. In addition to this, $F''(x,0)$ in $\tilde{x}-$direction is greatly increasing with positive values of Ri. At the end of the table, the influence of the thermal and solutal dispersions on $F''(x,0)$ and $W'(x,0)$ is presented. It is noticed from the table that, enhancing the thermal or solutal or both the dispersions leads to the reduction in surface drag and hence, both the skin-frictions $F''(x,0)$ and $W'(x,0)$ escalates.

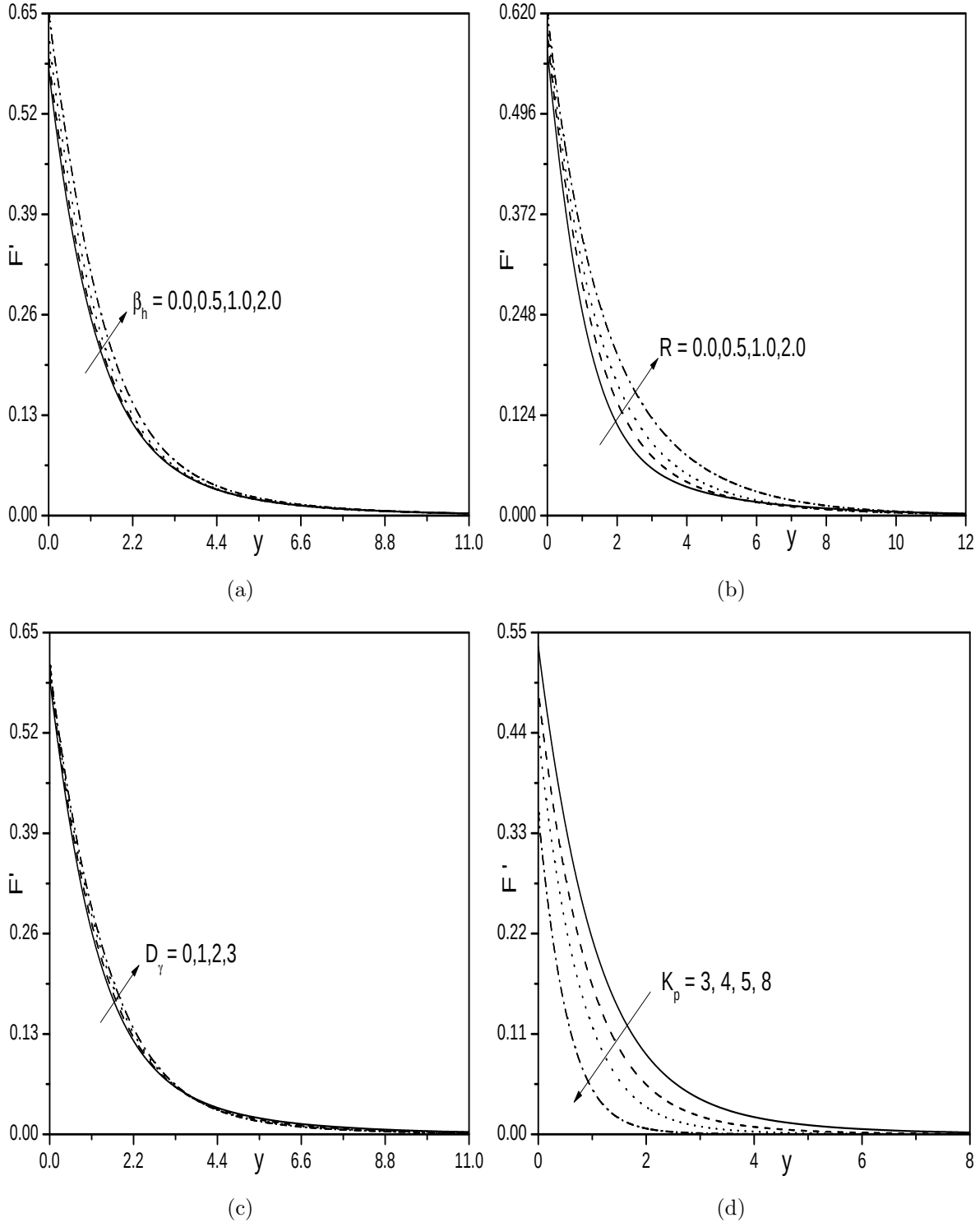

Figure 7.7: *Effect (a)β_h, (b)R, (c)D_γ and (d)K_p on tangential velocity.*

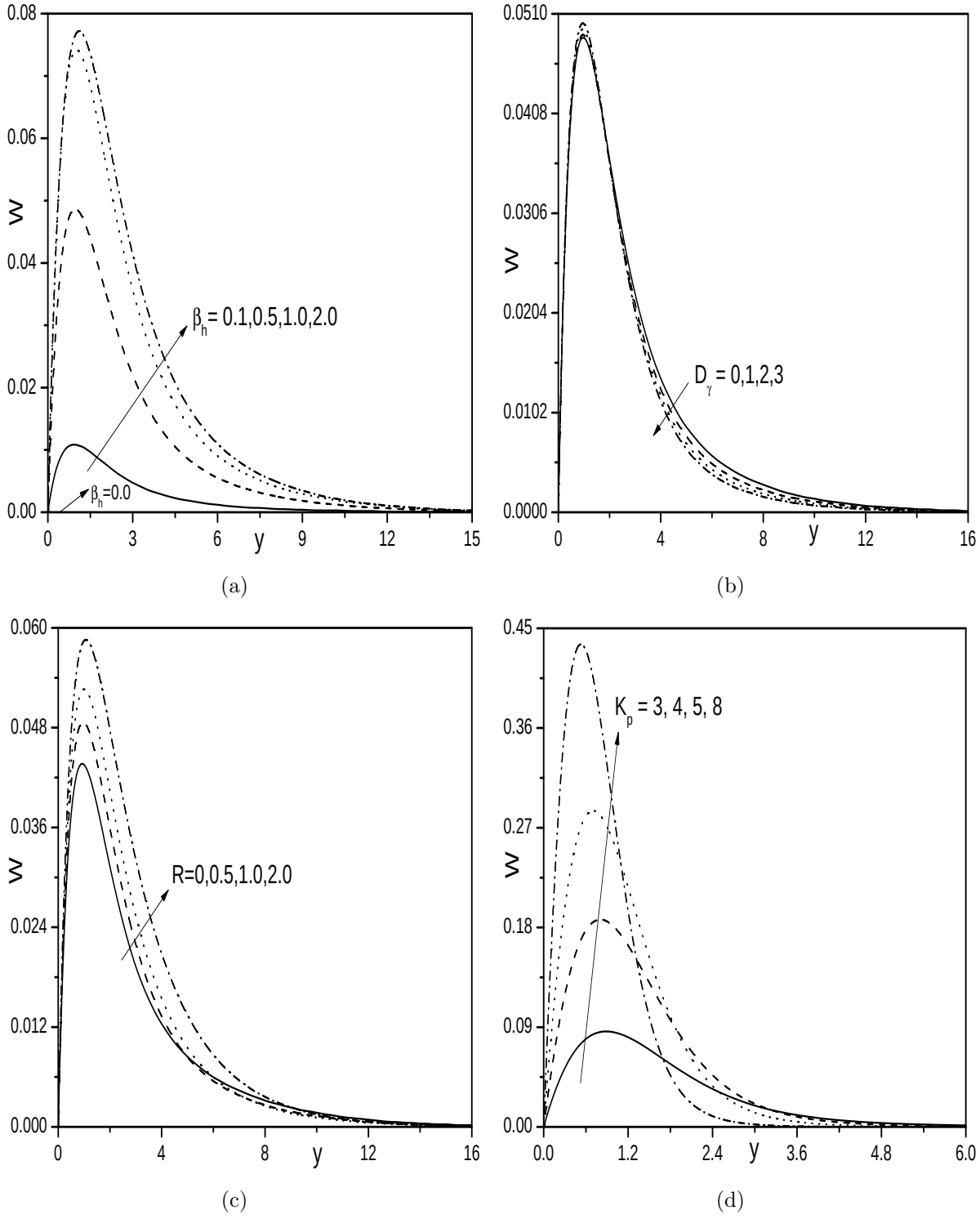

Figure 7.8: *Effect (a)β_h, (b)D_γ, (c)R and (d)K_p on transverse velocity.*

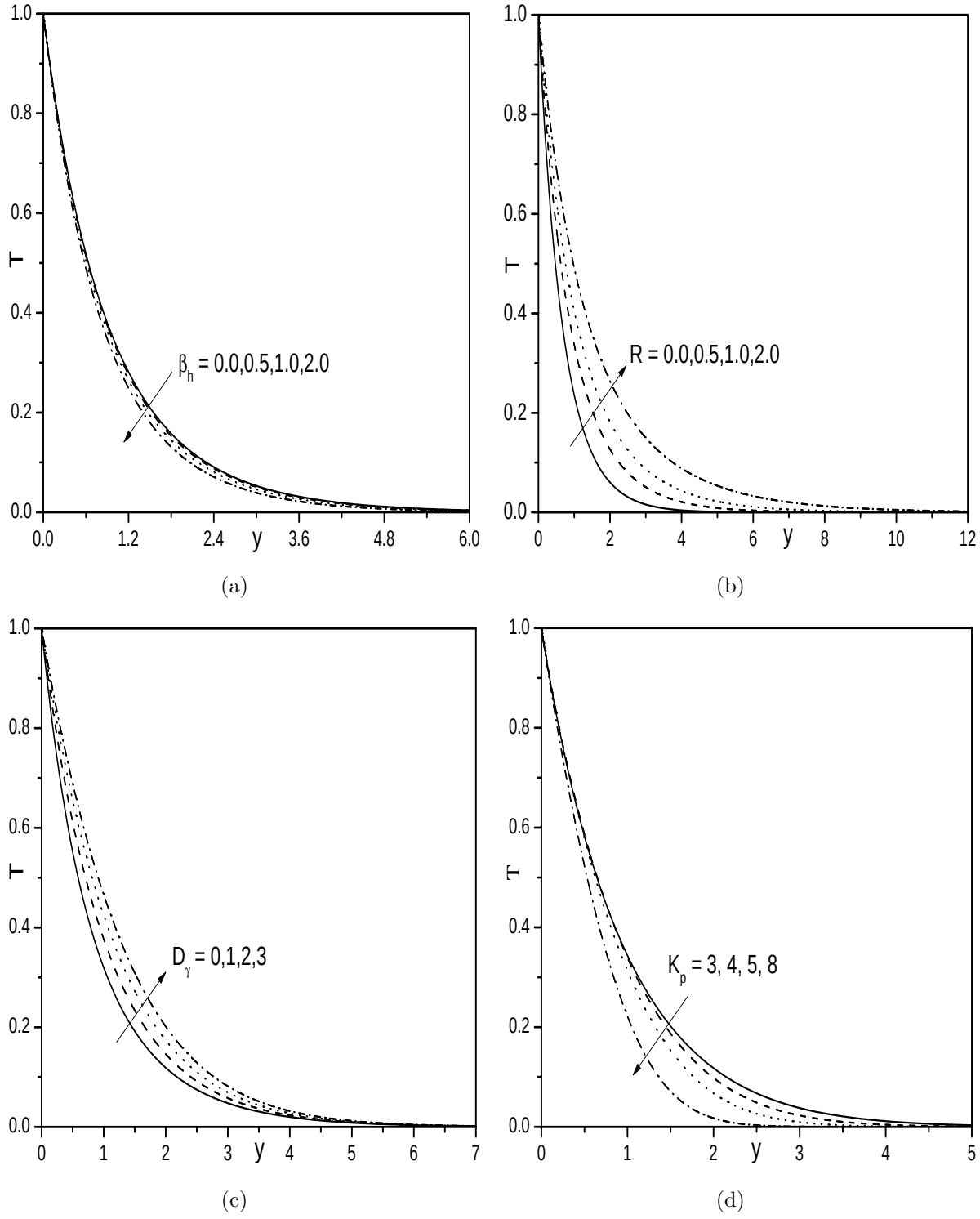

Figure 7.9: *Effect (a)β_h, (b)R, (c)D_γ and (d)K_p on temperature profile.*

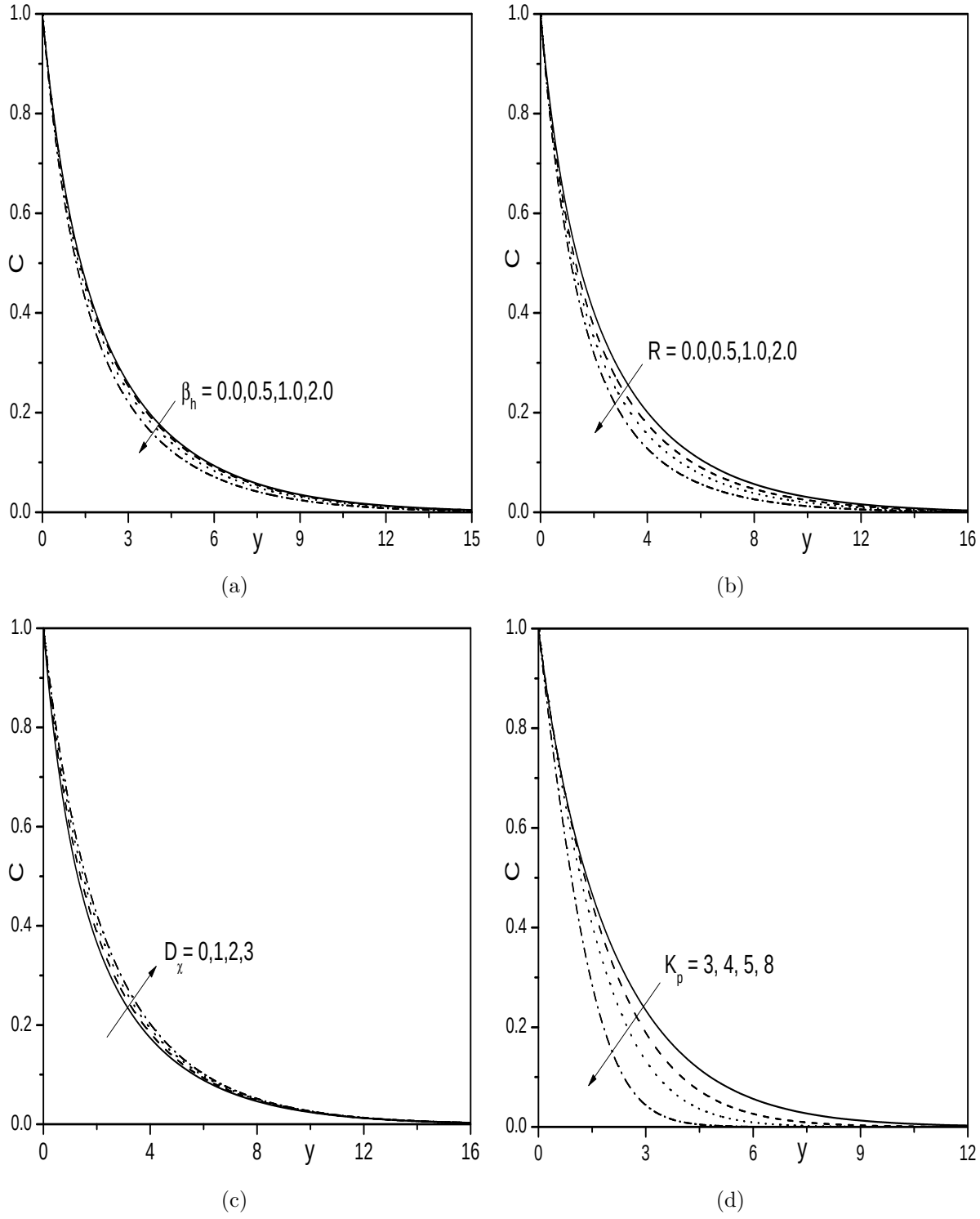

Figure 7.10: *Effect (a)β_h, (b)R, (c)D_χ and (d)K_p on concentration profile.*

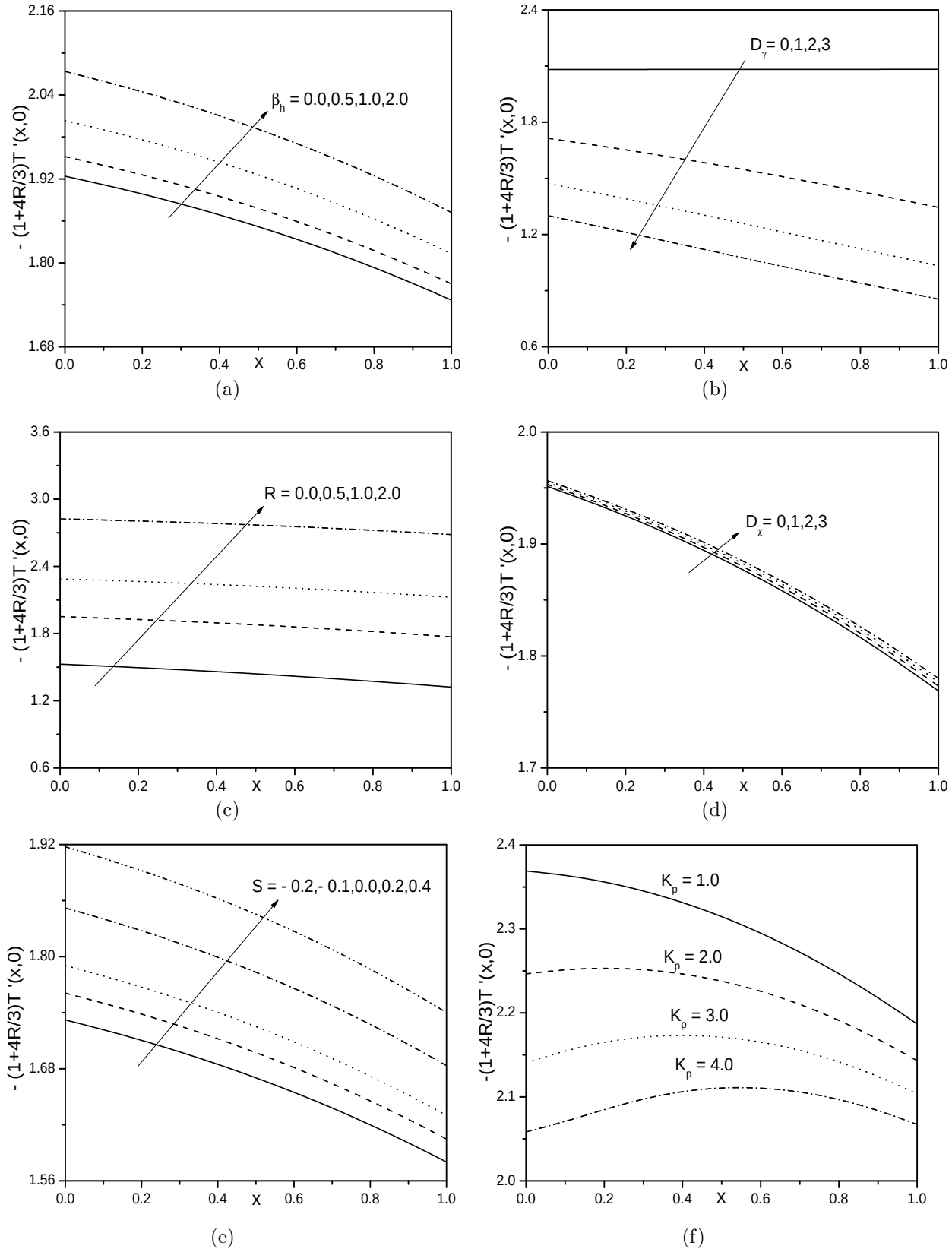

Figure 7.11: *Effect (a)β_h, (b)D_γ, (c)R, (d)D_χ, (e)S and (f)K_p on* $-\left(1+\frac{4R}{3}\right)T'(x,0)$

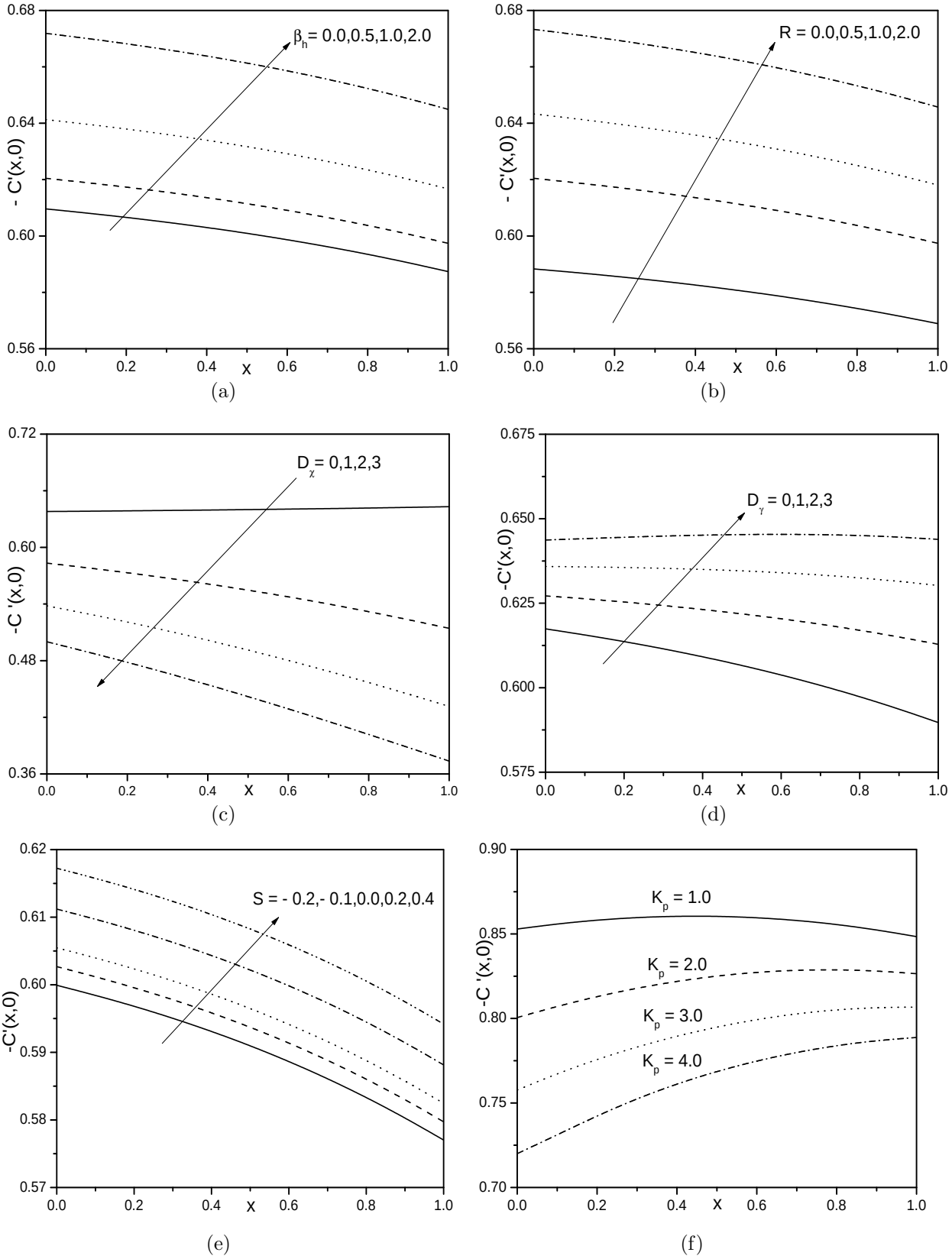

Figure 7.12: *Effect (a)β_h, (b)D_γ, (c)R, (d)D_χ, (e)S and (f)K_p on $-C'(x,0)$*

7.3 Conclusions

Numerical investigation of the influence of the thermal and solutal dispersions in the presence of thermal radiation on the laminar slip flow, heat and mass transfer of an incompressible viscous fluid over a porous sheet stretching exponentially is analyzed.

The temperature increases with an increase in the Biot number and decreases with an increase in the Hall parameter. In both the cases, the temperature increases with an increase in the thermal dispersion and radiation parameters. In both cases, the rate of heat transfer decreases with an increase in the thermal dispersion and porosity parameters and increases with an increase in the radiation parameter. While, in case (a), the rate of heat transfer increases with an increase in Biot number and in case (b), it increases with the increase in the Hall, solutal dispersion and suction parameters. In both cases, the concentration increases and the rate of mass transfer decrease with the increase in solutal dispersion parameter.

Chapter 8

Influence of homogeneous-heterogeneous reactions on the viscous flow on an exponentially stretching sheet [1]

8.1 Introduction

In the recent past, considerable attention has been given to study of combined heat and mass transfer problems with the effect of chemical reaction as it plays a crucial role in diverse applications such as drying, energy transfer in wet cooling surface, evaporation at the surface of the water body etc. There are two types of chemical reactions, namely, homogeneous and heterogeneous reactions. Chaudhary and Merkin [16] discussed the homogeneous-heterogeneous reactions in boundary layer flow. Nandkeolyar *et al.* [74] investigated the influence of internal heat generation in nanofluid flow with homogeneous-heterogeneous reactions. Sheikh and Abbas [96] studied the effect of homogeneousheterogeneous reaction in the boundary layer

[1] Case(a): Communicated to "**Nonlinear Engineering - Modeling and Application**",
Case(b) Communicated to "**International Journal of Chemical Reactor Engineering**"

flow of a non-Newtonian fluid near a stagnation point over a porous stretching/shrinking sheet with a constant suction.

In this Chapter, the effect of homogeneous-heterogeneous chemical reactions on the viscous fluid flow over an exponentially stretching permeable sheet in presence of thermal radiation is considered.

8.2 Mathematical Formulation

Consider a stretching sheet with a temperature $T_w(\tilde{x})$ and concentration $C_w(\tilde{x})$ in a laminar slip flow of electrically viscous incompressible fluid with a temperature and concentration as T_∞ and C_∞, respectively. The fluid is considered to be a gray, absorbing/emitting radiation, but non-scattering medium. The Rosseland approximation [102] is used to describe the radiative heat flux in the energy equation. It is assumed that a simple homogeneous-heterogeneous reaction model exists as proposed by Chaudary and Merkin [16] in the following form: For homogeneous reaction, cubic autocatalysis method is chosen, namely

$$\tilde{A} + 2\tilde{B} \to 3\tilde{B}, \quad rate = k_c \tilde{a}\,\tilde{b}^2$$

while on the catalyst surface, we have the single isothermal first order reaction

$$\tilde{A} \to \tilde{B}, \quad rate = k_s \tilde{a}$$

where $\tilde{a}$ and $\tilde{b}$ are concentrations of the chemical species $\tilde{A}$ and $\tilde{B}$, respectively, k_c and k_s are constants. Hence, with the above assumptions, the following are the equations which governs the flow problem in the presence of thermal radiation:

$$\frac{\partial \tilde{u}_x}{\partial \tilde{x}} + \frac{\partial \tilde{u}_y}{\partial \tilde{y}} = 0 \tag{8.1}$$

$$\tilde{u}_x \frac{\partial \tilde{u}_x}{\partial \tilde{x}} + \tilde{u}_y \frac{\partial \tilde{u}_x}{\partial \tilde{y}} = \nu \frac{\partial^2 \tilde{u}_x}{\partial \tilde{y}^2} \tag{8.2}$$

$$\tilde{u}_x \frac{\partial \tilde{T}}{\partial \tilde{x}} + \tilde{u}_y \frac{\partial \tilde{T}}{\partial \tilde{y}} = \alpha \frac{\partial^2 \tilde{T}}{\partial \tilde{y}^2} + \frac{16 T_\infty^3 \sigma^*}{3k^* \rho c_p} \frac{\partial^2 \tilde{T}}{\partial \tilde{y}^2} \tag{8.3}$$

$$\tilde{u}_x \frac{\partial \tilde{a}}{\partial \tilde{x}} + \tilde{u}_y \frac{\partial \tilde{a}}{\partial \tilde{y}} = D_A \frac{\partial^2 \tilde{a}}{\partial \tilde{y}^2} - k_c \tilde{a}\, \tilde{b}^2 \tag{8.4}$$

$$\tilde{u}_x \frac{\partial \tilde{b}}{\partial \tilde{x}} + \tilde{u}_y \frac{\partial \tilde{b}}{\partial \tilde{y}} = D_B \frac{\partial^2 \tilde{b}}{\partial \tilde{y}^2} + k_c \tilde{a}\, \tilde{b}^2 \tag{8.5}$$

8.2.1 Case(a): Convective Thermal Condition

Assume that the sheet is either cooled or heated convectively through a fluid with temperature T_f ($T_f > T_\infty$ corresponding to a heated surface and $T_f < T_\infty$ corresponding to a cooled surface, respectively) and which induces a heat transfer coefficient h_f, where $h_f = h\sqrt{\frac{U_0}{2L}} e^{\frac{\tilde{x}}{2L}}$.

The conditions on the boundary of the stretching surface are

$$\left.\begin{array}{l} \tilde{u}_x = U_* + N_* \nu \frac{\partial \tilde{u}_x}{\partial \tilde{y}},\ \tilde{u}_y = -V_*(\tilde{x}),\ h_f(T_f - \tilde{T}) = -\kappa \frac{\partial \tilde{T}}{\partial \tilde{y}}, \\ D_A \frac{\partial \tilde{a}}{\partial \tilde{y}} = k_s \tilde{a},\ D_B \frac{\partial \tilde{b}}{\partial \tilde{y}} = -k_s \tilde{a} \quad \text{at} \quad \tilde{y} = 0 \\ \tilde{u}_x \to 0,\ \tilde{T} \to T_\infty,\ \tilde{a} \to \tilde{a_0},\ \tilde{b} \to 0 \ \text{ as } \ \tilde{y} \to \infty \end{array}\right\} \tag{8.6}$$

where $\tilde{a_0}$ is a positive constant.

Introducing the stream functions through $\tilde{u}_x = -\frac{\partial \psi}{\partial \tilde{y}}$ and $\tilde{u}_y = \frac{\partial \psi}{\partial \tilde{x}}$ and then the following dimensionless variables

$$\left.\begin{array}{l} \tilde{x} = xL, \quad \tilde{y} = y\sqrt{\frac{2\nu L}{U_0}} e^{\frac{-\tilde{x}}{2L}},\ \psi = \sqrt{2\nu L U_0} e^{\frac{\tilde{x}}{2L}} F(x,y), \\ \tilde{T} = T_\infty + (T_f - T_\infty) T(x,y),\ \tilde{C} = \tilde{a_0} C, \quad \tilde{C_1} = \tilde{a_0} C_1 \end{array}\right\} \tag{8.7}$$

into Eqs. (8.1) - (8.5), we obtain

$$F''' + FF'' - 2F'^2 + 2\left(F'' \frac{\partial F}{\partial x} - F' \frac{\partial F'}{\partial x}\right) = 0 \tag{8.8}$$

$$\frac{1}{Pr}\left(1 + \frac{4R}{3}\right) T'' + FT' + 2\left(T' \frac{\partial F}{\partial x} - F' \frac{\partial T}{\partial x}\right) = 0 \tag{8.9}$$

$$\frac{1}{Sc}C'' + FC' - K\ e^{-x}CC_1^2 + 2\left(C'\frac{\partial F}{\partial x} - F'\frac{\partial C}{\partial x}\right) = 0 \tag{8.10}$$

$$\frac{\delta}{Sc}C_1'' + FC_1' + K\ e^{-x}CC_1^2 + 2\left(C_1'\frac{\partial F}{\partial x} - F'\frac{\partial C_1}{\partial x}\right) = 0 \tag{8.11}$$

The conditions at the boundary reduces to

$$\left.\begin{aligned} &F(x,0) + 2\tfrac{\partial F}{\partial x}(x,0) = S,\ F'(x,0) = 1 + \lambda F''(x,0), \\ &\qquad T'(x,0) = -Bi(1 - T(x,0)), \\ &C'(x,0) = K_s\ e^{-x/2}C(x,0), \quad \delta C_1'(x,0) = -K_s\ e^{-x/2}C(x,0), \\ &F'(x,y) \to 0,\ T(x,y) \to 0,\ C(x,y) \to 1, C_1(x,y) \to 0, \quad \text{as} \quad y \to \infty \end{aligned}\right\} \tag{8.12}$$

where $\delta = \frac{D_B}{D_A}$ is the duffusion ratio.

It is predicted that the diffusion coefficients of chemical species $\tilde{A}$ and $\tilde{B}$ are of comparable size, which undergo further assumption that diffusion coefficients D_A and D_B are equal, i.e., $\delta = 1$ [16]. This assumption leads to the following relation

$$C(x,y) + C_1(x,y) = 1 \tag{8.13}$$

Thus, Eqs. (8.10) and (8.11) reduce to

$$\frac{1}{Sc}C'' + FC' - K\ e^{-x}C(1-C)^2 + 2\left(C'\frac{\partial F}{\partial x} - F'\frac{\partial C}{\partial x}\right) = 0 \tag{8.14}$$

and the boundary condition in (8.12) reduce to

$$C'(x,0) = K_s e^{-x/2}C(x,0) \text{ and } \quad C(x,\infty) = 1 \tag{8.15}$$

$K = \frac{2Lk_c\tilde{a_0}^2}{U_0}$ is the measure of the strength of homogenous reaction, $K_s = \frac{\sqrt{2}Lk_sRe^{-1/2}}{D_A}$ is the measure of the strength of heterogeneous (surface) reaction.

The non-dimensional skin friction C_f and the local Nusselt number $Nu_{\tilde{x}}$ are given by

$$\frac{\sqrt{Re_x}}{\sqrt{2x/L}}\ C_f = F''(x,0) \quad \text{and} \quad \frac{Nu_x}{\sqrt{Lx/2}\sqrt{Re_x}} = -\left(1 + \frac{4R}{3}\right)T'(x,0) \tag{8.16}$$

where $Re_x = \frac{xU_*(x)}{\nu}$ is the local Reynolds number.

8.2.2 Method of Solution

The numerical solutions to Eqs. (8.8), (8.9) and (8.14) along with the boundary conditions (8.12) and (8.15), is solved numerically, as explained in case (a) of Chapter-3.

Proceeding in case (a) of Chapter-3, we obtain the following matrix equation

$$\mathbf{A}_{i-1}\mathbf{X}_i = \mathbf{R}_{i-1}, \tag{8.17}$$

In Eq. (8.17), $\mathbf{A}_{i-1}$ is a square matrix of order $(6N+6)$ and $\mathbf{X}_i$ and $\mathbf{R}_{i-1}$ are (6N + 6)×1 column vectors defined by

$$\mathbf{A}_{i-1} = [A_{rs}], \mathbf{R}_{i-1} = [\mathbf{E}_{r,i-1}], r, s = 1, 2, \cdots, 6, \quad \mathbf{X}_i = \begin{bmatrix} \mathbf{F}_i \\ \mathbf{\Theta}_i \\ \mathbf{\Phi}_i \\ \mathbf{G}_i \\ \mathbf{H}_i \\ \mathbf{K}_i \end{bmatrix} \tag{8.18}$$

where

$$\begin{aligned}
\mathbf{F}_i &= [F_i(\xi_0), F_i(\xi_1), F_i(\xi_2), ..., F_i(\xi_{N-1}), F_i(\xi_N)]^T, \\
\mathbf{\Theta}_i &= [T_i(\xi_0), T_i(\xi_1), T_i(\xi_2), ..., T_i(\xi_{N-1}), T_i(\xi_N)]^T, \\
\mathbf{\Phi}_i &= [C_i(\xi_0), C_i(\xi_1), C_i(\xi_2), ..., C_i(\xi_{N-1}), C_i(\xi_N)]^T, \\
\mathbf{G}_i &= [G_i(\xi_0), G_i(\xi_1), G_i(\xi_2), ..., G_i(\xi_{N-1}), G_i(\xi_N)]^T, \\
\mathbf{H}_i &= [H_i(\xi_0), H_i(\xi_1), H_i(\xi_2), ..., H_i(\xi_{N-1}), H_i(\xi_N)]^T, \\
\mathbf{K}_i &= [K_i(\xi_0), K_i(\xi_1), K_i(\xi_2), ..., K_i(\xi_{N-1}), K_i(\xi_N)]^T,
\end{aligned}$$

$$\mathbf{E}_{j,i-1} = [\zeta_{j,i-1}(\xi_0), \zeta_{j,i-1}(\xi_1), \zeta_{j,i-1}(\xi_2), ..., \zeta_{j,i-1}(\xi_{N-1}), \zeta_{j,i-1}(\xi_N)]^T, j = 1, 2, 3, 4, 5, 6$$
$$A_{11} = \mathbf{D}^3 + \chi_{11,i-1}\mathbf{D}^2 + \chi_{12,i-1}\mathbf{D} + \chi_{13,i-1}, \quad A_{12} = \mathbf{0}, \quad A_{13} = \mathbf{0},$$
$$A_{14} = \chi_{14,i-1}\mathbf{D} + \chi_{15,i-1}, \quad A_{15} = \mathbf{0}, \quad A_{16} = \mathbf{0}, \quad A_{21} = \chi_{21,i-1}\mathbf{D} + \chi_{22,i-1},$$
$$A_{22} = \frac{1}{Pr}\left(1 + \frac{4R}{3}\right)\mathbf{D}^2 + \chi_{23,i-1}\mathbf{D}, \quad A_{23} = \mathbf{0}, \quad A_{24} = \chi_{24,i-1}, \quad A_{25} = \chi_{25,i-1},$$
$$A_{26} = \mathbf{0}, \quad A_{31} = \chi_{31,i-1}\mathbf{D} + \chi_{32,i-1}, \quad A_{32} = \mathbf{0}, \quad A_{33} = \frac{1}{Sc}\mathbf{D}^2 + \chi_{33,i-1}\mathbf{D} + \chi_{34,i-1},$$
$$A_{34} = \chi_{35,i-1}, \quad A_{35} = \mathbf{0}, \quad A_{36} = \chi_{36,i-1}, \quad A_{41} = \chi_{41,i-1}\mathbf{D}^2 + \chi_{42,i-1}\mathbf{D} + \chi_{43,i-1},$$
$$A_{42} = \mathbf{0}, \quad A_{43} = \mathbf{0}, \quad A_{44} = \mathbf{D}^3 + \chi_{44,i-1}\mathbf{D}^2 + \chi_{45,i-1}\mathbf{D} + \chi_{46,i-1},$$
$$A_{45} = \mathbf{0}, \quad A_{46} = \mathbf{0}, \quad A_{51} = \chi_{51,i-1}, \quad A_{52} = \chi_{52,i-1}\mathbf{D}, \quad A_{53} = \mathbf{0},$$
$$A_{54} = \chi_{53,i-1}\mathbf{D} + \chi_{54,i-1}, \quad A_{55} = \frac{1}{Pr}\left(1 + \frac{4R}{3}\right)\mathbf{D}^2 + \chi_{55,i-1}\mathbf{D} + \chi_{56,i-1},$$
$$A_{56} = \mathbf{0}, \quad A_{61} = \chi_{61,i-1}, \quad A_{62} = \mathbf{0}, \quad A_{63} = \chi_{62,i-1}\mathbf{D} + \chi_{63,i-1},$$
$$A_{64} = \chi_{64,i-1}\mathbf{D} + \chi_{65,i-1}, \quad A_{65} = \mathbf{0}, \quad A_{66} = \frac{1}{Sc}\mathbf{D}^2 + \chi_{66,i-1}\mathbf{D} + \chi_{67,i-1},$$

where the coefficients $\chi_{lk,n-1}$ and $\zeta_{l,i-1}$, $(l = 1, 2, 3, ..., 6, k = 1, 2, 3, ..., 7)$ are approximations in terms of F_i, T_i and C_i, $(i = 1, 2, 3, ..., n-1)$ and their derivatives, $\mathbf{0}$ and $\mathbf{I}$ are null and identity matrices of size (N +1)×(N +1).

After modifying the matrix system (8.17) to incorporate boundary conditions, the solution is obtained as

$$\mathbf{X}_i = \mathbf{A}_{i-1}^{-1}\mathbf{R}_{i-1} \tag{8.19}$$

8.2.3 Result and Discussion

The variation of fluid velocity with slip parameter and suction/injection parameter is portrayed through the Figures (8.1(a)) - (8.1(b)). The velocity reduces with an increase in the slip parameter as shown in the Figure (8.1(a)). Figure (8.1(b)) depicts the variation of velocity with S. It is evident from the figure that velocity reduces with the wall suction and escalates with the injection. Figures (8.2(a)) and (8.2(b)) represent the variation of the skin-friction against x for distinct values of λ and S, respectively. It is observed from these figures that the skin-friction escalates with an increase in slip and falls down with an increase

in the fluid suction. The effect of the other parameters on the velocity and skin-friction are not much significant and hence graphs are not included.

Figures (8.3(a)) - (8.3(d)) exhibit the behaviour of temperature for different values of Bi, R, λ and S. It is known that the stronger convection leads to the higher surface temperatures which appreciably increases the temperature Therefore, the temperature rises with an increase in the value of Bi as shown in the Figure (8.3(a)). Further, for large large value of Biot number Bi, the convective thermal condition from (8.12) transforms to $T(0) \to 1$, which signifies the constant wall condition. It is seen from the Fig. (8.3(b)) that the temperature increases with the increasing values of thermal radiation, which in turn, intensifies the thermal boundary layer thickness. Figure (8.3(c)) illustrates that variation of the temperature with λ. The temperature escalates with a raise in λ as portrayed in the Fig. (8.3(c)). Reduction in temperature is observed with an increase in the fluid suction and enhancement with blowing as shown in the Fig. (8.3(d)).

The variation of the rate of heat transfer in the presence of Bi, R, λ and S against non-similar variable x is presented in the Figures (8.4(a)) - (8.4(d)). It is evident from the Fig. (8.4(a)) that the Biot number enhances the rate of heat transfer predominantly. The rate of heat transfer escalates with a rise in the value of the thermal radiation parameter R as depicted in the Fig. (8.4(b)). Figure (8.4(c)) shows that the rate of heat transfer diminishes with a raise in the slipperiness. Due to fluid suction the rate of heat transfer rises and reduces with injection as shown in the Fig. (8.4(d)).

The variation of concentration profile for distinct values of K and K_s, respectively, is shown in the Figures (8.5(a)) and (8.5(b)). An Enhancement in the values of K and K_s, i.e., strengthening the homogeneous-heterogeneous reactions, decreases the concentration of the fluid as shown in the Figs. (8.5(a)) and (8.5(b)). Further, Figs. (8.5(c)) and (8.5(d)) depicts the behaviour of species concentration for distinct values of λ and S. It is noticed from these figures that, as the value of slip parameter increases the concentration decreases and it increases with the fluid suction.

Figures (8.6(a)) - (8.6(d)) depicts the behaviour of mass transfer rate for different values

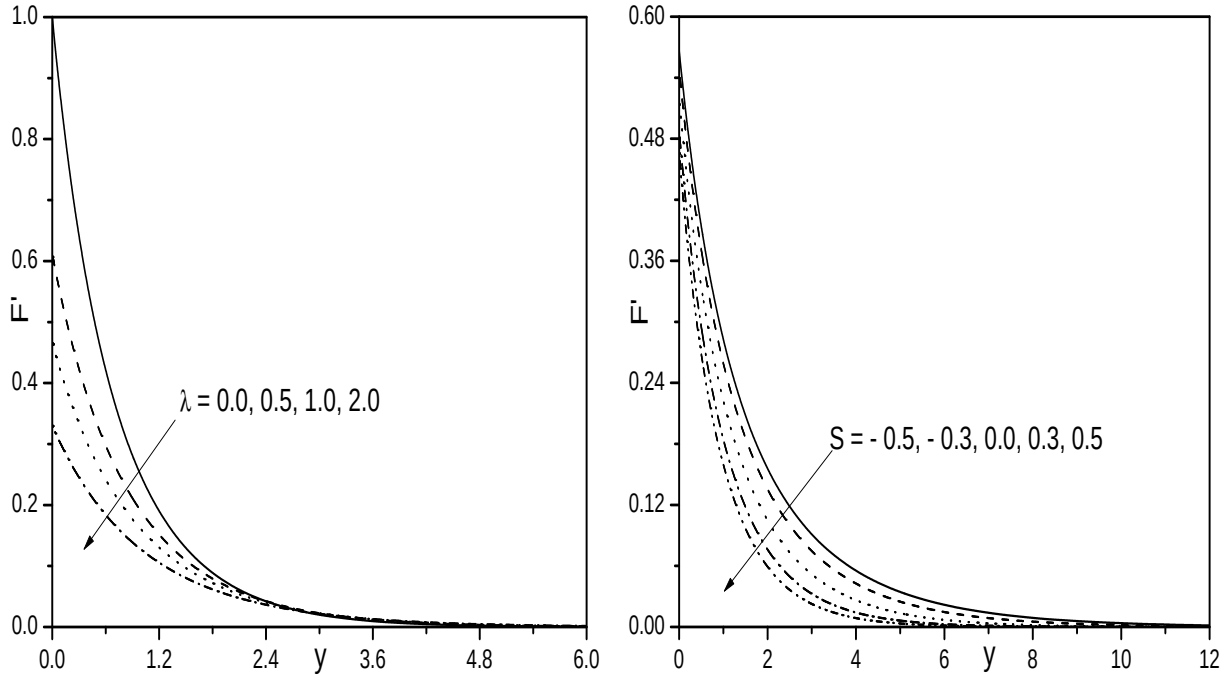

Figure 8.1: *Effect of(a) λ, and (b) S on F'.*

of K, K_s, λ and S against non-similar variable x. An increase in value of K and Ks, corresponds to an increase in the strengths of homogeneous and heterogeneous reaction rates, respectively. As the values of K and K_s escalates, the mass transfer rate reduces as portrayed in the figures (8.6(a)) and (8.6(b)), respectively. As the slipperiness escalates, the mass transfer is reducing as witnessed in the Fig. (8.6(c)). Further, it is noticed from the figure (8.6(d)) that the mass transfer escalates with the fluid suction and reduces with the fluid injection. Finally, mass transfer rate is increasing gradually with x.

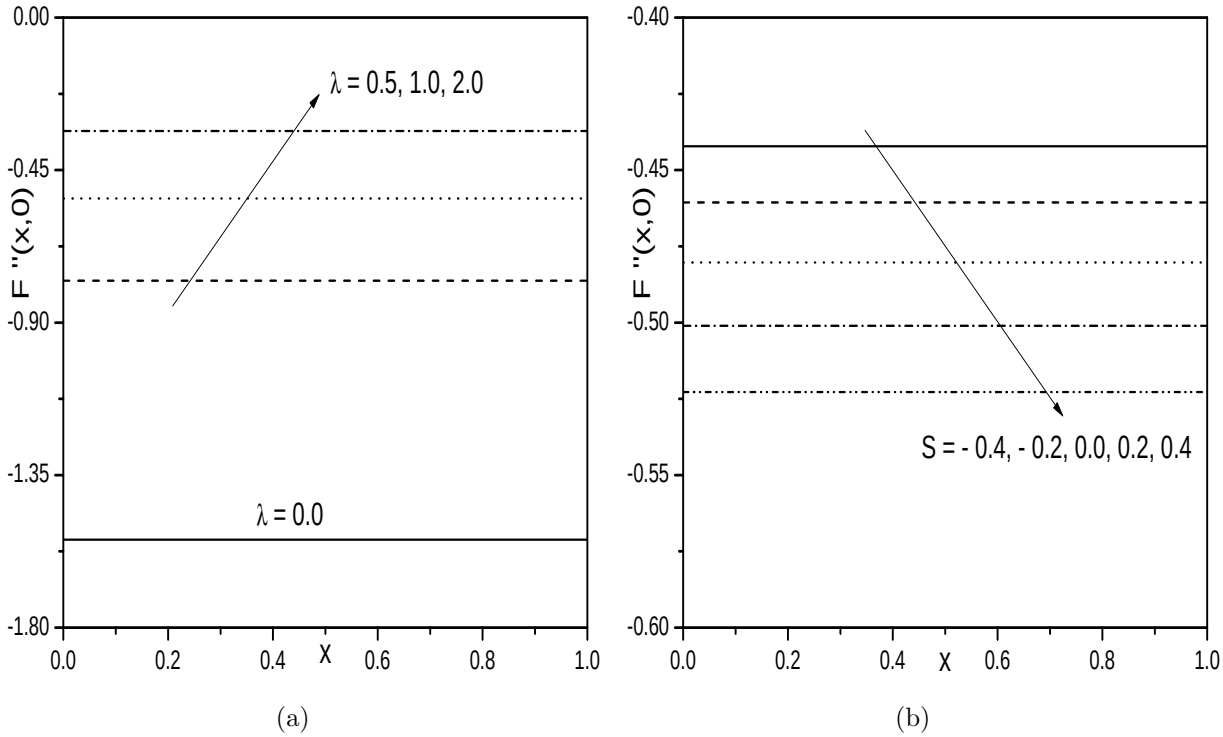

(a) (b)

Figure 8.2: *Effect of (a) λ, and (b) S on $F''(x, 0)$.*

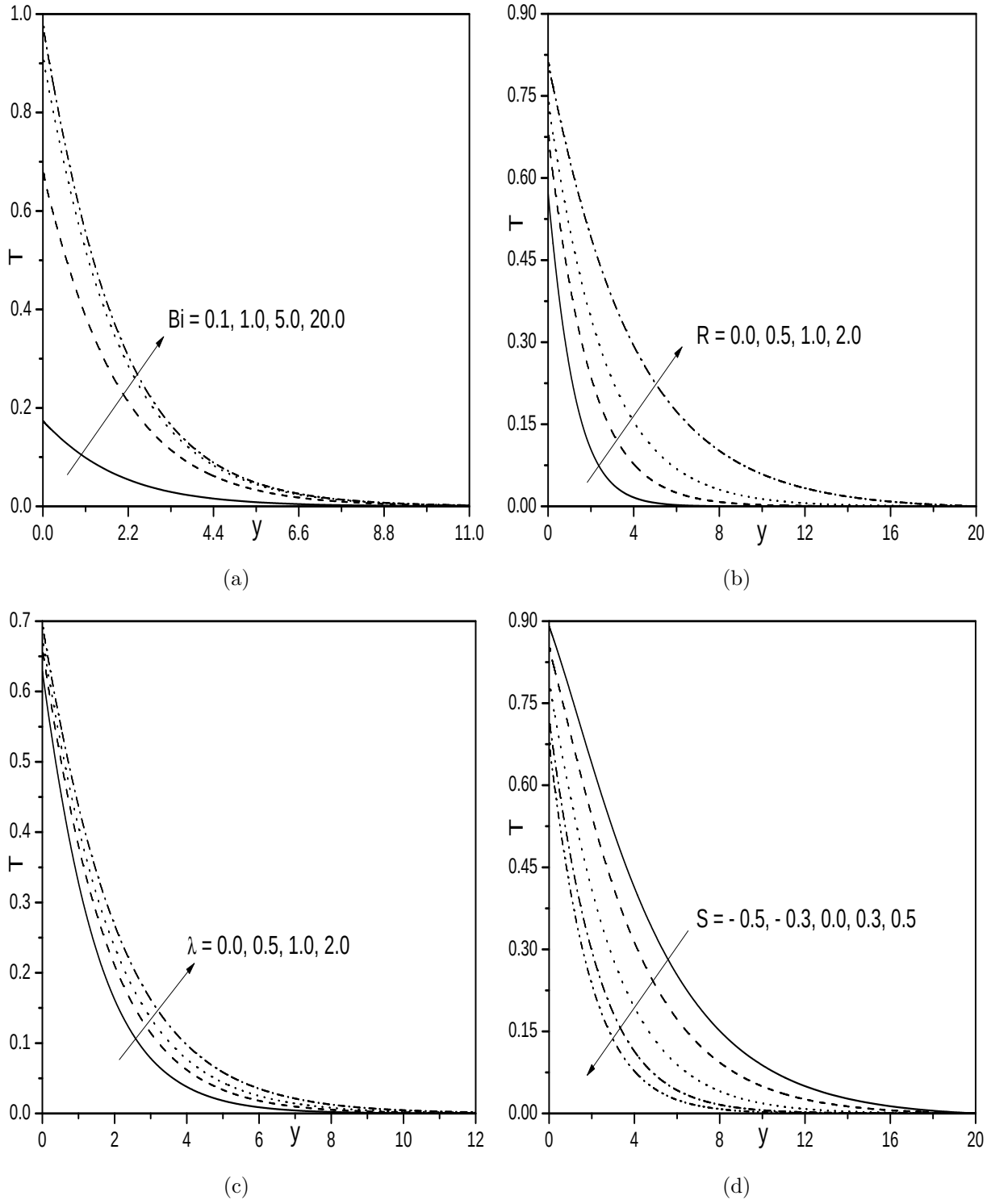

Figure 8.3: *"Effect of (a)Bi, (b)R, (c)λ, and (d)S on T".*

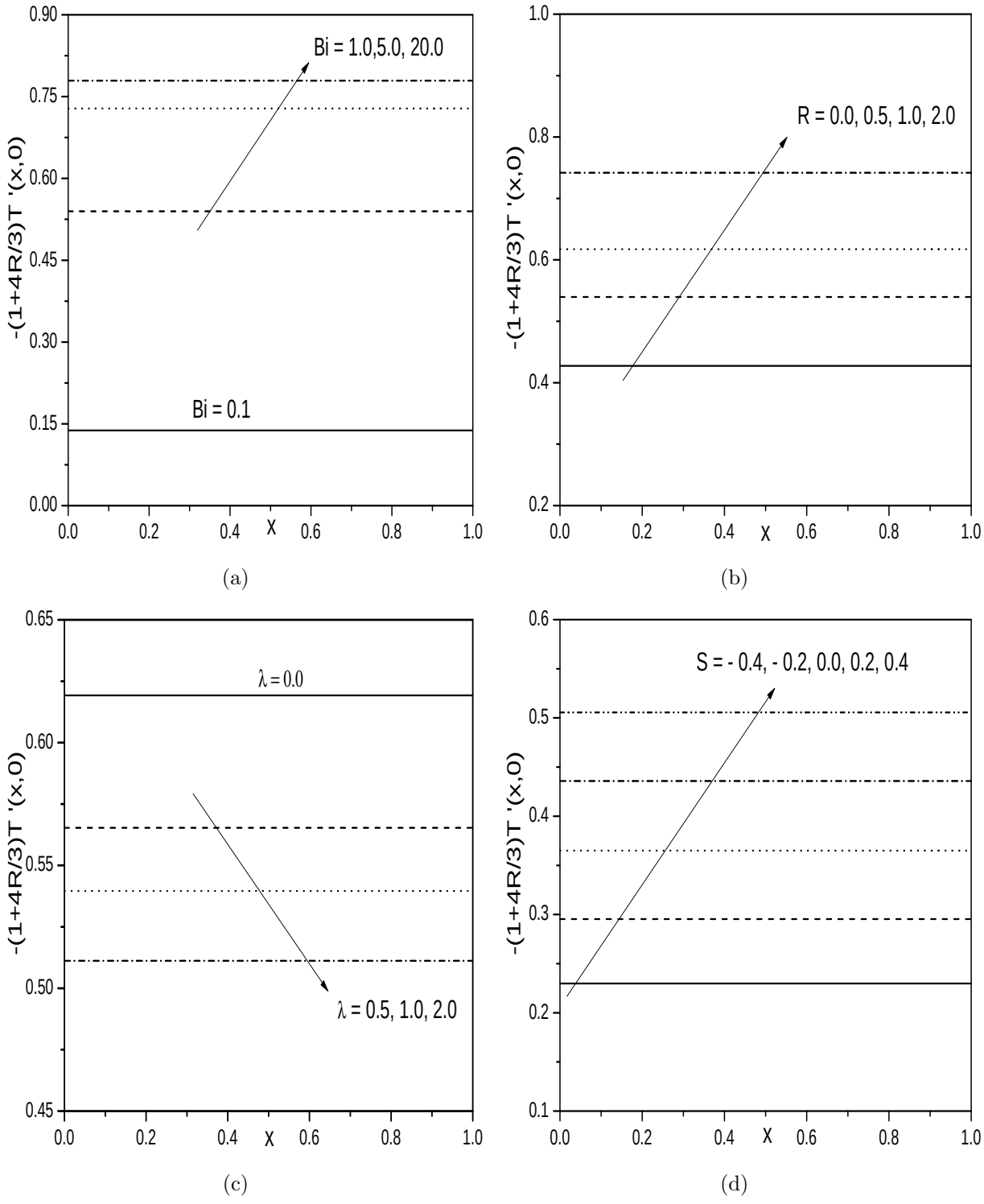

Figure 8.4: *"Effect of (a)Bi, (b)R, (c)λ, and (d)S on* $-\left(1+\frac{4R}{3}\right)T'(x,0)$*".*

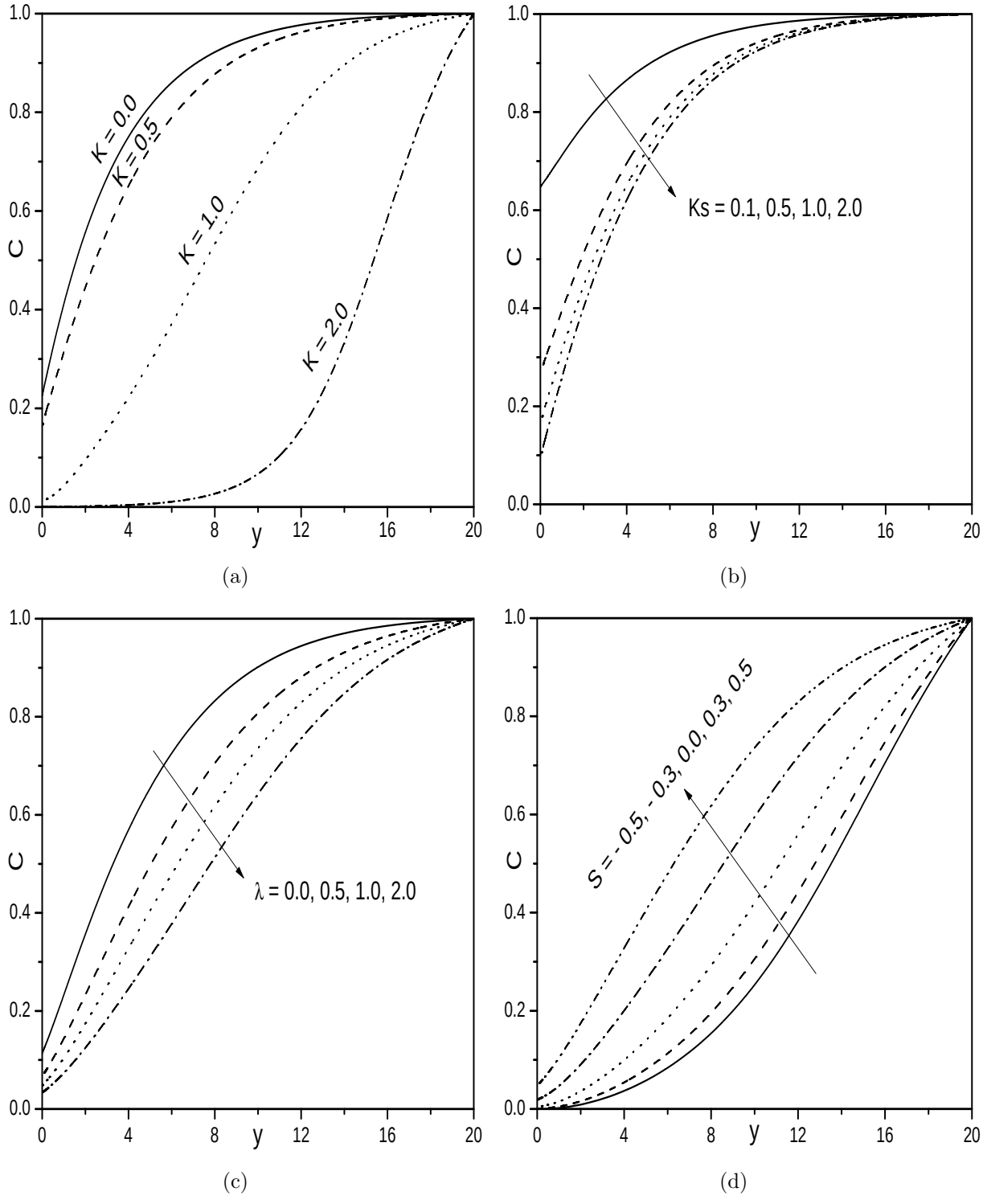

Figure 8.5: *"Effect of (a) K, (b) Ks, (c) λ, and (d) S on C".*

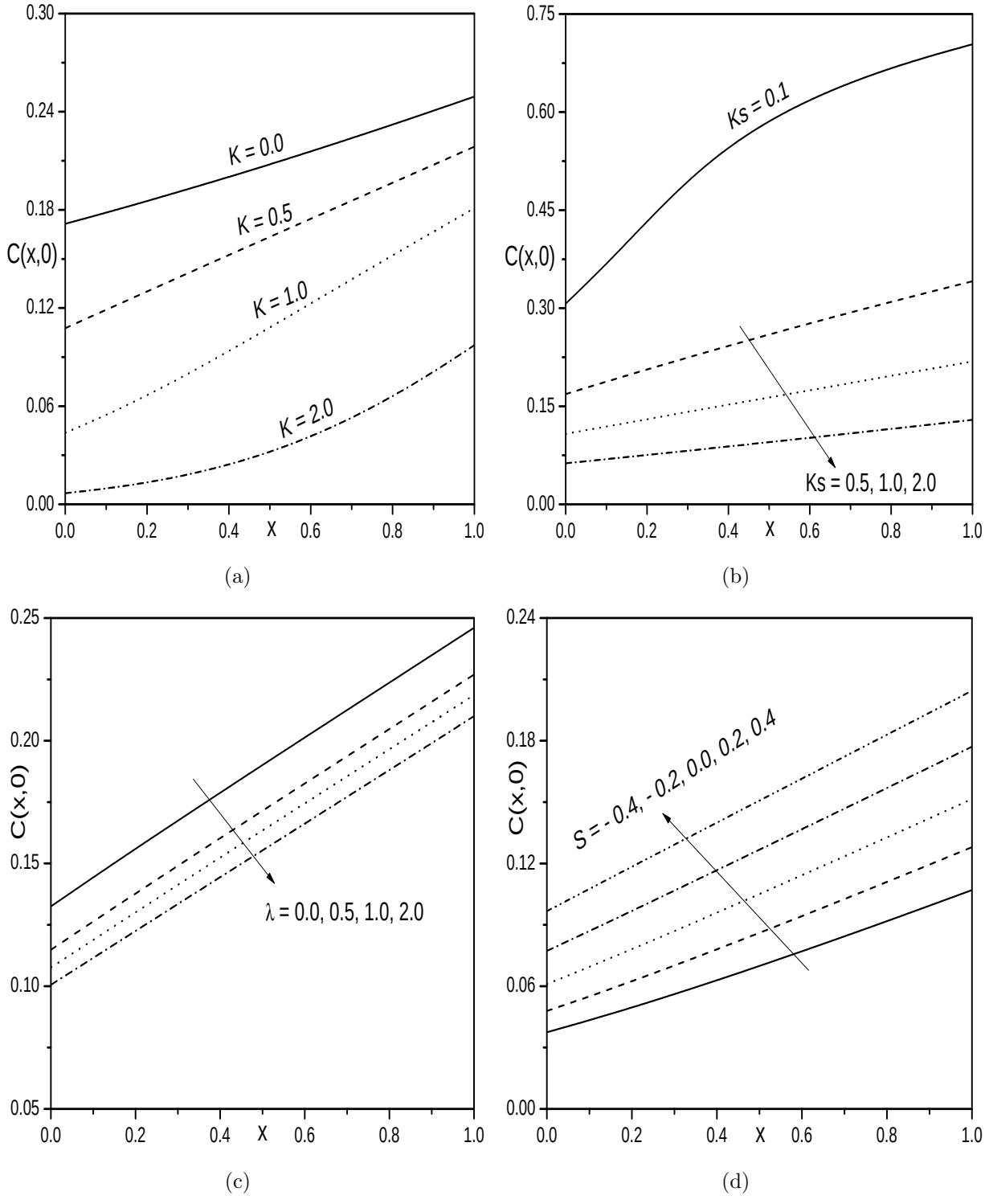

Figure 8.6: *"Effect of (a) K, (b) Ks, (c) λ, and (d) S on $C(x,0)$".*

8.2.4 Case(b): Uniform wall temperature with Hall effect

Assume that, a strong magnetic field of strength $B(\tilde{x}) = B_0 e^{\frac{\tilde{x}}{2L}}$ is applied in $\tilde{y}-$direction and the influence of Hall current is not neglected. Assume that magnetic Reynolds number is very small so that the induced magnetic field is negligible in comparison to applied magnetic field. The presence of Hall current induces a cross flow in $\tilde{z}$-direction and hence the flow becomes three-dimensional. Under the Boussinesq approximation, the flow is governed by the following non-dimensional equations

$$F''' + FF'' - 2F'^2 + 2Ri\ T - \frac{H_a}{1+\beta_h^2}(F' + \beta_h W) + 2\left(F''\frac{\partial F}{\partial x} - F'\frac{\partial F'}{\partial x}\right) = 0 \tag{8.20}$$

$$W'' - 2F'W + FW' + \frac{H_a}{1+\beta_h^2}(\beta_h F' - W) + 2\left(W'\frac{\partial F}{\partial x} - F'\frac{\partial W}{\partial x}\right) = 0 \tag{8.21}$$

$$\frac{1}{Pr}\left(1 + \frac{4R}{3}\right)T'' + FT' - 4F'T + 2\left(T'\frac{\partial F}{\partial x} - F'\frac{\partial T}{\partial x}\right) = 0 \tag{8.22}$$

$$\frac{1}{Sc}C'' + FC' - K\ e^{-x}CC_1^2 + 2\left(C'\frac{\partial F}{\partial x} - F'\frac{\partial C}{\partial x}\right) = 0 \tag{8.23}$$

$$\frac{\delta}{Sc}C_1'' + FC_1' + K\ e^{-x}CC_1^2 + 2\left(C_1'\frac{\partial F}{\partial x} - F'\frac{\partial C_1}{\partial x}\right) = 0 \tag{8.24}$$

The corresponding non-dimensional conditions on the boundary

$$\left.\begin{array}{c} F'(x,0) = 1 + \lambda F''(x,0),\ F(x,0) + 2\frac{\partial F}{\partial x}(x,0) = S, \quad W(x,0) = 0, \quad T(x,0) = 1, \\ C'(x,0) = K_s\ e^{-x/2}C(x,0), \quad \delta C_1'(x,0) = -K_s\ e^{-x/2}C(x,0), \\ F'(x,y) \to 0,\ W(x,y) \to 0,\ T(x,y) \to 0,\ C(x,y) \to 1, C_1(x,y) \to 0, \quad \text{as} \quad y \to \infty \end{array}\right\} \tag{8.25}$$

It is predicted that the diffusion coefficients of chemical species $\tilde{A}$ and $\tilde{B}$ are of comparable size, which undergo further assumption that diffusion coefficients D_A and D_B are equal, i.e., $\delta = 1$ [16]. This assumption leads to the following relation

$$C(x,y) + C_1(x,y) = 1 \tag{8.26}$$

Thus, Eqs. (8.23) and (8.24) reduce to

$$\frac{1}{Sc}C'' + FC' - K\ e^{-x}C(1-C)^2 + 2\left(C'\frac{\partial F}{\partial x} - F'\frac{\partial C}{\partial x}\right) = 0 \tag{8.27}$$

and the boundary condition in (8.25) reduce to

$$C'(x,0) = K_s e^{-x/2}C(x,0) \text{ and } \quad C(x,\infty) = 1 \tag{8.28}$$

The non-dimensional skin friction in $\tilde{x}-$direction $C_{F\tilde{x}}$, local skin-friction in $\tilde{z}-$direction $C_{F\tilde{z}}$ and the local Nusselt number $Nu_{\tilde{x}}$, are given by

$$\frac{\sqrt{Re_x}}{\sqrt{2x/L}}C_{F\tilde{x}} = F''(x,0),\ \frac{\sqrt{Re_x}}{\sqrt{2x/L}}C_{F\tilde{z}} = W'(x,0) \text{ and } \frac{Nu_x}{\sqrt{x/2L}\sqrt{Re_x}} = -\left(1+\frac{4R}{3}\right)T'(x,0)$$

where $Re_x = \frac{xU_*(x)}{\nu}$ is the local Reynolds number.

8.2.5 Method of Solution

To solve the system of Eqs. (8.20) - (8.22) and (8.27) along with the boundary conditions (8.25) and (8.28), is solved numerically, as explained in case (a) of Chapter-3.

Proceeding in case (a) of Chapter-3, we obtain the following matrix equation

$$\mathbf{A}_{i-1}\mathbf{X}_i = \mathbf{R}_{i-1}, \tag{8.29}$$

In Eq. (8.29), $\mathbf{A}_{i-1}$ is a square matrix of order $(8N+8)$ and $\mathbf{X}_i$ and $\mathbf{R}_{i-1}$ are (8N + 8)×1

column vectors defined by

$$\mathbf{A}_{i-1} = [A_{rs}], \mathbf{R}_{i-1} = [\mathbf{E}_{r,i-1}], r, s = 1, 2, \cdots, 8, \ \mathbf{X}_i = \begin{bmatrix} \mathbf{F}_i \\ \mathbf{W}_i \\ \mathbf{\Theta}_i \\ \mathbf{\Phi}_i \\ \mathbf{G}_i \\ \mathbf{H}_i \\ \mathbf{J}_i \\ \mathbf{K}_i \end{bmatrix} \tag{8.30}$$

where

$$\mathbf{F}_i = [F_i(\xi_0), F_i(\xi_1), F_i(\xi_2), ..., F_i(\xi_{N-1}), F_i(\xi_N)]^T,$$
$$\mathbf{W}_i = [W_i(\xi_0), W_i(\xi_1), W_i(\xi_2), ..., W_i(\xi_{N-1}), W_i(\xi_N)]^T,$$
$$\mathbf{\Theta}_i = [T_i(\xi_0), T_i(\xi_1), T_i(\xi_2), ..., T_i(\xi_{N-1}), T_i(\xi_N)]^T,$$
$$\mathbf{\Phi}_i = [C_i(\xi_0), C_i(\xi_1), C_i(\xi_2), ..., C_i(\xi_{N-1}), C_i(\xi_N)]^T,$$
$$\mathbf{G}_i = [G_i(\xi_0), G_i(\xi_1), G_i(\xi_2), ..., G_i(\xi_{N-1}), G_i(\xi_N)]^T,$$
$$\mathbf{H}_i = [H_i(\xi_0), H_i(\xi_1), H_i(\xi_2), ..., H_i(\xi_{N-1}), H_i(\xi_N)]^T,$$
$$\mathbf{J}_i = [J_i(\xi_0), J_i(\xi_1), J_i(\xi_2), ..., J_i(\xi_{N-1}), J_i(\xi_N)]^T,$$
$$\mathbf{K}_i = [K_i(\xi_0), K_i(\xi_1), K_i(\xi_2), ..., K_i(\xi_{N-1}), K_i(\xi_N)]^T,$$
$$\mathbf{E}_{j,i-1} = [\zeta_{j,i-1}(\xi_0), \zeta_{j,i-1}(\xi_1), \zeta_{j,i-1}(\xi_2), ..., \zeta_{j,i-1}(\xi_{N-1}), \zeta_{j,i-1}(\xi_N)]^T, j = 1, 2, 3, ..., 8$$
$$A_{11} = \mathbf{D}^3 + \chi_{11,i-1}\mathbf{D}^2 + \chi_{12,i-1}\mathbf{D} + \chi_{13,i-1}, \quad A_{12} = -\tfrac{H_a\beta_h}{1+\beta_h^2}\mathbf{I}, \quad A_{13} = 2Ri\mathbf{I},$$
$$A_{14} = \mathbf{0}, \quad A_{15} = \chi_{14,i-1}\mathbf{D} + \chi_{15,i-1}, \quad A_{16} = \mathbf{0}, \quad A_{17} = \mathbf{0}, \quad A_{18} = \mathbf{0},$$
$$A_{21} = \chi_{21,i-1}\mathbf{D} + \chi_{22,i-1}, \quad A_{22} = \mathbf{D}^2 + \chi_{23,i-1}\mathbf{D} + \chi_{24,i-1}, \quad A_{23} = \mathbf{0},$$
$$A_{24} = \mathbf{0}, \quad A_{25} = \chi_{25,i-1}, \quad A_{26} = \chi_{26,i-1}, \quad A_{27} = \mathbf{0}, \quad A_{28} = \mathbf{0}$$
$$A_{31} = \chi_{31,i-1}\mathbf{D} + \chi_{32,i-1}, \quad A_{32} = \mathbf{0}, \quad A_{33} = \tfrac{1}{Pr}\left(1 + \tfrac{4R}{3}\right)\mathbf{D}^2 + \chi_{33,i-1}\mathbf{D} + \chi_{34,i-1},$$
$$A_{34} = \mathbf{0}, \quad A_{35} = \chi_{35,i-1}, \quad A_{36} = \mathbf{0}, \quad A_{37} = \chi_{36,i-1}, \quad A_{38} = \mathbf{0}$$
$$A_{41} = \chi_{41,i-1}\mathbf{D} + \chi_{42,i-1}, \quad A_{42} = \mathbf{0}, \quad A_{43} = \mathbf{0}, \quad A_{44} = \tfrac{1}{Sc}\mathbf{D}^2 + \chi_{43,i-1}\mathbf{D} + \chi_{44,i-1},$$
$$A_{45} = \chi_{45,i-1}, \quad A_{46} = \mathbf{0}, \quad A_{47} = \mathbf{0}, \quad A_{48} = \chi_{46,i-1},$$
$$A_{51} = \chi_{51,i-1}\mathbf{D}^2 + \chi_{52,i-1}\mathbf{D} + \chi_{53,i-1}, \quad A_{52} = \mathbf{0}, \quad A_{53} = \mathbf{0}, \quad A_{54} = \mathbf{0},$$

$$A_{55} = \mathbf{D}^3 + \chi_{54,i-1}\mathbf{D}^2 + \chi_{55,i-1}\mathbf{D} + \chi_{56,i-1}, \quad A_{56} = -\frac{H_a\beta_h}{1+\beta_h^2}\mathbf{I}, \quad A_{57} = 2Ri\mathbf{I}, \quad A_{58} = \mathbf{0},$$
$$A_{61} = \chi_{61,i-1}\mathbf{D} + \chi_{62,i-1}, \quad A_{62} = \chi_{63,i-1}\mathbf{D} + \chi_{64,i-1}, \quad A_{63} = \mathbf{0}, \quad A_{64} = \mathbf{0},$$
$$A_{65} = \chi_{65,i-1}\mathbf{D} + \chi_{66,i-1}, \quad A_{66} = \mathbf{D}^2 + \chi_{67,i-1}\mathbf{D} + \chi_{68,i-1}, \quad A_{67} = \mathbf{0}, \quad A_{68} = \mathbf{0},$$
$$A_{71} = \chi_{71,i-1}\mathbf{D} + \chi_{72,i-1}, \quad A_{72} = \mathbf{0}, \quad A_{73} = \chi_{73,i-1}\mathbf{D} + \chi_{74,i-1}, \quad A_{74} = \mathbf{0},$$
$$A_{75} = \chi_{75,i-1}\mathbf{D} + \chi_{76,i-1}, \quad A_{76} = \mathbf{0}, \quad A_{77} = \frac{1}{Pr}\left(1 + \frac{4R}{3}\right)\mathbf{D}^2 + \chi_{77,i-1}\mathbf{D} + \chi_{78,i-1},$$
$$A_{78} = \mathbf{0}, \quad A_{81} = \chi_{81,i-1}, \quad A_{82} = \mathbf{0}, \quad A_{83} = \mathbf{0}, \quad A_{84} = \chi_{82,i-1}\mathbf{D} + \chi_{83,i-1},$$
$$A_{85} = \chi_{84,i-1}\mathbf{D} + \chi_{85,i-1}, \quad A_{86} = \mathbf{0}, \quad A_{87} = \mathbf{0}, \quad A_{88} = \frac{1}{Sc}\mathbf{D}^2 + \chi_{86,i-1}\mathbf{D} + \chi_{87,i-1},$$

where the coefficients $\chi_{lk,n-1}$ and $\zeta_{l,i-1}$, $(l, k = 1, 2, 3, ..., 8)$ are approximations in terms of F_i, W_i, T_i and C_i, $(i = 1, 2, 3, ..., n-1)$ and their derivatives, $\mathbf{0}$ and $\mathbf{I}$ are null and identity matrices of size (N +1)×(N +1).

After modifying the matrix system (8.29) to incorporate boundary conditions, the solution is obtained as

$$\mathbf{X}_i = \mathbf{A}_{i-1}^{-1}\mathbf{R}_{i-1} \tag{8.31}$$

8.2.6 Results and Discussion

Comparison analysis is presented between the present results and the results obtained by Magyari and Keller [56] as a special case by taking $\lambda = 0$, $S = 0$, $R = 0$, $Ri = 0$, $H_a = 0$ and $x = 0$ and found that they are in good agreement, as presented in Table (8.1). To study the effects of homogeneous-heterogeneous reaction parameters K and Ks, respectively, Hall parameter β_h, slip parameter λ, radiation parameter R, and suction/injection parameter S, computations have been carried out in the cases of $\lambda = 1.0$, $Ri = 0.5$, $\beta_h = 0.5$, $R = 0.5$, $S = 0.5$, $K = 0.5$, $K_s = 1.0$, $H_a = 1.0$ and $x = 0.2$

The variation of tangential velocity for distinct values of β_h, R, S and Ri is exhibited through the Figs. (8.7(a)) - (8.7(d)). An increase in the Hall parameter enhances the tangential velocity as depicted in the Fig. (8.7(a)). It is noticed from the Fig. (8.7(b)) that, an increase in the thermal radiation causes an increase in the velocity. It is seen from the

Table 8.1: *Comparison of* $-F''(0)$ *and* $F(\infty)$ *calculated by the present method for* $\lambda = 0$, $S = 0$, $R = 0$, $Ri = 0$, $H_a = 0$ *and* $x = 0$.

	Magyari and Keller [56]	Present
$-F''(0)$	1.281808	1.28180856
$F(\infty)$	0.905639	0.90564370

Fig. (8.7(c)) that the fluid velocity is less in the presence of fluid suction and more in the presence of injection. An increase in the value of Ri, induces a favorable pressure gradient which, in turn, enhances the fluid velocity in the boundary layer as portrayed in the Fig. (8.7(d)).

Figures (8.8(a)) - (8.8(d)) represents the variations of the transverse velocity for distinct values of β_h, R, S and Ri, respectively. It is noticed from the Fig. (8.8(a)), that there is no secondary flow velocity in the absence of Hall parameter. As the values of β_h increased, the cross flow is generated. An increase in the thermal radiation, the transverse velocity enhances as shown in the Fig. (8.8(b)). Fig. (8.8(c)) exhibits that the transverse velocity decreases with the fluid suction and increases with the injection. It is evident from the Fig. (8.8(d)) that the cross flow, generated due to Hall effect, escalates with an enhancement in the values Ri.

Figures (8.9(a)) - (8.9(d)) are due to the variation of temperature profile for distinct values of β_h, R, S and Ri. An enhancement in the value of β_h, the effective thermal conductivity of the fluid reduces and hence temperature diminishes as shown in the Fig. (8.9(a)). It is seen from the Fig. (8.9(b)) that the temperature escalates with the increasing values of thermal radiation, which in turn, intensifies the thermal boundary layer thickness. Figure (8.9(c)) shows that the fluid temperature decreases with the fluid suction and escalates with the injection. The temperature reduces with rise in Ri as shown in the Fig. (8.9(d)).

The variation of concentration profile for distinct values of K_s, K, R, Ri, β_h and S is portrayed in the Figs. (8.10(a)) - (8.10(f)). From Fig. (8.10(a)), it is seen that the concentration reduces as the strength of heterogeneous reaction enhances and decreases by strengthening the homogeneous reaction as shown in the Fig. (8.10(b)). This is due

to the fact that, reaction rates dominate diffusion coefficients. This is in tune with the general physical behavior of homogeneous and heterogeneous reactions. As the values of radiation, mixed convection and Hall parameter escalates, concentration boundary layer enhances and hence, concentration rises as shown in the Figs. (8.10(c)), (8.10(d)) and (8.10(e)), respectively. Moreover, it is observed that the concentration less influenced with Hall effect. Figure (8.10(f)) exhibits that concentration of the fluid enhances with the fluid suction and diminishes with the injection.

The influence of β_h, R, Ri and S on the rate of heat transfer against non-similar variable x is explored in the Figures (8.11(a)) - (8.11(d)). It is observed from the Fig. (8.11(a)) that the rate of heat transfer reduces with an increase in the value of β_h. The rate of heat transfer escalates with an increase in the value of thermal radiation parameter R as depicted in the Fig. (8.11(b)). Further, in the absence of thermal radiation, minimum rate of heat transfer occurred and as strengthening the radiation, the rate of heat transfer escalated as shown in the Fig. (8.11(b)). The effect of Ri on the rate of heat transfer is presented in the Fig. (8.11(c)). It is evident from the figure that the rate of heat transfer enhances with a raise in Ri. Figure (8.11(d)) shows that the rate of heat transfer enhances with a raise in the fluid suction and diminishes with the injection.

Figures (8.12(a)) - (8.12(f)) depict the behaviour of the rate of mass transfer for different values of K_s, K, R, Ri, β_h and S against non-similar variable x. It is known that increase in the value of K_s and K corresponds to increase in the strength of heterogeneous and homogeneous reactions. Figures (8.12(a)) and (8.12(b)) depicts that, the mass transfer rate decreases as the strength of heterogeneous and homogeneous reactions escalates. It is noticed that, the effect of heterogeneous reaction is more than that of homogeneous reaction. However, it is witnessed that both the concentration and mass transfer rate influenced uniformly by the strength of heterogeneous and homogeneous reactions. An increase in the values of the R, Ri, β_h and S, the mass transfer rate escalates as portrayed in the Figs. (8.12(c)) - (8.12(f)). Further, it is depicted that the rate of mass transfer enhances gradually as $x \to 1$.

The behaviour of $F''(x,0)$ and $W'(x,0)$ for different values of λ, β_h, R, Ri, K_s and K

are tabulated in the Table (8.2). It is evident from the table that the $F''(x,0)$ is increasing and $W'(x,0)$ is reducing with the slipperiness. In the presence of Hall parameter both the skin-frictions are increasing. It is also observed that the transverse velocity vanishes when $\beta_h = 0$ and hence in $\tilde{z}-$direction there is no skin-friction. Table (8.2) illustrates that, $F''(x,0)$ and $W'(x,0)$ are enhancing with a rise in the thermal radiation. The positive values of Ri increases both the skin-frictions. In addition to this, $F''(x,0)$ in $\tilde{x}-$direction is greatly increased with positive values of Ri. At the end of the table the influence of strength of homogeneous-heterogeneous reactions on $F''(x,0)$ and $W'(x,0)$ is presented. It is noticed from the table that, there is no effect of K_s and K on both the skin-friction.

Table 8.2: *Variation of skin friction in $\tilde{x}$- and $\tilde{z}$-directions for varying values of slip parameter λ, Hall parameter β_h, radiation parameter R, mixed convection parameter Ri, heterogeneous reaction parameter Ks, and homogeneous reaction parameeter K.*

λ	β_h	R	Ri	K_s	K	$F''(x,0)$	$W'(x,0)$
0.0	0.5	0.5	0.5	1.0	0.5	-1.452122	0.171179
0.5	0.5	0.5	0.5	1.0	0.5	-0.670978	0.138906
1.0	0.5	0.5	0.5	1.0	0.5	-0.442109	0.127885
2.0	0.5	0.5	0.5	1.0	0.5	-0.264181	0.118659
1.0	0.0	0.5	0.5	1.0	0.5	-0.455100	0.000000
1.0	0.5	0.5	0.5	1.0	0.5	-0.442109	0.127885
1.0	1.0	0.5	0.5	1.0	0.5	-0.419032	0.182813
1.0	1.5	0.5	0.5	1.0	0.5	-0.400926	0.187412
1.0	0.5	0.0	0.5	1.0	0.5	-0.464936	0.114359
1.0	0.5	0.5	0.5	1.0	0.5	-0.442109	0.127885
1.0	0.5	1.0	0.5	1.0	0.5	-0.428240	0.136786
1.0	0.5	2.0	0.5	1.0	0.5	-0.411402	0.148090
1.0	0.5	0.5	0.0	1.0	0.5	-0.598770	0.070074
1.0	0.5	0.5	0.1	1.0	0.5	-0.559650	0.088126
1.0	0.5	0.5	0.5	1.0	0.5	-0.442110	0.127885
1.0	0.5	0.5	1.0	1.0	0.5	-0.327710	0.157594
1.0	0.5	0.5	0.5	0.1	0.5	-0.442086	0.127950
1.0	0.5	0.5	0.5	0.5	0.5	-0.442086	0.127950
1.0	0.5	0.5	0.5	1.0	0.5	-0.442086	0.127950
1.0	0.5	0.5	0.5	2.0	0.5	-0.442086	0.127950
1.0	0.5	0.5	0.5	1.0	1.0	-0.444640	0.127212
1.0	0.5	0.5	0.5	1.0	2.0	-0.444640	0.127212
1.0	0.5	0.5	0.5	1.0	3.0	-0.444640	0.127212
1.0	0.5	0.5	0.5	1.0	4.0	-0.444640	0.127212

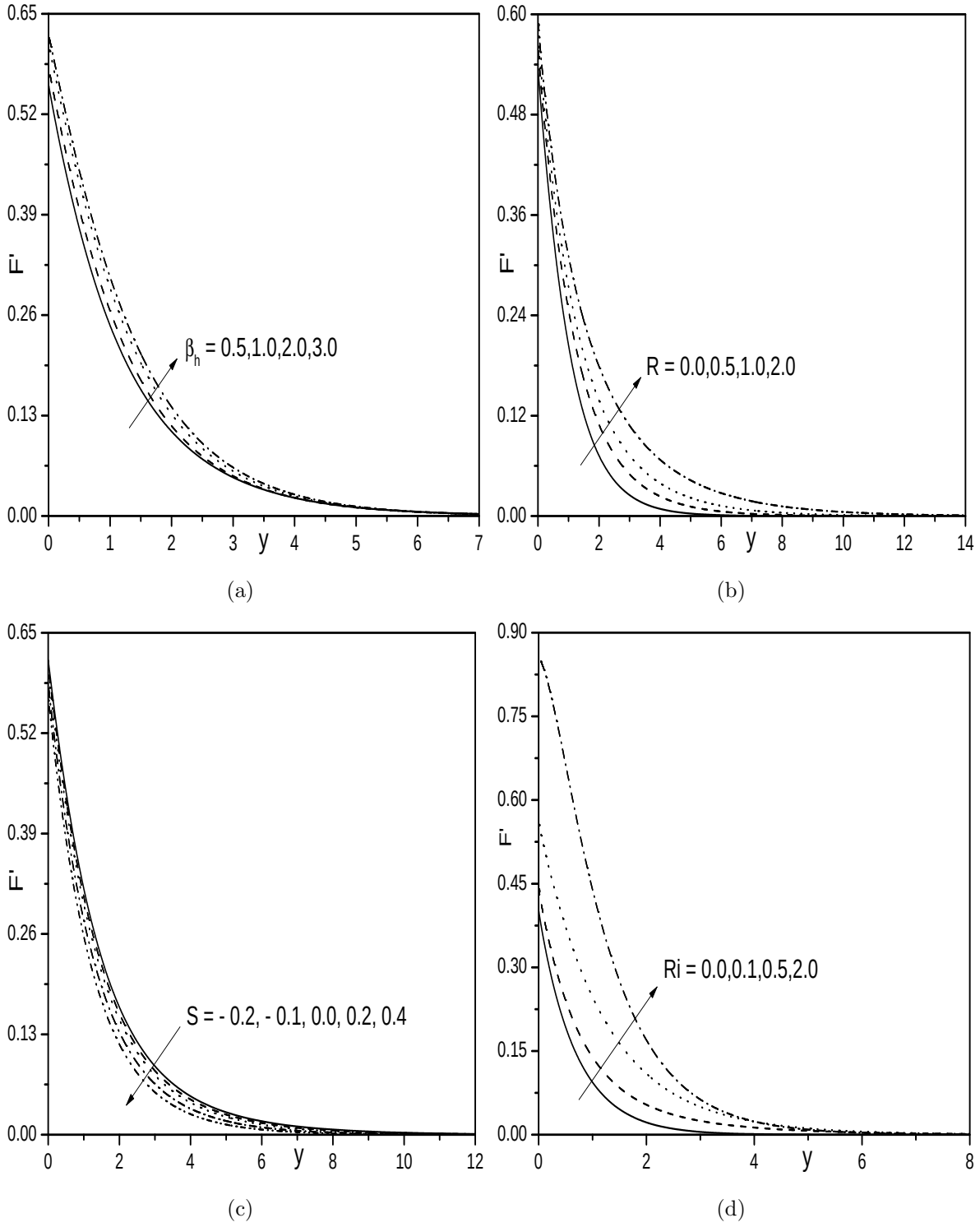

Figure 8.7: *"Effect (a)β_h, (b)R, (c)S, and (d)Ri on tangential velocity".*

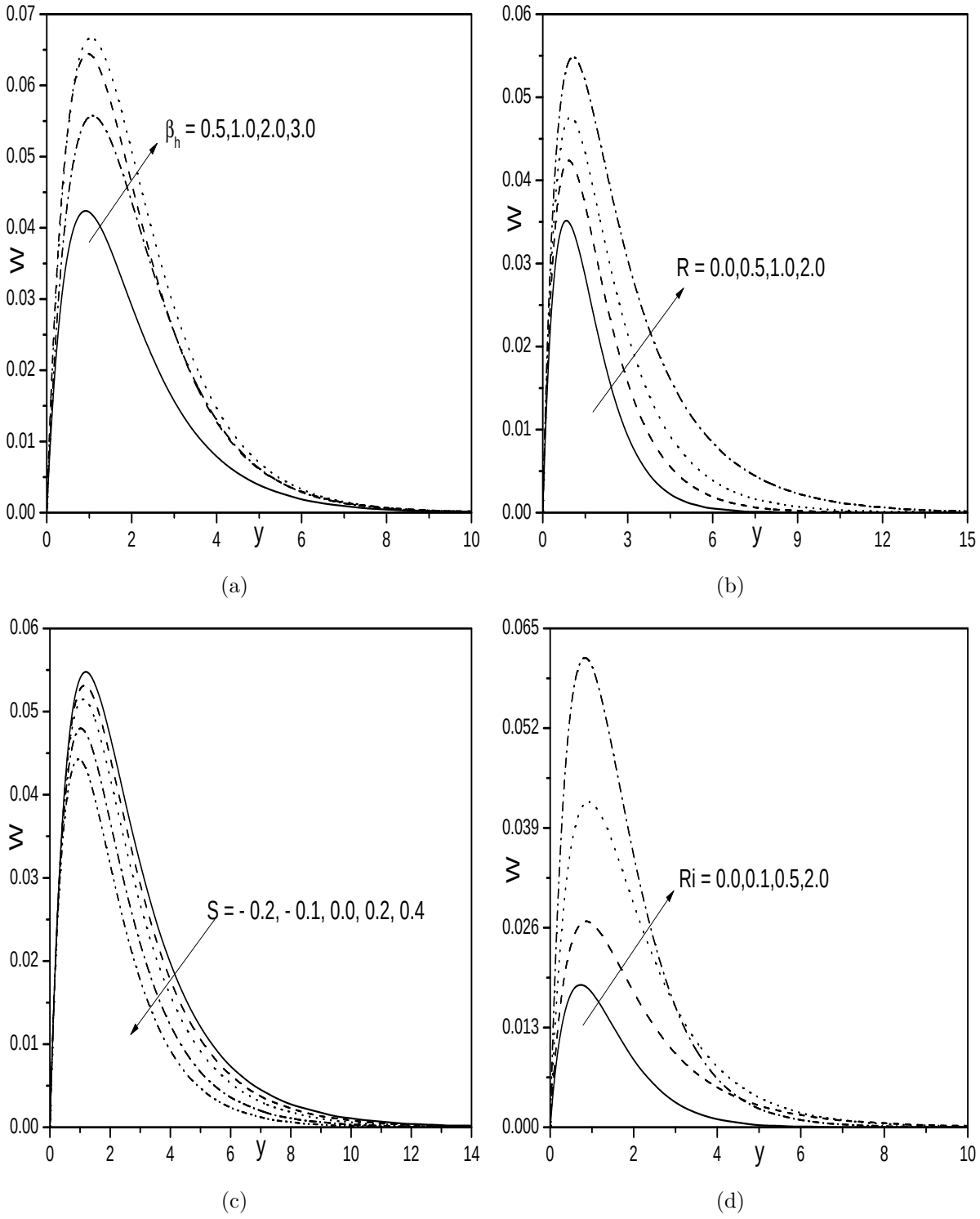

Figure 8.8: *"Effect (a)β_h, (b)R, (c)S, and (d)Ri on transverse velocity."*

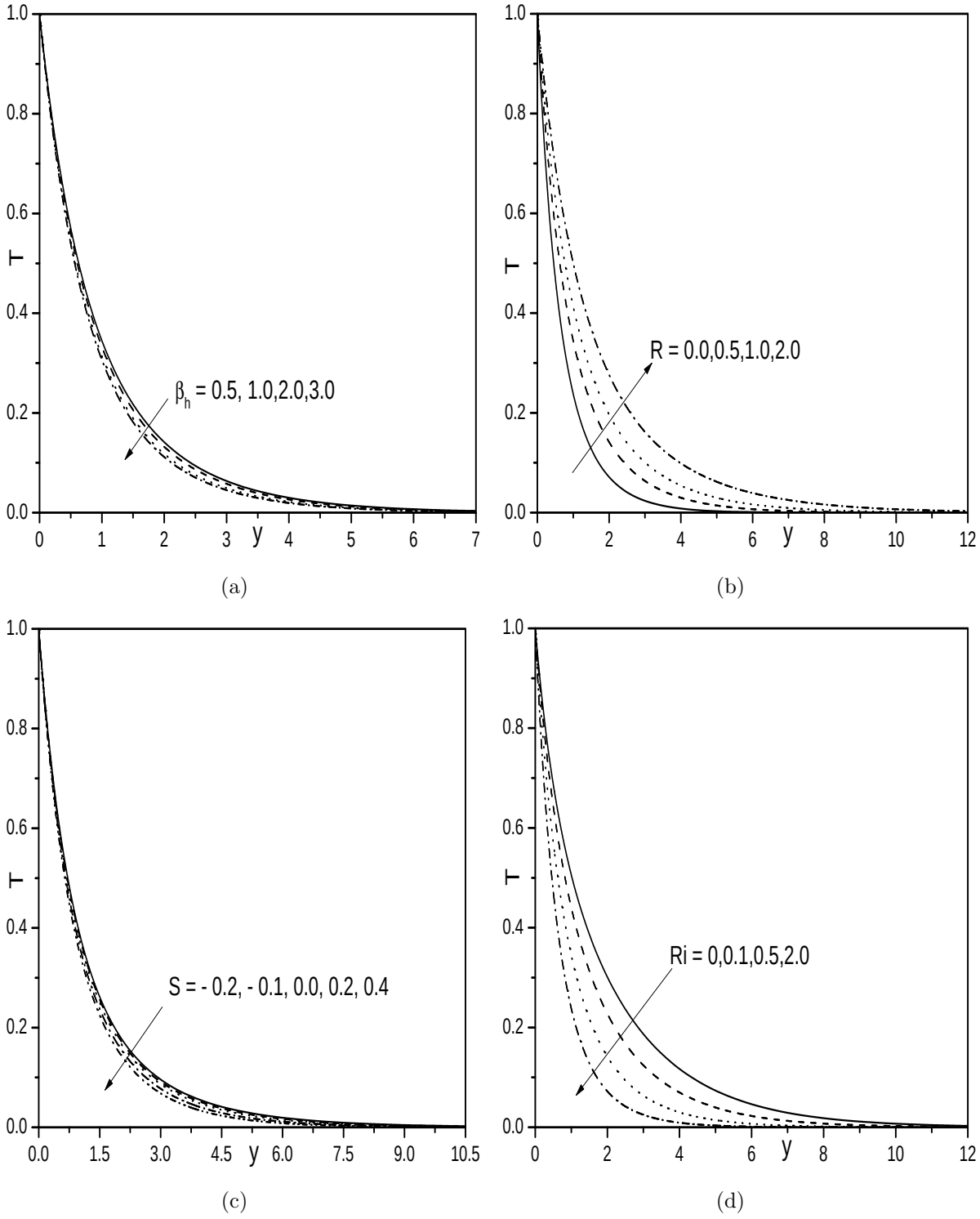

Figure 8.9: *"Effect (a)β_h, (b)R, (c)S, and (d)Ri on temperature profile".*

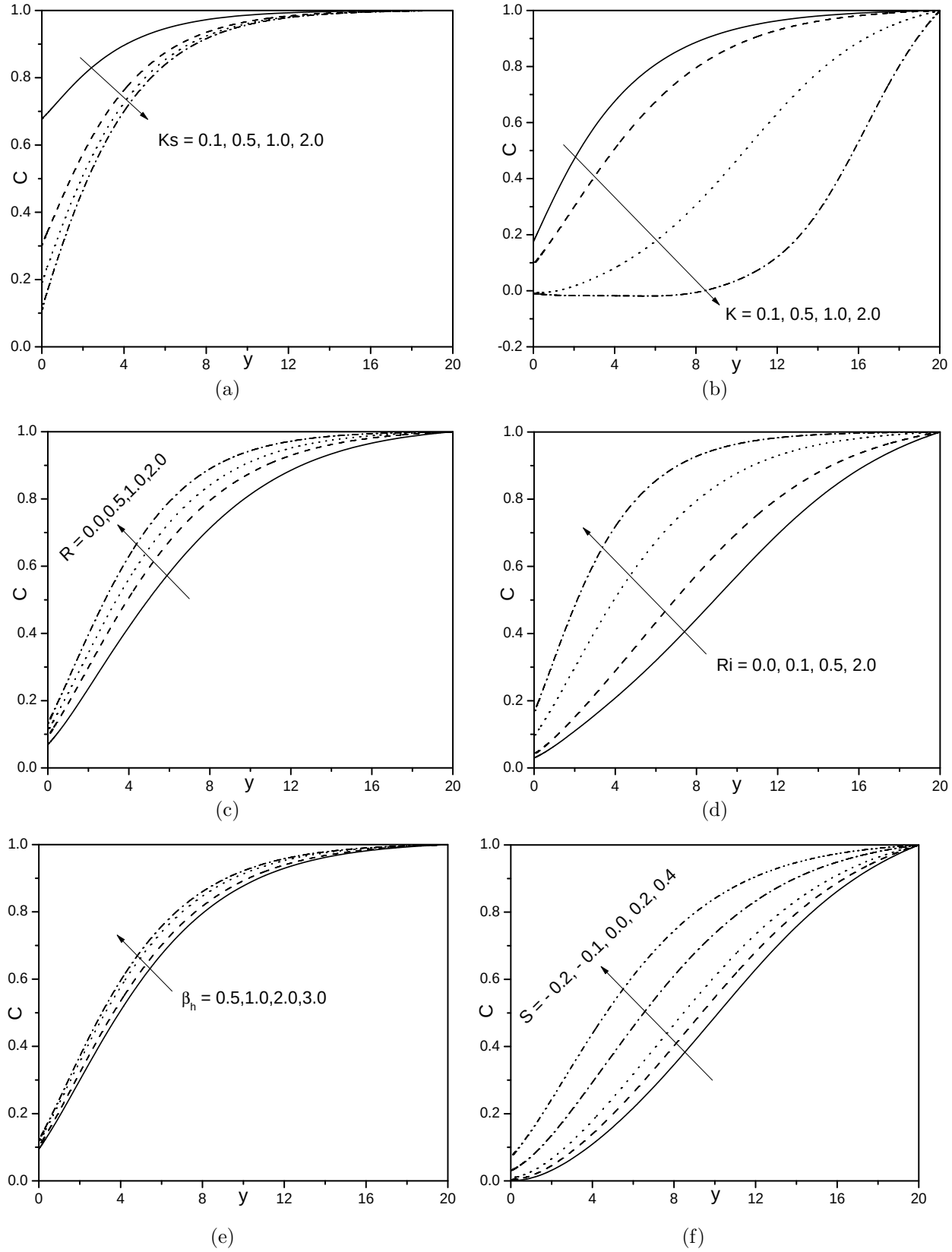

Figure 8.10: *"Effect (a)Ks, (b)K, (c)R, (d)Ri, (e)β_h and (f)S on C"*

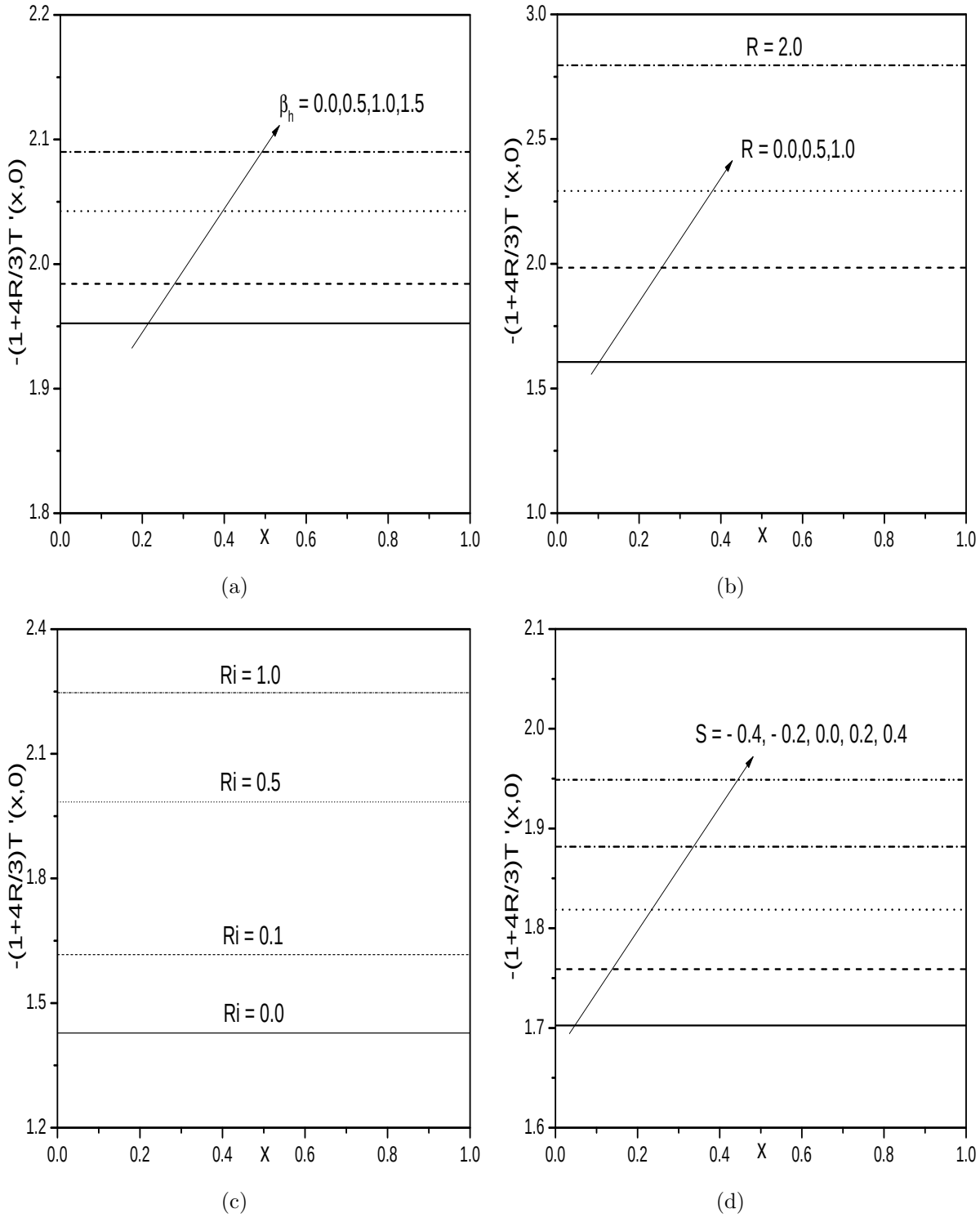

Figure 8.11: *"Effect (a)β_h, (b)R, (c)Ri, and (d)S on* $-\left(1+\frac{4R}{3}\right)T'(x,0)$*"*.

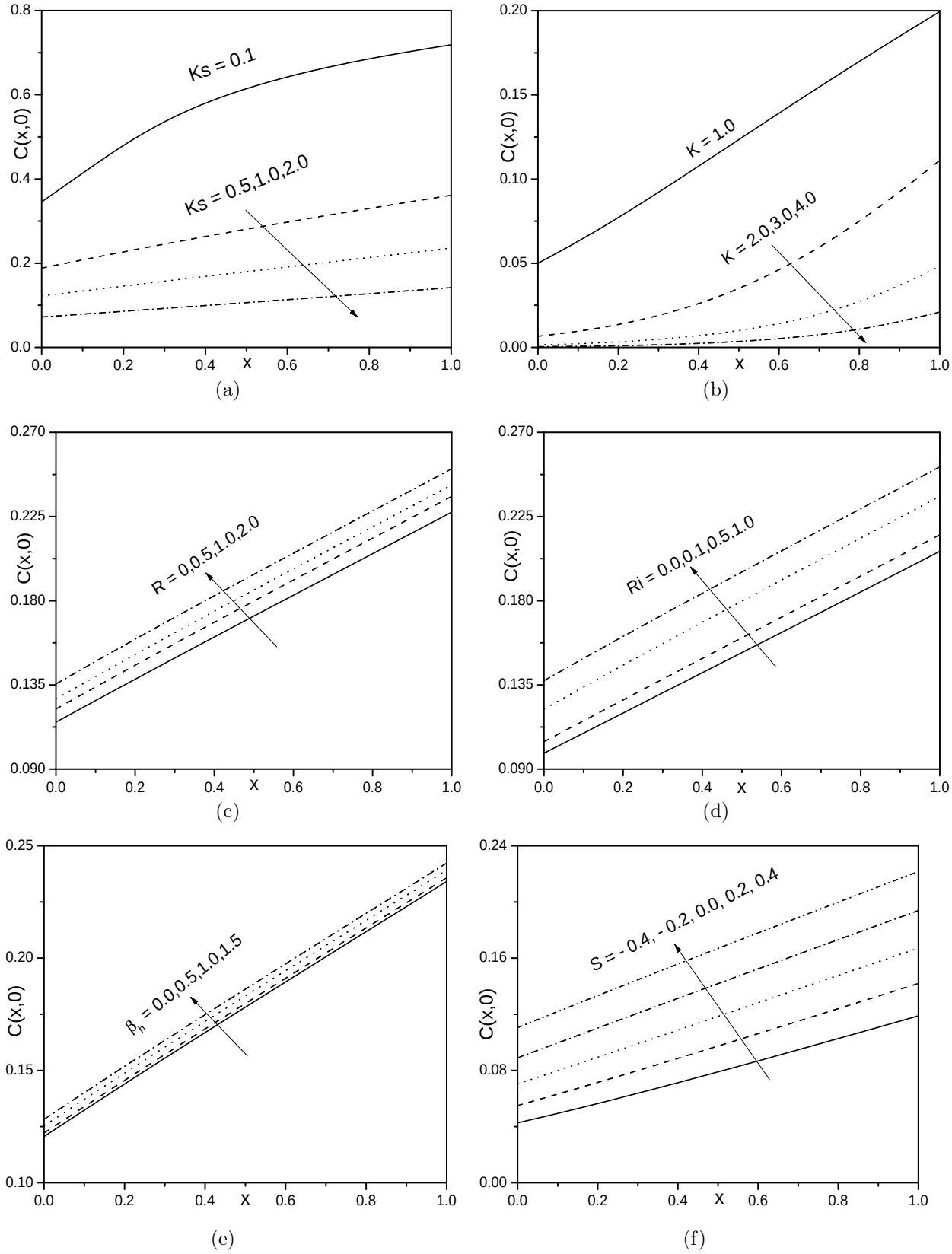

Figure 8.12: *"Effect (a)Ks, (b)K, (c)R, (d)Ri, (e)β_h and (f)S on $C(x,0)$"*

8.3 Conclusions

Numerical investigation of influence of homogeneous-heterogeneous reactions on the laminar slip flow, heat and mass transfer of a incompressible viscous fluid over a porous sheet stretching exponentially is analyzed in this chapter. Based on the analysis carried out the main conclusions are drawn:

In case (a) and (b), the velocity decreases with the fluid suction and the skin-friction increases with the slippage. In case (a), the temperature of the fluid increases with an increase in the Biot number and decreases with an increase in Hall parameter for case (b). In both the cases, the temperature increases with the thermal radiation. In both the cases, the concentration decreases with an increase in the strengths of homogeneous-heterogeneous reactions and increases with the fluid suction. The rate of heat transfer, in case (a), increases with an increase in the Biot number and increases with the Hall parameter in case (b). In both the cases, the rate of heat transfer increases with the thermal radiation and the fluid suction. In both the cases, the mass transfer rate decreases with an increase in the strengths of homogeneous-heterogeneous reactions .

Chapter 9

Summary and Conclusions

In this thesis, a steady, laminar viscous fluid flow over an exponentially stretching sheet is investigated. On the surface of the sheet two different types physical conditions were considered. The sheet is (i) subjected to thermal convective boundary condition and (ii) maintained at uniform wall temperature with Hall effect. The effect of various parameters i.e., convective heat transfer coefficient (Biot number), Hall parameter, thermal radiation, chemical reaction, Joule heating, cross-diffusion effects, variable viscosity, variable thermal conductivity, heat source or sink, thermophoresis, viscous dissipation, double dispersion effects, homogeneous and heterogeneous reactions on the flow characteristics such as velocity, temperature and concentration distributions along with the local heat and mass transfer coefficients were considered.

The governing equations of the flow in the Chapters 2, 4, 5 and case (b) of Chapter 3 and 6 are transformed into a system of nonlinear ordinary differential equations using similarity transformations. These non-linear ordinary differential equations and their associated boundary conditions are linearized by using successive linearization method. In the case (a) of Chapter 3 and 6, Chapters 7 and 8, the governing equations of the flow are reduced to a system of nonlinear partial differential equations using non-dimensional variables. A local similarity and non-similarity method is used to transform the governing partial differential equations into ordinary differential equations and then linearized by using Successive

linearization method. In all the chapters, the linearized equations together with corresponding boundary conditions were solved using Chebyshev spectral collocation method. The important observations made from this study are listed below.

- In the presence of the Hall parameter, both the velocities, the skin-friction and the rate of heat and mass transfer increase and the temperature and the concentration decrease. Whereas the temperature and the rate of heat transfer increase with the increase in the convective heat transfer coefficient.
- In the presence of the convective heat transfer coefficient, the rate of heat transfer and temperature increases with an increase in the radiation parameter. As the chemical reaction parameter increases, the concentration decreases and the rate of mass transfer increases. Whereas in the presence of the Hall effect, both the velocities, the temperature, the skin-friction, the rate of heat and mass transfers increase with an increase in the radiation parameter and both the velocities, the concentration, the skin-friction and the rate of heat transfer reduce with the increase in the chemical reaction parameter.
- An increase in the Joule heating parameter, the rate of heat transfer increases in both the cases. The temperature and concentration, increase and the rate of heat and mass transfers decrease with the increase in the magnetic parameter.
- The presence of the Hall effect increases both the velocities and the skin-friction with an increase in the Soret and Dufour numbers. In both the cases, the temperature and the rate of mass transfer decrease, the concentration and the rate of heat transfer increase with the increase in the Soret number. Whereas exactly an opposite trend is witnessed with the increase in the Dufour number.
- The rate of heat transfer increases with the increase in the viscosity parameter and decreases with an increase in the thermal conductivity and the heat source parameters. But, an opposite trend is observed in the rate of mass transfer. Further, in the presence of Hall effect the rate of heat and mass transfers decrease with the increase in slip parameter. In the absence of slip parameter, an opposite trend is observed with the increase in convective heat transfer coefficient.

- As the viscous dissipation parameter increases, the temperature increases and the rate of heat transfer decreases. Increase in the value of thermophoresis parameter, the concentration decreases and the rate of mass transfer increases.

- An increase in the thermal dispersion parameter increases the temperature and decreases the rate of heat transfer. On the other hand, the concentration increases and the rate of mass transfer decrease with an increase in the solutal dispersion parameter. But, in the presence of the Hall effect, the rate of heat transfer increases with an increase in the value of solutal dispersion parameter and the rate of mass transfer increases with an increase in the thermal dispersion parameter.

- The species concentration and mass transfer rate decrease with the increase in the strength of homogeneous and heterogeneous reaction parameter. The effect of homogeneous reaction is greater on species concentration as compared with heterogeneous reaction.

- The velocity, temperature and concentration decreases and the rate of heat and mass transfers increase with the fluid suction at the boundary of the stretching surface. While, in the presence of Hall and cross-diffusion effects, a dual trend is observed on the rate of mass transfer. The velocity, rate of heat and mass transfers reduce and the temperature and concentration increase with the fluid slippage at the boundary. But, in the presence of thermophoresis and convective heat transfer coefficient, the rate of heat transfer increases with the fluid slippage at the wall.

The work presented in the thesis can be extended to analyze the effect of double stratification, nonlinear convection, Arrhenius activation energy, binary chemical reaction, etc. Further, this work can be extended by studying the analysis in various non-Newtonian fluids like Couple stress fluids, Casson fluids, Jeffrey fluids, Power-law fluids and the geometry can be changed to oscillatory, inclined exponentially stretching sheet. This work can also be extended to porous media. Further, this work can be extended to study the heat and mass transfer analysis on free convection.

In the recent past, the study of stability analysis has attracted the curiosity of many researchers. Thus, the work presented in the thesis can be extended to study the stability and convergence analysis.

Bibliography

[1] Z. Abbas, M. Sheikh, and I. Pop. Stagnation-point flow of a hydromagnetic viscous fluid over stretching/shrinking sheet with generalized slip condition in the presence of homogeneousheterogeneous reactions. *Journal of the Taiwan Institute of Chemical Engineers*, 55:69–75, 2015.

[2] M.S. Abel, P.G. Siddheshwar, and M. Narayana. Numerical solution of the momentum and heat transfer equations for a hydromagnetic flow due to a stretching sheet of a non-uniform property micropolar liquid. *Applied Mathematics and Computation*, 217:5895–5909, 2011.

[3] A. Adeniyan and J.A. Adigun. Similarity solution of hydromagnetic flow and heat transfer past an exponentially stretching permeable vertical sheet with viscous dissipation, joulean and viscous heating effects. *ANNALS of Faculty Engineering Hunedoara International Journal of Engineering*, 14(2):113–120, 2016.

[4] R. Ahmad and M. Mustafa. Model and comparative study for rotating flow of nanofluids due to convectively heated exponentially stretching sheet. *Journal of Molecular Liquids*, 220:635–641, 2016.

[5] M.E. Ali. Heat transfer characteristics of a continuous stretching surface. *Wrme-und Stoffbertragung*, 29(4):227–234, 1994.

[6] I.L. Animasaun, E.A. Adebile, and A.I. Fagbade. Casson fluid flow with variable thermo-physical property along exponentially stretching sheet with suction and ex-

ponentially decaying internal heat generation using the homotopy analysis method. *Journal of the Nigerian Mathematical Society*, 35:1–17, 2016.

[7] F.G. Awad, P. Sibanda, and P.V.S.N. Murthy. A note on double dispersion effects in a nanofluid flow in a non-darcy porous medium. *Journal of Heat Transfer*, 137(104501):1–5, 2015.

[8] M.A.E. Aziz. Flow and heat transfer over an unsteady stretching surface with hall effect. *Meccanica*, 45(1):97–109, 2010.

[9] D.H. Babu and P.V.S. Narayana. Joule heating effects on mhd mixed convection of a jeffrey fluid over a stretching sheet with power law heat flux: A numerical study. *International Journal of Heat and Mass Transfer*, 412:185–193, 2016.

[10] N. Bachok, A. Ishak, and I. Pop. On the stagnation-point flow towards a stretching sheet with homogeneous-heterogeneous reactions effects. *Commun Nonlinear Sci Numer Simulat*, 16:4296–4302, 2011.

[11] B. Bidin and R. Nazar. Numerical solution of boundary layer flow over an exponentially stretching sheet with thermal radiatioin. *European journal of scientific research*, 33(4):710–717, 2009.

[12] C. Canuto, M.Y. Hussaini, A. Quarteroni, and T.A. Zang. Spectral methods-fundamentals in single domains. *Journal of Applied Mathematics and Mechanics*, 87(1), 2007.

[13] T.C. Chaim. Heat transfer with variable thermal conductivity in a stagnation-point flow towards a stretching sheet. *Int. Commun. Heat Mass Transfer*, 23(2):239–248, 1996.

[14] M.A. Chaudhary and J.H. Merkin. A simple isothermal model for homogeneous-heterogeneous reactions in boundary-layer flow. i- equal diffusivities. *Fluid Dynamics Research*, 16(6):311–333, 1995.

[15] M.A. Chaudhary and J.H. Merkin. A simple isothermal model for homogeneous-heterogeneous reactions in boundary-layer flow. ii- different diffusivities for reactant and autocatalyst. *Fluid Dynamics Research*, 16(6):335–359, 1995.

[16] M.A. Chaudhary and J.H. Merkin. Homogeneous-heterogeneous reactions in boundary-layer flow: Effects of loss of reactant. *Mathematical and computer modelling*, 24(3):21–28, 1996.

[17] S. Chaudhary, S. Singh, and S. Chaudhary. Thermal radiatioin effects on mhd boundary layer flow over an exponentially stretching surface. *Applied Mathematics*, 6(2):295–303, 2015.

[18] L.J. Crane. Flow past a stretching plate. *Journal of Applied Mathematics and Physics*, 21(4):645–647, 1970.

[19] Y.S. Daniel. Hydromagnetic nanofluid flow in the presence of radiation and heat generation/absorption past an exponential stretching sheet with slip boundary conditions using ham. *Journal of Aeronautics & Aerospace Engineering*, 4(152):1–8, 2015.

[20] L. Debnath, S.C. Ray, and A.K. Chatterjee. Effects of hall currents on unsteady hydromagnetic flow past a porous plate in a rotating fluid system. *Journal of Applied Mathematics and Mechanics*, 59(9):469–471, 1979.

[21] W.S. Don and A. Solomonoff. Accuracy and speed in computing the chebyshev collocation derivative. *SIAM J. Sci. Comput.*, 16:1253–1268, 1995.

[22] E. R. G. Eckert and R. M. Drake. *Analysis of Heat and Mass Transfer*. McGraw Hill, New York, 1972.

[23] M.R. Eid. Chemical reaction effect on mhd boundary-layer flow of two-phase nanofluid model over an exponentially stretching sheet with a heat generation. *Journal of Molecular Liquids*, 220:718–725, 2016.

[24] M.A El-Aziz. Viscous dissipation effect on mixed convection flow of a micropolar fluid over an exponentially stretching sheet. *Canadian Journal of Physics*, 87(4):359–368, 2009.

[25] E.M.A. Elbashbeshy. Heat transfer over an exponentially stretching continuous surface with suction. *Archives of Mechanics*, 53(6):643–651, 2001.

[26] E.M.A Eldahad and M.A.E. Aziz. Hall and ion-slip effects on mhd free convective heat generating flow past a semi-infinite vertical flat plate. *Physica Scripta*, 61(3):344–348, 2000.

[27] E.M.A. Eldahad, M.A.E. Aziz, A.M. Salem, and K.K. Jaber. Hall current effect on mhd mixed convection flow from an inclined continuously stretching surface with blowing/suction and internal heat generation/absorption. *Applied Mathematical Modelling*, 31(9):1829–1846, 2007.

[28] L.E. Erickson, L.T. Fan, and V.G. Fox. Heat and mass transfer on a moving continuous flat plate with suction or injection. *Industrial & Engineering Chemistry Fundamentals*, 5(1):19–25, 1966.

[29] E.G. Fisher. *Extrusion of Plastics*, volume III. Newnes-Butterworld, London, 1976.

[30] B. Gebhart. Effect of viscous dissipation in natural convection. *Journal of Fluid Mechanics*, 14:225–235, 1962.

[31] P. Goldsmith and F.G. May. Diffusiophoresis and thermophoresis in water vapour systems. *Aerosol science, Academic Press*, 39:163–194, 1966.

[32] S. Goldstein. *Modern Developments in Fluid Dynamics*, volume II. Oxford University Press(U.K.), England, 1965.

[33] R.M. Griffith. Velocity, temperature and concentration distributions during fiber spinning. *Industrial & Engineering Chemistry Fundamentals*, 3(3):245–250, 1964.

[34] L.J. Grubka and K.M. Bobba. Heat transfer characteristics of a continuous stretching surface with variable temperature. *Journal of Heat Transfer*, 107(1):248–250, 1985.

[35] A.S. Gupta. Steady and transient free convection of an electrically conducting fluid from a vertical plate in the presence of a magnetic field. *Applied Scientific Research*, 9(1):319–333, 1960.

[36] A.S. Gupta. Hydromagnetic flow past a porous flat plate with hall effects. *Acta Mechanica*, 22(3-4):281–287, 1975.

[37] P.S. Gupta and A.S. Gupta. Heat and mass transfer on a stretching sheet with suction or blowing. *The Canadian Journal of Cheinical Engineering*, 55(6):744–746, 1977.

[38] M.A.A. Hamad, Md.J. Uddin, and A.I.Md. Ismail. Investigation of combined heat and mass transfer by lie group analysis with variable diffusivity taking into account hydrodynamic slip and thermal convective boundary conditions. *International Journal of Heat and Mass Transfer*, 55:1355–1362, 2012.

[39] T. Hayat, G. Bashir, M. Waqas, and A. Alsaedi. Mhd flow of jeffrey liquid due to a nonlinear radially stretched sheet in presence of newtonian heating. *Results in Physics*, 6:817–823, 2016.

[40] T. Hayat, M. Imtiaz, and A. Alsaed. Unsteady flow of nanofluid with double stratification and magnetohydrodynamics. *International Journal of Heat and Mass Transfer*, 92:100–109, 2016.

[41] G.C. Hazarika and K. Goswami. Effects of variable viscosity and thermal conductivity on mhd flow over an exponentially stretching sheet. *International Journal of Modern Sciences and Engineering Technology*, 2(9):15–22, 2015.

[42] K.L. Hsiao. Micropolar nanofluid flow with mhd and viscous dissipation effects towards a stretching sheet with multimedia feature. *International Journal of Heat and Mass Transfer*, 112:983–990, 2017.

[43] T. Hussain, S.A. Shehzad, T. Hayat, A. Alsaedi, F. Al-Solamy, and M. Ramzan. Radiative hydromagnetic flow of jeffrey nanofluid by an exponentially stretching sheet. *Plus One*, 9(8):e103719, 2014.

[44] R.N. Jat and C. Gopi. Mhd flow and heat transfer over an exponentially stretching sheet with viscous dissipation and radiation effects. *Applied Mathematical Sciences*, 7(4):167–180, 2013.

[45] P.K. Kameswaran, M. Narayana, P. Sibanda, and G. Makanda. On radiation effects on hydromagnetic newtonian liquid flow due to an exponential stretching sheet. *Boundary Value Problems*, 2012(1):105, 2012.

[46] P.K. Kameswaran, S. Shaw, P. Sibanda, and P.V.S.N. Murthy. Homogeneousheterogeneous reactions in a nanofluid flow due to a porous stretching sheet. *International Journal of Heat and Mass Transfer*, 57:465–472, 2013.

[47] M. Katagiri. The effect of hall currents on the magnetohydrodynamic boundary layer flow past a semi-infinite flat plate. *Journal of the Physical Society of Japan*, 27(4):1051–1059, 1969.

[48] J.A. Khan, M. Mustafa, T. Hayat, and A. Alsaedi. Numerical study on three-dimensional flow of nanofluid past a convectively heated exponentially stretching sheet. *Canadian Journal of Physics*, 93(10):1131–1137, 2015.

[49] A.A. Khidir and P. Sibanda. Cross-diffusion, viscous dissipation and radiation effects on an exponentially stretching surface in porous media. *Mass Transfer-Advances in Sustainable Energy and Environment Oriented Numerical Modeling. InTech*, pages 125–143, 2013.

[50] V. Kumaran and G. Ramanaiah. A note on the flow over a stretching sheet. *Acta Mechanica*, 116(1-4):229–233, 1996.

[51] F.C. Lai and F.A. Kulacki. The effect of variable viscosity on convective heat transfer along a vertical surface in a saturated porous medium. *International Journal of Heat and Mass Transfer*, 33:1028–1031, 1991.

[52] A.I. Lare. Casson fluid flow of variable viscocity and thermal conductivity along exponentially stretching sheet embedded in a thermally stratified medium with exponentially heat generation. *Journal of heat and mass transfer research*, 2(2):63–78, 2015.

[53] T.F. Lin, K.H. Hawks, and W. Leidenfrost. Analysis of viscous dissipation effect on thermal entrance heat transfer in laminar pipe flows with convective boundary conditions. *Wrme-und stoffbertragung*, 17(2):97–105, 1983.

[54] P. Loganthan and C. Vimala. Mhd flow of nanofluids over an exponentially stretching sheet embedded in a stratified medium with suction and radiation effects. *Journal of Applied Fluid Mechanics*, 8(1):85–93, 2015.

[55] F. Mabood, W.A. Khan, and A.I.Md. Ismail. Mhd flow over exponential radiating stretching sheet using homotopy analysis method. *Journal of King Saud University Engineering Sciences*, 29:68–74, 2017.

[56] E. Magyari and B. Keller. Heat and mass transfer in the boundary layers on an exponentially stretching continuous surface. *Journal of Physics D: Applied Physics*, 32(5):577–585, 1999.

[57] B. Mahanthesh, B.J. Gireesha, and R.S.R. Gorla. Unsteady three-dimensional mhd flow of a nano eyring-powell fluid past a convectively heated stretching sheet in the presence of thermal radiation, viscous dissipation and joule heating. *Journal of the Association of Arab Universities for Basic and Applied Sciences*, 23:75–84, 2017.

[58] M.A.A. Mahmoud. Variable fluid properties effects on hydromagnetic fluid flow over an exponentially stretching sheet. *Open Science Journal of Mathematics and Application*, 3(2):26–33, 2015.

[59] Z.G. Makukula, S.S. Motsa, and P. Sibanda. On a new solution for the viscoelastic squeezing flow between two parallel plates. *Journal of Advanced Research in Applied Mathematics*, 2(4):31–38, 2010.

[60] Z.G. Makukula, P. Sibanda, and S.S. Motsa. A novel numerical technique for two dimensional laminar flow between two moving porous walls. *Mathematical problems in Engineering*, 2010:1–15, 2010.

[61] S. Mansur, A. Ishak, and I. Pop. Mhd homogeneous-heterogeneous reactions in a nanofluid due to a permeable shrinking surface. *Journal of Applied Fluid Mechanics*, 9(3):1073–1079, 2016.

[62] A. Megahed, S.R. Komy, and A. Afify. Similarity analysis in magnetohydrodynamics: Hall effects on free convection flow and mass transfer past a semi-infinite vertical flat plate. *International Journal of Non-Linear Mechanics*, 38(4):513–520, 2003.

[63] A.M. Megahed. Effect of slip velocity on casson thin film flow and heat transfer due to unsteady stretching sheet in presence of variable heat flux and viscous dissipation. *Applied Mathematics and Mechanics*, 36(10):1273–1284, 2015.

[64] A.M. Megahed. Flow and heat transfer of powell-eyring fluid due to an exponential stretching sheet with heat flux and variable thermal conductivity. *Journal for Nature Research B*, 70(3):163–169, 2015.

[65] J.H. Merkin. Natural-convection boundary-layer flow on a vertical surface with newtonian heating. *International Journal of Heat and Fluid Flow*, 15(5):392–398, 1994.

[66] A.F. Mills, X. Hang, and F. Ayazi. The effect of wall suction and thermophoresis on aerosol-particle deposition from a laminar boundary layer on a flat plate. *International Journal of Heat and Mass Transfer*, 27(7):1110–1113, 1984.

[67] W.J. Minkowycz and E.M. Sparrow. Local non-similar solution for natural convection on a vertical cylinder. *Journal of Heat Transfer*, 96(2):178–183, 1974.

[68] S.S. Motsa and S. Shateyi. Successive linearisation solution of free convection non-darcy flow with heat and mass transfer. *Advanced topics in mass transfer*, 19:425–438, 2006.

[69] S.S. Motsa and P. Sibanda. A new algorithm for solving singular ivps of lane-emden type. *Proceedings of the 4^{th} international conference on Applied mathematics, simulation and modelling*, NAUN International Conferences:176–180, 2010.

[70] S. Mukhopadhyay and R.S.R. Gorla. Effects of partial slip on boundary layer flow past a permeable exponential stretching sheet in presence of thermal radiation. *Heat and Mass Transfer*, 48(10):1773–1781, 2012.

[71] M. Mustafaa, T. Hayat, and S. Obaidat. Boundary layer flow of a nanofluid over an exponentially stretching sheet with convective boundary conditions. *International Journal of Numerical Methods for Heat & Fluid Flow*, 23(6):945–959, 2013.

[72] S. Nadeem, R. Ul-Haq, and Z.H. Khan. Heat transfer analysis of water-based nanofluid over an exponentially stretching sheet. *Alexandria Engineering Journal*, 53(1):219–224, 2014.

[73] Ch. Nagalakshmi, K. Sreelakshmi, and G. Sarojamma. Effects of hall currents on the boundary layer flow induced by an exponentially stretching surface. *Procedia Engineering*, 127:440–446, 2015.

[74] R. Nandkeolyar, P.K. Kameswaran, S. Shaw, and P. Sibanda. Heat transfer on nanofluid flow with homogeneous-heterogeneous reactions and internal heat generation. *Journal of Heat Transfer*, 136(12):122001–1–8, 2014.

[75] C.L.M. Navier. Sur les lois du mouvement des uides. *Memoires delAcademie Royale des Sciences*, 6:389–440, 1827.

[76] M.K. Nayak, N.S. Akbar, D. Tripathi, and V.S. Pandey. Three dimensional mhd flow of nanofluid over an exponential porous stretching sheet with convective boundary conditions. *Thermal Science and Engineering Progress*, 3:133–140, 2017.

[77] D. Pal. Hall current and mhd effects on heat transfer over an unsteady stretching permeable surface with thermal radiation. *Computers & Mathematics with Applications*, 66(7):1161–1180, 2013.

[78] M.K. Partha, P.V.S.N. Murthy, and G.P. Rajasekhar. Effect of viscous dissipation on the mixed convection heat transfer from an exponentially stretching surface. *Heat and Mass Transfer*, 41(4):360–366, 2005.

[79] P.M. Patil, S. Roy, and E. Momoniat. Thermal diffusion and diffusion-thermo effects on mixed convection from an exponentially impermeable stretching surface. *International Journal of Heat and Mass Transfer*, 100:482–489, 2016.

[80] I. Pop and V.M. Soundalgekar. Effects of hall current on hydromagnetic flow near a porous plate. *Acta Mechanica*, 20(3):315–318, 1974.

[81] I. Pop and T. Watanabe. Hall effects on magnetohydrodynamic free convection about a semi-infinite vertical flat plate. *International Journal of Engineering Science*, 32(12):1903–1911, 1994.

[82] G.M.A. Rahman. Effects of variable viscosity and thermal conductivity on unsteady mhd flow of non-newtonian fluid over a stretching porous sheet. *Thermal Science*, 17(4):1035–1047, 2013.

[83] M.M. Rahman, A.V. Rosca, and I. Pop. Boundary layer flow of a nanofluid past a permeable exponentially shrinking surface with convective boundary condition using buongiornos model. *International Journal of Numerical Methods for Heat & Fluid Flow*, 25(2):299–319, 2015.

[84] M.M. Rahman and K.M. Salahuddin. Study of hydromagnetic heat and mass transfer flow over an inclined heated surface with variable viscosity and electric conductivity. *Commun Nonlinear Sci Numer Simulation*, 15:2073–2085, 2010.

[85] C.S.K. Raju, N. Sandeep, V. Sugunamma, M.J. Babu, and J.V.R. Reddy. Heat and mass transfer in magnetohydrodynamic casson fluid over an exponentially permeable stretching surface. *Engineering Science and Technology, an International Journal*, 19:45–52, 2016.

[86] P.B.A. Reddy, S. Suneetha, and N.B Reddy. Numerical study of magnetohydrodynamics(mhd) boundary layer slip flow of a maxwell nanofluid over an exponentially stretching surface with convective boundary condition. *Propulsion and Power Research*, 6(4):259–268, 2017.

[87] F.U. Rehman, S. Nadeem, and R.U. Haq. Heat transfer analysis for three-dimensional stagnation-point flow over an exponentially stretching surface. *Chinese Journal of Physics*, 55:1552–1560, 2017.

[88] D.E. Remus and V. Marinca. Approximate solutions for steady boundary layer mhd viscous flow and radiative heat transfer over an exponentially porous stretching sheet. *Applied Mathematics and Computation*, 269:389–401, 2015.

[89] D.E. Rosner. Thermal(soret) diffusion effects on interfacial mass transport rates. *PhysicoChemical Hydrodynamics*, 1(2-3):159–185, 1980.

[90] B.R. Rout, S.K. Parida, and S. Panda. Mhd heat and mass transfer of chemical reaction fluid flow over a moving vertical plate in presence of heat source with convective surface boundary condition. *International Journal of Chemical Engineering*, 2013(296834):1–10, 2013.

[91] B.C. Sakiadis. The boundary layer on a continuous flat surface. *A.I.Ch.E. Journal*, 7(2):221–225, 1961.

[92] S. Sandeep and C. Sulochana. Dual solutions of radiative mhd nanofluid flow over an exponentially stretching sheet with heat generation/absorption. *Applied Nanoscience*, 6(1):131–139, 2016.

[93] H. Sato. The hall effect in the viscous flow of ionized gas between parallel plates under transverse magnetic field. *Journal of the Physical Society of Japan*, 16(7):1427–1433, 1961.

[94] Y.I. Seini and O.D. Makinde. Mhd boundary layer flow due to exponential stretching surface with radiation and chemical reaction. *Mathematical Problems in Engineering*, 2013(163614):1–7, 2013.

[95] S. Shateyi and S.S. Motsa. Boundary layer flow and double diffusion over an unsteady stretching surface with hall effect. *Chemical Engineering Communications*, 198(12):1545–1565, 2011.

[96] M. Sheikh and Z. Abbas. Homogeneous - heterogeneous reactions in stagnation point flow of casson fluid due to a stretching/shrinking sheet with uniform suction and slip effects. *Ain Shams Engineering Journal*, 8:467–474, 2017.

[97] P.G. Siddheshwar, G.N. Sekhar, and A.S. Chethan. Flow and heat transfer in a newtonian liquid with temperature dependent properties over an exponential stretching sheet. *Journal of Applied Fluid Mechanics*, 7(2):367–374, 2014.

[98] K.R. Singh and T.G. Cowling. Thermal convection in magnetohydrodynamics. *The Quarterly Journal of Mechanics and Applied Mathematics*, 16(1):1–15, 1963.

[99] V. Singh and S. Agarwal. Flow and heat transfer of maxwell mluid with variable viscosity and thermal conductivity over an exponentially stretching sheet. *American Journal of Fluid Dynamics*, 3(4):87–95, 2013.

[100] J.C. Slattery. Momentum, energy and mass transfer in continua. *Mc. Graw-Hill New York*, 1972.

[101] E.M. Sparrow and R.D. Cess. The effect of a magnetic field on free convection heat transfer. *International Journal of Heat and Mass Transfer*, 3(4):267–274, 1961.

[102] E.M. Sparrow and R.D. Cess. *Radiation Heat Transfer*. 1^{st} Ed., Series in Thermal and Fluids Engineering, McGraw-Hill, 1978.

[103] E.M. Sparrow and H.S. Yu. Local nonsimilarity thermal boundary-layer solutions. *Journal of Heat Transfer*, 93(4):328–334, 1971.

[104] C.S. Sravanthi. Homotopy analysis solution of mhd slip flow past an exponentially stretching inclined sheet with soret-dufour effects. *Journal of the Nigerian Mathematical Society*, 35:208–226, 2016.

[105] P. Sreenivasulu, T. Poornima, and N.B. Reddy. Thermal radiation effects on mhd boundary layer slip flow past a permeable exponential stretching sheet in the presence of joule heating and viscous dissipation. *Journal of Applied Fluid Mechanics*, 9(1):267–278, 2016.

[106] D. Srinivasacharya, R. Bhuvanavijaya, and B. Mallikarjuna. Dispersion effects on mixed convection over a vertical wavy surface in a porous medium with variable properties. *Procedia Engineering*, 127:271–278, 2015.

[107] D. Srinivasacharya and Ch. Ramreddy. Soret and dufour effects on mixed convection from an exponentially stretching surface. *International Journal of Nonlinear Science*, 12(1):60–68, 2011.

[108] D. Srinivasacharya and Ch. Ramreddy. Cross-diffusion effects on mixed convection from an exponentially stretching surface in non-darcy porous. *Heat Transfer-Asian Research*, 42(2):111–124, 2013.

[109] C. Sulochana, N. Sandeep, V. Sugunamma, and B.R. Kumar. Aligned magnetic field and cross-diffusion effects of a nanofluid over an exponentially stretching surface in porous medium. *Applied Nanoscience*, 6(5):1–10, 2016.

[110] G.W. Sutton and A. Sherman. Engineering magnetohydrodynamics. *McGraw-Hill, New York, NY, USA*, 1965.

[111] L. Talbot, R.K. Cheng, R.W. Schefer, and D.R. Willis. Thermophoresis of particles in a heated boundary layer. *Journal of Fluid Mechanics*, 101(4):737–758, 1980.

[112] L. N. Trefethen. *Spectral Methods in MATLAB, 10*. SIAM, 2000.

[113] D. J. Tritton. *Physical Fluid Dynamics*. Van Nostrand Reinhold(London), England, 1985.

[114] R. Tsai. A simple approach for evaluating the effect of wall suction and thermophoresis on aerosol particle deposition from a laminar flow over a flat plate. *International Communications in Heat and Mass Transfer*, 26(2):249–257, 1999.

[115] F.K. Tsou, E.M. Sparrow, and R.J. Goldstein. Flow and heat transfer in the boundary layer on a continuous moving surface. *International Journal of Heat and Mass Transfer*, 10(2):219–235, 1967.

[116] J. Vleggaar. Laminar boundary-layer behaviour on continuous, accelerating surfaces. *Chemical Engineering Science*, 32(12):1517–1525, 1977.

[117] N.A. Yacob and A. Ishak. Stagnation point flow towards a stretching/shrinking sheet in a micropolar fluid with a convective surface boundary condition. *Can. J. Chem. Eng.*, 90:621–626, 2012.

[118] R.S. Yadav and P.R. Sharma. Effects of radiation and viscous dissipation on mhd boundary layer flow due to an exponentially moving stretching sheet in porous medium. *Asian Journal of Multidisciplinary Studies*, 2(8):119–124, 2014.

[119] A. Zaib and S. Shafie. Thermal diffusion and diffusion thermo effects on unsteady mhd free convection flow over a stretching surface considering joule heating and viscous dissipation with thermal stratification, chemical reaction and hall current. *Journal of the Franklin Institute*, 351(3):1268–1287, 2014.

[120] A. Zaib, Md.S. Uddin, K. Bhattacharyya, and S. Shafiee. Micropolar fluid flow and heat transfer over an exponentially permeable shrinking sheet. *Propulsion and Power Research*, 5(4):310–317, 2016.

[121] H. Zaman, A. Sohail, A. Ali, and T. Abbas. Effects of hall current on flow of unsteady mhd axisymmetric second-grade fluid with suction and blowing over an exponentially stretching sheet. *Open Journal of Modelling and Simulation*, 2(2):23–33, 2014.